STATUS AND OVERVIEW OF THE DOE-FUNDED PROJECTS RELATED TO
CHEMICAL GAS STREAM CLEANUP PROGRAM

Daniel C. Cicero
Suresh C. Jain

Department of Energy
Morgantown Energy Technology Center
P.O. Box 880
Collins Ferry Road
Morgantown, West Virginia   26505

INTRODUCTION

The U.S. Department of Energy has undertaken a Chemical Gas Stream Cleanup Program to
simplify and improve methods for cleaning gas generated from coal either by gasifica-
tion or combustion. The projects which comprise this development program are mainly
aimed at gas streams generated at pressures greater than 6 atmospheres and tempera-
tures greater than 1,000°F. These elevated pressures and temperatures would be
associated with emerging technologies such as integrated gasification combined-cycle
molten carbonate fuel cell power plants, direct-fired coal turbines, and pressurized
fluidized-bed combustion. Control and removal of the contaminants is a technical
limitation and a major cost associated with these advanced coal utilization systems.

The overall program objective is to develop technologies economically to remove hot
gas stream contaminants such as sulfur compounds, nitrogen compounds, alkalis,
selected trace metals, and residual hydrocarbons which are detrimental to advanced
coal-fired systems (1). Selection and continuance of the projects is based on their
ability to meet performance and environmental requirements and to show promise of
significant cost reduction over available technologies.

The Department of Energy through the Morgantown Energy Technology Center (METC)
carries out development programs for many of the other fuel conversion and power-
generating components for advanced energy systems based on coal. Besides the Gas
Stream Cleanup Program, METC implements programs in Gasification, Heat Engines, Fuel
Cells, Fluidized-Bed Combustion, Components, and Solid Waste Management. A high
degree of coordination with these programs is maintained to insure compatibility and
proper integration of development efforts. Figure 1 depicts the integration of
Chemical Gas Stream Program.

DISCUSSION

The products of coal gasification or combustion contain contaminants which were part
of the coal feedstock. These contaminants include sulfur compounds, chlorides,
nitrogen compounds (HCN, NH_3, NO_x), alkalis, particulates, and trace elements.
Removal of the sulfur and nitrogen compounds and the particulates is necessary to
meet national air quality standards for SO_x, NO_x, and suspended solids. Removal of
the other contaminants is required for some applications to avoid equipment damage or
serious degradation in performance. In particular, gas turbines have a very low
tolerance for alkali compounds and molten carbonate fuel cells (MCFC) for sulfur com-
pounds. The fuel cell sulfur limit is well below the environmental requirements for
sulfur control. The effect of sulfur on cell operation has been studied both theo-
retically and experimentally. The results from the Institute of Gas Technology (2),
United Technologies Corporation (3), and General Electric (4) work indicate that
sulfur present in either the anode or cathode feed affects the performance of the
nickel anode.

The cleanup requirements for four applications (pressurized fluidized-bed combustion/turbine, integrated gasification combined-cycle, molten carbonate fuel cell, and direct coal-fired turbine) and six categories of contaminants (particulates, sulfur, alkali, nitrogen, trace metals, and chlorine) are given in Table 1. Two applications pertain to cleanup of products of combustion before entering a turbine, one application is for low-Btu gas for turbine use and one is for medium-Btu gas for fuel cells. Allowable level of particulates for the pressurized fluidized-bed combustion/turbine and integrated gasification combined-cycle applications are in the range of 1.7×10^{-4} to 0.01 grain (gr) per standard cubic feet (scf) and 4.1×10^{-3} to 0.24 gr per scf, respectively.

The DOE Chemical Gas Stream Cleanup program has centered on matching of cleanup subsystem temperature and pressure to that required by the end use process element and the upstream gasifier or combustor. This matching should provide attractive systems by eliminating heat recovery equipment and compressors or expanders. Figure 2 shows a temperature-pressure plot with various subsystems in their operating envelopes. With gasifier turbine power systems, an ideal match is achieved with fixed-bed gasifiers and a zinc ferrite desulfurization subsystem. This combination of gasifier and hot cleanup has been referred to as a "gasification island" concept by METC and has been receiving high priority in development. Molten carbonate fuel cells operate at about the same temperatures but at lower pressures than gas turbines; both the zinc ferrite subsystem and some novel sorbent subsystems would be an ideal temperature match. A relatively unknown area is that required for direct-fired turbines where temperatures can range from 2,000° to 2,800°F or higher. Although a temperature-pressure match is attractive, systems analysis is necessary to examine all factors that effect performance and cost.

The Chemical Gas Stream Cleanup Program, as shown in Figure 3, is divided into six contaminant removal areas, i.e., sulfur, alkali, tars, trace species, chloride, and nitrogen. Each removal area is briefly discussed below. Particulate removal is a separate project area pursued by METC and is not discussed in this presentation.

Sulfur Removal

The need to comply with environmental standards makes sulfur removal important for all coal gas applications. However, MCFC applications require sulfur levels below the 1 part per million (ppm) range (5), while other applications allow 100 ppm or more. Nevertheless, sulfur removal to below 10 ppm could be beneficial for turbine applications, because sulfur and alkalis interact to cause corrosion and/or deposition on turbine blades, and reducing sulfur may allow less stringent alkali removal requirements. Projects under sulfur removal are shown in Figure 4.

Figure 5 shows sulfur removal technologies for various temperatures of fuel gas. Many cold scrubbing technologies are available for removing fuel gases up to temperatures of about 350° to 400°F. These techniques can achieve very high sulfur removals if designed in stages with extensive recycle. For fuel gas temperatures from about 850° to 1,200°F, two systems have shown promise: an iron oxide sorbent and a zinc ferrite sorbent. Iron oxide was tested at METC in the 1970's on fuel gas from a fixed-bed gasifier. These tests showed feasibility of the sorbent for achieving up to 90 percent sulfur removal. IHI subsequently has been testing this process on a pilot scale.

Recent development work at METC has shown zinc ferrite to be a likely candidate for hot gas desulfurization, because it can remove all sulfur species in the gas to below 5 ppm except for that found in the tar. Five projects are underway to explore the questions that remain in zinc ferrite sorbent development. In addition, the zinc ferrite absorber will be scaled up and tested at the process development unit (PDU) fluidized-bed gasifier at the KRW Energy Systems, Inc., Waltz Mill site early in 1986.

2

TABLE 1

Allowable Level of Contamination in Cleaned Gas for Four Potential Commercial Applications

	Pressurized Fluidized-Bed Combustion/Turbine (Products of Combustion)	Integrated Gasification Combined Cycle (Low-Btu Gas)	Molten Carbonate Fuel Cell (d) (Medium-Btu Gas)	Direct Coal-Fired Turbine (Products of Combustion)
1. Particulates	.0044 gr/scf[b], NSPS for Coal-Fired Boiler 3.2 x 10^{-4} gr/scf, Brown-Boveri[7] 1.7 x 10^{-4} gr/scf, General Electric[7] 2.2 x 10^{-4} gr/scf, United Technologies .002 gr/scf, Westinghouse[8] .01 gr/scf, METC Proposed[1]	.106 gr/scf, NSPS for Coal-Fired Power Generation .0077 gr/scf, Brown-Boveri[7] .0041 gr/scf, General Electric[7] .0053 gr/scf, United Technologies[7] .048 gr/scf, Westinghouse[8] .24 gr/scf, METC Proposed[1] .01 gr/scf, Westinghouse Blast Furnace Gas[8]	TBD[e] .0056 PPM Weight[9]	TBD[e]
2. Sulfur	269 PPMV, NSPS for Coal-Fired Boilers[10] 101 PPMV, NSPS for Coal-Fired Power Generation (98% Reduction)[10]	1616 PPMV, NSPS for Turbines[10] 606 PPMV, NSPS for Coal-Fired Power Generation (90% Reduction)[10]	.1-1 PPMV H_2S + COS[11] 1 PPMV[9]	269 PPMV, NSPS for Gas Turbines[10] 101 PPMV, NSPS for Coal-Fired Power Generation (90% Reduction)[10]
3. Alkalis[c]	.0063 - .063 PPMW[f] .02 PPMV, GE Proposed[1]	.05 - .5 PPMW[f] .2 PPMV, METC Proposed[1]	TBD[e]	TBD[e]
4. Nitrogen	None; Low Bed Temperature Should Keep NO_x Low	25 PPMV, METC Proposed to Meet NO_x Standards	TBD[e] None[9]	25 PPMV, METC Proposed to Meet NO_x Standards
5. Trace Metals	V-.0063 - .025 PPMV[f] Ca = .125 PPMV[f]	V-.05 - .2 PPMV[f] Ca = 1 PPMV[f]	.1 - 1 PPM[11]	TBD[e]
6. Chlorine	None[8]	None[8]	.1 - 1 PPM HCl[11] 10 PPM HCl[9]	None[8]

(a) Particulates, alkalis, and trace metals are back-calculated from PFBC. Assumptions: 160 Btu/scf gas; air/gas to turbine, 5.0 (1,333°F heat rise); particulates are 75% carbon, which is consumed ahead of turbine inlet; cold gas efficiency of gasifier is 80%.

(b) Varies with air/coal ratios; coal HHV.

(c) Tolerances for alkali removal are expected to be much higher if sulfur removal is 10 PPMV.

(d) To obtain tolerances for low-Btu gas, divide by 2.

(e) To be determined; tolerances are either unknown or are not firm. Contracts planned or in place to determine tolerances.

(f) Manufacturers standards for fuel oil fired turbines[8].

3B:3-28-85:pb:4a

3

Another category of sorbents referred to as mixed metal oxide and novel sorbents has been under investigation. These sorbents have promise of achieving desulfurization at higher temperatures and potentially producing elemental sulfur on regeneration. The Institute of Gas Technology (IGT) mixed metal oxide process and Battelle Pacific Northwest Laboratories solid supported molten salt process are currently at the bench-scale development stage. In addition, Jet Propulsion Laboratories (JPL) is completing laboratory-scale tests on entirely new types of synthesized sorbents; the most promising sorbents will be tested at the bench scale late in 1986.

At temperatures from 1,500° to about 2,000°F, calcium-based sorbents have been tested and achieved over 95 percent sulfur removal. These processes are not currently being developed by DOE. Earlier work by CONOCO and others have shown the feasibility of these systems. METC is exploring the potential of combining sulfur removal with gasification processes, however, in tests in a fluid-bed gasifier under the METC gasification program.

The final determination of which of these processes will find use in sulfur removal systems will depend on economics. Two pieces of these economic studies are being carried out by Gilbert/Commonwealth, Incorporated, in studies of reactor costs, and Ralph M. Parsons Company in evaluations of tail gas treating systems.

    Zinc Ferrite Studies

A sulfur sorbent utilizing zinc ferrite has been under development at METC for the past 5 years. Initial tests were with gas mixtures that approximated gasifier fuel gases. Bench-scale evaluation in actual coal gas streams were then carried out and demonstrated that in the operating regime 1,000° to 1,200°F, 120 to 240 psig, and 1,000 to 2,000 h^{-1} space velocity, a zinc ferrite sorbent can function in a hot gas stream from a fixed-bed coal gasifier, removing low molecular weight sulfur compounds to a level of about 10 ppm. High molecular weight sulfur compounds, which are in tars, however, are not removed. The sorbent picks up about 30 percent of its weight in sulfur before breakthrough. It can be regenerated by air and steam mixtures at 1,400° to 1,500°F, to near its original condition with a residual sulfur content (as sulfate) of less than 1 weight percent. Absorption performance after three regenerations is close to that of fresh sorbent (6). Figure 6 is a plot of the exit hydrogen sulfide (H$_2$S) level attained over three cycles of absorption and regeneration. It can be seen that the H$_2$S level is about 1 to 5 ppm before breakthrough and there is no significant drop in the sorbent sulfur loading following regeneration.

Potential improvements which may be made to the zinc ferrite system include (a) understanding metal phase changes occurring at certain operating conditions which could degrade sorbent integrity and performance; (b) minimize sulfate formation, which can occur in gases with significant SO$_2$; and (c) reduce catalyst degradation which occurs with repeated cycling leading to reduced structural strength and loss of integrity and performance. Several contracted efforts are aimed at these improvements.

Louisiana State University is studying structural changes in hot metal oxide sorbents including zinc ferrite through adsorption and regeneration cycles. Results to date indicate that the relatively simple model is adequate to describe the time-conversion data. During most of the reaction, product layer diffusion appears to be the controlling resistance. Early in the reaction, before the product layer is fully developed, mass transfer is believed to be important.

SRI International is performing theoretical and empirical studies of phase boundaries of zinc ferrite during adsorption and regeneration. The Fe$_3$O$_4$/Fe, Fe$_3$O$_4$/wustite, carbon deposition, and carbide formation phase boundary compositions have been calculated for total pressures of 1, 5, 10, 15, and 20 atm at temperatures of 930°, 1,020°, 1,100°, 1,200°, and 1,300°F. Another SRI International study deals with sulfate formation and how it can be avoided. Fixed-bed reactor experiments were conducted at

4

SRI to determine the amount of sulfate formed as a function of several process varia-
bles. Higher sorbent temperature and lower oxygen partial pressure in the feed gas
lead to a decrease in the amount of sulfate remaining in the regenerated sorbent is
a function of duration of regeneration; longer duration decreases the amount of
residual sulfate. An increase in space velocity was found to decrease the sulfate
formation. In the range of particle size from 0.5 to 5 mm, the sulfate formation was
not affected by the particle size. The presence of SO_2 in the feed gas significantly
promotes the sulfate formation.

AMAX, Incorporated, is studying how to maximize zinc ferrite physical strength
and durability during the sorbent fabrication process. A sorbent which was formu-
lated with bentonite as a binder has shown improved physical and chemical performance
over the United Catalyst, Incorporated (UCI), zinc ferrite composition used in test-
ing at METC. The AMAX sorbent had shown double the physical crush strength and twice
the sulfur bearing capacity of the UCI sorbent. During the desulfurization testing,
the AMAX sorbent showed the capacity for retaining its initial surface area whereas
the UCI sorbent showed some loss of surface area through sintering. The AMAX sorbent
also had less fines attritioning during the desulfurization testing.

Novel Fuel Gas Sorbents

Novel sorbents can offer higher temperature applications and simpler tail gas treat-
ment. The Battelle solid supported molten salt (SSMS) system, under development
since 1974, is at the bench-scale development stage and features both sulfur com-
pounds and HCl removal from 6,000 ppm and 200 ppm to less than 1 ppm level, respec-
tively. The SSMS sorbent consisted of porous lithium aluminate ceramic pellets
loaded with low-calcium salt ($Li_{1.1}K_{0.7}Ca_{0.1}CO_3$). The sorbent can be regenerated
with carbon dioxide-steam mixture to produce a hydrogen sulfide-rich gas from which
elemental sulfur could be efficiently recovered. The IGT mixed metal oxide system,
under development since the late 1970's, employs two sorbents. One sorbent, cobalt
titanate, removes 70 percent of the sulfur and can be regenerated with $N_2/O_2/SO_2$ mix-
tures to produce elemental sulfur. The other oxide is one of many suitable for
removing sulfur compounds to low levels which can be regenerated with air and steam
or nitrogen to produce SO_2. Major examples are zinc oxide, iron oxide, and copper
oxide.

The current research program conducted at JPL aims at synthesizing high-temperature
sulfur removal sorbents that combine several desirable physicochemical properties.
Certain mixed oxide sorbents have been developed with rapid kinetics of absorption
and good sorbent regenerability at 930° to 1,300°F. The rapid absorption rates are
realized by eliminating or minimizing the resistance associated with solid state dif-
fusion. In one class of sorbents, stable high surface area can be obtained by eutec-
tic mixtures of metal oxide sorbents (e.g., $ZnO \cdot V_2O_5$, $CuMoO_4 MoO_3$), which form a melt
that coats the pore surface of a high surface area support. The other class of sor-
bents considered in this work consists of unsupported mixed oxides forming highly
dispersed solid solutions or solid compounds (e.g., $ZnFe_2O_4$, $CuFe_2O_4$, $CuFeAlO_x$,
$CuMo_xAl_yO_z$), characterized by their small crystalline size, high porosity and rela-
tively high surface area. All sorbents exhibit high sulfur removal efficiency,
stable conversion, minimal pore plugging, and good regenerability.

Direct-Fired Turbine Sorbents

Physical Sciences, Inc. (PSI) is undertaking a combined theoretical and bench-scale
experimental program to study the feasibility of using micronized coal and coal-water
mixtures (CWM) as fuels in heat engines. This project addresses two major interre-
lated consequences arising from the introduction of these fuels into gas turbine
combustors. The first is the release of coal-bound mineral matter into the combus-
tion product stream. A second consequence of firing coal is the emissions of sulfur
oxides which have been identified as precursors to acid rain. PSI will quantify sul-
fur and alkali removal rates by solid sorbents and will determine the effects of the

sorbents on deposition. Westinghouse Research and Development Center will develop
information on the feasibility of using limestone and dolomite sorbents for sulfur
capture in post-combustion gas streams under temperature and pressure conditions
typical of direct coal-fired turbine operation. Both of these projects are in early
stages with findings not at a stage to report.

Economic System Studies

While various types of sulfur removal systems are in various stages of development,
Ralph M. Parsons Company and Gilbert/Commonwealth, Incorporated, are conducting
studies for cost optimization of the sulfur removal technology in a plant complex to
produce 100 megawatts of electrical power. The Gilbert study focuses on various coal
gasifier and fixed-/fluidized-bed sulfur absorber and sorbent regeneration systems
using the Morgantown Energy Technology Center's zinc ferrite process, the Institute
of Gas Technology's metal oxide process, and the Battelle Pacific Northwest Labora-
tory's solid-supported molten salt process. This study includes 11 cases for gasi-
fier, hot gas cleanup, and regeneration system configurations as summarized in Table 2.
The Parsons study deals exclusively with state-of-the-art sulfur recovery from regen-
eration gases. This study includes 11 process configurations as summarized in Table 3.
Both of these studies are in the early stages and conclusions have not been reached
concerning them.

Alkali Removal

Presence of alkali metal is a major concern in gas turbines, which operate at tem-
peratures of 1,800°F and higher. Allowable levels of alkali metals in expansion
gases for turbines to prevent corrosion or deposition on blades, stators, and rotors
can be readily derived from standards for alkali content for liquid turbine fuel (.5
to 5 ppm). These standards correspond to a .05 to .5 ppm allowance for alkali metals
in low-Btu gas. Encouraging results were achieved in measurements of alkali levels
during a test at the General Electric Company gasifier in November 1984. The gasi-
fier is a stirred-bed operated in an air-blown mode. Cleanup consisted of a single
cyclone. Alkali levels were measured, less than 1 ppm, and approximated that calcu-
lated from alkali content in the feed coal ash.

Alkali metal tolerances for MCFC applications have not been established. A
study ongoing by Energy Research Corporation (ERC) to determine the effect of trace
metals on fuel cells will establish alkali tolerances if in fact they are needed.
Figures 7 and 8 show the work being conducted in the areas of fundamental studies,
alkali measurement, and alkali control.

Fundamental studies of release mechanisms, capture mechanisms, and fate of alkali
metals are being conducted by METC, Midwest Research Institute, and the University of
Arizona. Aerodyne Corporation is updating and modifying a computer model for inter-
phase condensation of alkali metals in pressurized fluidized-bed combustion processes.

Three methods of alkali metal control are each being explored by Westinghouse,
Argonne National Laboratory, and the University of Pittsburgh. The Argonne study is
aimed at PFBC applications, the Westinghouse study is directed at pressurized coal
gasification applications, while the University of Pittsburgh study is concerned with
products of entrained gasification using solid collectors to trap contaminant species.

Fundamental Studies

A University of Arizona study is investigating the formation of alkali metal vapor in
entrained flow gasification and combustion at various temperatures, and the potential
for capture of these vapors with powdered kaolite or limestone. Midwest Research
Institute is studying fundamental combustion chemistry in PFBC applications with the
goal of verifying predictability of alkali metal concentrations in off gases by
existing computer models. One such model, the PACKAGE code, is being modified,
upgraded, and more fully documented by the Aerodyne Corporation.

6

TABLE 2. Summary of Hot Gas Cleanup Cases Studied
by Gilbert/Commonwealth, Incorporated

Cases Sorbent Process				Hot Gas Cleanup Reactor	Sulfided Sorbent Regenerator
METC[a]	Battelle[b]	IGT[c]	Gasifier		
1	6	9	Air -- Fixed-Bed Dry Ash	Fixed	Fixed
2	7	10	O_2 -- Texaco Quench	Fixed	Fixed
3	8	11	O_2 -- Westinghouse Fluid Bed	Fixed	Fixed
4			O_2 -- Westinghouse Fluid Bed	Fluid	Fluid
5			O_2 -- Fixed-Bed Dry Ash	Fixed	Fixed

[a] Zinc ferrite.

[b] Solid-supported molten salt.

[c] Mixed metal oxides.

TABLE 3. Summary of Configurations of 11 "Short-List" Process
Candidates Assessed by The Ralph M. Parsons Company

Candidate Process Grouping No.	Case No.	SO_2 Recovery/ Concentration Process	Sulfur Reduction/ Production Process	Tail Gas Process
1	1A	Wellman-Lord	Resox	BSR/Claus
	1B	Wellman-Lord	Resox	Recylce to W-L
	1C	Wellman-Lord	Resox	BSR/MDEA
	1D	Wellman-Lord	Resox	BSR/Stretford
2	2A	Wellman-Lord	Allied Chemical (2 Claus Stages)	None
	2B	Wellman-Lord	Allied Chemical (2 Claus Stages)	Recycle to W-L
	2C	Wellman-Lord	Allied Chemical (3 Claus Stages)	None
3	3	Wellman-Lord	Beavon Sulfur Removal (BSR)	Stretford
4	4A	Wellman-Lord	Modified Claus	BSR/Selectox
	4B	Wellman-Lord	Modified Claus	BSR/Stretford
	4C	Wellman-Lord	Modified Claus	Recycle to W-L

BSR -- Beavon Sulfur Removal.

W-L -- Wellman-Lord.

MDEA -- Methyl-di-ethanol-amine.

Alkali Measurement

In addition to fundamental studies and development of control technology, Ames
National Laboratory has developed an on-line alkali measuring device, which was
further developed by METC to be capable of measuring alkali content to 10 ppb. The
meter has been successfully tested at the process development unit (PDU) scale at
METC and at GE Research Center, Schenectady site. The meter will be used to measure
the alkali levels at the PDU scale at KRW Energy Systems, Inc., Waltz Mill site.

Alkali Control

Westinghouse, Incorporated, has conducted research into the alkali-gettering concept
since October 1978. The results of their work and that of others like Argonne
National Laboratories (ANL) led to the conclusion that a fixed bed of cylindrical
pellets, 1/8 inch in diameter by 1/4 inch long, of emathlite, a fuller's earth, is
the best method of hot gas removal of alkali metals from products of coal gasifica-
tion. Current development is at bench scale.

A recent 100-hour test conducted by Westinghouse using a shallow packed bed showed a
range of 2.0 to 4.2 weight percent capture of sodium by the emathlite. The feed gas
sodium concentration was reduced from 10 ppm to approximately 2 ppm. In laboratory
tests at Argonne, activated bauxite shows a similar ability for sodium capture, but
has the additional advantage of being regenerable via water leaching.

ANL has pioneered the development of granular sorbents suitable for use in a granular
bed for the removal of alkali vapor from hot PFBC flue gas. After extensive screen-
ing of potential candidate sorbents, activated bauxite and diatomaceous earth were
found to be the most effective sorbents in capturing NaCl, KCl, and K_2SO_4 vapors from
a simulated hot PFBC flue gas at atmospheric pressure.

In recent laboratory-scale, fixed-bed sorption studies at ANL, performed at condi-
tions that closely simulate the actual PFBC flue gas (temperature, 1,560°F; pressure
10 atm absolute; gaseous composition, 3 percent O_2, 16 percent CO_2, 5 percent H_2O,
250 ppmV SO_2, few ppmV NaCl vapor, and the balance N_2), NaCl-vapor removal efficien-
cies greater than 99 percent were achieved for both activated bauxite and diatomace-
ous earth sorbents. It was also demonstrated that activated bauxite can be easily
and effectively regenerated for reuse by a simple water-leaching process. A prelimi-
nary evaluation indicated that the fixed granular-bed filter concept for the control
of alkali vapors from PFBC flue gas is economically attractive.

A research project has been initiated at the University of Pittsburgh whose objective
is the control of emissions of alkali metals, trace metals, and aromatic hydrocarbons
that occur in advanced coal conversion processes such as pulverized coal combustion
for turbine applications. The process is the adsorption of the undesirable components
onto the surface of a solid collector, such as pulverized alumina, which is injected
into the flame mixed with the feed coal. The particle size of the collector will be
such that it can be easily removed from the flue gas by a cyclone or other separator.

Tar Removal

The problem of removing tar and other lighter hydrocarbons from hot coal gas streams
is of interest primarily for integrated coal gasification/molten carbonate fuel cell
power plant applications using fixed-bed gasifiers. These hydrocarbons also carry a
nontrivial fraction of sulfur which could impact the performance of the molten carbon-
ate fuel cell. Tar removal is irrelevant for gas turbine use, and tar and all but the
lightest hydrocarbons are absent from products of other than fixed-bed gasifiers.
Figure 9 shows the work being conducted in the area of tar removal.

The Chemical Gas Stream Cleanup Program includes a study by Washington State Univer-
sity on the fundamentals of tar formation in fixed-bed gasifiers and preliminary

development of three broad approaches to cracking hydrocarbons in hot product gas streams from fixed-bed gasifiers by Battelle Pacific Northwest Laboratory (Battelle), Physical Sciences, Incorporated (PSI), and Massachusetts Institute of Technology (MIT).

Fundamentals of Tar Formation and Removal

Tars and lighter hydrocarbons appear in the raw product gas streams of fixed-bed gasifiers because conditions at the top of the bed of coal permit coal to devolatilize, but the products of devolatilization only partially break down. The type and yields of tars and lighter hydrocarbons from fixed-bed gasifiers at various conditions and the subject of coal devolatilization in general has been studied rather extensively. A METC-sponsored study by Washington State University will provide a compilation of fundamental facts about tar formation in fixed-bed gasifiers and their destruction by catalytic or thermal cracking. The study also includes empirical work to fill in gaps in information required to design MCFC power plants incorporating methods of eliminating tars from the fuel cell feed gases. Also, studies sponsored by the DOE gasification program are providing new data on tar formation mechanisms.

The Effects of Tar and Other Contaminants on Fuel Cell Performance and Life

Previous studies have shown particulates, soot, hydrocarbons, and trace elements to be potentially deleterious to MCFC performance and life. Soot formation is an important concern for efficient utilization of coal gas in MCFC systems. Coal gas is generally formed at temperatures greater than the MCFC operating temperatures (~ 1,830°F for a gasifier compared with ~ 1,200°F for MCFC) and tends to deposit carbon in the fuel cell unless its gas composition is properly "stabilized," and the surfaces and the conditions that promote carbon deposition are minimized. The presence of hydrocarbons, tars and oils, etc., can further aggravate this problem. The effect of particulate matter present in coal gas (even after various cleanup steps) has not been characterized so far, except for some theoretical modeling under a Westinghouse/Energy Research Corporation (ERC) study performed for METC. Similarly, only some thermodynamic calculations have been performed on the possible effects of ammonia, arsenic, and other trace elements. A very limited amount of experimental data is available on the possible effects of these contaminants.

Tar Cracking

Three preliminary development projects at Battelle, PSI, and MIT for tar removal sponsored by METC involve the use of a cracking catalyst. Since sulfur removal to below 1 ppm is required for MCFC, a preliminary goal is to remove a sufficient quantity of tar and/or desulfurize the remaining tar so that the tar sulfur content does not prevent achievement of desulfurization requirements. The Battelle study is directed to convert the sulfur in the tar to a form (such as H_2S) which can be removed by a hot gas desulfurization process. The results of the catalytic cracking of coal tars are shown in Figure 10. The PSI study is aimed at in-process destruction of aromatic hydrocarbons, while the MIT study is concerned with quantitative understanding of the thermal reactions of aromatic contaminants with calcium oxide.

Trace Species Removal

A research program in support of a high-temperature process for the removal of sulfur and arsenic containing compounds as well as other trace contaminants from coal-derived fuel gas was initiated at ERC. The process to be explored utilizes a nickel sorbent system which may be regenerable with steam and hydrogen or oxygen. This concept is supported by the fact that nickel has a strong affinity for both sulfur and arsenic even at low concentrations (< 10 ppm). Both the contaminants are known poisons for the nickel catalysts. The adsorption of sulfur on nickel occurs by reversible dissociative chemisorption. A number of studies indicate that a gas stream can be purified

to very low levels of sulfur with a nickel-based catalyst, which may be regenerable as well. Figure 11a shows the work being conducted in the areas of trace species control and measurement.

Chloride Removal

Chloride removal to .1 to 10 ppm has been established as a requirement for MCFC applications. Requirements for other applications have not been established, but they are not expected to be as stringent. SRI International is developing a laboratory-scale process to remove HCl to below 1 ppm. Figure 11b shows the work being conducted in the area of chloride removal.

Nitrogen Removal

Most of the ammonia emitted from a typical gas producer has been determined to come from the reduction of the nitrogen in the fuel. The temperature-pressure relation-ships in an atmospheric or low-pressure gas producer are sufficient for the breakdown of ammonia in the presence of a catalyst. A large number of such catalysts have been manufactured and tested. In general, these catalysts tend to be expensive and susceptible to irreversible poisoning by hydrogen sulfide (H_2S). Previous experi-mental work has indicated that the irreversible poisoning of the catalyst could be avoided by removing the H_2S from the producer gas prior to exposure to the catalyst. It has also been suggested that combining these catalysts with the fuel in the gasifier would avoid contact of the evolving H_2S gas with the catalyst and achieve the desired reduction.

A project will soon be initiated to explore both methods of ammonia decomposition, develop preliminary process economics, and make some preliminary determinations of their applicability to full-scale coal-powered gasification systems.

CONCLUSION

The results obtained from the ongoing DOE-funded projects related to the chemical gas stream cleanup are encouraging. The design data will be available for process engi-neers to develop hot gas desulfurization/regeneration systems design using zinc fer-rite as the sorbent. Novel sorbents have been identified for potential removal of H_2S, COS, and HCl to less than 1 ppm.

An alkali meter has been developed which can be used wherever on-line measurements of trace alkali metal concentration in hot dirty gas or combustion product streams are required. Alkali sorbents have also been identified to remove alkalis to very low levels when required. Promising results have been obtained using the novel sorbents to convert the sulfur in the tar to hydrogen sulfide which can be removed by a hot gas desulfurization process. These sorbents can also convert the tars to compounds which will not crack and deposit coke on the electrodes of a molten carbonate fuel cell. Another sorbent has been identified for hot removal of the trace contaminants (sulfur and arsenic) present in coal gas to sub-ppm levels for MCFC applications.

The results obtained through efforts on these projects promise to show marked improvements in the development of advanced cleanup concepts for controlling and/or removing contaminants economically from coal-derived gas streams. Advanced research efforts will continue as well as efforts to determine the overall technical and economic feasibility of these concepts for possible future commercialization by the private sector. Successful eventual commercialization of cleanup unit operations using these concepts could provide advanced coal conversion/utilization system with emissions far below these seen from today's coal-fueled power systems.

14A:3-22-85:slc:4a

References

1. FY 85 Implementation Plan for the Gas Stream Cleanup Program, Gas Stream Cleanup Section, U.S. Department of Energy, Morgantown Energy Technology Center, August 20, 1984.

2. Benjamin, T. G., E. H. Camara, and L. G. Marianowski, "Handbook of Fuel Cell Performance," Prepared by Institute of Gas Technology for the U.S. Department of Energy, Contract No. EC-77-C-03-1545, May 1980.

3. Healy, H. C., et al., "Development of Molten Carbonate Fuel Cell Power Plant Technology," Quarterly Technical Progress Report No. 2, Prepared by United Technologies Corporation for the Department of Energy, Contract No. DE-AC01-79ET15440, August 1980.

4. Reinstrom, R. M., et al., "Development of Molten Carbonate Fuel Cell Power Plant," Quarterly Technical Progress Report for May-July 1980, Prepared by General Electric Company for the Department of Energy, Contract No. DE-AC02-80ET17019, September 1980.

5. Monitoring Contaminants in Coal-Derived Gas for Molten Carbonate Fuel Cells, "DOE/METC/82-44," Final Report by TRW, Prepared for Argonne National Laboratory, Contract No. 31-109-38-6108, May 1981.

6. Grindley, T. and G. Steinfeld, "Desulfurization of Hot Coal Gas by Zinc Ferrite," Prepared for Publication in "Acid and Sour Gas Treating Processes" by Gulf Publishing Company, June 1984.

7. Meyer, J. P. and M. S. Edwards, "Survey of Industrial Coal Conversion Equipment Capabilities: High-Temperature, High-Pressure Gas Purification," ORNL/TM-6072, Oak Ridge National Laboratory, June 1978.

8. High-Temperature Turbine Technology Program, FE-2290-27, Phase I, Program and System Definition, Topical Report, "Fuels Cleanup and Turbine Tolerance," Westinghouse Electric Corporation, February 1977.

9. Vidt, E. J., G. Jablonski, J. R. Hamm, M. A. Alvin, R. A. Wenglarz, and B. Patel, "Evaluation of Gasification and Gas Cleanup Processes for Use in Molten Carbonate Fuel Cell Power Plants," DOE/MC/16220-1306, Final Report, Westinghouse and Davy McKee for the U.S. Department of Energy, Morgantown Energy Technology Center.

10. "Protection of Environment," 40, Code of Federal Regulations, Parts 53 to 80, Office of the Federal Register, July 1, 1982.

11. Frumerman, R., "Gasification Cleanup Requirements," presented at the Second Annual Contractors' Meeting on Contaminant Control in Hot Coal-Derived Gas Streams, Morgantown, West Virginia, February 17 to 19, 1982.
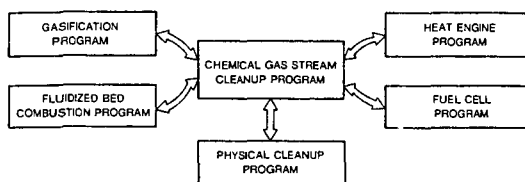
13A:3-22-85:slc:4a

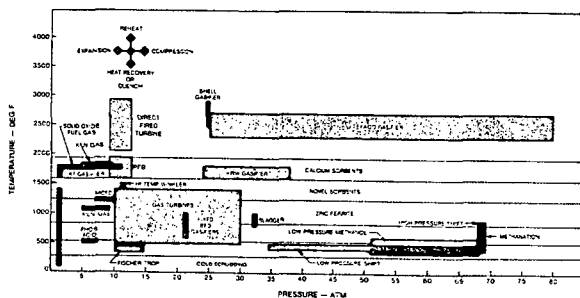Figure 1.   Cleanup Program Integration

Figure 2.   Temperature-Pressure Envelopes
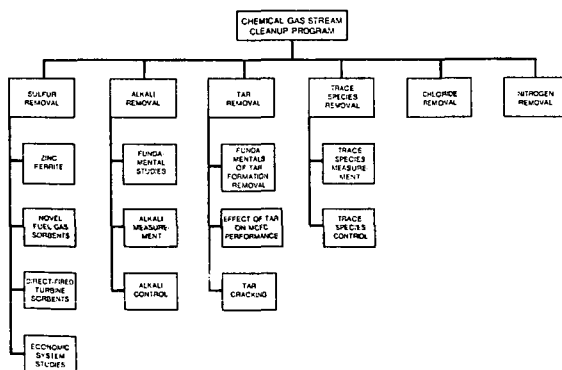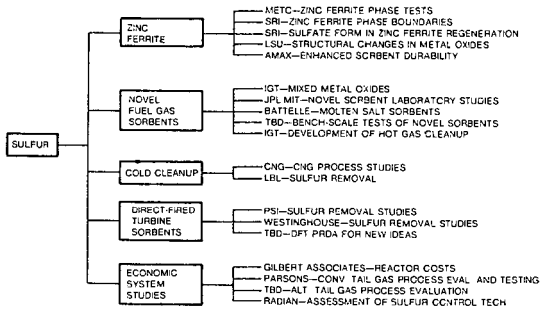

Figure 3.   Chemical Gas Stream Cleanup Program
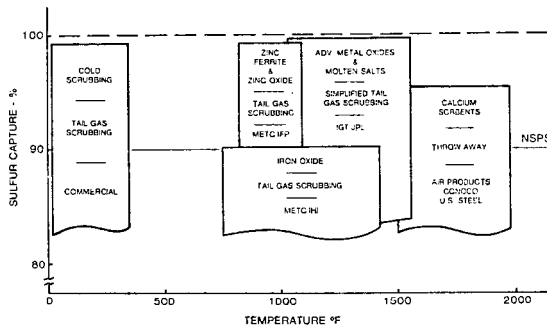
12

Figure 4. Sulfur Removal Projects

Figure 5. Fuel Gas Desulfurization

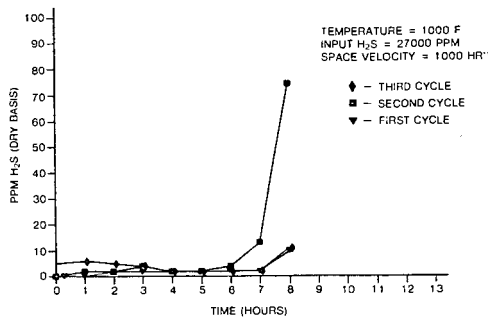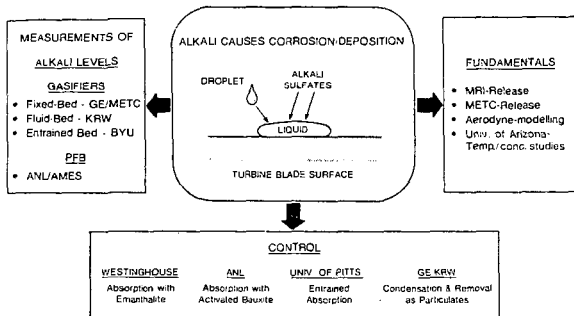

Figure 6. Zinc Ferrite Sulfidation

13

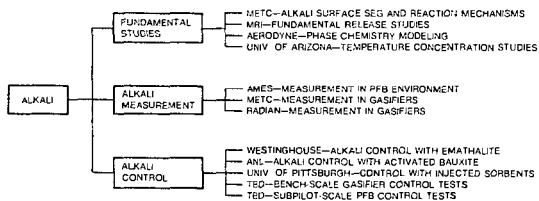Figure 7. Alakli Removal Projects
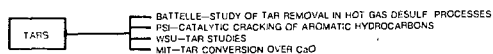

Figure 8. Alkali Removal Projects
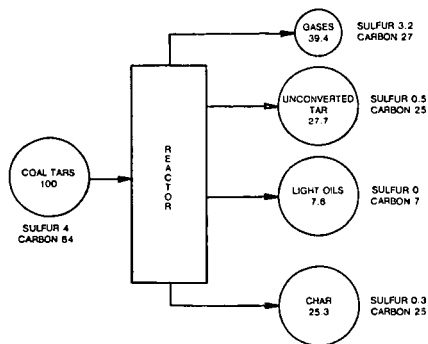

Figure 9. Tar Removal Projects

14

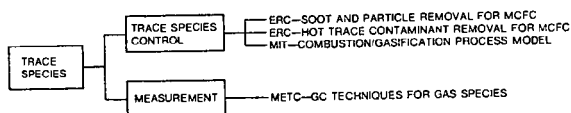Figure 10. Catalytic Cracking of Coal Tars (Battelle-PNL)

Figure 11a. Trace Species Removal Projects

Figure 11b. Chloride Removal Projects

HIGH-TEMPERATURE REGENERATIVE REMOVAL OF H_2S BY POROUS MIXED OXIDE SORBENTS

M. Flytzani-Stephanopoulos, S.S. Tamhankar,[†] G.R. Gavalas,[†]
M.J. Bagajewicz,[†] and P.K. Sharma

Jet Propulsion Laboratory and[†] Department of Chemical Engineering
California Institute of Technology
Pasadena, California 91109

ABSTRACT

Several mixed-metal oxides ($ZnFe_2O_4$, $CuFe_2O_4$, $CuAl_2O_4$, Cu-Fe-Al-O) were investigated as regenerable sorbents for the high-temperature removal of H_2S. A special technique was used to prepare the sorbents in a highly porous form. The sorbents were subjected to successive sulfidation/regeneration cycles in a packed bed microreactor. Sulfidation was carried out at 538-650°C with H_2S-H_2O-H_2-N_2 mixtures, regeneration with O_2-N_2-H_2O mixtures. The fresh, sulfided and regenerated sorbents were analyzed by XRD. Solid conversion and pre-breakthrough exit H_2S concentration are discussed in terms of physical structure and thermodynamic properties of the sorbents. In the case of $CuFe_2O_4$, $CuAl_2O_4$ and $CuFeAlO_x$, sorbent performance is discussed in terms of changes in the oxidation states of copper and iron during sulfidation.

INTRODUCTION

High temperature desulfurization of coal-derived fuel gas offers potential improvements on the thermal efficiency of systems using coal gasification such as power plants (high temperature fuel cells, combined cycle) and synthesis gas conversion plants (ammonia, methanol). Over the last ten years, several sorbents have been proposed and investigated for the regenerative removal of the main sulfur compound, i.e. hydrogen sulfide, from fuel gas at high temperatures. The level of H_2S removal needed depends on the end use of the fuel gas. For power plant combustion purposes, removal down to about 100 ppm is adequate, but for molten carbonate fuel cell applications removal down to a level of 1 ppm may be required.

The thermodynamics of various sorbents have been analyzed in (1) and (2) among other reports. Comprehensive surveys of experimental work encompassing various high temperature sorbents have also been published (1-7).

The overall performance of a sorbent depends on a variety of properties. Thermodynamics and kinetics of sulfidation are obvious factors, for they determine the overall sulfur capacity before breakthrough of some predetermined level of H_2S. Kinetics encompasses the rates of purely chemical steps as well as the rate of pore diffusion and, more crucially, diffusion in the sulfide product layer. Surface area and pore size distribution are very important sorbent properties as they determine the rate of these diffusional processes. Zinc oxide, one of the most promising and widely studied sorbents, has very high equilibrium constant for sulfidation but in its unsupported form suffers from slow kinetics limiting its sulfidation capacity. Iron oxide, on the other hand, has rapid kinetics but its equilibrium constant for sulfidation is not adequate for the degree of H_2S removal required in the molten carbonate fuel cell application.

The other important sorbent properties refer to stability or regenerability in extended use, the operating conditions required for regeneration, and the composition of the regeneration off-gas, which largely determines the choice of a downstream sulfur recovery process. Using zinc oxide as an example again, it is well known that evaporative loss of metallic zinc places an upper limit on the sulfidation temperature. Loss of surface area during regeneration places an upper limit on the temperature or necessitates a more complicated regenerative treatment. The regeneration off-gas including sulfur dioxide, hydrogen sulfide and elemental sulfur requires further treatment for sulfur recovery. When the yield of elemental sulfur

is sufficiently high, sulfur recovery can be simplified with significant overall cost benefits (6).

With several of the thermodynamically favorable H_2S sorbents reported to date, slow rates of reaction and pore diffusion, sintering, and pore plugging limit sorbent capacity and degree of purification under practical conditions. Such is the case with some commercial ZnO sorbents where reported conversions at breakthrough were less than 20 percent.

Recent research has shifted from pure to mixed metal oxides with the goal of improving sorbent performance. For example, zinc ferrite has been found to possess better capacity and regenerability than pure zinc oxide (5). Mixed ZnO-CuO has been studied for its better resistance to surface area loss (8) and various other mixtures including $ZnO-Cr_2O_3$ and $ZnO-Al_2O_3$ have been studied with the objective of increasing the yield of elemental sulfur during regeneration (6). Mixed oxides form various distinct crystalline phases or solid compounds, and should generally possess different thermodynamic properties and reactivity with respect to reduction, sulfidation, and regeneration reactions. This has so far received limited attention.

The preceding discussion emphasizes the variety of properties impacting sorbent performance and points out the need for synthesis of sorbents combining several desirable properties. On-going research at the Jet Propulsion Laboratory aims at developing improved sorbents for desulfurization of hot coal-derived gas streams. Two classes or sorbents have been developed (9,10) both characterized by rapid kinetics of absorption and good sorbent regenerability during operation at 500-700°C. Detailed description of the first class of sorbents, which consist of supported mixed oxides that form eutectic melts coating the pores of high surface area supports at the operating temperatures, can be found in recent reports (9,10). In this paper, we limit our discussion to the second class of sorbents investigated in our work. This consists of unsupported mixed oxides forming highly dispersed solid solutions or solid compounds characterized by small crystallite size, high porosity and relatively high surface areas. The sorbent is a mixture of Cu or Zn oxides with one or both of Al and Fe oxides prepared in a special manner which provides the sorbent in a highly porous form with a range of pore sizes. This prevents fouling of the sorbent during absorption and/or regeneration cycles.

EXPERIMENTAL

a) Sorbent Preparation

Several methods are described in the literature (11-14) for synthesizing highly dispersed mixed oxides. Early attempts to form high surface area metal oxide sorbents by precipitating mixed carbonates from homogenous salt solutions followed by drying and calcining resulted in materials of low surface area, about 5-8m²/g. The bulk sorbents either in single or mixed form were then prepared by a technique that resulted in high pore volume and surface area. Following a general procedure suggested in the literature (14), an aqueous solution of thermally decomposable metal salts in the desired proportion and an organic polyfunctional acid containing at least one hydroxy - and at least one carboxylic function is rapidly dehydrated under vacuum at a temperature of 70°C. An amorphous solid foam forms which is calcined at an elevated temperature above 300°C, usually 500°C to 600°C, to form a mixed oxide phase. The crystallized mixed oxides thus formed are homogenous and highly porous.

This method was used to prepare the bulk sorbens CF ($CuFe_2O_4$) ZF ($ZnFe_2O_4$), CA ($CuAl_2O_4$), CFA ($2CuO\ Fe_2O_3\ Al_2O_3$), and others. All these materials were prepared as dispersed microcrystalline solids with high porosity. To illustrate the porous structure of these solids, scanning electron micrographs (SEM) of copper ferrite ($CuFe_2O_4$), before and after sulfidation, are depicted in Figure 1. The micrographs show very large ($\geq 10\mu m$) as well as submicron size pores. The gross porous structure before and after sulfidation, appears very similar. X-ray diffraction analysis (XRD) using Cu $K\alpha$ source on a Siemens Allis D 500 instrument showed that the mixed oxides $ZnO-Fe_2O_3$ and $CuO-Fe_2O_3$ had the ferrite-spinel structure, $ZnFe_2O_4$ and $CuFe_2O_4$, respectively, while $CuO-Al_2O_3$ formed the aluminate spinel $CuAl_2O_4$. The CFA sorbent had
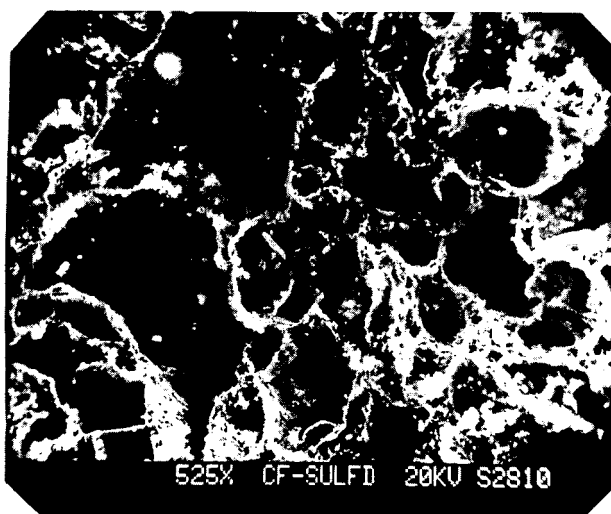
17
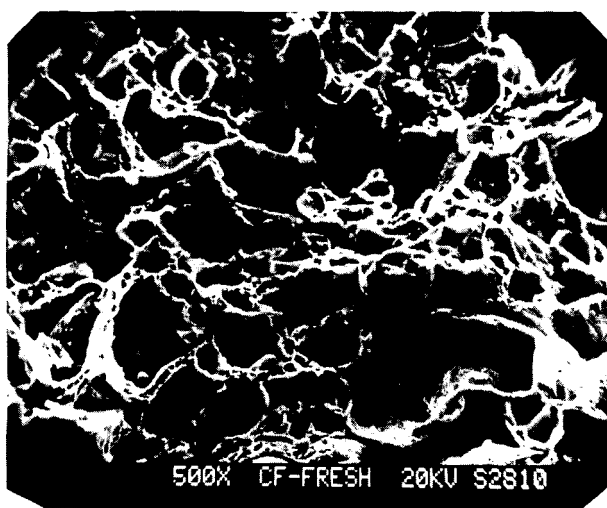
20μm

Figure 1. Scanning Electron Micrographs of Fresh and Sulfided Copper Ferrite.

a surface area of 26 m^2/g and consisted of crystalline CuO, $FeAl_2O_4$, $CuFe_2O_4$, and amorphous Al_2O_3 phases. Low angle XRD analysis of $ZnFe_2O_4$ revealed a microcrystalline structure with average crystallite size of 890Å.

b) Reactor System and Experimental Procedures

The experiments were performed in a quartz microreactor, 1 cm I.D. x 41 cm length, mounted vertically inside an electric furnace and instrumented with a K-type thermocouple moving inside a quartz thermowell (0.3 cm I.D.) concentric to the reactor. The sorbents were loaded in the microreactor as -20+40 mesh particles. The unsupported sorbents were mixed with low surface area zirconia or alumina particles, which served as an inert filler. The use of the inert particles allows to compress the experimental run time by decreasing the bed capacity, while maintaining the same space velocity. Different gases from cylinders passed through purifiers and then throu.'i calibrated flowmeters into a common gas line. The gas mixture then passed through the reactor in the upward or downward direction. The lines leading to the reactor were heated and insulated. Nitrogen bubbling through water maintained at constant temperature in a 3-neck flask assembly was used to introduce known amounts of water vapor into the feed gas stream. Temperatures at various locations in the reactor system were monitored by K-type thermocouples connected to a multi-channel digital readout. The reactor pressure in all cases was slightly above atmospheric.

The experiments consisted of consecutive sulfidation and regeneration runs. In a sulfidation run, the sulfur-free sorbent was exposed to a feed gas containing H_2(15-30%), H_2O(7-25%), H_2S(0.2-1%) and N_2 (balance). The temperature was in the range of 500-700°C and was held fixed for the duration of sulfidation. Sulfided sorbents were regenerated using a nitrogen-air or steam-air mixture at temperatures of 600-750°C. The product gas was passed through ice traps to condense any elemental sulfur formed and was analyzed for H_2S and SO_2 by a gas chromatograph HP-5830A equipped with a flame photometric detector. An absorber loop containing iodine solution, installed in the exit line from the gas-sampling valve, was used for the analysis of the total sulfur gases (H_2S, SO_2) produced during regeneration. The amount of sulfur gases absorbed was determined by titrating the excess iodine with a sodium thiosulfate solution. Elemental sulfur collected in the traps was dissolved in a sodium sulfite solution and analyzed by a standard iodometric titration method.

EXPERIMENTAL RESULTS AND DISCUSSION

The results presented in this section concern the concentration of hydrogen sulfide in the product gas during sorbent sulfidation. In a typical experiment this concentration rises very slowly at first until a certain time after which it rises rapidly to the inlet value. The time of this abrupt change of slope is called the breakthrough time, and the whole concentration vs. time curve is sometimes called a breakthrough curve. In the absence of transport and kinetic limitations the breakthrough curve would be the step function, $y=y^e$ at $t<t^*$, $y=y^o$ at $t>t^*$, where y^e, y^o are the equilibrium and inlet mole fractions of hydrogen sulfide, and t^* is the theoretical breakthrough time, i.e., the time required for complete sulfidation of the sorbent. Finite reaction and diffusion rates, axial dispersion and channeling produce experimental breakthrough curves that are smoothly sloping. The fractional conversion at the actual breakthrough time provides a measure of sorbent utilization efficiency, while the level of H_2S before breakthrough is also an important measure of sorbent performance.

The results below are presented and discussed in terms of the mole fraction of H_2S in the product gas versus the normalized time t/t^* (sorbent conversion).

$ZnFe_2O_4$ Sorbents

Zinc ferrite is one of the most efficient H_2S sorbents. Extensive lab-and/ bench-scale tests with $ZnFe_2O_4$ have been performed at DOE/METC (5). The material used in that work was prepared by United Catalysts, Inc., by the conventional technique of high-temperature (>800°C) heating of mixtures of the pure oxide powders.

The surface area of this zinc ferrite, designated METC-ZF, is ~5 m^2/g and its pore volume ~0.3 cc/g.

The performance of porous zinc ferrite (ZF) synthesized in this work with high surface area and large pore size was tested in the quartz microreactor and compared to the METC-ZF sorbent at the same operating conditions. Both sorbents were used as -20 +40 mesh particles mixed with low surface area alumina particles.

At 538°C (1000°F) sulfidation temperature, the stable pre-breakthrough conversion of ZF sorbent was >0.75, while that of METC-ZF was 0.35-0.40. Both sorbents were capable of removing H_2S from ~2500 ppm to less than 1 ppm level with a feed gas containing 20 vol% H_2 and 6.5 vol% H_2O. The higher conversion of ZF must be attributed to its different physical properties. SEM micrographs of the sulfided ZF and METC-ZF sorbents show that the pore structure of the two is very different, with METC-ZF lacking the large pores of ZF. The gross morphological features of the latter were the same before and after sulfidation which is indicative of high accessibility to H_2S and limited or no pore mouth blocking.

Similarly high conversion (>0.75) was obtained with ZF at all temperatures 538-650°C and with a sulfidation gas containing 15-20% H_2, 7-25% H_2O, 0.21% H_2S, balance N_2 by volume. Figure 2 shows H_2S breakthrough curves with the ZF sorbent at 600°C sulfidation/regeneration. Very sharp elution profiles, indicative of fast reaction and diffusion rates, are observed in this figure. A limitation of all zinc ferrite sorbents, however, is that at sulfidation temperatures >600°C, zinc metal loss takes place (via reduction of ZnO). In deposits collected from the cooler part of the reactor tube, zinc has been identified by Atomic Absorption (AA) analysis. Loss of zinc could not be prevented even with high H_2O and low H_2 concentrations in the feed gas. At 600°C, at the conditions of Figure 2, the rate of evaporative Zn loss was 8 and 26 weight percent per 1000 hours at space velocities of 2100 and 6900 hr^{-1}, respectively. The corresponding content of Zn vapor in the gas phase was ~1.3 ppm, close to the equilibrium value for the ZnO reduction. Therefore, under typical sulfidation conditions, ZnO reduction will rapidly reach equilibrium. A slow decline in conversion, observed between the first and fourth cycles of sulfidation / regeneration in Figure 2, may be attributed to zinc metal loss.

$CuFe_2O_4$ Sorbents

Bulk porous copper ferrite was investigated with the hope of avoiding two difficulties that arise with zinc-based sorbents, namely the loss of metallic zinc at temperatures >600°C and the high (>700°C) regeneration temperatures required for decomposition of zinc sulfate.

Copper oxide by itself is known to reduce to the metal under the conditions of temperature and feed composition employed. Metallic copper, in turn, is sulfided according to the reaction

$$2 Cu + H_2S = Cu_2S + H_2 \qquad\qquad 1)$$

For a feed gas with 20 mol% H_2, the equilibrium H_2S level is 44.5 ppm at 538°C and 89 ppm at 650°C. Although these levels are quite high it was thought that the equilibrium with copper ferrite could be lower because of its different crystal structure.

The copper ferrite (CF) sorbent was prepared by the technique described earlier. H_2S breakthrough curves in several sulfidation cycles at 538°C showed that the pre-breakthrough sorbent conversion was high (~0.80) and stable (over 6 cycles), Figure 3. In all cases the pre-breakthrough H_2S level was below the value of 44.5 ppm calculated for the equilibrium of reaction 1. In fact, the H_2S level remained below 2 ppm until 0.5 conversion and then gradually increased to <10 ppm when the conversion reached 0.78.

In two sulfidation/regeneration cycles carried out at 600°C, sub-equilibrium H_2S levels were again measured till breakthrough, which occurred at ~0.80 sorbent conversion. At 650°C sulfidation temperature, however, while a similarly high and stable sorbent conversion took place, the pre-breakthrough H_2S level at 0.80
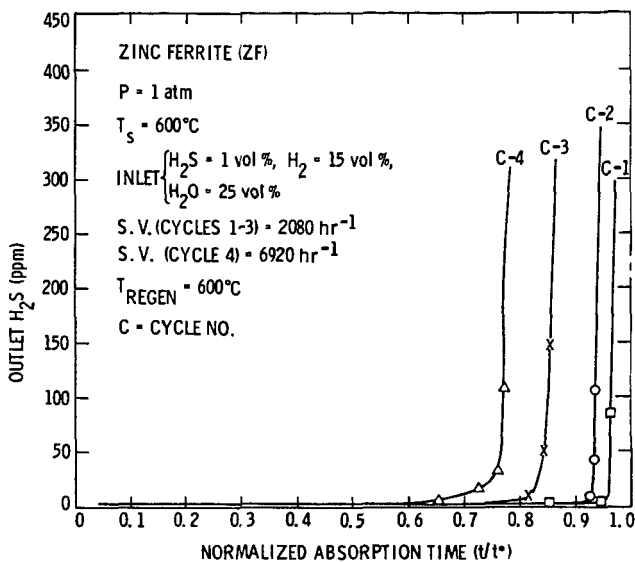
Figure 2. Breakthrough Curves in Successive Sulfidation Cycles of ZF Sorbent (ZnFe$_2$O$_4$) at 600°C.
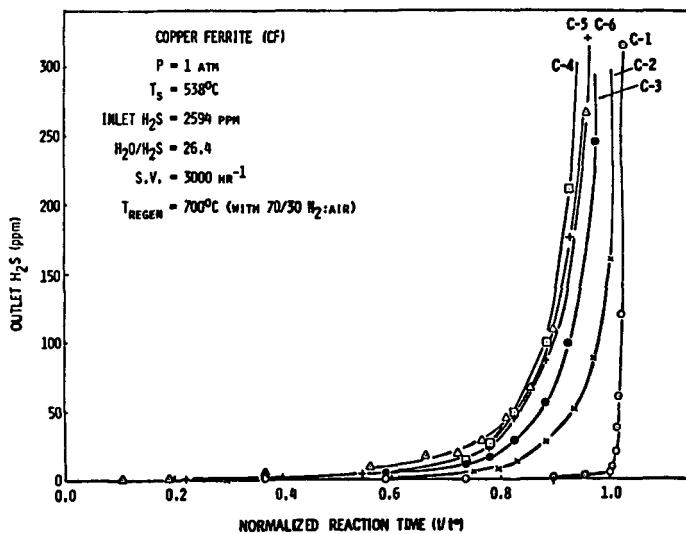

Figure 3. Breakthrough Curves in Successive Sulfidation Cycles of Copper Ferrite.

21

sorbent conversion was 85-90 ppm, close to the equilibrium for reaction 1. Up to 0.20 sorbent conversion, sub-equilibrium H_2S levels were measured, perhaps indicative of chemisorption effects.

Characterization of fresh, sulfided and regenerated samples of CF-sorbents was performed by SEM and XRD analyses. As shown in Figure 1, the gross porous structure of the sorbent before and after sulfidation appeared very similar in SEM (as in the case of zinc ferrite). XRD analysis of the sorbent sulfided at 538°C identified the mixed sulfide compound $CuFeS_2$ (chalcopyrite) along with $Fe_{1-x}S$, Fe_3O_4, unconverted $CuFe_2O_4$ and some amorphous material. In the sample sulfided at 650°C, the phase $CuFeS_2$ was absent, while there was indication of a poorly crystalline Cu_2S phase.

These results suggest that at 538-600°C sulfidation temperatures, CuO is stabilized towards reduction in the ferrite-spinel. The presence of $CuFeS_2$ in the sample sulfided at 538°C along with the observed pre-breakthrough H_2S levels correspond to the sulfidation reaction:

$$CuFeO_2 + H_2S = CuFeS_2 + H_2O \qquad\qquad 2)$$
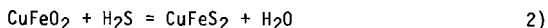
The intermediate compound $CuFeO_2$ indicates a step-wise reduction of $CuFe_2O_4$. The equilibrium H_2S levels for reaction 2 were calculated by using thermodynamic values for the compound $Cu_2O \cdot Fe_2O_3$ (15). These are in agreement with the experimental H_2S levels, and much below the values for metallic copper sulfidation, reaction 1. At the higher sulfidation temperature of 650°C, reduction to metallic copper is very fast, and controls the pre-breakthrough levels of H_2S after an initial sorbent conversion of 0.15-0.20 at sub-equilibrium H_2S exit levels.

$CuAl_2O_4$ Sorbents

The stability of _porous_ copper aluminate (CA) of the spinel crystal structure was investigated in a series of sulfidation/regeneration tests at 538-650°C. The results were very similar to copper ferrite. Thus, at 538-600°C, the H_2S pre-breakthrough levels were below the equilibrium for reaction 1, and high (>0.75, based on Cu_2S) and stable (over 5-6 cycles) sorbent conversion was observed. Copper in the +2 or +1 oxidation state was apparently stabilized in the alumina matrix and controlled the exit level of H_2S till breakthrough. At 650°C, the H_2S exit levels after ~0.20 sorbent conversion corresponded to sulfidation of metallic copper. With copper aluminate, however, structural changes that occurred at 650°C were reversed when the temperature was lowered to 538°C. This was not true with copper ferrite sorbents.

Mixed Cu-Fe-Al-O (CFA) Sorbents

In view of the enhanced stabilization of copper oxide in copper aluminate sorbents, a mixed copper ferrite-copper aluminate material, CFA, with $2CuO:Fe_2O_3:Al_2O_3$ molar ratio was prepared in porous bulk form (with 26 m^2/g surface area) as a potential sorbent for higher (>600°C) temperature H_2S removal. Under similar operating conditions, this sorbent was superior to either copper ferrite or copper aluminate in regard to pre-breakthrough H_2S levels, which were lower than the equilibrium of reaction 1 at all temperatures, 538-650°C. An example is shown in Figure 4 for 650°C sulfidation temperature with a gas containing 20 vol% H_2, 25 vol% H_2O, 1 vol% H_2S, balance N_2. The performance was stable over five cycles of sulfidation/regeneration with a high pre-breakthrough sorbent conversion of 0.75. In addition, remarkably high H_2S removal efficiency was achieved by this sorbent, with pre-breakthrough H_2S levels in the range of 0-10 ppm up to 0.50 sorbent conversion and less than 35-40 ppm at breakthrough. These levels are well below the corresponding equilibrium (89 ppm) for metallic copper sulfidation at 650°C.

XRD analysis of the fresh and sulfided (after cycle 4) CFA sorbent was performed to identify stable crystalline phases that may be responsible for the improved performance of this sorbent. The fresh CFA consisted of $CuFe_2O_4$, CuO, $FeAl_2O_4$ and some amorphous material (probably Al_2O_3), with $FeAl_2O_4$ (iron aluminate) in highly-
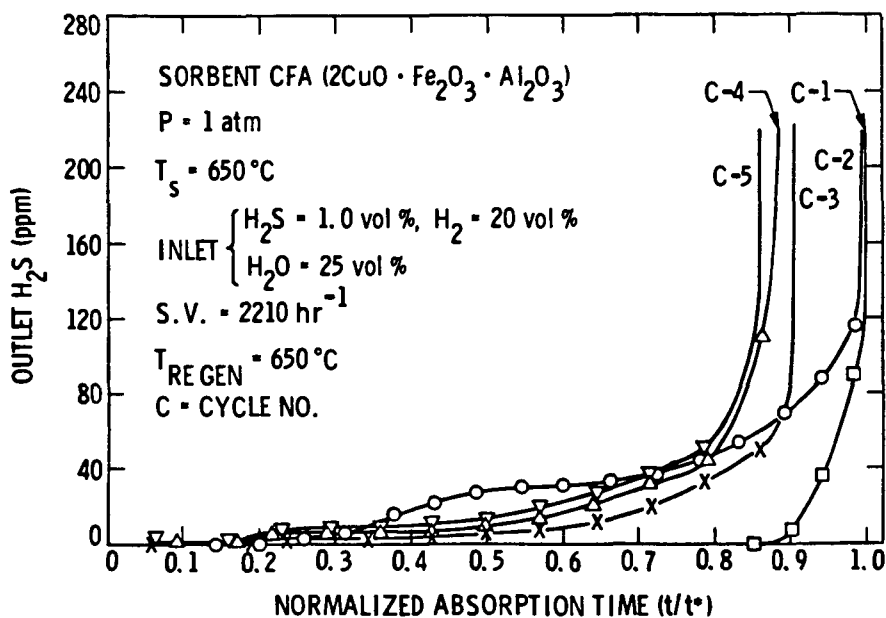
22

Figure 4. Breakthrough Curves in Successive Sulfidation Cycles of Sorbent CFA at 650°C.

microcrystalline form. The sulfided sample contained CuS, FeS and $CuFe_2S_3$ along with amorphous (to XRD) alumina. These results are very important, indicative of stabilization of both Cu^{2+} and Fe^{2+} in the sorbent matrix and associated improved absorption equilibria.

Additional testing of the stability and performance of the CFA sorbent was conducted with a coal gasifier gas simulant containing 17% H_2, 12% CO, 10%CO_2, 24% H_2O, 0.5-1% H_2S, balance N_2 by volume. Similar results to those shown in Figure 4 were obtained. Different conditions used in regeneration did not affect the performance of the sorbent. Other parametric studies with CFA included testing at a lower ($\sim$1000 hr^{-1}) space velocity, and different H_2S concentrations in the sulfidation gas. No significant effect on the sorbent performance was observed. A total of fourteen cycles of sulfidation/regeneration were run with CFA at 650°C. The surface area of the sulfided sorbent at the end of the fourteenth cycle was $\sim$8m^2/g, still a moderately high value, especially after the frequent and extended use of CFA at 700°C (during regeneration).

Another series of tests with a different batch of CFA sorbent were conducted at the higher temperature of 830°C with a reactant mixture containing 30 mol% H_2, 17 mol% H_2O, 1 mol% H_2S, balance N_2, simulating the Texaco gasifier-fuel gas. In three cycles, breakthrough of H_2S took place at complete (100%) sorbent conversion, while the pre-breakthrough H_2S level was zero up to $\sim$0.20 sorbent conversion and 250-270 ppm until final breakthrough. These results indicate that the CFA sorbent formulation has potential for higher temperature (up to $\sim$800°C) applications, such as molten carbonate fuel cells and combined-cycle power plants employing gas turbines.

CONCLUSIONS

Sorbents prepared in this work with large pore size (0.5-10μm) and relatively high surface area (10-25m^2/g) have been found to exhibit improved performance for hot gas cleanup applications over conventional sintered materials. This is displayed by sharp H_2S elution profiles indicating rapid reaction and diffusion rates, and minimal pore plugging, which all result in high absorption capacity, stability and good regenerability of sorbents.

Novel mixed oxide porous sorbents have been synthesized in this work which exhibit improved thermodynamic properties in addition to their physical attributes. For example, the mixed Cu-Fe-Al-O (CFA) sorbent shows much higher H_2S removal efficiency than each of the pure constituents alone. ZnO-containing sorbents have been found to lose zinc during sulfidation (via reduction of ZnO) at temperatures $\geq$600°C. For higher temperature applications the Cu-based sorbents appear to be more attractive. In particular, the CFA sorbent has shown stable and high performance over a variety of sulfidation conditions at 650°C. The H_2S removal efficiency of this sorbent and supporting XRD analysis data correlate well with complex reaction intermediates retaining copper at a higher oxidation state (+2 or +1) with associated better sulfidation equilibria.

Additional, more detailed testing and characterization of these types of sorbents are planned in future work to elucidate the mechanism of high-temperature solid-phase transformations and reactions responsible for the observed sorbent performance and stability.

REFERENCES

1. "Chemistry of Hot Gas Cleanup in Coal Gasification and Combustion," MERC Hot Gas Cleanup Task Force. MERC/SP-78/2, February 1978.

2. "Studies Involving High Temperature Desulfurization/Regeneration Reactions of Metal Oxides for the Fuel Cell Program," Final Report to DOE, Contract No. 31-109- 38-5804, by Giner, Inc., Waltham Massachusetts, February 1981.

3. Westmoreland, P.R., Gibson, J.B. and Harrison, D.P., Environ. Sci. Technol. 11, 488 (1977).

REFERENCES (cont.)

4. Westmoreland, P.R. and Harrison, D.P., Environ. Sci. Technol. $\underline{10}$, 659 (1976).

5. Grindley, T. and Steinfeld, G., "Development and Testing of Regenerable Hot Coal Gas Desulfurization Sorbents," METC, DOE/MC/16545-1125, October 1981.

6. Anderson, G.L. and Garrigan, P.C., "Gas Processing Technology for Integrating Coal Gasifiers with Molten Carbonate Fuel Cells." Paper presented at the Electrochemical Society Meeting, Montreal, Quebec, Canada, May 10-12, 1982.

7. Stegen, G.E., "Development of a Solid Absorption Process for Removal of Sulfur from Fuel Gas," Final Report DE-AC21-79ET11028 Battelle, Pacific Northwest Laboratories, March 1982.

8. Jalan, V., "Studies Involving High Temperature Desulfurization/Regeneration Reactions of Metal Oxides for Fuel Cell Development," Final Report, DOE/MC/16021-1486, October 1983.

9. Flytzani-Stephanopoulos, M., Gavalas, G.R. and Tamhankar, S.S., "Novel Sorbents for High-Temperature Regenerative H_2S Removal," Topical Report to DOE, DOE/MC/20417-3, Jet Propulsion Laboratory, July 1984.

10. Flytzani-Stephanopoulos, M., Gavalas, G.R., Tamhankar, S.S. and Sharma, P.K., "Novel Sorbents for High-Temperature Regenerative H_2S Removal," Quarterly Report to DOE, DOE/MC/20417-4, Jet Propulsion Laboratory, December 1984.

11. Longo, J.M., Horowitz, H.S. and Clavenna, L.R., "A Low Temperature Route to Complex Oxides," Advances in Chemistry Series No. 186, p. 139, American Chemical Society, Washington, D.C., 1980.

12. Singh, B.N., Banerjee, R.K. and Arora, B.R., J. Thermal Analysis $\underline{18}$, 5 (1980).

13. Kolta, G.A., El-Tawil, S.Z., Ibrahim, A.A. and Felix, N.S., Thermochim. Acta $\underline{36}$, 359 (1980).

14. Marcilly, C., Courty, P. and Delmon, B., J. Am. Cer. Soc. $\underline{53}$, No.1, 56 (1970).

15. Barrin, I. and Knacke, O., "Thermochemical Properties of Inorganic Substances," Springer Verlag, 1973.

ACKNOWLEDGEMENT

SOLID SUPPORTED MOLTEN SALT HOT GAS CLEANUP
FOR CARBONATE FUEL CELL POWER PLANTS.

S. E. Lyke

Battelle, Pacific Northwest Laboratories
P.O. Box 999, Richland, Washington   99352.

INTRODUCTION

A regenerable sorbent for removing sulfur from hot fuel gas was developed at Battelle, Pacific Northwest Laboratories by supporting molten carbonates in porous ceramic pellets. Recent development work has shown the sorbent to be a promising candidate to meet the stringent cleanup requirements for coal gasification molten carbonate fuel cell power plants while allowing elemental sulfur recovery and maintaining high power production efficiency. Solid supported molten salt (SSMS) differs from other methods of hot gas cleanup in that the reaction products dissolve in the molten carbonate matrix resulting in a theoretically unlimited extent of contaminant removal. If only a solid reaction product is formed, removal cannot proceed below the level at which the contaminant in the cleaned gas is in equilibrium with that solid. At the clean end of an SSMS absorber the concentrations of reaction product sulfides and chlorides in the sorbent approach zero and the concentration of contaminants in the cleaned gas can also approach zero. The approach is limited only by the size of the bed, mass transfer efficiency and the degree of regeneration.

This paper begins by presenting the background and the overall approach and scope of the recent developmental effort. More detail is then given on equilibrium measurements, mass transfer performance and modeling of the H_2S absorption and regeneration steps. The paper closes with a discussion of process flowsheet development and preliminary economics.

BACKGROUND

The reversible reaction of H_2S with molten carbonates has been under study at Battelle Northwest since 1974[1].

$$MCO_3 \; (\ell) + H_2S(g) = MS(\ell) + CO_2(g) + H_2O(g), \hspace{3cm} 1)$$
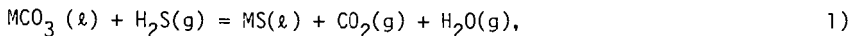
Where "M" represents Li_2, Na_2, K_2 or Ca.

A process was first developed based on continuous, countercurrent gas liquid contacting [2]. Absorption of H_2S and particulates, deentrainment and regeneration of the carbonate were demonstrated in a process development unit (PDU) operating with gas from an air blown, fixed—bed coal gasifier. A venturi scrubber provided the first sulfur absorption stage and also circulated the molten salt between bubble-cap absorption and stripping columns. In the latter, steam and CO_2 were used to recover H_2S. Use of the hot, corrosive molten salt in a countercurrent contactor led to severe equipment problems, and operation was never sustained for more than a few hours at a time.

The SSMS concept was developed as a practical means for handling the corrosive molten carbonates (3). Several ceramics were investigated as potential supports. Lithium aluminate was chosen for chemical stability and for ease of fabrication of strong, porous pellets. Use in a cyclically-operated fixed-bed allowed the advantages of a gas-liquid equilibrium system to be exploited through breakthrough behavior rather than countercurrent contacting. Operation was relatively trouble-free with bench-scale absorption cycles of up to 7 hours duration. Laboratory and bench-scale testing demonstrated up to 99.5% sulfur removal (adequate for the combined cycle application under study) from a feed gas containing 1% H_2S and produced regeneration gases containing up to 50% H_2S on a dry basis. The tests showed that COS was generated during absorption breakthrough and regeneration in amounts consistent with equilibrium by the gas phase reaction:

$$H_2S(g) + CO_2(g) = H_2O(g) + COS(g), \hspace{3cm} 2)$$

which could not be distinguished from the direct regeneration reaction:

$$2CO_2(g) + MS(\ell) = MCO_3(\ell) + COS(g), \hspace{3cm} 3)$$

The same study identified redox reactions involving H_2 and CO which may involve several oxidation states of sulfur such as poly sulfides or sulfites but can be characterized by:

$$nCO_2(g) + (4-n) H_2O(g) + MS(\ell) = MSO_4(\ell) + nCO(g) + (4-n) H_2(g), \hspace{1cm} 4)$$
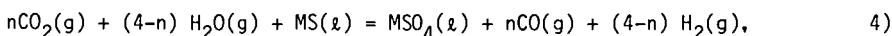
Where n = 0, 1, 2, 3 or 4. It was found that H_2 or CO had to be included in the regeneration feed gas to avoid leaving traces of oxidized sulfur in the bed that would be reduced during the subsequent absorption contaminating the product gas before breakthrough.


DEVELOPMENT FOR PRESSURIZED FUEL CELLS

The molten carbonate fuel cell application addressed by the recent study requires: 1) operation at elevated pressure which has a detrimental effect on the absorption equilibrium, Equation 1; 2) design for removal to less than 1 ppm through multiple cycles; 3) removal of COS and HCl as well as H_2S; and 4) design for an air-blown gasifier making the H_2 and CO needed to avoid oxidation, Equation 4, available only in streams diluted with nitrogen.

Laboratory equilibrium experiments to optimize salt composition, bench scale experiments to establish mass transfer performance and modeling efforts were directed primarily toward the first two requirements. Results will be discussed in more detail later in the paper.

The third requirement was addressed by including COS and HCl in feed gases and by a few experiments directed solely at HCl behavior. The method used for effluent COS (4) analysis had a detection limit of 1 to 10 ppm depending upon experimental conditions. Removal from 1000 to less than 10 ppm was demonstrated in most cases but in several cases COS was detected in absorber effluent at more than 1 ppm when H_2S levels were lower. Because of the high detection limits, results are not conclusive but COS removal may be slower than H_2S under some conditions.

Hydrogen chloride removal occurs by chloride formation:

$$2HCl(g) + MCO_3(\ell) = 2MCl(\ell) + H_2O(g) + CO_2(g), \qquad\qquad 5)$$
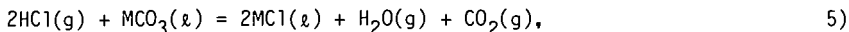
which has an equilibrium shifted well to the right under hot cleanup conditions. Equilibrium tests confirmed the thermodynamics and removal from 200 to less than 1 ppm was demonstrated in several tests. Because of the high equilibrium conversion by Equation 5, no regeneration tests during representative sulfur cycles achieved high enough HCl concentrations for practicle chloride removal. A separate method for HCl regeneration appears necessary. The behaviors of chlorides and COS in the SSMS system both require additional study.

The fourth fuel cell application requirement was addressed by using nitrogen diluted feed gas such as would be available in an air-blown gasification plant. Thermodynamic calculations (4) based on published data (5, 6, 7) indicated 5 to 10% CO + H_2 is required to avoid oxidation (Equation 4) during regeneration. About 10% was used throughout and found to be adequate. Because the exact level used does affect process efficiency, a direct study of Equation 4 would eventually be necessary for commercial design.

EQUILIBRIUM MEASUREMENTS

The sulfide/carbonate equilibrium was measured in various mixtures of molten Li, Na, K and Ca carbonates to select an optimum composition for use in the MCFC application.

APPARATUS AND METHODS: A pressure-capable experimental apparatus was designed and constructed for use in both equilibrium and subsequent bench-scale mass transfer tests. Gases (metered into the system under cylinder pressure) and water (pumped into a steam generator by a high pressure feed pump) were used to generate simulated coal gas of the desired composition. Accuracy of metering the fuel gas, contaminant and steam streams is estimated to have been $\pm 5\%$ or less of each component. A section of Incoloy 800H pipe served as a pressure vessel (rated for 250 psig at 1600°F) and was heated by ceramic fiber heaters. An alumina thimble suspended inside the pipe contained free liquid or solid supported molten carbonate. Smaller tubes sealed through the top flange provided a thermowell and access to the thimble through its loose fitting lid. A small nitrogen purge into the pipe assured that system gases remained inside the alumina. Heat traced, teflon lined tubes conducted effluent gas to stainless steel scrubbers where circulating sodium hydroxide solutions condensed steam and absorbed contaminants for analysis. The solutions were monitored for sulfide by specific ion potentiometry giving an effective detection limit of 0.5 ppmv for H_2S. A letdown valve after the scrubbers provided pressure control. Gas samples were taken downstream of the valve and analyzed by gas chromatography. Using the known composition of the fuel gas as a standard, changes in the CO/H_2 ratio and the CO + H_2 balance were measured. Because of drift in the CO response factor the CO/H_2 ratios and CO + H_2 balance are only considered accurate to $\pm 10\%$.

Equilibrium measurements were performed by melting the desired salt composition in the thimble, loading it with H_2S, purging simulated fuel gas

through the molten liquid and measuring the effluent gas composition as a function of the sulfide content determined by material balance. Purge gas without H_2S or with slightly more than the expected effluent level was used to check approach to equilibrium from below or above. Equilibrium constants were calculated assuming ideal gas and liquid solutions.

RESULTS: Screening experiments for sulfide capacity were completed with four different salt mixtures (Table 1) at atmospheric pressure. Salt mix #1 is the composition used by Moore et. al. (8) and Stegen (3) as unsupported and supported sorbents respectively at atmospheric pressure. Sodium in the mixed carbonate sorbent represents a possible source of contamination to a Li/K-eutectic fuel cell. The elimination of sodium was tested with salt mix #2. Higher calcium and lower lithium contents were tested with salt mix #3 and salt mix #4, respectively. Adjusting to 750°C and averaging gives K_1 = 1.6, 1.7, 2.0 and 1.8 all $\pm$ 0.2 atm for salt mix #1, #2, #3 and #4, respectively. It is apparent that the sulfide/carbonate equilibrium is relatively insensitive to the cation mix.

TABLE 1. Carbonate Mixtures Screened for Sulfide Capacity, mole %

Salt Mix	Li_2CO_3	Na_2CO_3	K_2CO_3	$CaCO_3$
1	37.5	23.4	19.3	19.8
2	48.9	0	25.2	25.8
3	35.1	0	33.8	31.1
4	23.3	0	53.9	22.9

Figure 1 shows that calcium content can be used to correlate the results of this work with the calcium-free results of Moore. Moore's data with calcium showed a low temperature dependence relative to pure component thermodynamics. Although pure component solid thermodynamic data (5) would indicate a stronger effect of calcium, the high estimated melting point for CaS (2725K, 9) relative to $CaCO_3$ (1500K, 10) apparently leads to lower relative stability in the liquid phase. Projecting data from (5) into the subcooled liquid range, assuming entropies of fusion at reported (5, 9, 10) melting points for Li_2S, $CaCO_3$ and CaS of 5, 6 and 6 cal/degree/mole and assuming constant liquid heat capacities of 22, 33 and 16 cal/degree/mole respectively, allows the calculation of pure component equilibrium constants for Reaction 1. These are compared with the full range of experimental data from this work in Figure 2. The lower constants found for mixed carbonates probably reflect the stability of the inter-alkali carbonate eutectics. Although Figure 2 would indicate a lower activity for calcium than potassium, the correlation of Figure 1 apparently shows that calcium sulfide is relatively more stable in the carbonate matrix than the alkali metal sulfides. Precipitation of solid calcium sulfide cannot be eliminated as a possibility but was judged unlikely at the low sulfur concentrations (less than 3 mole%) used in the screening studies.

BENCH SCALE MASS TRANSFER EXPERIMENTS

Mass transfer data on the absorption/regeneration cycle were obtained by experiments with packed beds of solid supported sorbent. Methods and an overview of results are presented here. Results are discussed in more detail in connection with the mass transfer model.

29

METHODS: Porous, lithium aluminate ceramic pellets (1.4 to 2.8 mm size range) were fabricated by methods developed in previous work (3). The pellets were loaded close to saturation with molten salt (0.36 to 0.42g of salt per bulk cc of sorbent). In the apparatus already described a ceramic thimble of 4.6 or 9.1 cm^2 cross section served as an absorber. The smaller thimble was filled with a 25 cm bed of pellets. The larger thimble was operated at both 25 and 50 cm depths. Sorbent was supported on dense alumina beads (1/16 in. diameter) and, at the 50 cm depth, topped with a layer of the same beads to provide gas distribution.

For each absorption experiment the bed was brought to temperature and pressure under a nitrogen atmosphere, a simulated coal gas flow started, contaminant gas added and effluent concentration monitored as a function of time by methods described earlier under "Equilibrium Measurements." For regenerations, temperature was adjusted (generally 100°C cooler) and a CO_2-H_2O rich fuel gas fed in the opposite direction.

RESULTS: Sorbents with two different salt compositions were tested in the smaller absorber. The first, $Li_{0.86}K_{0.54}Ca_{.3}CO_3$, selected from the equilibrium results, demonstrated poor mass transfer (broad breakthrough curves). A low-calcium composition, $Li_{1.1}K_{0.7}Ca_{0.1}CO_3$, showed better mass transfer performance and was used for all tests in the larger absorber. It was postulated that the high-calcium salt precipitated solid calcium sulfide which interfered with both absorption and regeneration.

After thorough regeneration, both salt compositions removed H_2S to less than 1 ppm with the length of time before breakthrough ("breakthrough time") limited by equilibrium and mass transfer effects. Incomplete regeneration further shortened breakthrough time and/or added a background level of H_2S before breakthrough. Projecting breakthrough curves to one half the inlet H_2S^* concentration checked with "equilibrium times" for saturation of the bed with feed gas calculated from results of the equilibrium measurements. Similar treatmnet of low-calcium results allowed the estimation of thermodynamic constants, Table 2, for the carbonate/sulfide equilibrium which are consistent with Figure 1 and with mass transfer results over the range studied.

TABLE 2. Thermodynamic Constants for Reaction 1 (900 to 1100°K, 1 to 15 atm)

Salt	$Li_{.86}K_{.54}Ca_{0.3}CO_3$	$Li_{1.1}K_{0.7}Ca_{0.1}CO_3$
Heat of Reaction	26K cal/mole	27K cal/mole
Entropy of Reaction	26.8 cal/mole-K	26.4 cal/mole-K

Varying space velocity and gas composition changed the breakthrough and equilibrium times but the general shape of the breakthrough curves remained the same. A total of 16 absorption and regeneration experiments were completed with the same half or full load of sorbent in the larger absorber. Space velocities from 300 to 2300 per hour, absorption temperatures of 750 and 800°C, pressures of 100 and 180 psig and several levels of steam-carbon

---

* actually, 1/2 inlet H_2S + COS minus equilibrium COS for that concentration.

dioxide back pressure were tested. A complete presentation and discussion of laboratory and bench scale results obtained in this study has been reported elsewhere (4).

MASS TRANSFER MODEL

Having shown the significant effect of mass transfer resistance on breakthrough time for SSMS cleanup under the desired conditions, a quantitative treatment was developed as a basis for design and optimization. It was found that simple two-film mass transfer theory used with the equilibrium expressions presented earlier gave a good representation of both absorption and regeneration behavior. The mass transfer equation:

$$N = k_g a(y-y_i) = k_p a(x_i-x), \qquad 6)$$

must be solved in an unsteady state material balance framework:

$$\varepsilon dy/dt + \rho_b dx/dt + Gdy/dh = 0 \qquad 7)$$

In these expressions: N = interphase molar flux per unit volume, k_g and k_p = gas and pellet mass transfer coefficients, a = surface area per unit volume, y and x = gas and liquid mole fractions with the subscript "i" representing interface concentrations (assumed at equilibrium), ε = void fraction, t = time, ρ_b = molar density of liquid (salt) in the bulk pellets, G = superficial molar velocity of gas and h = distance through the bed.

Rigorous analytical solutions of Equation 7 are possible (11) but restricted to linear equilibrium and simple boundary conditions. For the non-linear equilibrium that results from Equation 1 and the arbitrary concentration (x) profile from a preceding absorption or regeneration, a model was developed using finite elements of time and distance (4). Preliminary calculations showed that the ε dy/dt term was relatively small and that particle phase transfer should control. The void volume term was eliminated from Equation 7 and although $k_g a$ was retained in Equation 6 it was assigned an arbitrarily high value so that the values of the combined term "$k_p a$" used to fit the data were in effect overall particle-phase mass transfer coefficients.

Figures 3 and 4 show calculated and typical experimental results for a low-calcium absorption and regeneration respectively. Dead volume in the experimental system caused a delay and reduction of the regeneration peak. The data are plotted on an adjusted time scale to show that the regeneration decay slope is matched by the model. A value of 2 X 10^{-5} g-moles/cm^3/sec fitted the low-calcium absorption data at 750°C and was adjusted for a linear decrease in diffusivity with absolute temperature to fit the regeneration data at 650°C. The model does not reflect the pre-breakthrough background H$_2$S during absorptions or a break in decay slope observed during extended regenerations. Both phenomena were highly temperature sensitive and may be the effect of a trace side reaction such as oxidation (Equation 4).

Slow mass transfer in the SSMS pellets studied probably results from a low surface to volume ratio. Loading more porous pellets to a lower degree of saturation with molten salt could lead to a significant improvement.

31

PROCESS DESIGN

Cyclic regeneration for sulfur recovery and the need to include contaminant-free reducing gas in the regeneration feed to avoid oxidation of sulfur to sulfate suggest several flowsheet options. The source of regeneration gas, choice of sulfur recovery process, disposition of the tail gas from sulfur recovery, operating temperature and pressure and the use of temperature and/or pressure cycling for regeneration all must be determined. This section reviews flowsheet development and preliminary estimates of efficiency and economics with reference to a study performed by Stone and Webster Engineering Corporation (SWEC) and suggests additional options outside the scope of that study.

FLOWSHEET DEVELOPMENT: Seven flowsheet options were evaluated by SWEC. Six used temperature cycling to effect regeneration while the seventh used only increased CO_2 and steam content. A blend of anode feed and exhaust gas made up the regeneration feed. The reader is referred to our final report (4) for a complete description of the options. Because experimental data were obtained for essentially isothermal operation during absorption and regeneration, SWEC added separate heating and cooling cycles requiring two beds in addition to those in the absorption or regeneration positions. It is likely that the cooling and heating periods can be incorporated into the regeneration cycle eliminating the extra beds.

SWEC used commercially available sulfur recovery technology which dilutes the sulfur-bearing regeneration product stream with the air required to oxidize H_2S to elemental sulfur. As a result, the energy value of the CO, H_2 and CH_4 in that stream could only be recovered by incineration to raise steam. Use of advanced sulfur recovery technology (12) that removes and recovers CO_2 and sulfur without adding air could allow recycle of sulfur recovery tail gas to the MCFC which would recover the energy value at higher efficiency.

The difficulties involved in heating and cooling large beds of sorbent could be avoided by using a pressure cycle to obtain the necessary driving force for regeneration. After absorption at the fuel cell feed pressure regeneration could be performed with CO_2 (from a CO_2 recovery unit) and steam, both of which could easily be supplied at high pressure. Adding a relatively small amount of cooled and compressed fuel cell feed gas would supply the necessary CO and H_2. Stone and Webster's flowsheet used a swing from 4.4% CO_2 and 14.4% steam to 32.9% CO_2 and 27.3% steam plus a 126°F temperature swing to effect regeneration while suffering a pressure reduction from 150 to 110 psia. Increasing regeneration gas steam and CO_2 contents to about 39% each and pressure to 215 psia would more than compensate for the loss of the equilibrium advantage from the temperature swing. This option could reduce capital cost by eliminating the inter-bed coolers as well as reducing the number of beds. It could also increase process efficiency by eliminating the dilution and thermal losses associated with the temperature cycle.

EFFICIENCY: The primary reason for considering hot gas cleanup is increased power generation efficiency. The net power production efficiency calcualted by SWEC for an integrated coal gasification/molten carbonate fuel cell power plant with SSMS hot gas cleanup was 45.6% or 7478 Btu/KwH (4). This figure compares well with conventional technology and with 7300 to 7700 Btu/kWh

calculated by Westinghouse (13) for air blown gasification with other developmental hot gas cleanup systems. Further improvement is likely upon optimization of the coal gasification-SSMS-MCFC system.

CAPITAL AND OPERATING COSTS: Capital and operating costs were calculated by SWEC for an integrated coal gasification/MCFC power plant with SSMS hot gas cleanup (4). The commercial plant burning 1000 tons/day of coal and producing 135.9 MW net power had an estimated investment of 216 million dollars. Operating costs were estimated for the power recovery, absorption/ regeneration, sulfur recovery and incineration sections at 11.8 million dollars per year or about one cent per kilowatt-hour.

    The overall investment figure was developed for comparison with other cost estimates. The Westinghouse hot gas cleanup study (13) reported total costs based on other developmental cleanup systems representing 169 to 188 million dollars when adjusted to the same time and scale. SWEC performed detailed cost analysis only for sections of the plant directly affected by the SSMS system. A more complete process optimization/cost study is in progress. The most significant result of the SWEC study is that the absorption/regeneration section accounts for 34% of the power plant cost. With process and/or sorbent optimization, a reduction in cost of the SSMS system by 50% appears possible which would make the estimated cost of coal gasification/MCFC power plants using SSMS cleanup competitive with the published estimates for other hot gas cleanup systems.

REFERENCES

(1) Moore, R. H., C. H. Allen, G. F. Schiefelbein and R. J. Maness. 1974. "A Process for Cleaning and Removal of Sulfur Compounds from Low Btu Gases." Interim Report October 1972 - August 1974, GPO Cat. No. I:63, 10:100/Int. 1.

(2) Moore, R. H. et al. 1979. Process for Cleaning and Removal of Sulfur Compounds from Low Btu Gas. PNL-2851 PT 1, Pacific Northwest Laboratory, Richland, Washington.

(3) Stegen, G. E. 1982. Development of a Solid Absorption Process for Removal of Sulfur from Fuel Gas. DOE/ET/11028-9, prepared for the U.S. Department of Energy under Contract DE-AC21-79ET11028 by Battelle, Pacific Northwest Laboratories, Richland, Washington.

(4) Lyke, S. E., L. J. Sealock, Jr. and G. L. Roberts. 1985. Development of a Hot Gas Cleanup System for Integrated Coal Gasification/Molten Carbonate Fuel Cell Power Plants, Final Report for the period from October 1982 to January 1985. Prepared for the United States Department of Energy, under Contract DE-AC21-82MC19077 by Battelle, Pacific Northwest Laboratories, Richland, Washington.

(5) Barin, I. and O. Knack. 1973. Thermochemical Properties of Inorganic Substances. Springer-Verlog, Berlin.

(6) Pelton, A. D., C. W. Bale and P. L. Lin. 1981. Calculation of Thermodynamic Equilibria in the Carbonate Fuel Cell. DOE/ET/15416-2. Ecol Polytechnique, Montreal, Quebec.

(7) Smith, S. W. and S. M. Kapelner. 1983. "The Equilibrium Constant for the Reaction $H_2S + 3H_2O + (Li_{0.66}K_{0.34})_2CO_3 = 4H_2 + CO_2 + (Li_{0.66}K_{0.34})_2SO_4$ at Elevated Temperature." Journal of the Electrochemical Society: Electrochemical Science and Technology, Volume 130 (2), pp. 405-407.

(8) Moore, R. H., G. F. Schiefelbein and G. E. Stegen. 1976. Molten Salt Scrubbing Process for Removal of Particles and Sulfur Compounds from Low Btu Fuel Gases. BNWL-SA-6030, Pacific Northwest Laboratory, Richland, Washington.

(9) Leung, C. H. and L. H. Van Vlack. 1979. "Solubility Limits in Binary (Ca, Mn) Chalcogenides" J. American Ceramic Soc. 62 (11-12)613-616.

(10) Forland,, J. 1955. "An Investigation of the Activity of Calcium Carbonate in Mixtures of Fused Salts" J. Phys. Chem., 59, 152.

(11) Furnas, C. C. 1930. Trans. Am. Inst. Chem. Engrs., Vol. 24, pp. 142-193.

(12) Lynn, S., R. Demyanovich, D. Neumann and S. Sciamanno. 1984. "The Removal of Hydrogen Sulfide from Gasified Coal." In Proceedings of the Fourth Annual Advanced Gasification Projects Contractor's Meeting, Morgantown, West Virginia, June 26-28, 1984.

(13) Jablonski et al. 1982. Evaluation of Gasification and Gas Cleanup Processes for Use in Molten Carbonate Fuel Cell Power Plants, Final Report, DOE/MC/16220-1306. Prepared for Morgantown Energy Technology Center by Westinghouse R&D Center, Pittsburgh, Pennsylvania.
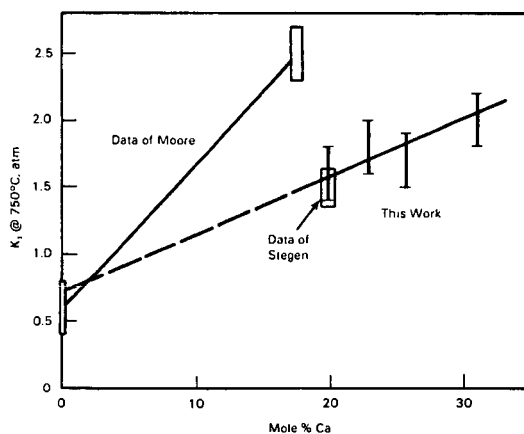
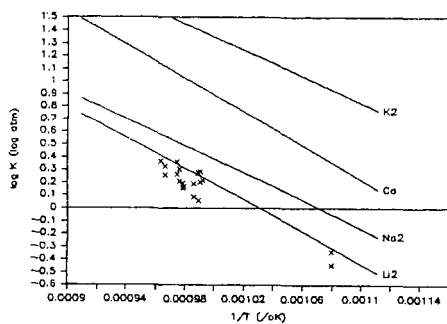Figure 1. Correlation of Carbonate/Sulfide Equilibrium with Calcium Content.

Figure 2. Estimated Pure Liquid Carbonate/Sulfide Equilibria and Data for Mixed Liquids.
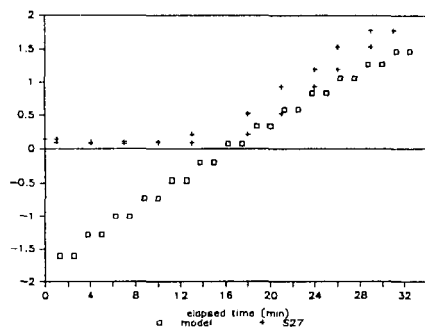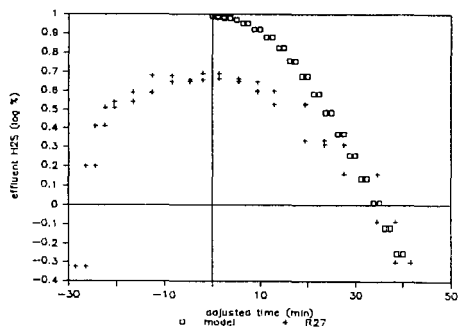

Figure 3. Absorption S27 and Model.

Figure 4. Regeneration R27 and Model.

35

APPLICATION OF NICKEL SORBENTS TO REMOVE TRACE
CONTAMINANTS FROM HOT COAL GAS

P.S. Patel, S.M. Rich, and H.C. Maru

Energy Research Corporation
3 Great Pasture Road
Danbury, CT 06810

INTRODUCTION

    Coal gas offers a low cost feed option for efficient generation
of electricity using turbines or fuel cells as generators. However,
coal derived gases contain contaminants such as sulfur and arsenic
compounds, halides, etc., which are known to detrimentally affect the
generator performance (1,2,3). These contaminants must be kept below
a certain, permissible level for long-term, cost effective operation
of a coal gas fueled power plant. Based on contaminant tolerance data
for the related catalysts and the limited data available for fuel cell
performance, it is desirable that the sulfur and arsenic compounds be
reduced to sub-ppm levels. The commercially available low temperature
cleanup processes are not cost effective as they require
quenching/reheating operations. An energy efficient and economically
viable high temperature coal gas purification process to minimize the
heat exchange requirements is highly desirable. Several high
temperature processes based on regenerative adsorption appear to be
capable of removing H_2S from coal gas to a 2-10 ppmv level
(4,5,6,7,8), but further reduction to a sub-ppm level is required.
This paper describes a regenerable process to achieve this sub-ppm
contaminant cleanup using nickel sorbents.

    Supported nickel catalysts were investigated for their capability
to remove sulfur compounds in coal gas to sub-ppm levels and to study
the effect of other contaminants such as arsenic on sorbent
performance. This concept is supported by the fact that these
contaminants are known poisons towards nickel catalysts, even at low
(<10 ppm) concentrations (9,10). The adsorption of sulfur on nickel
occurs by reversible, dissociative chemisorption at concentrations of
approximately 10 ppmv H_2S or less (11,12). The removal of chemisorbed
sulfur has also been studied to recover the activity of nickel
catalysts used in processes such as reforming, methanation, etc.
(13,14,15). Sorption and regeneration experiments were performed with
commercially available dispersed nickel sorbents to determine rate and
capacity for sulfur removal from coal gas at high temperatures
(500-700°C). A parametric analysis and process design study were
performed to develop major guidelines for the trace contaminant
removal reactor system.

EXPERIMENTAL METHODS

    The coal gas contaminants, sulfur and arsenic, possess strong
affinity for many materials of constructions. A test apparatus and
analytical techniques capable of handling and monitoring trace amounts
of these contaminants in the presence of major coal gas components
with good reproducibility were developed.

    APPARATUS. The experimental studies were carried out with a
bench-scale, isothermal fixed-bed reactor at atmospheric pressure to

36

establish sulfur and arsenic sorption and regeneration characteristics of the nickel catalysts chosen. The reactor system was constructed of quartz and Teflon to minimize secondary adsorption effects. The model coal gas was simulated via mixing of the appropriate gaseous components, with steam introduced by humidifier evaporation. The gas delivery lines were heated to prevent steam condensation. All components, except H_2S were introduced from compressed gas cylinders (99.999% purity). Trace levels of H_2S (1-10 ppmv) were provided from a certified permeation tube and introduced after the humidifier to prevent dissolution of the H_2S.

ANALYTICAL. The major coal gas constituents were monitored with a microprocessor controlled gas chromatograph(GC) equipped with a thermal conductivity detector(TCD). Trace contaminant measurements at the reactor exit and entry were accomplished with the GC using a photoionization detector(PID). Lower detection limits of 20 ppbv H_2S and 20 ppbv AsH_3 were achieved with this apparatus using appropriate combination of GC columns and operating conditions such as carrier flow rate, oven temperature, etc. Consistent and reproducible measurements were obtained in the presence of H_2O, H_2, CO, CO_2, etc. to establish long-term reliability of the analytical method. When required, gas detector tubes were used to determine certain trace by-products, such as CS_2 and SO_2.

The total adsorbed contaminants and their location on the sorbents were determined with SEM, X-ray fluorescence, and X-ray EDS, supplemented by wet chemical analysis when appropriate. Total arsenic content was determined by spectrophotometric determination with silver diethyl-dithiocarbamate. The physical structural changes in the sorbents were characterized by BET surface area, selective chemisorption, and porosimetry measurements.

SORPTION/REGENERATION CONDITIONS. The preliminary screening of commercial nickel catalysts was performed under a fixed set of most favorable conditions with a constant driving force (P_{H_2S}/P_{H}). This was accomplished by using 10 ppmv H_2S in a N_2/H_2 environment at 500°C, 2000 hr^{-1} space velocity and no carbon species during initial sorption runs. Prior to a sorption run, each sorbent was subjected to a 4-hour reduction period in H_2 at 450°C. Data acquisition was performed with the automated GC/PID system until 1 ppmv H_2S was observed in the exit stream. Sulfur sorption capacity and breakthrough times for 20 and 100 ppb H_2S in the exit coal gas were used for performance comparison purposes. Pre- and post-test analyses were performed to characterize sorbent stability. Two of the most promising sorbents were chosen for further testing with a simulated coal gas. Table 1 illustrates the conditions used for a parametric evaluation of the effects of arsenic and other contaminants on the sulfur sorption characteristics. Various regeneration media such as steam, hydrogen, and air in appropriate combination were also tested at 500-700°C and 500, 5000 hr^{-1} space velocities to identify a preferred set of regeneration conditions.

RESULTS AND DISCUSSION

Based on input from catalyst manufacturers, consultants, and past experience in applications similar to coal gas, over 120 commercial nickel catalysts were qualitatively assessed for their suitability in removing the trace contaminants regeneratively. From hydrothermal

stability considerations, alumina appeared to be a preferred catalyst support. Ten candidates were chosen for preliminary screening on a comparative basis. All the sorbents were able to purify a dry H_2/N_2 stream from 10 ppmv to less than 20 ppbv H_2S, although breakthrough times varied. Sorbents containing additives such as copper or cobalt, as expected, did provide better regenerability. However, their sulfur sorption capacities were significantly lower and experienced significant losses in surface area. As can be seen in Figure 1, the breakthrough time showed a linear dependence on the nickel content indicating that high nickel contents should be preferred to achieve large sulfur removal capacities. However, the catalysts with high (50-60%) nickel contents showed a greater level of sintering, which may lead to a loss of activity in subsequent sorption cycles. Based on the sulfur sorption capacity, extent of regeneration, and the catalyst stability, two of the candidate sorbents, 3% Ni/14% MoO_3 on alumina (Ni/Mo) and 20% Ni on alumina were selected for further testing.

During preliminary screening with dry gases, the Ni/Mo sorbent exhibited an extremely high sulfur sorption capacity (16,600 ppmwS) and almost complete regeneration. When tested in the presence of a model coal gas, its performance was seriously impaired. As verified by the manufacturer and by elemental analysis, approximately 0.3% sulfur was found in the fresh sorbent. The sulfur evolved as H_2S in the presence of steam in the coal gas. When this sulfur was removed from a fresh sample before testing, the sulfur sorption capacity and the 20 ppbv H_2S breakthrough time decreased to such an extent as to make it unattractive as a trace contaminant cleanup sorbent. Unlike the Ni/Mo sorbent, 20 wt% Ni on alumina maintained the desired sulfur cleanup levels under a variety of operating conditions and changes in the coal gas composition (Table 2). Major observations related to the desirable operating conditions are summarized below.

- The sulfur sorption capacity increased with decreasing space velocity. The breakthrough time behavior suggests that the use of lower space velocities (500-2000 hr.$^{-1}$) may promote a higher contaminant removal efficiency.

- The sulfur sorption capacity increased slightly with decreasing steam content in the model coal gas. Carbon deposition occurs at lower steam content ($\sim$7%) and may be a limiting design parameter.

- Effect of decreasing temperature was to increase sulfur sorption capacity with the largest capacity observed at 500°C (Figure 2).

- In presence of arsine, the sorbent exhibited $\sim$25% reduction in the sulfur sorption capacity, possibly due to a competition between the two contaminants for the available nickel sites (Figure 3).

- Regeneration of the sulfur spent sorbents indicates that chemisorption of sulfur on the nickel surface is reversible depending on the experimental conditions used. With 70% $H_2O/30\%$ H_2 as a regeneration medium, 60-80% regeneration may be achieved at 600-700°C. Other regeneration media, such as steam, steam with $\sim$1% air, simulated fuel cell cathode

exhaust, and high steam/hydrogen ratios at 500°C did not provide satisfactory regeneration.

- The structural stability of the nickel sorbents appeared to be affected when relatively high regeneration temperatures (700°C) were used. This resulted in a drop in sorption activity in the next sorption cycle. However, the subsequent sorption/regeneration cycles indicated a stabilization of the sorbent performance (Figure 4).

CONCLUSIONS

This investigation has demonstrated that commercial, supported nickel sorbents are able to remove trace amounts of H_2S from hot coal gas to the desired sub-ppm levels for extended periods of time. The selected sorbent, 20 wt% Ni on alumina, can provide sulfur sorption capacities of 2000-10,000 ppmw S, depending on the operating conditions. All of the sorbents tested are regenerable towards sulfur. Optimum sorption/regeneration conditions exist which may make the application of these sorbents for trace contaminant cleanup of coal gas economically viable. The analytical methods developed for the coal gas cleanup application are capable of measuring sub-ppm levels of H_2S and AsH_3 and reliable for extended period of experimental runs.

ACKNOWLEDGEMENT

REFERENCES

1. E.J. Vidt, et al., "Evaluation of Gasification and Gas Clean-up Processes for use in MCFC Power Plants," Final Report prepared by Westinghouse-ERC for DOE Contract No. DE-AC21-81MC16220, 1981.

2. TRW, "Monitoring Contaminants in Coal-Derived Gas for Molten Carbonate Fuel Cells," Final Report prepared for Argonne National Laboratory, DOE/METC/82-44, 1981.

3. Morgantown Energy Technology Center, "Advanced Environmental Control Technology," Topical Report, DOE/METC/SP-187.

4. T. Grindley, "Development and Testing of Regenerable Hot Coal Gas Desulfurization Sorbents for Molten Carbonate Fuel Cell Application," DOE/Morgantown Energy Technology Center, IR No. 1133, October 1981; IR No. 1386, November 1982.

5. Katalco, "Catalyst Handbook," Springer-Verlag, New York Inc., 1970.

6. Giner, Inc., a) "Molten Carbonate Fuel Cell Power Plant Desulfurization Systems," DOE Contract No. DE-AC03-78-ET15370; b) "Studies Involving High-Temperature Desulfurization/Regeneration Reactions of Metal Oxides for the Fuel Cell Program," for Argonne National Laboratory, Contract No. 31-109-38-5804; c) Studies Involving High-Temperature Desulfurization/Regeneration reactions

of Metal Oxides for Fuel Cell Development," for DOE/Morgantown Energy Technology Center, DOE, Contract No. DE-AC21-81MC16021.

7. Institute of Gas Technology, a) "Coal Gasification Pilot Plant Support Studies," for U.S. Department of Energy, Contract No. ET-78-C-01-2806; b) "Development of a Hot Gas Cleanup System for Integrated Coal Gasification/Molten Carbonate Fuel Cell Power Plants," for DOE/Morgantown Energy Technology Center, Contract No. DE-AC21-82MC19043.

8. Battelle Pacific Northwest Laboratories, a) "Development of a Solid Absorption Process for Removal of Sulfur from Fuel Gas," for DOE/Morgantown Energy Technology Center, DOE Contract No. DE-AC21-79ET11028; b) "Development of a Hot Gas Cleanup System for Integrated Coal Gasification/Molten Carbonate Fuel Cell Power Plants," DOE/Morgantown Energy Technology Center, Contract No. DE-AC21-82MC19077.

9. J.R. Rostrup-Nielsen, J. Catal., 71, 220 (1968).

10. I.M. Al-Daher and J.M. Salih, J. Phys Chem., 76 (20), 2851-7, 1972.

11. I.E. Den Besten and P.W. Selwood, J. Catal, 1, 93, 1962.

12. J.G. McCarty, and H. Wise, J. Chem Phys., 72, 6332 1980.

13. I. Alstreys, et al., Appl. Catal., 1, 303 1981.

14. J.G. McCarty, et al., Final Report prepared by SRI International for U.S. DOE Contract No. AC21-79MC11323, December 1981.

15. J.R. Rostrup-Nielsen, J. Catal. 21, 171, 1971.

TABLE 1.   RANGE OF EXPERIMENTAL PARAMETERS EVALUATED FOR
           TRACE CONTAMINANT REMOVAL FROM HOT COAL GAS

COMPONENT		RANGE
Model Coal Gas:	H_2	15-20 vol%
	N_2	30-50
	CO	10-20
	CO_2	5-15
	H_2O	5-40
Trace Contaminants:	H_2S	1-10 ppmv
	AsH_3	1-10 ppmv
Temperature		500-700°C
Pressure		1 atm
Gas Space Velocity		500-5000 hr.$^{-1}$

Feed Gas: 10 ppmv H_2S; 20% H_2, 80% N_2
Temperature: 500°C
Space Velocity: 2000 hr^{-1}
Sorbents: Nickel on alumina

Breakthrough time
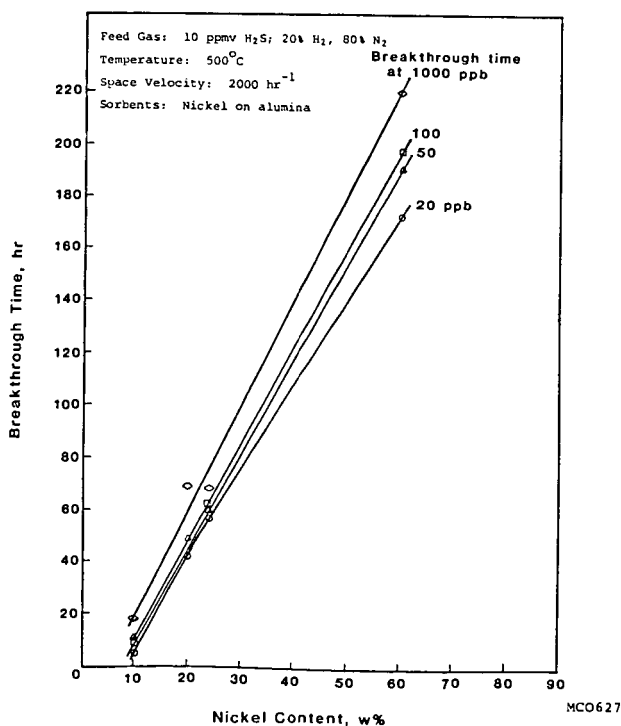at 1000 ppb
100
50
20 ppb

MCO627

FIGURE 1.   THE BREAKTHROUGH TIME SHOWS A LINEAR DEPENDENCE
            ON THE NICKEL CONTENT

41

TABLE 2. IMPACT OF OPERATING CONDITIONS ON THE PERFORMANCE OF 20 WT% Ni ON ALUMINA SORBENT

COMPOSITION OF FEED COAL GAS							TEMP °C	SP VEL hr⁻¹	SULFUR SORPTION CAPACITY g S/g Ni		COMMENTS
%H$_2$O	%H$_2$	%CO	%CO$_2$	%N$_2$	ppmH$_2$S	ppmAsH$_3$			@ 20 ppbv H$_2$S BREAKTHROUGH*	@ 100 ppbv H$_2$S BREAKTHROUGH*	
-	20	-	-	-	15	-	500	2000	9500	12,500	
7	16	20	7	50	12	-	500	2150	-	-	C-deposition observed; run terminated due to excessive increase in pressure drop.
40	10	13	5	32	10	-	500	2150	7150	9750	No C-deposition observed
25	13	16	6	40	11	-	500	2000	8850	10,650	No C-deposition observed
25	13	16	6	40	10	-	500	5000	5200	6200	
25	13	16	6	40	10	-	600	5070	4150	5500	
25	13	16	6	40	9	-	700	4900	2100	3900	
25	13	16	6	40	11	10	500	5000	3850	4650	Arsenic decreases sulfur sorption capacity.

*Breakthrough is defined as the time or event at which the specified amount of contaminant is observed in the reactor exit effluent.
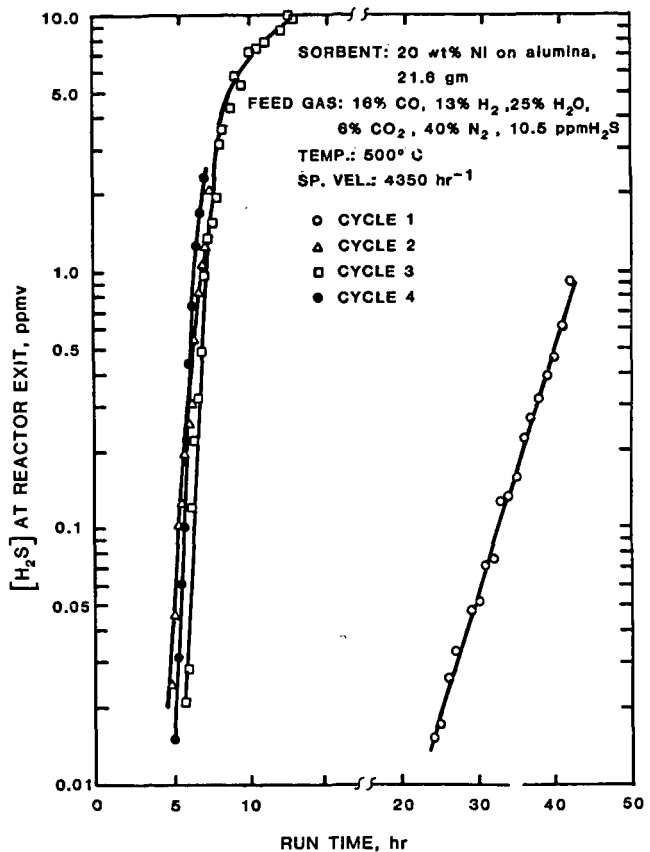
42
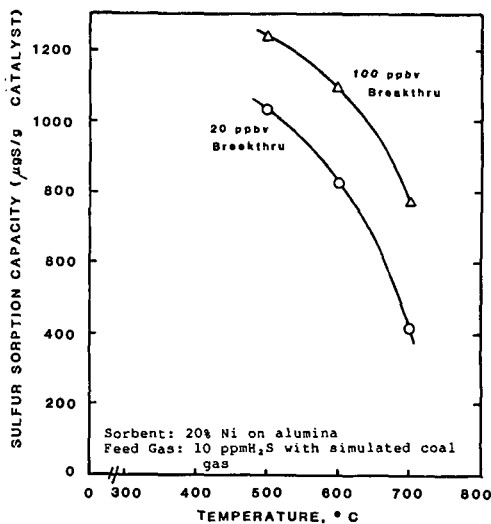
FIGURE 2.   EFFECT OF TEMPERATURE ON SORBENT PERFORMANCE
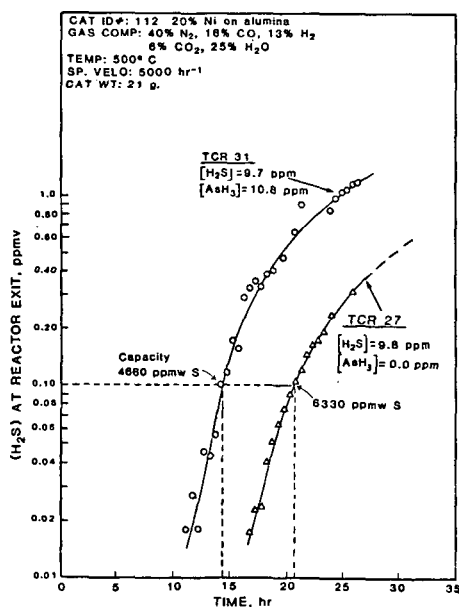
FIGURE 3.   EFFECT OF ARSENIC ON SORBENT PERFORMANCE

43

FIGURE 4. EFFECT OF SORPTION/REGENERATION ON
SORBENT PERFORMANCE

44

A STUDY OF SULFATE FORMATION DURING REGENERATION OF ZINC FERRITE SORBENTS

G.N. Krishnan, G.T. Tong, R.H. Lamoreaux, R.D. Brittain and B.J. Wood

SRI International
333, Ravenswood avenue, Menlo Park, CA 94025.

INTRODUCTION

Zinc ferrite ($ZnO \cdot Fe_2O_3$) is a promising regenerable sorbent for the high temperature (800 - 925 K) removal of hydrogen sulfide from coal gas to be fed to molten carbonate fuel cells[1]. For the desulfurization process to be economically attractive, the spent sorbent needs to be regenerated and reused. During the coal gas desulfurization step the zinc and iron oxides are converted into the corresponding sulfides. Regeneration back to the oxides is accomplished by the use of oxidizing gases such as oxygen (or air) and steam at elevated temperatures. Ideally, the regeneration should be carried out at sufficiently high temperatures to eliminate or minimize side reactions such as formation of sulfates. However, severe sintering may occur at such elevated temperatures leading to decreased sorbent desufurization capacity. Thus, to minimize sintering it is necessary to regenerate at lower temperatures where a significant degree of sulfate formation can occur.

The presence of sulfates is detrimental to the subsequent coal gas desulfurization performance of the sorbent. It not only reduces the sulfur capacity of the sorbent, but also leads to the introduction of secondary contaminants, such as SO_2, into the hot coal gas stream. These sulfur species[2] are just as undesirable as H_2S. Hence for zinc ferrite to be useful as a hot coal gas desulfurization sorbent it is essential that during regeneration sulfate formation should be minimized. An experimental and theoretical study was undertaken to define conditions where sulfate formation would occur during regeneration of spent zinc ferrite sorbents.

METHODS, APPARATUS AND PROCEDURES

Thermodynamic calculations were performed to define equilibrium conditions favorable for sulfate formation during regeneration and to predict the reaction products resulting from the interaction of zinc sulfate with hot coal gas. The regions of stabilities of oxides, sulfides and sulfates of both zinc and iron as functions of partial pressures of O_2 and SO_2 were determined. Gibbs energy minimization methods were used to calculate the equilibrium compositions of gases and solids under desulfurization and regeneration conditions. Fifty gaseous species and seventeen solid phases were inlcuded in these calculations.

The formation of zinc and iron oxides from corresponding sulfides results in a decrease of the mass of the specimen, whereas the formation of sulfates leads to an increase of the mass. Hence a thermogravimetric system incorporating a Cahn RG electrobalance and a programmable electronic temperature controller was used to monitor the mass of the specimen as the specimen was heated in a mixture of air and steam.

A laboratory-scale fixed-bed reactor system was used to determine the extent of sulfate formation as a function of process variables. The effluent gases from the reactor were analyzed for SO_2, H_2S, and residual O_2 using gas chromatography. At the end of a reaction period the specimen was rapidly quenched to preserve its chemical composition that existed at the reaction temperature.

The zinc ferrite used in this study was manufactured by United Catalysts Inc. in the form of extruded pellets. For our experiments it was crushed and sieved to a particle size range of 300 -, 500 μm. To provide a uniform starting material for the regeneration experiments, the zinc ferrite sorbent was sulfided at 873 K using a simulated coal gas of the following composition: 15% H_2, 15% CO, 11% CO_2, 24% H_2O, 3% H_2S, 32% N_2. After sulfidation the sorbent had a composition (wt%) of 40.7% Zn, 24% Fe, and 35% S. The crystalline phases were α and β ZnS and $Fe_{0.88}S$ (pyrrohtite).

45

RESULTS AND DISCUSSION

Equilibrium Calculations

The equilibrium conditions necessary for the various solid phases to be stable in the Zn-Fe-O-S system can be conveniently expressed in the form of a stability diagram. A calculated stability diagram for a temperature of 873 K is shown in Figure 1. It illustrates that the oxides are stable at high partial pressures of O_2 and low partial pressures of SO_2. For sulfates to be stable partial pressures of both O_2 and SO_2 need to be high. The stability diagrams for other temperatures indicated that as the temperature is increased higher partial pressures of O_2 and SO_2 are necessary for the stabilization of zinc and iron sulfates.

The stability diagram can be used to predict the composition of solid phases under equilibrium regeneration conditions. For example, the dotted line in Figure 1 represents a locus of points of total pressure of 0.01 atm of a mixture of O_2 and SO_2 (corresponding to a feed gas of 5% air – 95% steam). Initially in a fully sulfided sorbent, the equlibrium solid phases will be $Fe_{0.88}S$ and ZnS (upper left portion of the diagram). At the start of the regeneration the $p(O_2)$ will be less than 10^{-18} atm and $p(SO_2)$ will be about 0.01 atm. As the regeneration proceeds $p(O_2)$ will begin to increase (going from left to right on the abscissa). Initially $Fe_{0.88}S$ will be converted to Fe_3O_4. As the $P(O_2)$ increases above 2×10^{-16} atm both ZnS and Fe_3O_4 will be oxidized to form zinc ferrite. With further increase in $p(O_2)$ (>6×10^{-14} atm) ZnO. 2ZnSO$_4$ is formed. As $p(O_2)$ approaches feedstock level ZnO . 2ZnSO$_4$ and $Fe_2(SO_4)_3$ become the equilibrium phases. At the end of conversion of sulfides $p(SO_2)$ decreases and the sulfates decompose to the oxides.

The equilbrium composition of the solid phases as a function of the extent of regeneration was also calculated using a Gibbs energy minimization method. In this calculation, 1 mole of ZnS. 2.3 $Fe_{0.88}S$ was equilibrated with different quantities of a regeneration gas (air-steam-SO_2 mixtures). The reaction extent was defined as unity when the quantity of oxygen present in the feed gas was sufficient for the stoichiometric conversion of sulfides to oxides (ZnO. Fe_2O_3). An example of this calculation for the case when regeneration is carried out at 873 K using 90% air – 10% SO_2 at 20 atm total pressure is shown in Figure 2.

These computations, which included a large number of chemical species in addition to O_2 and SO_2, confirm the general sequence of chemical reactions inferred from the stability diagrams. Initially, $Fe_{0.88}S$ is oxidized to Fe_3O_4. At the end of oxidation of this phase $ZnFe_2O_4$ is formed by the oxidation of ZnS to ZnO and Fe_3O_4 to Fe_2O_3. At greater than stoichiometric levels of the regeneration gas, $FeSO_4$ and ZnO.2ZnSO$_4$ are formed. Finally, when the regeneration is complete the sulfates have decomposed to the oxides.

Thermogravimetric Experiments

The results of TGA experiments with different gas mixtures are shown in Figure 3. On heating from ambient to 625 K at 5 K/min the specimens gained mass. At higher temperatures the mass of the specimens decreased up to a temperature of about 650 K. Above 650 K, depending on the oxygen content of the feed gas the specimens either gained or lost mass. The second mass gain peak, when present, reached a maximium in a temperature range of 825 – 925 K. Above 925 K a decrease in mass was observed with all gas compostions.

The chemical reactions associated with the various mass changes were deduced from X-ray diffraction analyses of the solid remnant quenched from various temperatures. Table 1 shows these chemical reactions. The initial mass gain is due to the oxidation of $Fe_{0.88}S$ to FeS_2 and Fe_2O_3. At temperatures above 625 K, FeS_2 is also oxidized to Fe_2O_3 resulting in a mass loss. The observed mass increase above 650 K is due to the oxidation of ZnS to ZnSO$_4$. The extent of ZnSO$_4$ formation is a function of the oxygen content of the feed gas. Higher amounts of sulfates are formed when $p(O_2)$ is high. Above 925 K ZnSO$_4$ decomposes to ZnO and any residual ZnS is also oxidized resulting in a mass loss.

To determine the role of iron oxides in the formation of ZnSO$_4$, TGA experiments were conducted with a sulfided ZnO sorbent (ZnS). During heating of the ZnS in an

atmosphere of 50% air – 48% N_2 and 2% steam no mass change was observed below 925 K, but a mass loss was observed above this temperature. This indicates that $ZnSO_4$ formation is significantly reduced in the absence of Fe_2O_3. The presence of Fe_2O_3 has been reported to accelerate the formation of $ZnSO_4$ by catalyzing the formation[3,4] of SO_3.

Fixed Bed Reactor Experiments

In these experiments, about 2 g samples of sulfided zinc ferrite sorbents were regenerated isothermally using gas mixtures with various air-steam ratios. Gas chromatographic analysis of the reactor effluent gases indicated oxygen was completely consumed initially and during a major portion of the regeneration period. During regeneration with air - steam mixtures small amounts of H_2S (0.2 vol%) and elemental sulfur were prduced, but the major gaseous species was SO_2. The formation of H_2S and elemental sulfur is due to the reaction of iron sulfides with steam.

Table 2 lists the weight percentages of sulfides and sulfates of specimens regenerated for various periods of time. It indicates that the sulfide content of the specimen is progressively reduced as the duration of regeneration increases. In contrast, the amount of sulfate remaining in the sorbent initially increases, reaches a maximum when about 99% of the sulfide is converted and then decreases. The occurrence of such a maximum in sulfate content was predicted by the thermodynamic calculations.

Table 3 lists the weight percentages of sulfate remaining in the sorbents regenerated at various temperatures. The regeneration was carried out until the concentration of SO_2 in the reactor effluent decreased below 0.5 vol%. This condition occurred typically when the total amount of feed gas supplied was about 150% of that required for stoichiometric conversion of the sulfides to oxides. The results of these experiments (Table 3) indicate that sulfate formation is favored by lower temperatures and higher partial pressures of O_2.

Other parameters in the regeneration process exhibit a minor influence on the extent of sulfate formation. Increasing the space velocity appeared to decrease the amount of sulfate formed. This may be due to either an increase in the surface temperature of the sorbent during the exothermic oxidation or to a decrease in the contact time between SO_2 and the sorbent. Particle size of the sorbent over the range 0.5 to 5 mm had no observable effect on the amount of sulfate remaining in the sorbents. Furthermore, replacing steam with nitrogen as a diluent in the regeneration feed gas had no effect on the residual sulfate level. However, the presence of SO_2, even in the amount of 0.5 vol%, significantly increases sulfate formation below 975 K. Above 975 K, SO_2 in the feed gas had only a small effect on the amount of residual sulfate in the sorbent. Other conditions being equal, cycling between sulfidation and regeneration did not significantly change the amount of sulfate formed during regeneration. Finally, sulfided zinc oxide sorbents regenerated in air – steam mixtures contained a significantly lower amount of sulfate than zinc ferrite sorbents regenerated under similar conditions.

Behavior of Sulfates in Hot Coal Gas Atmosphere

The zinc sulfate present in the regenerated sorbent decomposes under the reducing conditions of hot coal gas releasing SO_2 and SO_3. Figure 4 illustrates the concentration of SO_2 observed in the reactor effluent when a regenerated sorbent containing zinc sulfate is exposed to a simulated coal gas. The SO_2 content is initially high but it declines with time in an approximately exponential manner. At higher temperatures the SO_2 level generally is high because of more rapid decomposition of the sulfate. Gas chroatography was incapable of measuring the SO_3 released. However, high temperature Knudsen cell mass spectrometric experiments indicated that the SO_3/SO_2 ratio is about 0.2.

The SO_2 and SO_3 released into the hot coal gas can be reduced and removed by another bed of fresh zinc ferrite sorbent provided sufficient concentration of hydrogen is available in the hot coal gas stream. In the initial stages of desulfurization, the hydrogen present in the coal gas is consumed in converting the Fe_2O_3 to Fe_3O_4.

$$3\ Fe_2O_3 + H_2\ =\ 2\ Fe_3O_4 + H_2O$$

When the reduction of Fe_2O_3 is complete $p(H_2)$ in the coal gas stream increases. At this stage the SO_2 and SO_3 will be reduced and react with zinc ferrite to form ZnS.

$$SO_3 + H_2 = SO_2 + H_2O$$
$$SO_2 + 3 H_2 = H_2S + 2 H_2O$$
$$ZnO + H_2S = ZnS + H_2O$$
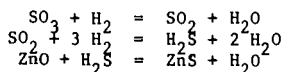
SO_2 concentrations of less than 1 ppm level were achieved by the use of a two bed system and addition of hydrogen when a regenerated sorbent containing 6 wt% sulfate was used for coal gas desulfurization.

CONCLUSIONS

Thermodynamic calculations and experimental studies have shown that zinc sulfate is formed during regeneration of sulfided zinc ferrite sorbents. The formation of sulfate is a dynamic process requiring the simultaneous presence of SO_2 and O_2. Hence it reaches a maximum level under conditions when all the sulfides in the spent sorbent have been converted to oxides and sulfates. Sulfate formation is enhanced by lower temperatures and high oxygen partial pressures in the feed gas. The formation of the sulfate is promoted by the presence of the iron oxide component of the zinc ferrite sorbent.

During subsequent desulfurization use the zinc sulfate present in the regenerated sorbent releases SO_2 and SO_3 into the hot coal gas stream. These sulfur oxides can be removed by another bed of zinc ferrite provided a sufficient concentration of hydrogen is available in the coal gas stream.

ACKNOWLEDGEMENT

REFERENCES

1. T. Grindley and G. Steinfield, "Development and Testing of Regenerable Hot Gas Desulfurization Sorbents", U.S. Department of Energy Report DOE/MC/16545 - 1125, (1981).

2. L.G. Marianowski, "An Update of the Sulfur Tolerance of Molten Carbonate Fuel Cells", in 3rd Annual Contaminant Control in Hot Coal Derived Gas Streams - Contractors Review Meeting", U.S. Department of Energy Report DOE/METC/84-6 (1984).

3. R. Dimitrov, G. Bakalov, and I. Vasilev, Rudodobiv. Met., 23, 46 (1968).

4. V.V. Pechkovskii, J. Inorg. Chem. USSR, 3, 1483 (1958).

Table 1

PROGRESSION OF OXIDATION OF SULFIDED ZINCE FERRITE
DURING THERMOGRAVIMETRIC EXPERIMENTS

Step 1

$$ZnS + 2.27\ Fe_{0.88}S + 1.02\ O_2 \rightarrow ZnS + FeS_2 + 0.5\ Fe_2O_3 + 0.27\ SO_2$$

$$\Delta m = +5.5\%$$

Step 2

$$ZnS + FeS_2 + 0.5\ Fe_2O_3 + 1.75O_2 \rightarrow ZnS + Fe_2O_3 + SO_2$$

$$\Delta m = -8.7\%$$

Step 3a

$$ZnS + Fe_2O_3 + 2\ O_2 \rightarrow ZnSO_4 + Fe_2O_3$$

$$\Delta m = 14.0\%$$

Step 3b

$$ZnS + Fe_2O_3 + 3/2\ O_2 \rightarrow ZnFe_2O_4 + SO_2$$

$$\Delta m = -14.4\%$$

Step 4

$$ZnSO_4 + Fe_2O_3 \rightarrow ZnO \cdot Fe_2O_3 + SO_2 + 1/2\ O_2$$
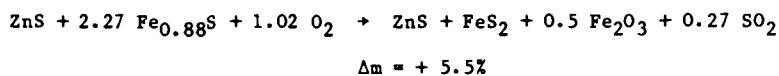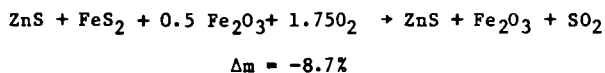
$$\Delta m = -14.4\%$$
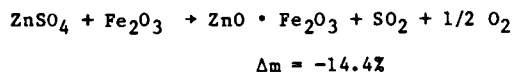
Note: The mass gain is based on the initial sample mass.

Table 2

SULFATE AND SULFIDE CONTENTS OF REGENERATED
SORBENTS AS A FUNCTION OF REGENERATION TIME[a]

Regeneration Time (min)	Fractional Conversion[b]	Sulfate (wt%)	Sulfide (wt%)
0	0	0	35.5
30	0.27	1.17	18.15
60	0.54	1.32	7.82
90	0.81	4.77	0.35
120	1.1	8.31	0.093
145	1.31	7.32	0.09

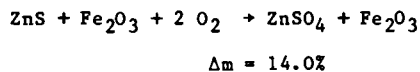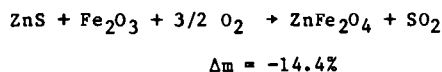[a]Feed gas composition: 58% air – 42% steam; space velocity: 2420 hr[1]

[b]Fractional conversion is unity when the amount of feed gas passed is sufficient for stoichiometric conversion of sulfides to oxides.

Table 3

EFFECT OF GAS COMPOSITION AND TEMPERATURE ON SULFATE FORMATION

Temperature (K)	Wt% Sulfate		
	100% air – 0% steam	58% air 42% steam	25% air – 75% steam
823	13.8	14.5	3.5
873	11.3	14.9	2.4
923	9.3	5.4	
973		4.5	
1073		2.2	
1173		0.45	
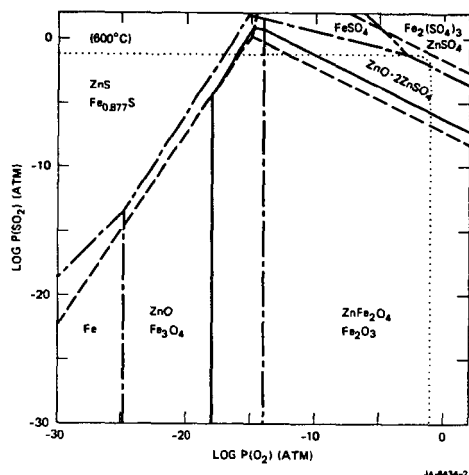
Figure 1. Stability Diagram of the Fe-Zn-O-S System at 873 K. $ZnFe_2O_4$
Phase Field (——), Zn-O-S Phases (- - -), Fe-O-S (—— - ——).
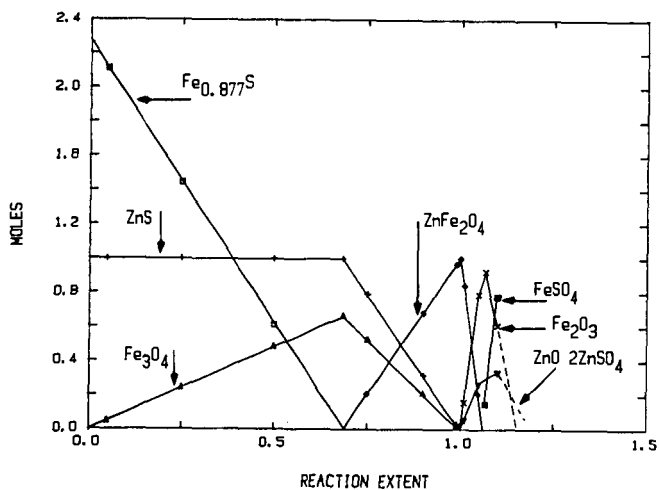
Figure 2. Equilibrium Solid Phase Products During Regeneration of Spent
Zinc Ferrite Sorbents with a Gas Mixture of 90% Air – 10% SO_2
at 873 K.
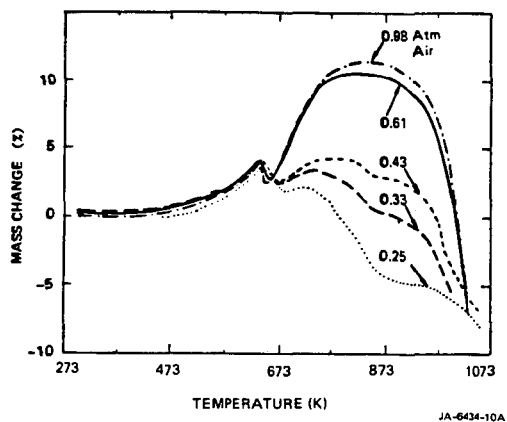
Figure 3. Temperature Programmed Thermogravimetry of Reaction of Spent Zinc Ferrite Sorbents with Various Air-N_2-H_2O Mixtures. P_{H_2O} = 0.02 atm, P_{air} is shown and Balance P_{N_2} at 1 atm.

Figure 4. Release of SO_2 into Hot Coal Gas at 873 K by $SO_4^=$ (13.5 wt%) Present in Regenerated Zinc Ferrite Sorbent.

52

Separation and Characterization of Hydroxyl Aromatics in Oils
and Asphaltenes from Nondistillable, Pyridine Soluble Coal-Liquids

R. J. Hurtubise, H. A. Cooper, and T. W. Allen

Department of Chemistry, University of Wyoming, Laramie, WY 82071

and

H. F. Silver

Chemical Engineering Department, University of Wyoming, Laramie, WY 82071

Introduction

Hydroxyl aromatics are an important class of compounds in coal liquefaction processes (1-6). The separation and characterization of hydroxyl aromatics are particularly important for the development of coal liquefaction processes and for an understanding of coal liquefaction chemistry. It has been shown that oils and asphaltenes in high-boiling distillates an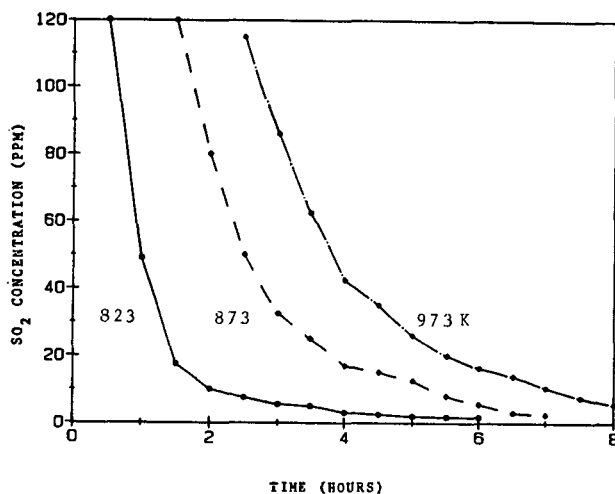d nondistillable, pyridine soluble coal-liquid samples produced in an SRC-I process consist of the same major compound classes: hydrocarbons, nitrogen compounds, and hydroxyl aromatics (5). However, as reported by Boduszynski et al. (5) oils and asphaltenes differ in the concentrations of hydrocarbons, nitrogen compounds, and hydroxyl aromatics. In this work, hydroxyl aromatic fractions were isolated from oils and asphaltenes in nondistillable (> 427°C) Wyodak and Kentucky pyridine soluble coal-liquid samples using procedures developed by Boduszynski et al. (7, 8). The fractions were further separated by normal-phase and reversed-phase liquid chromatography and then characterized by nuclear magnetic resonance, infrared, and field-ionization mass spectrometry. In addition, elemental analysis data were obtained on some of the fractions.

Experimental

Using methods developed by Boduszynski et al. (7, 8) nondistillable, pyridine soluble coal-liquid samples were separated into solvent-derived fractions and compound-class fractions. Coal-liquid fractions rich in hydroxyl aromatics from oils and asphaltenes were obtained from both Wyodak and Kentucky pyridine soluble coal-liquid samples. Each of these hydroxyl aromatic fractions was then separated into fractions containing monohydroxyl and dihydroxyl aromatics by liquid chromatography with a bonded-phase amino column and chloroform:2-propanol mobile phases. The monohydroxyl aromatic fraction was first eluted from the bonded-phase amino column with chloroform:2-propanol (95:5, v/v), and the dihydroxyl aromatic fraction was subsequently eluted with chloroform:2-propanol (75:25, v/v).

Fractions containing monohydroxyl aromatics from oils were isolated with the bonded-phase amino column and further separated by reversed-phase liquid chromatography. In reversed-phase liquid chromatography experiments, the monohydroxyl fraction from Wyodak oils was separated in two steps. First, isocratic conditions with a Resolvex C_8 column and a acetonitrile:tetrahydrofuran:water (15.2:27.8: 57.0, v/v/v) mobile phase were used. Then, a linear gradient to 100% tetrahydrofuran was employed.

Field-ionization mass spectral data were obtained from SRI International, Menlo Park, California on several of the monohydroxyl and dihydroxyl aromatic fractions from oils and asphaltenes. Elemental analysis data were obtained from Huffman Laboratories, Inc., Wheatridge, Colorado.

Results and Discussion

Weight Percent and Elemental Analysis Data

Table I gives the approximate weight percent (wt%) data for fractions containing monohydroxyl aromatics and dihydroxyl aromatics isolated from the oils and asphaltenes of Kentucky and Wyodak nondistillable, pyridine soluble coal-liquid samples. It is clear from the data in Table I that the monohydroxyl aromatic fractions contain significantly more material than the dihydroxyl aromatic fractions. Table II gives the elemental analysis data obtained for three of the monohydroxyl aromatic fractions and one of the dihydroxyl aromatic fractions. The elemental analysis data clearly show that the fractions contain a large amount of oxygen; however, nitrogen is also present but in smaller amounts. Infrared data and the chromatographic data indicated that hydroxyl oxygen was present in the fractions. The infrared experiments also showed that pyrrolic nitrogen was in most of the fractions.

Chromatographic and Field-Ionization Mass Spectral Data

Chromatographic data from thirty-four monohydroxyl and dihydroxyl aromatic standards indicated that these compounds could be separated into monohydroxyl and dihydroxyl aromatic fractions with a bonded-phase amino column and chloroform:2-propanol mobile phases. Application of this approach to hydroxyl fractions from coal-derived oils and asphaltenes yielded two distinct fractions which had retention characteristics similar to the model monohydroxyl and dihydroxyl aromatic compounds, respectively.

Field-ionization mass spectral data were obtained from eight monohydroxyl and dihydroxyl aromatic fractions isolated from Wyodak and Kentucky nondistillable, pyridine soluble coal-liquid samples. The spectra revealed the extreme complexity of these samples. Table III gives the weight average molecular weight for the fractions.

To obtain field-ionization mass spectra that were less complex, the monohydroxyl aromatics from Kentucky oils were divided into four fractions using a bonded-phase amino column. Then field-ionization mass spectra were obtained from these four fractions. Even though the field-ionization mass spectra were simplified, relatively complex spectra were still observed. However, major structural assignments were made and several homologous series were characterized.

Reversed-phase liquid chromatography experiments with the monohydroxyl fraction from Wyodak oils showed that the compounds could be completely eluted from a reversed-phase column. Under the reversed-phase conditions, first a highly resolved chromatographic profile of low molecular weight compounds was obtained, and then with the application of a reversed-phase gradient elution step, two major chromatographic bands were observed. Figure 1 shows the overall chromatogram obtained from the monohydroxyl fraction from Wyodak oils. In related experiments, field-ionization mass spectra were obtained from the total material of the highly resolved chromatographic bands and the total material from the reversed-phase gradient step from the monohydroxyl fraction of Kentucky oils. The field-ionization mass spectrum of the highly resolved chromatographic bands was somewhat simple, giving a weight average molecular weight of 291. The spectrum from the reversed-phase gradient step was rather complex and showed a weight average molecular weight of 465.

Acknowledgement

References

1. Whitehurst, D. D.; Mitchell, T. O.; Farcasiu M. "Coal Liquefaction"; Academic Press: New York, 1980.

2. Kamiya, Y.; Sato, H.; Yao, T. Fuel 1978, 57, 681.

3. Schiller, J. E.; Mathiason, D. R. Anal. Chem. 1977, 49, 1225.

4. White, C. M.; Li, N. C. Anal. Chem. 1982, 54, 1570.

5. Boduszynski, M. M.; Hurtubise, R. J.; Silver, H. F. Fuel 1984, 63, 93.

6. Cronauer, D. C.; McNeil, R. I.; Galya, L. G.; Danner, D. A. Am. Chem. Soc., Div. Fuel Chem. Preprints 1984, 29(5), 130.

7. Boduszynski, M. M.; Hurtubise, R. J.; Silver, H. F. Anal. Chem. 1982, 54, 372.

8. Boduszynski, M. M.; Hurtubise, R. J.; Silver, H. F. Anal. Chem. 1982, 54, 375.

Table I. Approximate wt % Values of Monohydroxyl Aromatic and Dihydroxyl Aromatic Fractions From Oils and Asphaltenes in Solvent-Refined Coal-Liquid Samples

Oils

Wyodak		Kentucky	
Monohydroxyl	Dihydroxyl	Monohydroxyl	Dihydroxyl
4.3	1.0	3.8	0.2

Asphaltenes

Wyodak		Kentucky	
Monohydroxyl	Dihydroxyl	Monohydroxyl	Dihydroxyl
17.0	7.4	17.8	5.2

Table II. Elemental Analysis Data for Monohydroxyl and Dihydroxyl Aromatic
          Fractions[1]

Oils	C	H	O	N
			Wt%	
Wyodak-monohydroxyl	81.1	7.3	9.1	0.73
Kentucky-monohydroxyl	80.6	7.5	9.5	0.47
Asphaltenes				
Wyodak-monohydroxyl	84.3	6.3	8.5	1.0
Wyodak-dihydroxyl	80.1	6.2	11.3	0.90

[1]Data provided by Huffman Laboratories, Inc.

Table III. Weight Average Molecular Weight for Hydroxyl Aromatic Fractions[1]

Oils

Wyodak		Kentucky	
Monohydroxyl	Dihydroxyl	Monohydroxyl	Dihydroxyl
496	503	477	505

Asphaltenes

Wyodak		Kentucky	
Monohydroxyl	Dihydroxyl	Monohydroxyl	Dihydroxyl
571	543	566	556

[1]Data provided by SRI International.

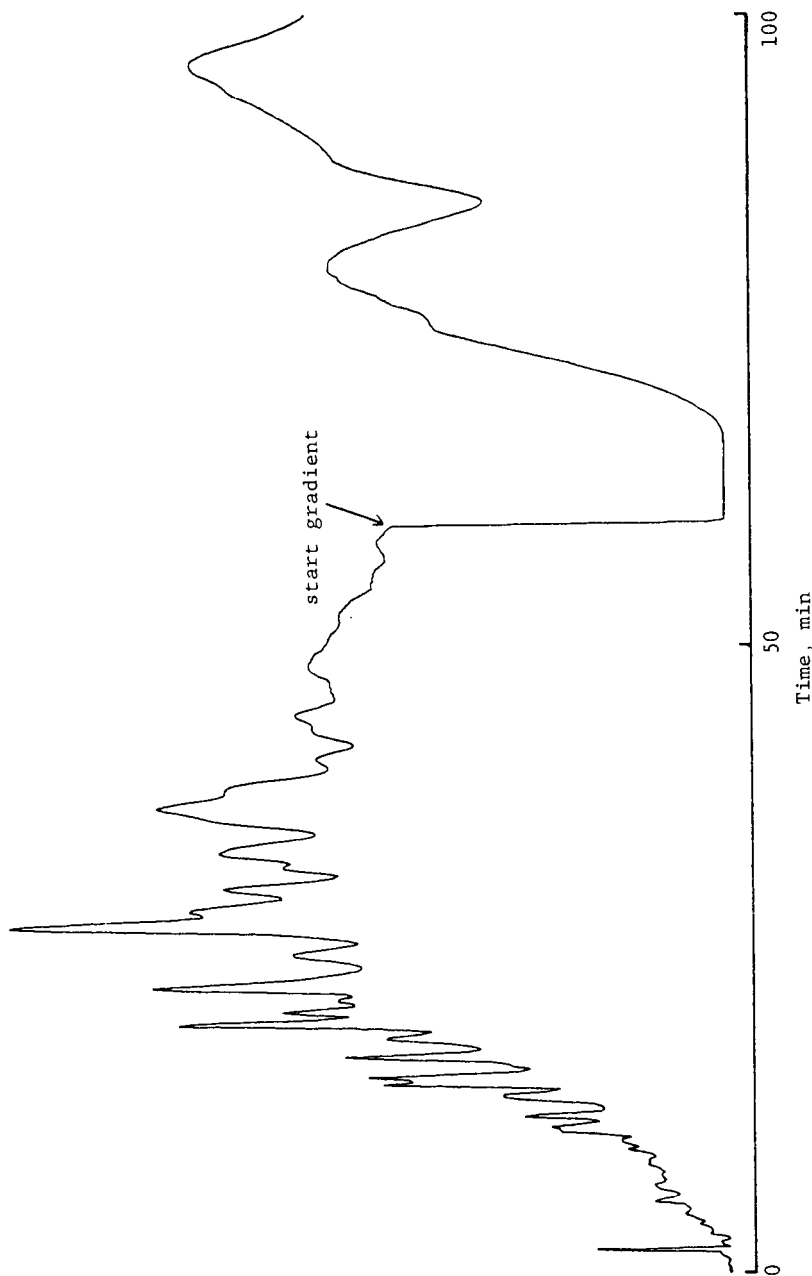Figure 1. Reversed-phase chromatogram obtained from the monohydroxyl fraction from Wyodak oils with a C8 column and acetonitrile:tetrahydrofuran:water (15.2:27.8:57.0, v:v:v) mobile phase (0-60 min) and a gradient step to 100% tetrahydrofuran (60-100 min) at 1.0 mL/min. The chromatogram from 0-60 min represents about 22% of the fraction and the chromatogram from 60-100 min represents about 78% of the fraction.

57

CHARACTERIZATION OF CHEMICAL SPECIES IN COAL LIQUIDS USING AUTOMATED

SIZE EXCLUSION CHROMATOGRAPHY - GAS CHROMATOGRAPHY (SEC-GC)

C. V. Philip and R. G. Anthony

Kinetic, Catalysis and Reaction Enginering Laboratory
Dept. of Chemical Engineering, Texas A&M University
College Station, Texas 77843

Introduction

Both size exclusion chromatography (SEC) and distillation are used to characterize species based on molecular weights which are determined indirectly either from SEC separation pattern (molecular size separation) (1-6) or from an ASTM distillation pattern. Boiling points can be used to estimate the molecular weight of the species but it is inadequate for chemical species characterization. The molecular separation by SEC is a powerful tool for determining molecular weights of polymers of known chemical structure. Although knowledge about the chemical structure of the component species are essential for the successful use of SEC,(5) it has certain advantages over distillations. SEC separations are less time consuming and can be used for both volatile and nonvolatile materials. Due to its simplicity, distillation is the most popular technique used for large and small separations and for the characterization of hydrocarbon fluids such as petroleum crudes, synthetic crudes, coal liquids and their refinery products. The performance of distillation cuts such as gasoline, kerosene and various lubricants are monitored and blended for standardizing performance rather than using the chemical composition for predicting the performance.

The high efficiency gel columns packed with 5μm particles have increased the efficiency and decreased the analysis time of size exclusion chromatography (SEC). Since relatively large samples can be separated in a time as short as 20 minutes, SEC can be used as a preliminary separation technique prior to other analytical techniques such as gas chromatography (GC) and gas chromatography-mass spectroscopy (GC-MS). Such SEC separation of coal liquids, petroleum crudes and their distillation cuts into four or five fractions, followed by the analysis of the SEC fractions by GC and GC-MS have been reported elsewhere (7-21). The fraction collection and concentration of fractions were performed manually. This procedures was inefficient, and susceptible to human error. The Automated fraction collection followed by injection of the fraction into the GC reduces analysis time, and offers and option for collecting a desired number of fractions at predetermined time intervals.

The SEC separates coal liquids into fractions containing species with similar linear molecular sizes. Since similar molecular size species in coal liquid happened to have similar functionalities, the size separation enables the separation of fractions containing similar chemical species. When tetrahydrofuran (THF) is used as the mobil phase the coal liquid can be separated into four fractions containing heavy nonvolatiles, long chain alkanes mixed with light nonvolatile, phenols and aromatics.

When the number of fractions are increased, less complex chromatograms with fewer peaks are obtained. The results of SEC-GC analysis of coal liquids indicate that the coal liquids are composed of a very large number of species but with similar structural blocks and functionalgroups. Lumping of similar components into four distinct groups such as nonvolatiles, alkanes (nonaromatic hydrocarbons), alkylated phenols and aromatics is seen as practical means of characterizing coal liquids.

In petroleum refinery industry the composition of distillation cuts are plotted versus distillation temperature. A similar technique is used for lumping of chemical species in coal liquid where the chemical composition is plotted versus elution volume (i.e. decreasing molecular size). In the SEC-GC set-up, the gas chromatograph can be visualized as a detector for SEC effluents. The GC out-put is used to determine the composition of SEC efficients. The instrumentation, SEC-GC analysis and chemical lumping of coal liquids are presented in this paper.

Experimental

A western Kentucky synthoil and lignite derived recycle solvents from the Energy Research Center, University of North Dakota were the samples used for the analysis. Dry, additive-free tetrahydrofuran (THF) under helium atmosphere was used for preparing sample solutions and as the mobile phase in the size exclusion chromatograph (SEC). Although the synthoil could be injected without dilution, a 50% solution was preferred in order to reduce possible peak spreading and tailing. Since the recycle solvents were very viscous, 25% solutions were used. All the solutions were filtered through 0.5 μm Millipore filters using modest heat (but not high enough to boil THF) from a hot air gun and 30 psi nitrogen pressure.

The instrumentation included a liquid chromatograph (LC, Waters ALC/SEC Model 202) equipped with a 60 cm, 5μm 100 Å PL gel column (Polymer Laboratories) and a refractive index detector (Waters Model R401) a Varian Chromatographic system (GC, VISTA 44) equipped with a 30 meter x 0.32 mm ID DB-5 capillary column (bonded phase fused silica column manufactured by J&W Scientific Co.) an autosampler (Varian 8000), a flame ionization detector (FID) and a nitrogen specific detector (thermionic ion specific - TSD) and a microcomputer system (IBM CS 9000) with 1000 K bytes RAM and dual 8" floppy disc drives for collecting raw chromatographic data.

The continuous sample separations on the gel column followed by the GC analysis of selected fractions was achieved by the operation of two sixport valves and a 34 port valve (All from Valco Instrument Company) as illustrated in Fig. 1. Sample injection into the LC was performed by a sixport valve (V_1) with a 2 ml sample loop and fitted with a syringe-needleport for variable sample size injection. The combined operation of another sixport switching valve and the 34 port valve (V_3) with 16 sample loops (100 μl) enabled the linking of the liquid chromatograph with the autosampler of the gas chromatograph. The autosampler was modified to handle 100 μl samples directly from the fraction collection loops of V_3. When V_2 was turned clockwise, it kept V_3 in line of LC effluents so that the fractions of separated sample could be collected and also the autosampler was bypassed. V_2 at its counter clockwise position kept V_3 in line with the autosampler for sample injection but bypassed the LC stream. Generally 0.1 μl sample size was used for GC analysis. The real time monitoring of the GC was possible on both Varian and IBM systems and the raw chromatographic data were stored on the 8" floppy discs. The fraction collection, sample injection into the GC as well as the data collection was performed by the integrated system composed of a Varian Automation System (VISTA 401) and the IBM microcomputer (CS 9000). For each sample injection into the SEC column, up to 16 fractions were collected and analyzed by the GC using appropriate gas chromatographic programs stored in the memory without any manual interaction.

Results and Discussion

The sample size recommended by column manufacturers for size exclusion chromato-
graphy is less than 1 mg in 10µls for good analytical separations. Increasing the
sample size can cause increase in peak width as well as loss of resolution. The
effect of sample size is demonstrated in Figure 10. Currently the gel columns are
available with high plate counts and high sample loading capacity. Larger smaples can
be loaded with some peak broadening which can be tolerated. When a sample like coal
liquid which is composed of a very large number of components, the sample sizes with
respect to individual species are small. Even overloading of the column with a large
coal liquid sample can give good separation of most species in coal liquid. Straight
chain alkanes are the one group of species which are present in relatively large
concentrations. The effect of coal liquid sample size is illustrated in Figure 11.
When the concentration of alkanes in the sample is small only few alkane peaks are
present in the gc of 0.1 µl SEC effluent. As the alkane concentration is increased
the peak spreading causes the several alkanes to spread into the 0.1µl fracation
analysed for the next interval. When the sample size is increased the peak intensi-
ties due to individual alkane do not increase proportionally but larger number of
alkanes are observed in the 0.1µl effluent "window". The overloading has a positive
effect on SEC fraction collection intervals. The smaller samples need frequent
intervals of fraction collection for GC analysis to identify all the components.
When the sample size is increased the column overloading will cause the species to
spread into a wider range and the fraction collection interval time can be increased.

The recycled solvent produced from Wyodak coal is selected to illustrate the
chemcial species in coal liquids using SEC-GC. A large sample size is selected and
the SEC column is overloaded with respect to alkanes. The gas chromatograms similar
to those in Figure 8 were obtained. The raw data from a blank run, where 0.1µl THF
was injected with out any coal liquid species, were subtracted from each raw data
using a base subtraction program, to obtain the reconstructed, gas chromatograms as
shown in Figure 12. Each of the 12 GC's represents the analysis SEC fraction: (see
Figure 7b for SEC separation Wyodak recycle solvent). Once question which arise at
this point is how much overlapping of species is there between the species found in
two 0.1µl SEC slices or how many of the gc peaks are not present in the previous
sample slice. In order to determine the new species and the species which are in
larger concentrations than the previous sample slice, the raw data of the previous
gas chromatogram is subratacted from that each GC raw data. (Only base line is
subtracted from the first one. First GC run data is subtracted from the second, the
second is subtracted from the third and so on). Figure 13 shows GC's with new peaks
and peaks which are larger than those in the previous GC.

When SEC-GC is used for coal liquid analysis, .1µl fractions of SEC effluents
are analyzed by GC to produce simpler gas chromatograms. Some of these gas chromato-
grams, for example the GC of longer alkanes, are composed chemically similar
components. The flame ionization detector (FID) response factor (based on mass), is
essentially the same for these larger alkanes. The total area counts of such gas
chromatograms excluding solvent peak, the area count of which represents the sample
volume (6.1µl), multiplied by the response factor will give the amount of alkanes
"lumped" together for the SEC fraction analyzed. Certain SEC fractions are composed
of two or more different chemical species due to the over lapping effect of similar
size species. For example the low boiling point alkanes mixed with the high boiling
point phenols where the linear molecular sizes of the species are similar. The
alkanes appear at low retention times whereas phenols appear at longer retention
times as expected. In these cases the area counts have to be lumped into two groups,
one for alkanes and another one for phenols. Each of these area counts multiplied by
the corresponding FID response factor indicate the amount of alkanes or phenols
present in the 0.1µl SEC fractions. All the sixteen or more GC of selected SEC .1µl
fractions of coal liquid or recycle solvents are individually analyzed for various
"lumped chemical" species in the fractions. Coal liquid sample separated by
distillation estimates the nonvolatile content. The SEC of nonvolatiles, volatiles

are reconstructed to show both in the same SEC output. These data along with SEC-GC data and used to reconstruct SEC of Wyodak coal derived recycle solvent as shown in Fig. 6.

The chemical lumping pattern shown in Fig. 6 is very similar to the plotting of distillation temperatures vs. composition, a technique commonly used in petroleum refining to simulate the composition of distillate as a function of temperature. Since SEC includes nonvolatiles, information on its size distribution is also shown. In each chemical lump the molecular weight decreases as SEC retention volume increases. The individual chemical lump has a SEC separation pattern similar to distillation temperature vs. molecular weight plot.

The chemical lump of alkanes is the simplest. Straight alkanes are distributed through out the range in a continuous pattern. Such a pattern does not exist for phenols and aromatics. Both of them have similar aromatic nucleus such as benzene, indan and naphthalene. The presence of hydroxy groups distinguishes the phenols from the aromatics. The alkyl side chains ranging mostly from C_1 to C_3 all attached to the simple aromatic nucleus result is larger molecules of phenols and aromatics. As the number of side chains increases, the number of isomers increase exponentially. The mass distribution of phenols and aromatics peaks at a certain molecular weight and then decreases at higher molecular weights. At the lower end of the mass distribution pattern, since a number of isomers possibly are smaller, the GC is well resolved and composed of larger well resolved peaks. At the higher molecular weight end, a very large number of isomers are possible in a small mass, the GC shows an upward shift in the base line which is due to a large number of species that are appearing unresolved. Since phenols have an inherent tendency for tailing, the large phenols are not at all resolved. In the case of large aromatics, the enormous number of isomers are appearing with quite a few peaks partially resolved.

The species which are unkown and have not been identified as one of the major chemical lump such as alkanes, phenols and aromatics are lumped together as unidentified. The addition of the ms to our system will enable identification of these species. However, the species in this lump include saturated and unsaturated cyclo-alkanes with or without side chains, which resembles the naphthenes, a petroleum refinery product group. A number of well known species in coal liquid are not mentioned in this lumping scheme. Such as heterocyclic compounds with sulfur, nitrogen or oxygen as the hetero atom, and other hetero atoms containing species. Some of these compounds appear with aromatics (eg. thiophenes, quinolines) and with phenols (eg. aromatic amines), and most of them are lumped with the unidentified species lump.

Since SEC-GC can be equipped with a number of specific detectors such as nitrogen specific detector (TSD), flame photometric detector for sulfur (FPD) and mass spectrometer, the lumping of chemical species can be performed for any selected group of species such as polycyclic aromatics, thiophenes and nitrogen species.

Conclusions

Although SEC and GC are two powerful chromatographic techniques, their combined use for analyzing complex mitures has been limited due to the time consuming steps involved. The two valve interface which links the liquid chromatograph to gas chromatograph and the computer system which automate the system, reduce the analysis time as well as the frequency of manual interaction during the analysis which may take 8-10 hours for a coal liquid sample. By adding a mass spectrometer as a third detector to the GC, an extensive analysis of a rather complex sample such as coal liquid, petroleum crude and their refinery products can be achieved.

With the help of additional devices such as MS, SEC-GC is not expected to identify all the components of coal liquids. It may very well be true that all the positively identified components may represent only a fraction of all the components

and the mass fractions of all the identified species may very well represent only a minor fraction of the coal liquid. But the lumping of chemical species into fewer groups will be for the whole sample and the chemical nature of large number of species which are not totally identified are recognized for their structure based on similarity on of functional groups or main structural block. The lumping of chemical species as shown in Figure 14 is a good approximation which needs varification by detailed analysis.

Acknowledgements

Literature Cited

1.   Hendrickson, J.G., Anal. Chem., 1968, 40: 49.
2.   Majors, R.E.J., Chromatog. Sci., 1980, 18: 488.
3.   Hendrickson, J.G. and Moore, J.C., J. Polym. Sci. Part A-1, 1966, 4: (1966).
4.   Cazes, J. and Gaskill, D.R., Sep. Sci., 1969 4: 15.
5.   Krishen, A. and Tucker, R.G., Anal. Chem., 1977 49: 898.
6. Snyder, R.L. and Kirkland, J.J., Introduction to Modern Liquid Chromatography, John Wiley and Sons, Inc., New York, 1974.
7.   Philip, C.V., Anthony, R.G., Fuel Processing Technology, 1980, 3, 285.
8.   Philip, C.V., Anthony, R.G., Proc. Coal Technology, 1978, 2 p. 710.
9.   Philip, C.V., Anthony, R.G., Preprints ACS Org. Coat & Polym. Div., 1980 (August 20).
10. Zingaro, R.A., Philip, C.V., Anthony, R.G., Vindiola, A., Fuel Processing Technology, 1981, 4, 169.
11. Philip, C.V., Anthony, R.G., Am. Chem. Soc. Div. Fuel Chem. Preprints, (1979), 24, (3), 204.
12. Philip, C.V., Zingaro, R.A, Anthony, R.G., Am. Chem. Soc. Fuel Chem. Preprints, 1980, 25, (1), 47.
13. Philip, C.V., Zingaro, R.A., Anthony, R.G. in "Upgrading of Coal Liquids," Ed. Sullivan, R.F., ACS Symposium Series No. 156, 1981;p. 239.
14. Philip, C.V., Anthony, R.G., Am. Chem. Soc. Div. Fuel Chem. Preprints, 1977, 22, (5), 31.
15. Philip, C.V., Anthony, R.G. in "Organic Chemistry of Coal," Ed. Larsen, J.W., ACS Symp. Series, 1978, p. 258.
16. Philip, C.V., Anthony, R.G., Fuel, 1982, 61, 351.
17. Philip, C.V., Anthony, R.G., Fuel, 1982, 61, 357.
18. Philip, C.V. and Anthony, R.G., "Size Exclusion Chromatography", Ed. Prouder, T., ACS Symp. Series, 1984, 245, 257.
19. Philip, C.V., Anthony, R.G. and Cui, Z.D., "Chemistry of Low-Rank Coals, Ed. Schobert, H.H., ACS Symp. Series, 1984, 264, 287.
20. Philip, C.V., Bullin, J.A. and Anthony, R.G., Fuel Processing Technology, 1984, 9, 189.
21. Sheu, Y.H.E., Philip, C.V., Anthony, R.G. and Soltes, E.J., Chromatographic Science, 1984, 22, 497.
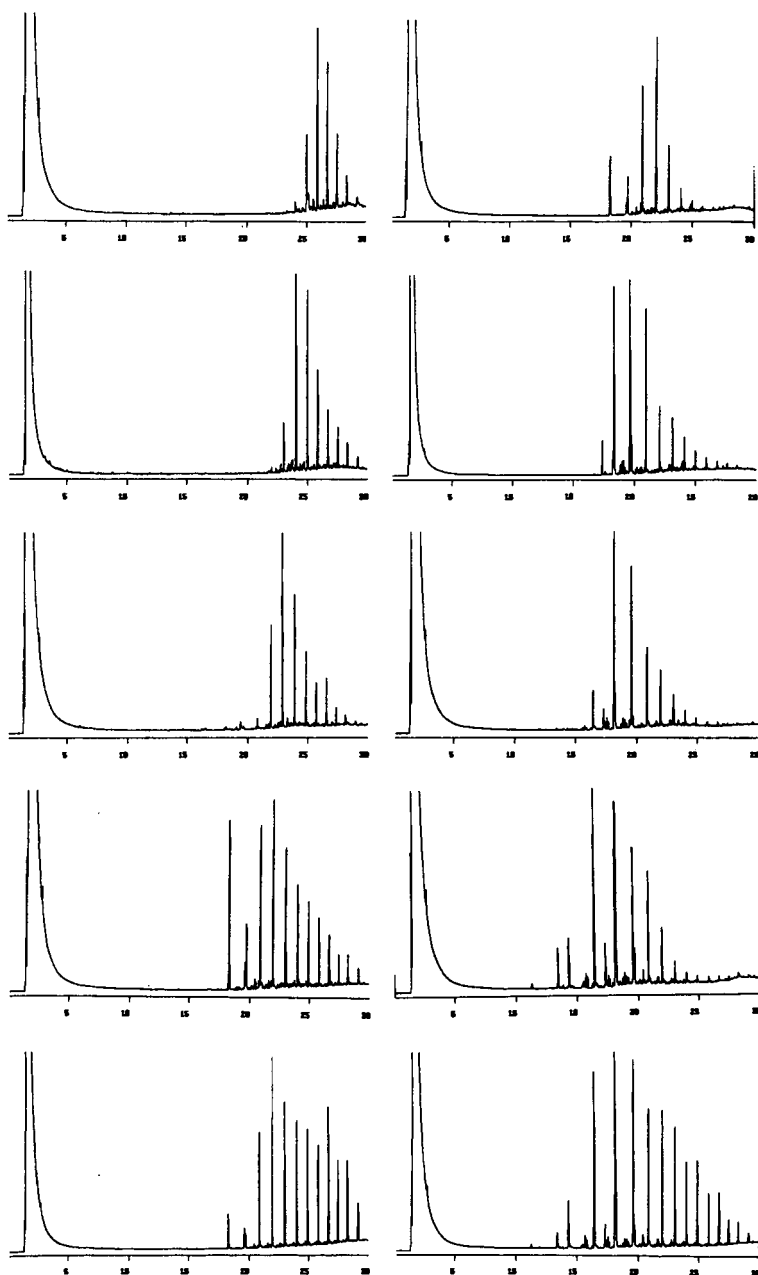
Figure 3:   The effect of column overloading by alkanes of coal liquids. Top to bottom: 20 mg synthoil, 50 mg synthoil, 50 mg ZAP recycle solvent, 50 mg Texas Big Brown recycle solvent, 50 mg Wyodak recycle solvent.

63
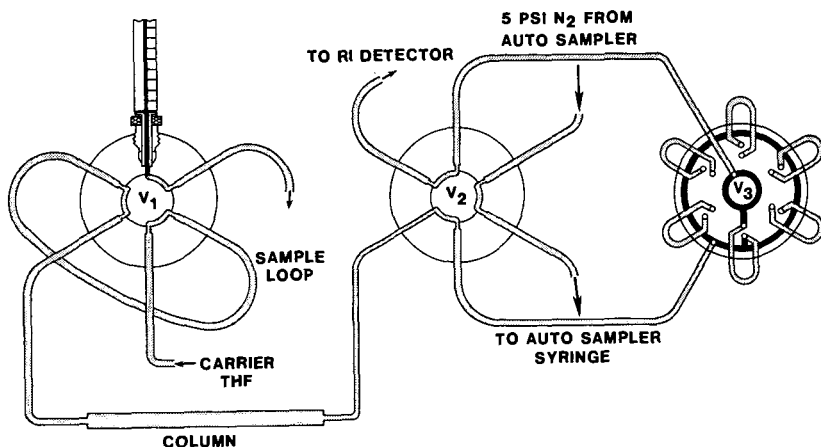
Figure 1:   SEC-GC interface. Note: V_3 has sixteen loops instead of
              six.

1. HEAVY NONVOLATILES
2. LIGHT NONVOLATILES +
   LONG CHAIN HYDROCARBONS
3. PHENOLS
4. AROMATICS

Figure 2:   SEC separation of Wydak coal derived recycle solvent (1)
              SEC-GC interface bypassed (b) 16 fraction were collected by
              SEC-GC interface.
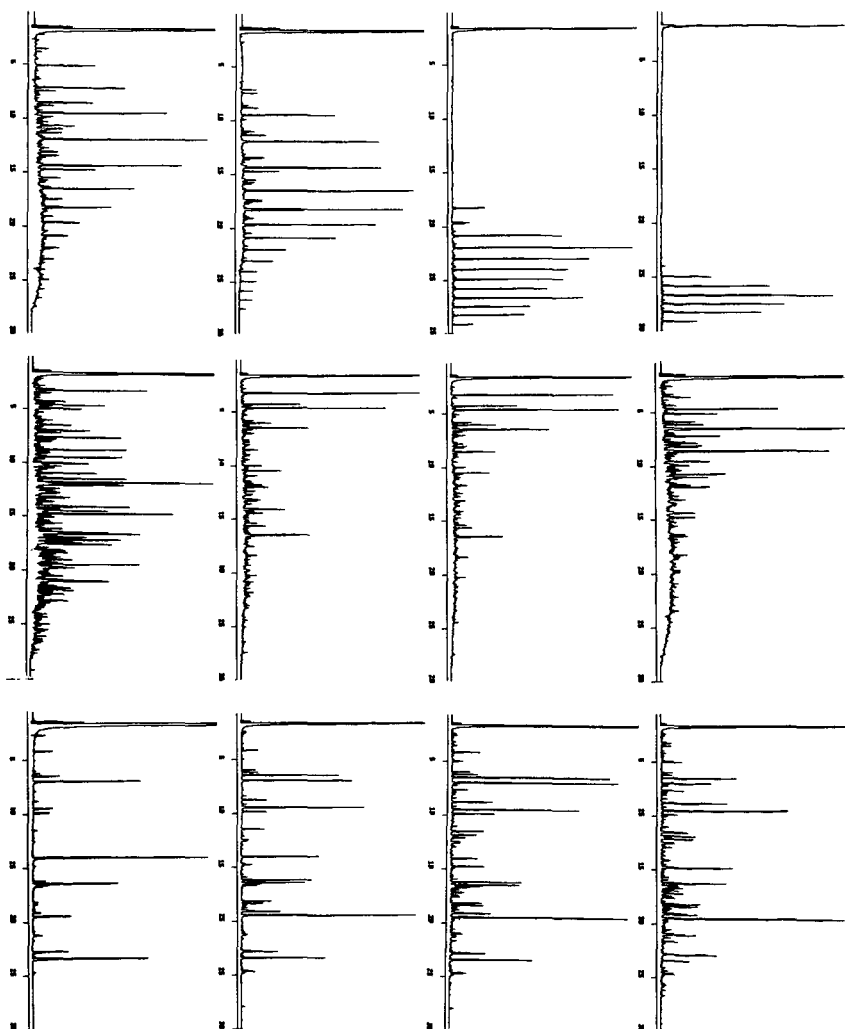
Figure 4: Gas chromatograms of SEC fractions from Wyodak recycle solvent. Base lin subtraction

65
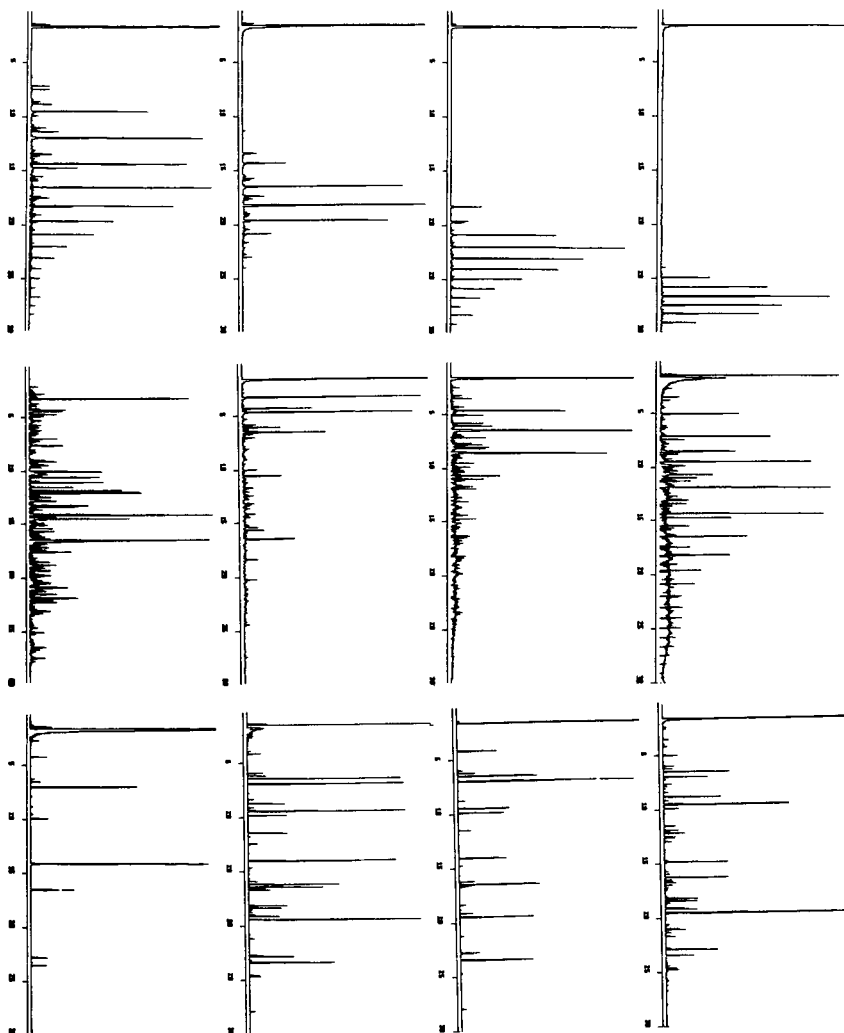
Figure 5:   Reconstructed gas chromatogram showing only new peaks
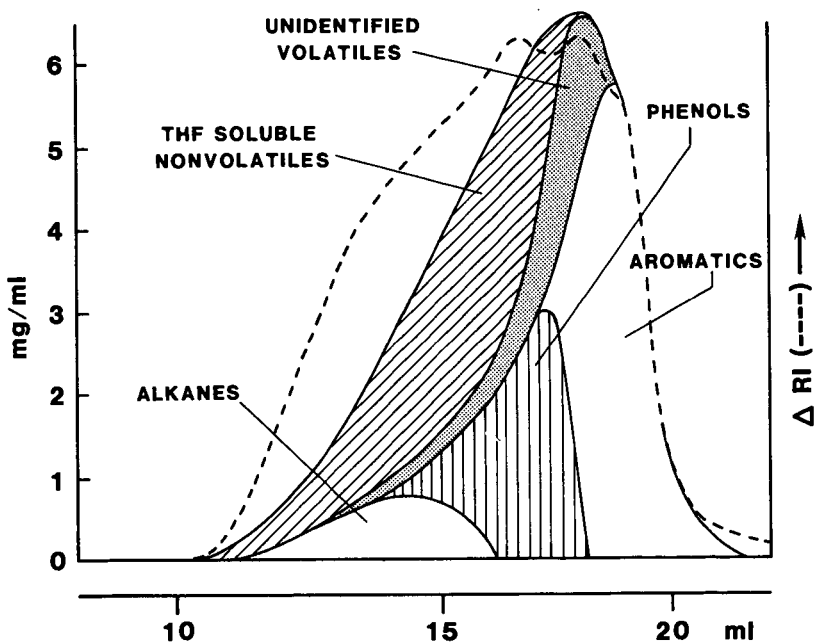
Figure 6: Lumping of chemical species in Wyodak recycle solvent.

Tandem Mass Spectrometry and the Structure of Coal Derivatives

Karl V. Wood

Engine/Fuels Laboratory
Department of Chemistry
Purdue University
West Lafayette, IN 47907

R.G. Cooks

Department of Chemistry
Purdue University
West Lafayette, IN 47907

Introduction

The chemical nature of products derived from coal, whether resulting from liquefaction or some form of chemical degradation, is of particular interest 1) as a means of probing the chemical structure of coal, and 2) in order to optimize the products for potential uses, for example as a fuel or chemical feedstock. Studies of this nature can be enhanced by tandem mass spectrometry (MS/MS) which is particularly well-suited to the analysis of complex mixtures (1-4). Previous investigations have shown the applicability of MS/MS to the analysis of both polynuclear aromatic hydrocarbons (PNAs) and related compounds. Particular examples include hydrodenitrogenation products incl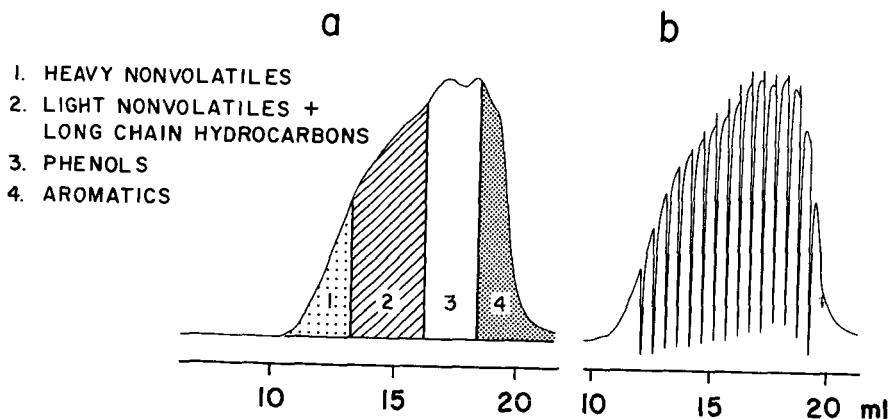uding tetrahydro nitrogen-containing PNAs (5), long chain alkyl PNAs in a boghead coal (6), and sulfur-containing PNAs in a coal liquid examined after chemical reduction (7). These analyses have made use of all three of the principal scanning modes (8) of MS/MS: daughter spectra for identification of specific constituents, parent spectra for characterization of components having a common substructure, and neutral loss spectra for characterization of constituents having a common functional group. A daughter spectrum is obtained by selecting the ion of interest in the first stage of mass analysis and passing it into the collision cell where it undergoes collision induced dissociation (CID). The resulting fragment ions are then mass analyzed with the second mass analyzer. To obtain a parent spectrum, the second mass analyzer is set to pass a selected fragment ion which results from CID and represents the substructure of interest. The first mass analyzer is scanned over the entire mass range of interest. Neutral loss spectra are obtained by scanning both mass analyzers simultaneously with a mass offset between the two analyzers corresponding to the mass of the selected functional group which is lost as a result of CID. Combining MS/MS with specific chemical degradation reactions as well as using differing modes of ionization, further enhances the utility of MS/MS as a means for addressing the complex nature of fuel materials. The focus of this paper is an attempt to tie a number of investigations, including characterization of products of specific chemical degradations, liquefaction processes and optimization of processing conditions, to a central theme; characterization of the chemical nature of coal.

EXPERIMENTAL

The MS/MS results were obtained using a Finnigan MAT triple quadrupole mass spectrometer (9,10). The samples were admitted into the mass spectrometer via the direct insertion probe. Isobutane chemical ionization was employed at a source pressure of 0.4 torr for a typical case. Argon was used as the collision gas and multiple collision conditions, 2 mtorr, were

chosen to increase the extent of fragmentation. The collision energy chosen was 20 eV.

The specific chemical degradation reactions which have been employed include: ruthenium tetroxide oxidation using ruthenium (III) trichloride in a mixture of water, acetonitrile and carbon tetrachloride at ambient temperature (11), calcium/mixed amine reduction (12), supercritical (steam) extraction (13) and potassium/crown ether reduction (14). In each instance the collaborators referenced provided the chemically degraded materials.

RESULTS AND DISCUSSION

Central to this work has been the identification of specific components not only to characterize them for their intrinsic importance but also to use this information to probe the nature of their possible precursors. Additionally, this work has focussed on the value of MS/MS as a method for comparing product distributions 1) as a means of improving processing conditions for obtaining the desired end product, and 2) to better understand the chemical nature of the original starting material, coal. With these objectives in mind, the differing types of specific chemical degradations as well as scan modes and ionization techniques amenable to MS/MS can be seen to represent an integrated approach to a well-defined problem.

A novel approach to the analysis of sulfur-containing PNAs used a calcium/mixed amine reduction of an SRC II middle heavy distillate (7). Using negative ion chemical ionization (NICI), a series of alkylbenzothiophenes were identified from their reduction products by obtaining a parent scan of m/z 122. The ion at m/z 122 corresponds to the thiotropylium radical anion which is a characteristic fragment of o-ethylthiophenol, the reduction product of benzothiophene. This methodology has been extended to an SRC II heavy distillate fraction as well as four coal samples with varying degrees of both total and organic sulfur content. Interestingly, the heavy distillates did not show the presence of alkylbenzothiophenes but rather displayed a series of alkyldibenzothiophenes, again characterized using a parent scan of m/z 122. (The ion at m/z 122 is also a characteristic fragment ion of o-cyclohexylthiophenol, the reduction product of dibenzothiophene.) Furthermore, a number of higher molecular weight sulfur-containing PNAs have also been tentatively identified (using different parent scans) including a series of alkylnaphthothiophenes as well as alkylbenzonaphthothiophenes. The reduced coal sample with the highest organic sulfur content, PSOC 740, was found to have a large abundance of dibenzothiophene, as indicated by the presence of the reduction product at m/z 191 in the parent scan of m/z 122 (Figure 1). This brings up an interesting question with regard to the dibenzothiphene in the coal - is it part of the macromolecular network or interstitially trapped material. The amount of dibenzothiophene identified in the other three coal samples was negligible. All four coals had a significant amount of S_x present as determined by a NICI parent scan of m/z 64, which can correspond to S_2^-. The amount of S_x found can be roughly correlated with the inorganic sulfur content of the four coal samples (see Table 1).

Another chemical reduction scheme, involving potassium/crown ether in tetrahydrofuran, has been used in a similar type of investigation. The emphasis of this work has been to probe the chemical structure of coal because this reaction, carried out at room temperature and normal pressure, may reduce the extent of breakdown of the macromolecular structure. Detailed carbon and hydrogen NMR studies from the reduction products of an Illinois No. 6 coal have indicated an abundance of extended chain methylenes, partially hydrogenated PNAs and significant amounts of the hydroxy functionality. Figure 2 is a comparison of the daughter spectrum of m/z 131 an abundant ion in the spectrum of the reduced coal product,

with the daughter spectrum of protonated dihydronaphthalene. The dihydro-naphthalene, the presence of which is inferred from the similarity of frag-mentation with the authentic compound, and its alkyl homologs may result from a Birch-type reduction of the corresponding alkyl naphthalenes. A series of protonated alkyl phenols extending to C_7 was identified in the same sample using a parent scan of m/z 95 (Figure 3). The first two members of the series protonated phenol (m/z 95) and protonated methyl-phenol (m/z 109) do not undergo CID to m/z 95 and therefore are not present in the parent spectrum. However, the presence of these two components as well as the other protonated alkyl phenols, m/z 123, 137, 151, 165, 179, and 193, were confirmed using daughter spectra. The principal components identified by MS/MS therefore correlate with structures determined in the NMR studies. Considering the mild reaction conditions it is possible the identified components result from enhanced solubilization and not breakdown of the macromolecular structure.

In addition to the MS/MS analysis of reduction products, the ruthenium tetroxide oxidation products of an Illinois No. 2 coal have been examined (15). In this study the carboxylic acids resulting from oxidation have been identified using both positive ion chemical ionization (PICI) as well as NICI. The emphasis of this work lies not in the identification of given components per se but rather in correlating the components identified with possible precursor structures present in the unreacted coal. For example, aliphatic dicarboxylic acids are a major reaction product of ruthenium tetroxide oxidation. Since this reaction occurs via oxidation of an aromatic carbon, these dicarboxylic acids can be postulated as resulting from alkyl bridges, for example, oxidation of tetralin can result in a significant amount of adipic acid (Figure 4). Comparison of the daughter spectrum of protonated adipic acid with the daughter spectrum of m/z 147 from the oxidized coal sample confirms the presence of adipic acid. Table II lists the most abundant types of compounds which have been identified. The presence of aromatic di, tri, and tetra carboxylic acids, can be correlated with oxidation of fused-ringed systems. It should be noted that aromatic carboxylic acids are detected as the corresponding anhydrides as a result of dehydration occurring in the hot mass spectrometer ion source. The absence of malonic acid in the oxidation product does not indicate the absence of methylene linkages but rather arises because of the added reacti-vity of the enolizable protons which can promote further oxidation.

In addition to the identification of specific components, tandem mass spectrometry is valuable as a tool for comparing the character of different samples. An example involves the analysis of the liquefaction products of hand-sorted coal macerals (16), exinite and vitrinite, in order to assess possible chemical differences. Three different fractions of the tetralin-liquefied macerals were examined by MS/MS; maltenes, asphaltenes, and pre-asphaltenes. The mass and MS/MS spectra of the maltene and asphaltene frac-tions indicated that maceral-related differences were quite small. Parent scans, however, provided ample information with regard to the presence of alkylbenzenes and naphthalenes. Likewise, the preasphaltene samples also produced little in the way of maceral-related differences. While the compounds identified in the two preasphaltene samples were essentially the same, differences in the relative amounts between the two samples were observed. Twelve different series of alkylhydroxyaromatics, including phenols, pyridinols, dihydroxybenzenes, indenols, indanols, naphthols, di and tetrahydronaphthols, dihydroxynaphthalenes, acenaphthols, anthracenols, and naphthylphenols, were confirmed using both parent and daughter scans. The same series of compounds were present in each maceral sample but the exinite sample had roughly ten times the concentration of hydroxyaromatics as did the vitrinite.

MS/MS can also be used as an aid to maximizing the information obtained from a chemical process. One such process on which this approach has been tested involved the supercritical steam extraction of sulfur from coal. Studies of this type are aimed at finding both economical and efficient means for reducing the sulfur content in coal prior to its being burned. Initial MS/MS studies used a parent scan of m/z 184 to identify the targeted species – alkyl dibenzothiophenes. However, no effect on the relative abundance of dibenzothiophene in the extracted residue was found when either the pressure or extraction time of the process was varied, in spite of large differences in total sulfur removed. Further studies in progress are aimed at extending the number of forms of sulfur being tested as well as including some additional process variables in the sampling scheme.

Tandem mass spectrometry is an efficient way of seeking differences in fuel samples. This can be illustrated by a case involving nine different samples obtained from the same coal, Illinois No. 6, using a variety of extraction and liquefaction conditions. This work is aimed at providing information on the guest-host model for coal structure. That is, are there conditions which can release a signficiant concentration of small molecules which are entrapped in the macromolecular network. The hexane-soluble extracts of these nine samples were analyzed by MS/MS. While the amount of hexane-soluble material extracted varied from sample to sample, the major alkyl series identified were essentially the same in all nine samples, being dominated by a series of alkyl acenaphthenes (Figure 5). The alkyl chain extends to C_9 as shown in the parent spectrum of m/z 155 from one of the tetralin-liquefied samples. The C_2-C_5 alkylated acenaphthenes (m/z 183, 197, 211, 225) appear to be the most abundant. This is also consistent with the chemical ionization mass spectrum. These results imply that while progressively harsher extraction/liquefaction conditions can release more material, the chemical nature of that material, in terms of components as well as the alkyl nature, is very similar, at least within the narrow confines of this investigation.

Tandem mass spectrometry has been used to probe a number of questions involving the chemical nature of fuel-related materials. With the available scan modes – daughter, parent, and neutral loss – and ionization techniques it is possible to probe increasingly complex questions concerning the structure of coal. This allows the identification of specific components in coal-derived materials for coal structure characterization and liquefaction product analysis, in addition to comparative studies for process optimization, maceral-related comparisons and investigation of the guest/host coal structure model.

References

1. McLafferty, F.W., Ed., <u>Tandem Mass Spectrometry</u>, John Wiley and Sons, New York, 1983.

2. Cooks, R.G. and Busch, K.L., <u>J. Chem. Ed.</u>, <u>59</u> (1982) 926.

3. Ciupek, J.D., Zakett, D., Cooks, R.G., and Wood, K.V., <u>Anal. Chem.</u>, <u>54</u> (1982) 2215.

4. Cooks, R.G. and Glish, G.L., <u>Chem. Eng. News.</u>, <u>59</u> (1981) 40.

5. Wood, K.V., Schmidt, C.E., Cooks, R.G., and Batts, B.D., <u>Anal. Chem.</u>, <u>56</u> (1984) 1335.

6. Wood, K.V., Cooks, R.G., Mudamburi, Z., and Given, P.H., <u>Org. Geochem.</u>, <u>7</u> (1984) 169.

7. Wood, K.V., Cooks, R.G., Laugal, J.A., and Benkeser, R.A., <u>Anal. Chem.</u>, <u>57</u> (1985) 692.

8. Ciupek, J.D., Cooks, R.G., Wood, K.V., and Ferguson, C.R., <u>Fuel</u>, <u>62</u> (1983) 829.

9. Slayback, J.R.B. and Story, M.S., <u>Ind. Res. Dev.</u>, Feb. (1981) 129.

10. Yost, R.A. and Fetterolf, D.D., <u>Mass Spectrom. Rev.</u>, <u>2</u> (1983) 1.

11. Stock, L.M. and Tse, K.T., <u>Fuel</u>, <u>62</u> (1983) 974.

12. Benkeser, R.A., Belmonte, F.G., and Kang, J.J., <u>J. Org. Chem.</u>, <u>48</u> (1983) 2796.

13. Tu, S.T., Mallinson, R.G., Greenkorn, R.A., and Chao, K.C., Presented at AIChE 1984 Winter Meeting, Atlanta, GA, March 1984.

14. Narayan, R. and Tsao, G.T., ACS Div. Fuel Preprints, <u>28</u> (1983) 261.

15. Singleton, K.E., Cooks, R.G., Wood, K.V., Tse, K.T., and Stock, L.M., submitted.

16. Wood, K.V., Albright, L.F., Brodbelt, J.S., and Cooks, R.G., <u>Anal. Chim. Acta</u>, in press.

Table I. Comparison of the amount of S_x determined from a parent spectrum of m/z 64 (S_2^-) with the inorganic sulfur content of the four coals studied.

Coal	Inorganic Sulfur	Counts of S_x (x10^3)
PSOC 685	1.3%	not detected
PSOC 1300	2.2%	2
PSOC 740	2.3%	7.5
PSOC 1143	3.9%	38

Table II. Dominant carboxylic acids identified in the ruthenium tetroxide oxidation of an Illinois No. 2 coal.

Dibasic Aliphatic Acids	$HOOC(CH_2)_x COOH$, x = 0,2-8
Dibasic Aromatic Acids	C_0-C_2
Tribasic Aromatics Acids	C_0-C_2
Tetrabasic Aromatic Acids	C_0-C_2
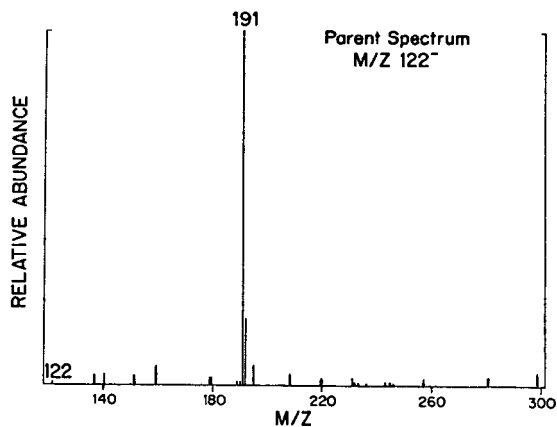
Figure 1. Parent spectrum of m/z 122 (negative ions) from the calcium/mixed amines reduction of a PSOC 740 coal sample, indicating the presence of the reduction product of dibenzothiophene (collision energy 20 eV; argon collision gas pressure 2.0 mtorr).

73
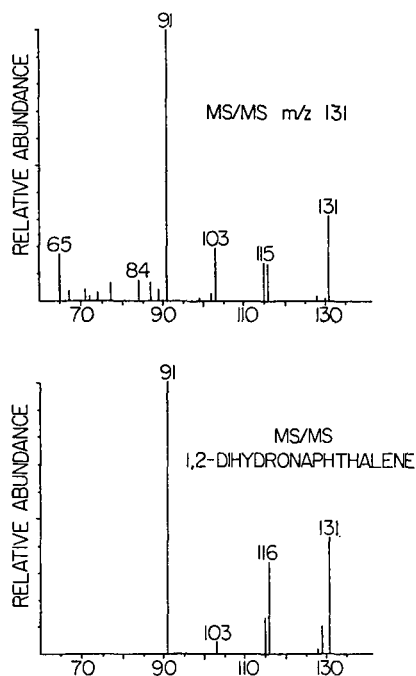
Figure 2. Comparison of the daughter spectrum of protonated dihydronaphthalene with the daughter spectrum of m/z 131 from the potassium/crown ether reduction of an Illinois No. 6 coal (collision energy 20 eV; argon collision gas pressure 2.0 mtorr).
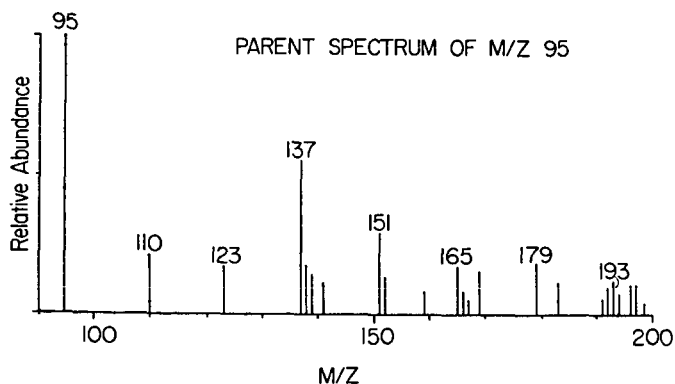
Figure 3. Parent spectrum of m/z 95, for the presence of alkyl phenols, from the potassium/crown ether reduction of an Illinois No. 6 coal (collision energy 20 eV; argon collision gas pressure 2.0 mtorr).

74

Parents of 155⁺

Figure 5. Parent spectrum of m/z 155, for the presence of alkylacenaphthenes, from the tetralin-liquefied Illinois No. 6 coal hexane soluble fraction (collision energy 20 eV; argon collision gas pressure 2.0 mtorr).

oxidized coal

$HOOC(CH_2)_4COOH_2^+$

Figure 4. Comparison of the daughter spectrum of protonated adipic acid with the daughter spectrum of m/z 147 from the ruthenium tetroxide oxidation of an Illinois No. 2 coal (collision energy 20 eV; argon collision as pressure 2.0 mtorr).

Analysis of Commercial Diesel Fuels by Preparative High Performance Liquid Chromatography and Gas Chromatography – Mass Spectrometry

S. G. Thomas, J. P. Kleiman and V. O. Brandt

Ethyl Corporation
Ethyl Technical Center
P. O. Box 14799
Baton Rouge, LA 70898

INTRODUCTION

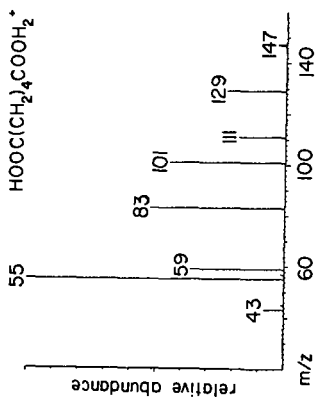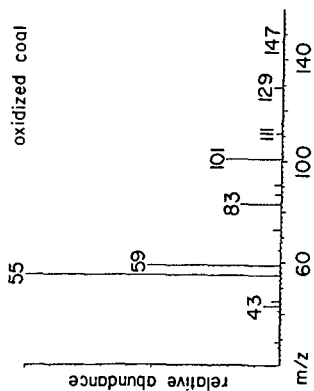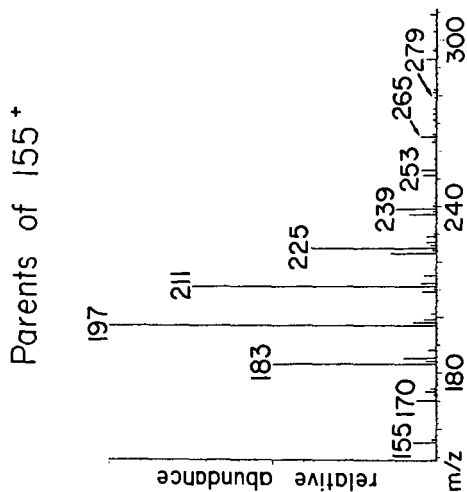Diesel fuel is a complex mixture of hydrocarbons with a boiling range from about 400 to 670°F. Recently, the emphasis on the diesel engine in passenger cars increased (1). It is expected that the demand for middle distillates will increase while the quality of feedstocks will decrease (2-5). Cetane number and stability are two measures of diesel fuel quality. Nozzle coking in diesel engines for passenger cars is another problem (6). This expected lower quality is related to the increased use of blending components from heavy oil cracking processes. The ability to define diesel fuel composition will become increasingly important to understand the relationship between fuel composition and cetane number, stability, coking tendency and other performance parameters.

A major problem is the separation and identification of pure compounds or classes of compounds from the complex hydrocarbon mixtures in diesel fuel. Many refinery test laboratories use the fluorescent indicator analysis method (FIA; ASTM D-1319) to separate and quantify saturates, olefins and aromatic hydrocarbons in diesel fuels. Another approach is to determine aromatic content by nuclear magnetic resonance spectroscopy (7). As pointed out by M. E. Myers (7) these methods do not give the same result because they do not measure the same properties.

Types of hydrocarbons in middle distillates may be determined by a combination of silica gel chromatography and mass spectrometry (ASTM D-2425 and -2549). A major disadvantage to this approach is the slowness of open column chromatography. We have developed an alternate to this ASTM procedure by using a preparative High Performance Liquid Chromatograph and a Gas Chromatograph-Mass Spectrometer to analyze two commercial diesel fuels. This modified ASTM method is faster and provides more efficient separations than ASTM D-2549. In this paper, this modified ASTM procedure will be described and the results compared to those obtained from the FIA (ASTM D-1319) and NMR procedures (7). Application of solvent extraction and clay chromatography also is demonstrated. These techniques separate polar components and polynuclear aromatics from other diesel fuel components.

EXPERIMENTAL

Instrumentation

The prep HPLC used to separate the diesel fuels into hydrocarbon group types was a Prep LC/System 500 with a refractive index detector from Waters Associates. An ultraviolet detector from Gow Mac was also used to monitor aromatic components. Qualitative hydrocarbon group types in chromatographic fractions were obtained with a Hewlett-Packard

5993 GC-MS while quantitative estimates were obtained with a Finnigan MAT-4000 GC-MS. ASTM D-2425 was employed for these quantitative estimates. A Varian FT-80A NMR was used for proton NMR analysis.

Chromatographic Separations

About 10 grams of diesel fuel was added to a silica gel column on the Prep HPLC. HPLC grade hexane was used to separate the sample into seven 250 mL fractions. Hexane was removed from each fraction with a rotary evaporator. Each fraction was weighed and analyzed by GC-MS for hydrocarbon type. Recovery from the chromatographic column with hexane was about 90 wt%.

Gas Chromatographic Analysis of Paraffin Fraction

The column was stainless steel (6 ft by 1/8 inch) with 10% OV-101 on 80/100 W HP. Initial column temperature was 75°C and programmed at a rate of 5°C/min to a final temperature of 330°C. A thermal conductivity detector was used with helium as a carrier gas (30 cc/min) and a 1.5 µl injection volume.

Dimethylsulfoxide Extraction

200 mL of diesel fuel was extracted with 50 mL of reagent grade dimethylsulfoxide (DMSO). The bottom DMSO layer was separated from the top hydrocarbon layer. About 120 mL of distilled water was added to the DMSO layer. A ring of dark colored liquid separated on top, which was the polar components. 10 mL of heptane was then added and the contents mixed. This top organic layer was isolated, dried with sodium sulfate and filtered. The heptane was evaporated under a stream of nitrogen and this organic layer analyzed by GC-MS.

Clay Chromatography

The procedure, which was developed by Pei, Britton and Hsu and described in reference (8) was used.

RESULTS AND DISCUSSION

Hydrocarbon Composition of Diesel Fuels

Two 38 cetane number (ASTM D613) commercial diesel fuels were separated on silica gel into fractions. Hydrocarbon composition of each fraction was determined by qualitative and quantitative (ASTM D-2425) GC-MS.

Qualitative GC-MS analyses confirmed that silica gel chromatographic separation yields fractions rich in paraffins and cycloparaffins, alkylbenzenes, indanes or tetralins, naphthalene, alkyl naphthalenes, acenaphthenes and biphenyls and tricyclic aromatics. The separation of each group type of hydrocarbons in "Fuel B" as a function of elution volume (polarity) is summarized in Figure 1. Because this separation is done on a preparative scale, each class of hydrocarbons in not completely separated. Each fraction contains two or more classes of hydrocarbons. In the conventional ASTM method, individual hydrocarbon types or classes are not separated. Aromatics are separated from non-aromatics and characterized by mass spectrometry.

Although individual hydrocarbon classes are not separated

completely, this modified quantitative GC–MS approach allows a comparison of the concentration of group types of hydrocarbons of different fuels. A comparison between "Fuel A" and "Fuel B" is summarized in Table 1.

The major difference in hydrocarbon composition between the two fuels is in alkyl naphthalene concentration. Naphthalenes are present at 31 wt% concentration in "Fuel B" and 9.1 wt% in "Fuel A." Other differences are in alkylbenzenes and indanes or tetralins present. We are not certain that differences in alkylbenzene concentration are analytically significant (7.7 wt% in "Fuel B" and 11.7 wt% in "Fuel A"), whereas we believe that differences in indane or tetralin are significant. "Fuel A" has a higher concentration of indanes or tetralins (10.3 wt%) than "Fuel B" (1.2 wt%). Other differences found are of the order of the reproducibility of ASTM D–2425.

Although aromatic content is about the same in both fuels by FIA analysis (40.5 vol% in "Fuel A" and 42 vol% in "Fuel B"), they differ by proton NMR (7) analysis (28.9 mole% in "Fuel A" and 36.7% in "Fuel B"). This difference is due to the fact that only aromatic moieties (carbons) are counted by NMR whereas alkyl aromatics and indane types are counted in the FIA method. Total weight percent of alkylbenzenes, indanes or tetralins and alkylnaphthalenes in "Fuel A" (31 wt%) are equal to the total amount of alkylnaphthalenes found in "Fuel B" (31 wt%). The higher number of aromatic carbons in naphthalenes versus benzenes or indanes or tetralins is the reason that "Fuel B" shows a higher amount of aromatics by NMR than "Fuel A."

The total concentration of aromatics found by GC–MS is about the same as that found by FIA analysis (about 40.4 wt% in "Fuel A" and 42.8 wt% in "Fuel B." One difference between the methods is that GC–MS measures weight percent and FIA volume percent. Both methods use a silica gel column for the separation and count as aromatic the total weight or volume of any components that contain aromatic rings. For these reasons, it is not surprising that both methods give similar results. However, neither FIA nor NMR should be used alone to obtain aromatic content. The combination provides some insight into the type of aromatics that may be present and a more accurate picture of total aromatic composition.

Composition of Paraffinic Fraction

The paraffinic fraction composition of two fuels was studied by gas chromatography and revealed more than 45 peaks. About 52-54 normalized weight percent of the paraffinic fractions were normal paraffins with the remainder being branched paraffins, olefins and/or cycloparaffins. "Fuel A" has a higher relative concentration of C_{10} to C_{13} n-paraffins, while "Fuel B" is higher in C_{14} to C_{21} n-paraffins. These results are summarized in Table 2.

Polar Components in Fuels

"Fuel A" and "Fuel B" were extracted with dimethylsulfoxide to isolate polar components for identification. GC/MS analysis of this polar fraction showed alkylated condensed aromatic derivatives of naphthalene, anthracene, phenanthrene, dibenzothiophene, carbazole and dibenzofuran.

About 1 gallon of "Fuel B" was chromatographed on a clay

column (prep HPLC) to remove polar components for identification. GC–MS of the polar fraction identified it to be alkylated carbazoles.

Table 3 lists example structures of components found in polar fractions.

SUMMARY

Compositions of hydrocarbons in two commercial diesel fuels have been obtained by a combination of preparative High Performance Liquid Chromatography (prep HPLC) and Gas Chromatography-Mass Spectroscopy (GC-MS). Two different GC-MS approaches are used; the first is qualitative and the second quantitative (modified ASTM-D-2425). Fuels are separated on a preparative silica gel column with a hexane solvent into group hydrocarbon types: paraffins, alkylbenzenes, indanes or tetralins and alkyl naphthalenes. Concentrations of each class of identified hydrocarbons are measured and compared for the two fuels.

Each commercial fuel also was analyzed by Nuclear Magnetic Resonance (NMR) and the Fluorescent Indicator Analysis (FIA ASTM-D-1319) specifically for aromatic content. Differences in aromatic content obtained for each fuel by these two techniques are explained by results from the prep HPLC/GC-MS approach. This paper demonstrates how aromatic content obtained by either the NMR or FIA methods alone is not adequate and may be misleading.

It is important to understand the relationships between fuel composition and cetane number, stability and coking tendency. By studying and understanding these relationships, the refiner will be able to more accurately prescribe treat levels of diesel ignition improvers (such as Ethyl's DII-3) or broader treatment products (such as Ethyl's DPI's) which reduce coking, enhance stability and provide other benefits.

In an effort to isolate and identify polar components in fuels, two approaches have been explored: (1) dimethylsulfoxide (DMSO) extraction; and (2) clay chromatography in combination with GC-MS. The following types of polar compounds and polynuclear hydrocarbons were identified in DMSO fuel extracts: anthracenes, naphthalenes, phenanthrenes, carbazoles, dibenzothiophenes, dibenzofurans, etc. Preparative clay chromatography of one of these 38 cetane number diesel fuels selectively allows separation of only carbazoles.

Besides providing detailed fuel composition, multigram quantities of selected hydrocarbons, can be isolated by the preparative chromatography approach outlined in this paper. These hydrocarbons could be used as analytical standards, further separated and analyzed or tested with or without additives in a bench test or engine. Results from this test work could provide a more fundamental understanding of the relationship between fuel structure and additive response.

ACKNOWLEDGEMENT

REFERENCES

1. Collins, J. M., and Unzelman, G. H., "Diesel Trends Emphasize Cetane Economics, Quality and Production," 47th Midyear API Refining Meeting, New York, May 1982.

2. Schrepfer, M. W., Arnold, R. J., and Stansky, C. A., "Distillate Stability Ensured by Testing Treatment," Oil & Gas Journal, pp. 79-84, January, 1984.

3. Fortangel, J., Hardenburg, H. O., and Gairing, M. "Requirements of Diesel Fuel Quality - Effects of Poor Quality Fuels," American Petroleum Institute, 47th Midyear Refining Meeting, New York, May 11, 1982.

4. Carnus, M. J., "Influence dus carburant sur les performances et les ´emissions du moteur Diesel," Ingenieurs De L´ Automobile, April-May, 1981.

5. Regneault, M., Pierz, J., and Cahill, G. F., "Improvements of Combustion of a Diesel Oil by Means of Additives," AGELFI European Automotive Symposium, Brussels, Belgium, October 20-21, 1983.

6. Lenane, D. L., Gluckstein, M. E., and Reid, R. C., Jr., "Impact of Diesel Fuel Quality Trends and Effects of Diesel Performance Improver Additives," Japan Petroleum Institute Conference, Tokyo, Japan, October 18-19, 1984.

7. Myers, M. E., "Determination of the Aromatic Content of Diesel Fuels by Proton and Carbon-13 Nuclear Magnetic Resonance Spectrometry," prepared for presentation before a meeting of the Coordinating Research Council Air Pollution Research Advisory Committee, Composition of Diesel Particulate Exhaust Chemical Characterization Panel, Dearborn, Michigan, March 3, 1981, GM Research Paper No. 3621, GM Research Laboratories, Warren, Michigan.

8. Pei, P., Britton, J., Hsu, S., Journal of Liquid Chromatography, 6(4), 627-645 (1983).

FIGURE 1

Separation of "Fuel B" into Hydrocarbon
Group Types on Silica Gel

Tricyclic Aromatics

Acenaphthenes & Biphenyls

Alkyl Naphthalenes

Naphthalene

Indanes or Tetralins

Alkylbenzenes

Paraffins and Cycloparaffins

0	0.25	0.50	0.75	1.0	1.25	1.50	1.75

Elution Volume (liters) of Hexane on Silica Gel

Hydrocarbon Group Type

81
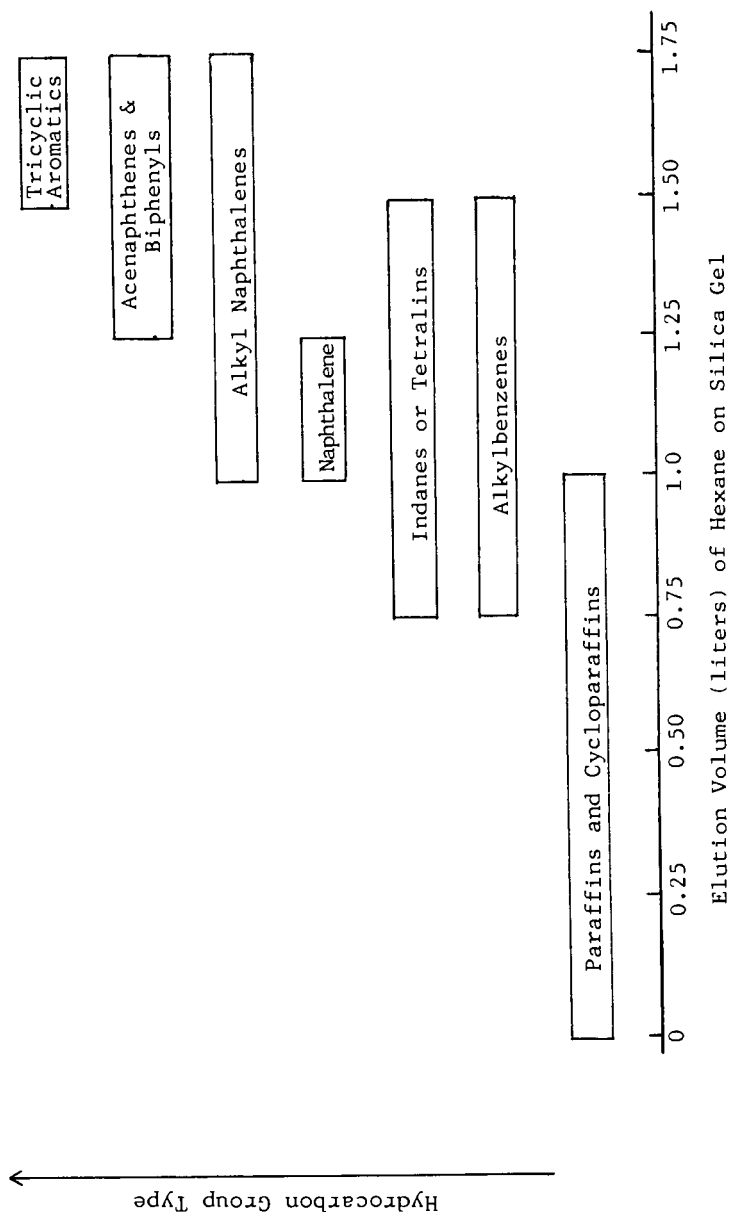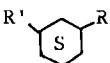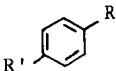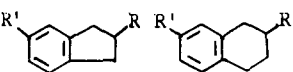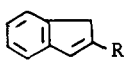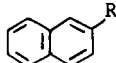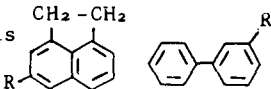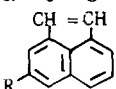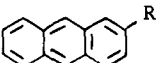
TABLE 1

Hydrocarbon Composition of "Fuel A" and "Fuel B"

by Gas Chromatography - Mass Spectrometry (ASTM D2425)

Hydrocarbon Group Type	Example	"Fuel B" (wt%)	"Fuel A" (wt%)
Paraffins	$CH_3-(CH_2)_{14}-CH_3$	46.2	50
Monocycloparaffins		2.2	1
Alkylbenzenes		7.7	11.7
Indanes or Tetralins		1.2	10.3
Indenes		0	1.1
Naphthalene		0.1	0.6
Alkyl Naphthalenes		31.0	9.1
Acenapthenes and biphenyls		2.9	3.9
Acenaphthylenes		0.5	1
Tricyclic aromatics		0.1	2.2
Material Balance Total Diesel Fuel Components Accounted For		91.9	91.5
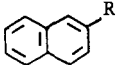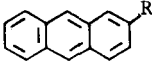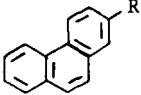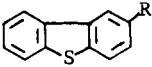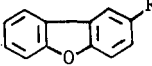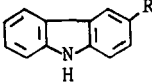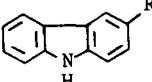
R' and R - alkyl groups or hydrogen

82

TABLE 2

Relative Amounts of Normal Paraffins

in Paraffinic Fractions of Diesel Fuels by Gas Chromatography

Normal Paraffin	Normalized Wt%	
	"Fuel A"	"Fuel B"
C_{10}	0.9	0.4
C_{11}	2.9	1.1
C_{12}	4.9	2.0
C_{13}	6.7	3.8
C_{14}	8.5	8.9
C_{15}	8.0	9.9
C_{16}	7.4	9.0
C_{17}	6.0	8.6
C_{18}	2.8	3.8
C_{19}	1.3	3.0
C_{20}	0.8	1.6
C_{21}	0.7	0.9
C_{22}	0.5	0.5
C_{23}	0.3	–
Total Weight Percent	51.7	53.5

TABLE 3

Example Structures of Components in Polar Diesel Fuel Fractions

Identified by Gas Chromatography – Mass Spectrometry

Fuel	Method	Components	Name
"Fuel A" and "Fuel B"	Dimethylsulfoxide Extraction		alkyl naphthalene
			alkyl anthracene
			alkyl phenanthrene
			alkyl dibenzothiophene
			alkyl dibenzofuran
			alkyl carbazole
"Fuel B"	Clay Chromatography		alkyl carbazole

R - alkyl groups

COMPUTER ENHANCED SEPARATION OF COMPOUND CLASSES IN FUEL MIXTURES
USING A COMBINED LC-MS APPROACH

Barbara L. Hoesterey, William H. McClennen, Willem Windig and Henk L.C. Meuzelaar

University of Utah, Biomaterials Profiling Center
391 S. Chipeta Way, Suite F, Research Park
Salt Lake City, Utah 84108

INTRODUCTION

Liquid Chromatography (LC) methods play an important role in coal liquid analysis
both as pre-separation techniques for further analytical studies as well as coal
liquid characterization methods in their own right. Among the many different LC
separation methods for coal liquids, those described by Farcasiu (1) and Dark *et al.*
(2) have gained relatively wide acceptance. A modified version of an open column
silica gel separation method developed by Rubin *et al.*(3) was described by McClennen
et al.(4) and adapted for GC/MS as well as direct low voltage MS studies. This
modified technique involves the use of four increasingly polar eluents: namely
pentane, pentane/benzene (8:1), benzene/ether (4:1) and benzene/methanol (1:1). Low
voltage MS analysis of the four subfractions obtained from coal tars produced by a
range of different liquefaction methods consistently reveals the following compound
categories: (1st subfraction) aliphatic, naphthenic and aromatic hydrocarbons; (2nd
subfraction) polynuclear aromatic hydrocarbons; (3rd subfraction) hydroxyaromatics;
and (4th subfraction) polyfunctional and nitrogen compounds (4,5).

In most instances, the first (pentane) fraction is still too complex for a useful
degree of compound class quantitation since this fraction contains a variety of
aliphatic compound series as well as alicyclic, hydroaromatic and aromatic series.
On the basis of elementary LC principles, however, it can be predicted that the
various hydrocarbon compound classes will elute at slightly different points in
time. In view of the broad range of molecular sizes as well as structures involved
it would be unrealistic to expect a complete separation, even when using sophisti-
cated HPLC methods, therefore considerable overlap will occur among the various
compound series. Nevertheless, combination with MS techniques opens up the possi-
bility of achieving numerically enhanced separation between incompletely resolved
chromatographic peaks. This approach is widely used in combined GC/MS techniques.
However, whereas on-line GC/MS instrumentation is widely available, on-line LC/MS
methods are still under development and require expensive, dedicated equipment. In
contrast, off-line LC/MS procedures can be carried out with relatively simple LC and
MS equipment as demonstrated by Meuzelaar *et al.* (5). Preliminary results of such
an off-line LC-MS approach as applied to the pentane LC fraction of a heavy coal
pyrolysis tar, will be reported here.

EXPERIMENTAL

The pentane LC fraction of a heavy pyrolysis tar produced by a pilot plant scale
Lurgi retort run of a Blind Canyon seam (Wasatch Plateau field, Utah) coal was
prepared according to the method described by McClennen *et al.* (4). Subsequently,
this pentane fraction was subfractionated over a 0.7 cm dia. X 29 cm long glass
column packed with activated 120/200 mesh silica gel (Baker analyzed reagent) using
hexane (pesticide grade) as the eluent. Approximately 0.7 g of the pentane LC
fraction (a viscous liquid) were layered on the silica gel column. Thirty ml of
hexane were used to elute the tar fraction. The first ten fractions were collected
every 0.5 to 0.75 ml. Fractions 11 to 17 were collected every 1 to 1.5 ml.
Fractions 18 and 19 were collected every 2 ml. Fractions were evaporated with a
flow of nitrogen gas to between one half and one fourth volume.

The nineteen subfractions were analyzed by low voltage (12 eV) mass spectrometry using a heated inlet and capillary tube sample introduction procedure as described by McClennen et al. (5). Eight hundred scans over the mass range m/z 20 to 260 were summed for each subfraction. Data analysis was performed using the factor analysis routine of the SPSS program package (6) in combination with factor rotation methods developed by Windig et al. (7).

RESULTS AND DISCUSSION

The low voltage mass spectra of the original Lurgi tar and its pentane LC fraction, shown in Figure 1, illustrate the effectiveness of the LC procedure in separating hydroxyaromatic series (e.g., phenols and indanols) which appear in the benzene/-ether fraction (49% yield; not shown) from the hydrocarbon components. Moreover, although some three and four ring aromatic hydrocarbons, e.g., phenanthrene/-anthracene and pyrene, appear in the pentane fraction (Figure 1b) their relative abundance is decreased in comparison with the spectrum of the whole tar (Figure 1a). This is due to the fact that polynuclear aromatic hydrocarbon series are concentrated in the second (pentane/benzene) fraction (not shown; see reference 8) which accounts for 9% of the total tar.

When evaluating Figure 1, it should be pointed out that not all of the Lurgi tar was vacuum distillable (residue at 400°C ~5%; see reference 8). Therefore, Figure 1a represents a combined evaporation/pyrolysis mass spectrum. Moreover, some of the higher boiling tar components (e.g., vacuum distillable between 200°C and 400°C) may have been lost by condensation in the mass spectrometer inlet. To a lesser extent, a similar problem may exist with the pentane fraction in Figure 1b. Furthermore, it should be pointed out that the chemical identities of the ion species outlined in Figure 1, as well as in subsequent figures, are tentative only since these were based on prior experience with other coal tars (4,8,9) rather than on positive identification by combined GC/MS (4) or MS/MS (10) techniques.

Figure 2 shows that the expected separation of hydrocarbon compound classes during elution with hexane (or pentane) from the silica gel column does indeed take place. Subfractions 1 (Figure 2a), 11 (Figure 2b) and 19 (Figure 2c) are found to contain primarily aliphatic hydrocarbons, cyclic terpenoids and alkylsubstituted aromatics, respectively. The aliphatic pattern in Figure 1a exhibits the familiar alkane/-alkene/diene triplets up to C_{18} (probably continuing beyond the recorded mass range) illustrating that good quality aliphatic hydrocarbon spectra are obtained under the low voltage electron ionization conditions used in this experiment. Through subsequent fractions the relative contribution of the alkane components diminishes in favor of the olefinic compound series (not shown) until isoprenoid-type spectral patterns appear in fractions 10 and 11. The terpenoid pattern in fraction 11 (Figure 2b) is dominated by the characteristic rearrangement-type fragment ion series from decalins and higher terpanes at m/z 82, 96 and 110 as well as equally characteristic fragment ions at m/z 163 ($C_{12}H_{19}^+$) and 191 ($C_{14}H_{23}^+$). The fragment ion at m/z 191 is often used in GC/MS studies of hydrocarbon fractions of geo-chemical origin to identify cyclic terpanes and terpenes (including sesqui-, di- and triterpanes and -terpenes) (11,12,13) although it is also a major fragment ion of the acyclic isoprenoid pristane (14). A closer inspection of the sesquiterpenoid molecular ion region of the spectrum in Figure 2b reveals the expected peaks at m/z 208 (sesquiterpanes) and 206 (sesquiterpenes). Upon following the evolution of these patterns through subsequent hexane fractions (e.g., 12 and 13; not shown) a gradual shift towards more unsaturated sesquiterpenoids (e.g., at m/z 204 and 202) can be observed, finally cumulating in the jump to m/z 198 (cadalene) at the start of the alkylnaphthalene series in the last four fractions (see fraction 19 in Figure 2c).

The foregoing discussion illustrates that at least three (aliphatics, naphthenics and aromatics), and perhaps as much as five (alkanes, olefins, alicyclics, hydro-aromatics and aromatics), compound classes can be seen to elute in consecutive fashion and, thus, can be evaluated qualitatively. However, significant problems are encountered when trying to obtain a quantitative estimate of the relative abundances and yields of these compound classes by means of selected ion intensities. Whereas m/z 191 and 156 are found to provide good elution profiles for the terpenoid and two ring aromatic fractions, respectively (see Figure 3), no completely satisfactory fragment ion signals are found for the aliphatic components, due to strong overlap with the alicyclic and aromatic compound groups, as shown in Figure 4.

In view of the fact the single variables prove unsatisfactory for quantitation purposes, multivariate approaches such as factor analysis appear to be indicated in this case. Figure 5 shows a plot of the scores of the first two factors obtained on the low voltage mass spectra of 17 of the original 19 subfractions (subfractions 3 and 14 were eliminated because of aberrant behavior in the factor analysis). Together these two factors explain as much as 72.9% of the total variance in the mass spectra. In other words, the intrinsic ("true") dimensionality of the data set is close to 2. This is typical of situations where only three components dominate the behavior of the data set. The ternary mixture nature of the subfractions is further indicated by the near triangular arrangement of the data points in Figure 5 with aliphatics (alkanes + olefinics), naphthenics (alicyclics + hydroaromatics) and aromatics representing the three corner points of the triangle. As shown in previous multivariate analysis studies of mass spectra of ternary mixtures (5,7,15) the relative concentration of the components in such mixtures can be directly estimated from the factor analysis scores. The factor scores of the three component axes A, B and C representing aliphatic, naphthenic and aromatic components, respectively, are plotted in Figure 6 and show the relative concentrations of these compound classes during elution of the subfractions from the silica gel column. However, calculation of absolute concentration values requires the availability of suitable reference standards (e.g, reference mixtures obtained by repeated LC analysis of representative coal tars) and has not been attempted here.

It should be noted that the factor score plot in Figure 6 shows a numerically enhanced separation of the aliphatic and naphthenic compound classes in comparison to the selected ion intensity plots in Figure 4. Finally, it should be pointed out that the aliphatic and naphthenic compound classes in Figure 6 may each be subdivided further into at least two classes (as indicated by arrows) by using additional factor analysis data (factor III represents 12.7% of the total variance). This would result in a total of five compound classes: alkanes, olefins, alicyclics, hydroaromatics and aromatics.

REFERENCES

1. Farcasiu, M., Fuel 56, (1977) 9.

2. Dark, W.A., McFadden, W.H., Bradford, D.L., J. Chromatogr. Sci. 15, (1977) 454.

3. Rubin, I.B., Guerin, M.R., Hardigree, A.A., Epler, J.L., Environ. Res. 12, (1976) 358.

4. McClennen, W.H., Meuzelaar, H.L.C., Metcalf, G.S., Hill, G.R., Fuel 62, (1983) 1422.

5. Meuzelaar, H.L.C., McClennen, W.H., Final report to USAF, contract 416-84-004, "Tandem Mass Spectrometric Analysis (MS/MS) of Jet Fuels; Part II: Quantitative Aspects of Direct MS Analysis", 1984.

6. Nie, N.H., Hull, C.H.G., Jenkins, J.G., Steinbrenner, K., Bent, W.H., tistical Package for the Social Sciences:, 2nd Ed.; McGraw-Hill: New York, 1975.

7. Windig, W., Meuzelaar, H.L.C., Anal. Chem. 56, (1984) 2297.

8. Meuzelaar, H.L.C., Hoesterey, B.M., McClennen, W.H., Hill, G.R., "Composition and Stability of Pyrolytic Tars from HVB Wasatch Plateau Coals", Proceedings of EPRI's Clean Liquid and Solid Fuels Contractors' Conference, 1985.

9. Meuzelaar, H.L.C., Harper, A.M., Hill, G.R., Given, P.H., Fuel 63, (1984) 640.

10. Meuzelaar, H.L.C., McClennen, W.H., Tomlinson, J.H., Pope, D.L. "A Multimode Curie-point MS System for Rapid Characterization of Fossil Fuels and their Liquefaction Products", Proc. Int. Conf. on Coal Science, Dusseldorf, 1981, pp. 816-821.

11. Gallegos, E.J., J. Chromatogr. Sci. 19, (1981) 156.

12. Gallegos, E.J., Anal. Chem. 47, (1975) 1524.

13. Larter, S.R., in "Analytical Pyrolysis, Techniques and Applications", ed. K.J. Voorhees, publ. Butterworth, 1984, p. 212.

14. Given, P.H., "An Essay on the Organic Geochemistry of Coal" in Coal Science, Vol. 3, eds. M.L. Gorbaty, J.W. Larsen, and I. Wender, publ. Academic Press, 1984, p. 63.

15. Windig, W., Haverkamp, J., Kistemaker, P.G., Anal. Chem. 55, (1983) 81.

ACKNOWLEDGEMENTS
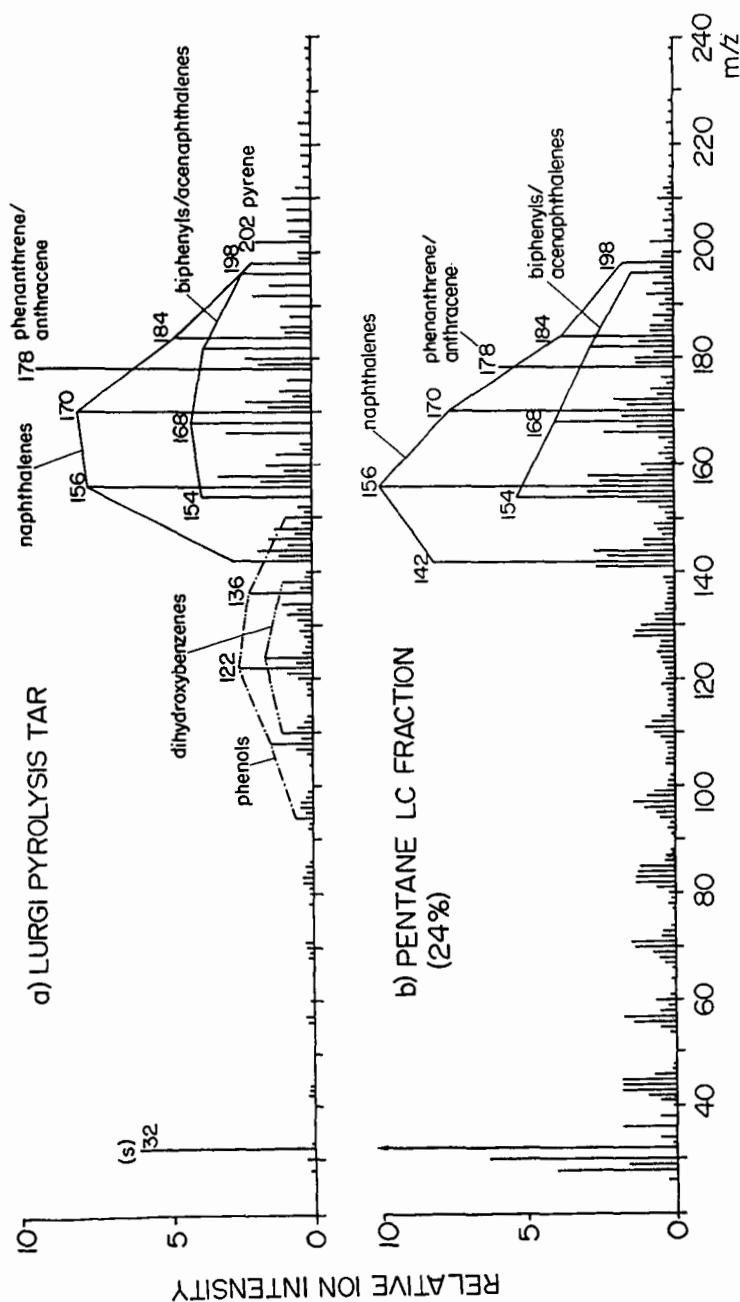
Figure 1. Low voltage volatilization/pyrolysis mass spectra of (a) the Lurgi pyrolysis tar and (b) the pentane LC fraction of the tar (24 wt. %) which was used in the subfractionation procedure. Note the absence of phenols and dihydroxybenzenes in the pentane fraction.
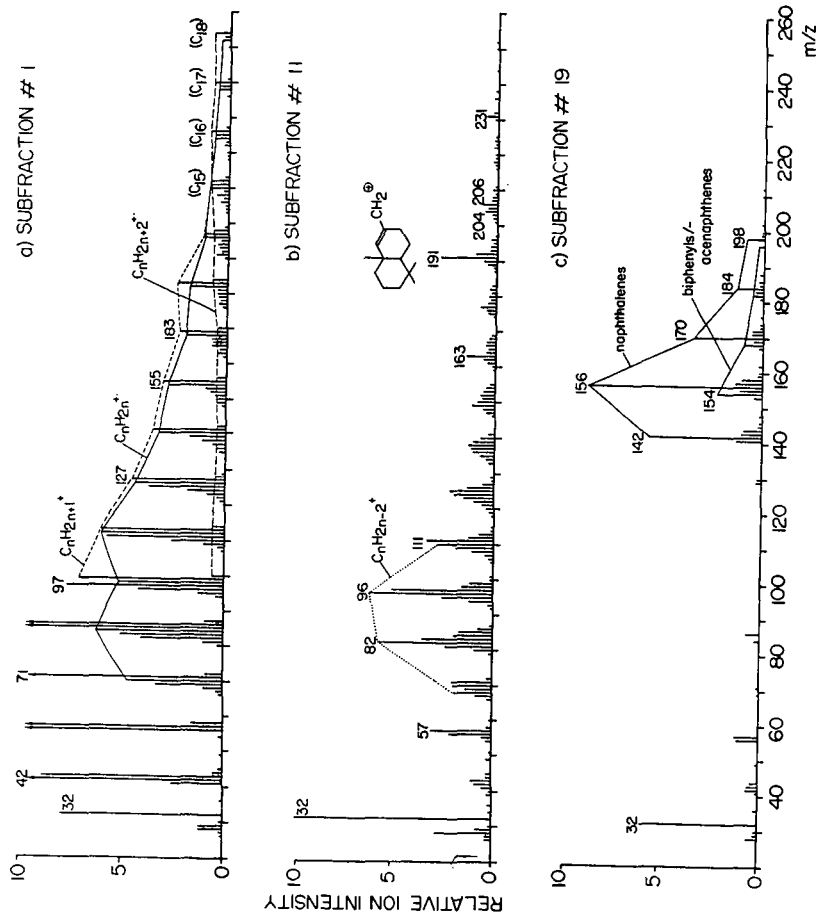
Figure 2. Low voltage mass spectra of selected subfractions of the pentane LC tar fraction. In (a) fraction 1, alkane and alkene molecular ions and fragments predominate; in (b) fraction 11, polyisoprenoid signals are evident; and in (c) fraction 19, naphthalene and acenaphthene and/or biphenyl molecular ions are present.
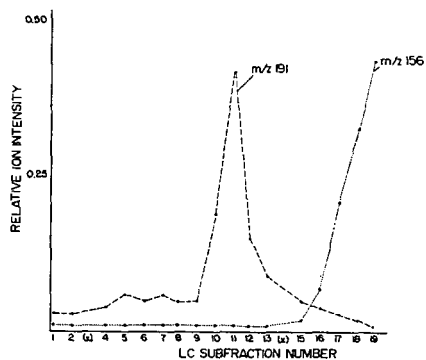
Figure 3. Relative ion intensities of selected ion intensities representing specific compound classes present in the subfractions. See text for details.
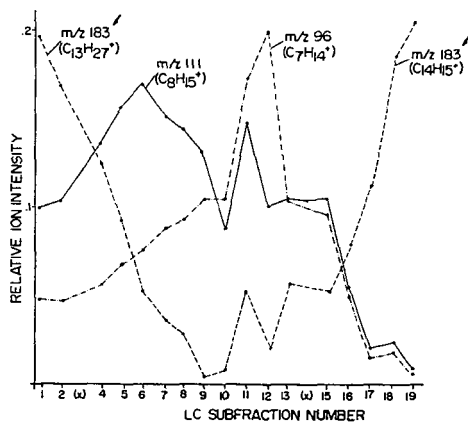
Figure 4. Relative ion intensities of selected fragment ions representing general compound classes present in the subfractions.

91
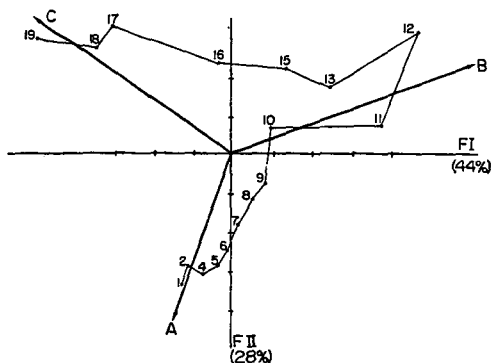
Figure 5. Score plot of subfractions on factors 1 and 2 with component axes indicated. Note resemblance to a ternary mixture diagram.
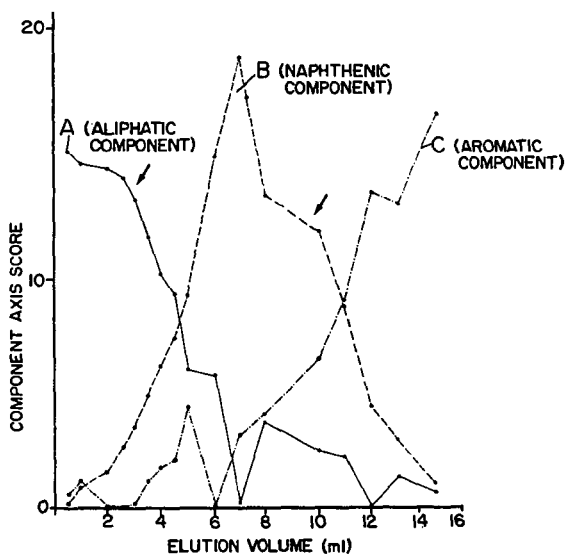
Figure 6. Relative scores of subfractions on components A, B, and C versus elution volume (calculated from factor score plot in Figure 5).

92

DETERMINATION OF POLYCYCLIC AROMATIC COMPOUNDS CONTAINING BOTH SULFUR AND NITROGEN HETEROATOMS IN COAL-DERIVED PRODUCTS

Masaharu Nishioka, Philip A. Smith, Gary M. Booth, and Milton L. Lee

Departments of Chemistry and Zoology, Brigham Young University, Provo, Utah 84602

Hirotaka Kudo, Daniel R. Muchiri, and Raymond N. Castle

Department of Chemistry, University of South Florida, Tampa, Florida 33620

LeRoy, H. Klemm

Department of Chemistry, University of Oregon, Eugene, Oregon 97403

Coal-derived products are extremely complex mixtures of organic chemicals, the majority of which are polycyclic aromatic compounds (PAC). While the polycyclic aromatic hydrocarbons (PAH) comprise the largest chemical class fraction of most coal products, there are substantial amounts of nitrogen-, sulfur-, and oxygen-containing PAC. After fractionation of the nitrogen-containing PAC fraction, it was found that the amino polycyclic aromatic hydrocarbons (APAH), which are present in low concentrations (usually less than 1%), were responsible for the major part of the mutagenicity (1-4). The nitrogen heterocycles were generally much less mutagenic than the APAH. This result has prompted the investigation of other possible trace components in coal products, particularly the PAC that contain two heteroatoms, that may be responsible for some of the observed biological activity.

In this paper, the analysis of a solvent-refined coal liquid and a coal tar for PAC which contain both nitrogen and sulfur heteroatoms is described. Capillary column gas chromatography with sulfur-selective flame photometric detection and mass spectrometry were used to identify several new compounds which were previously unreported. Pure reference compounds were also synthesized and tested for genotoxicity.

EXPERIMENTAL

The solvent-refined coal heavy distillate (SRC II HD: 260-450°C boiling point range) was obtained from the Fort Lewis, Washington, pilot plant (operated by the Pittsburgh & Midway Coal Mining Co.). The coal tar was obtained from S.A. Wise (National Bureau of Standards, Washington, D.C.). The four aminodibenzothiophene isomers and azathiophenic compounds used in this study were not commercially available and, therefore, had to be synthesized in our own laboratories. The synthetic procedures are reported elsewhere (5,6).

The SRC II HD material and coal tar were fractionated into chemical classes by adsorption chromatography on neutral alumina and silicic acid according to the procedure of Later et al. (7). The third fraction (A-3) which was composed of the nitrogen-containing PAC, the second silicic acid fraction (S-2) which was composed of the APAH, and the third silicic acid fraction (S-3) which was composed of the tertiary nitrogen-containing PAC were analyzed in this study. Acid extraction with H_2SO_4, and derivatization with pentafluoropropionic anhydride (PFPA) were previously described (8).

A Hewlett-Packard Model 5880 gas chromatograph equipped with a sulfur-selective flame photometric detector (FPD), and operated in the splitless injection mode was used to obtain chromatographic retention data. Hydrogen was used as the carrier gas at a linear velocity of 100 cm s^{-1}. The capillary column used in this study was prepared by coating a 20 m x 0.31 mm i.d. length of fused silica tubing (Hewlett-Packard, Avondale, PA) with a 25% biphenyl polymethylsiloxane stationary phase (0.25 μm film thickness) (9). A Hewlett-Packard Model 5982A GC-MS system was used to obtain mass spectral confirmation of identified compounds. The same chromatographic column was used as for gas chromatography, and the mass spectrometer was operated in the electron impact mode at 70 eV electron energy. The Ames mutagenicity assay was performed as described by Ames et al. (10) with minor modifications.

RESULTS AND DISCUSSION

The chromatogram of the SRC II HD A-3 fraction on the 25% biphenyl methylpolysiloxane stationary phase is shown in Figure 1. Retention times were compared with the newly synthesized standard samples, and the 1- to 4-aminodibenzothiophenes and various azathiophenic compounds were identified. Several small peaks (most likely sulfur-containing secondary nitrogen heterocycles) were eliminated after acid extraction of the fraction. A modification of the method described by Later et al. (11) was used to distinguish the sulfur/tertiary nitrogen-containing PAH and sulfur/amino-containing PAH. Comparison of the chromatogram of the PFP derivatives with Figure 1 showed that some of the peaks shifted in retention time after derivatization. Retention times for the PFP amide derivatives decreased because the polar amino groups were blocked by the PFP groups, causing less dipole/induced dipole interactions with the polarizable biphenyl stationary phase. Identification of the four aminodibenzothiophene isomers was confirmed by comparing the retention times of the PFP-derivatized standards with the retention times of the shifted peaks in the chromatogram of the PFP-derivatized A-3 fraction. A chromatogram of the S-2 APAH fraction of the SRC II HD showed only aminodibenzothiophenes and alkylated aminodibenzothiophenes.

The chromatogram of the coal tar A-3 fraction on the 25% biphenyl methylpolysiloxane stationary phase is shown in Figure 2. Retention times of compounds in both the A-3 and S-3 fractions were compared with the reference samples, and 3 isomers of the azabenzothiophenes and all isomers of the azadibenzothiophenes were identified. In contrast to the SRC II HD, azathiophenic compounds were major components and aminodibenzothiophenes were not found.

Further confirmation of peak identities was obtained by GC-MS analysis. Table 1 lists the relative retention times of the PAC containing both sulfur and nitrogen identified in this study and the result of semi-quantitation of several of these compounds in the samples.

Tertiary nitrogen heterocycles are more thermally stable than amino-containing PAC, and are major nitrogen-containing PAC in coal-derived products (12). Azathiophenic compounds were tentatively identified in an anthracene oil and coal tar using GC-MS by Burchill et al.(12,13). However, the amino-dibenzothiophenes were the major nitrogen/sulfur-containing heterocycles in this coal liquid, while the azathiophenic compounds were the major ones in the coal tar. The difference between the two coal-derived products apparently relates to the reaction conditions. In the SRC II process, hydrogen was used
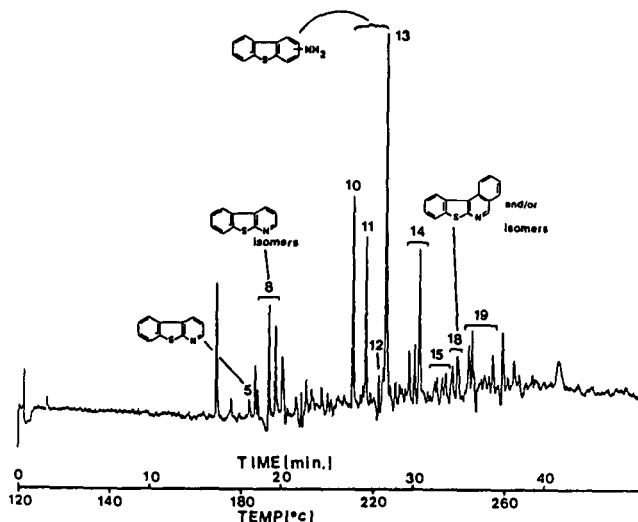
Figure 1. FPD chromatogram of the SRC II HD A-3 fraction on a 25% biphenyl polysiloxane stationary phase. Conditions: temperature program from 120°C to 265°C at 4°C min⁻¹, after an initial 2-min isothermal period; hydrogen carrier gas at 100 cm s⁻¹. Peak assignments are listed in Table 1.
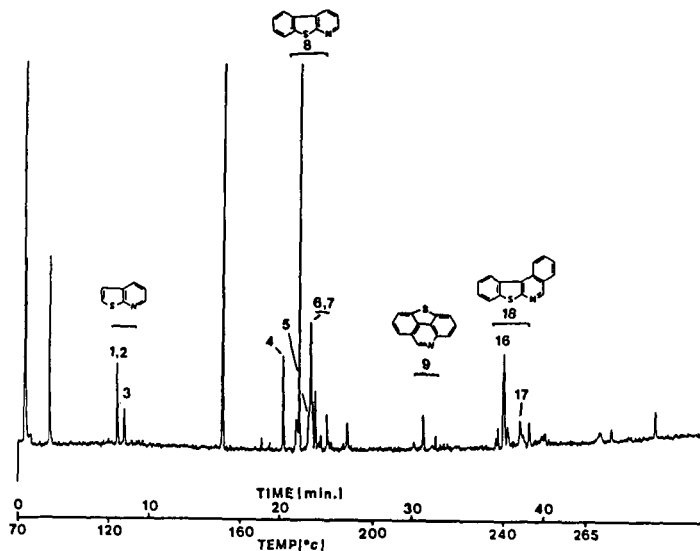
Figure 2. FPD chromatogram of the coal tar A-3 fraction on a 25% biphenyl polysiloxane stationary phase. Conditions: temperature program from 70 °C to 120°C at 10°C min⁻¹, then from 120°C to 265°C at 4°C min⁻¹, after an initial 2-min isothermal period; hydrogen carrier gas at 100 cm s⁻¹. Peak assignments are listed in Table 1.

Table 1. Relative retention times and semi-quantitation (selected examples) of PAC containing both sulfur and nitrogen in an SRC II heavy distillate coal liquid and a coal tar.

Peak No.	Compound[a]	Relative Retention Time[b]	Concentration[c] (µg/g)	
			SRC II HD	Coal Tar
1	4-azabenzothiophene	0.361		
3	6-azabenzothiophene	0.380		0.18
2	7-azabenzothiophene	0.361		
4	1-azadibenzothiophene	0.956		1.7
6	2-azadibenzothiophene	1.05		
7	3-azadibenzothiophene	1.05		
5	4-azadibenzothiophene	1.04		
8	azadibenzothiophene isomers	-		
-	1-azanaphtho[2,1-b]thiophene	0.979		
9	azaphenanthro[4,5-b,c,d]thiophene isomers	-		
11	1-aminodibenzothiophene	1.47	0.32	
12	2-aminodibenzothiophene	1.52	0.11	
13	3-aminodibenzothiophene	1.54	2.5	
10	4-aminodibenzothiophene	1.43	0.33	
14	C_1 aminodibenzothiophene	-		
15	C_2 aminodibenzothiophene	-		
16	3-azaphenanthro[9,10-b]thiophene	1.74		
-	3-azaphenanthro[2,1-b]thiophene	1.78		
17	3-azaphenanthro[4,3-b]thiophene	1.80		
-	1-azaphenanthro[1,2-b]thiophene	-[d]		
-	5-azabenzo[b]naphtho[1,2-d]thiophene	-[d]		
18	azabenzonaphthothiophene isomers	-		
19	C_1 azabenzonaphthothiophene isomers	-		

[a]Compounds which are not numbered were not found in these coal-derived products.
[b]Retention relative to naphto[2,3-b]thiophene.
[c]Approximate concentration in µg/g in the crude SRC II heavy distillate and the coal tar.
[d]Compound did not elute under the chromatographic conditions used.

in the reaction, and metals contained in the recycle oil were utilized as catalysts (14). Therefore, aminodibenzothiophenes seem to be more abundant than azathiophenic compounds in the coal liquid because of hydrogenation in the process. On the other hand, sulfur/tertiary nitrogen-containing PAC were thought to be major components in the high-temperature treated coal tar sample. Similarly, the easily desulfurized sulfur heterocycles such as naphtho[2,3-b]thiophene, 4- and 5-ring sulfur heterocycles derived from naphtho[2,3-b]thiophene were not found in SRC II sample, while these sulfur heterocycles were present in the same coal tar as reported elsewhere (15).

The mutagenicities of all isomers of the aminodibenzothiophenes and the

Table 2. Ames mutagenicity of the aminodibenzothiophenes and azadibenzo-
thiophenes.

Compound	rev/μg[a]	R^2
1-aminodibenzothiophene		
0% S9[b]	c	--
4% S9[d]	2.36	0.96
2-aminodibenzothiophene		
0% S9[b]	9.07	0.98
4% S9[e]	1.94×10^4	0.97
3-aminodibenzothiophene		
0% S9[b]	4.74	0.90
4% S9[f]	3.43×10^3	0.97
4-aminodibenzothiophene		
0% S9[b]	c	--
4% S9[d]	c	--
1-azadibenzothiophene		
4% S9[g]	c	--
2-azadibenzothiophene		
4% S9[h]	c	--
3-azadibenzothiophene		
4% S9[h]	c	--
4-azadibenzothiophene		
4% S9[g]	c	--

[a]Linear response region used to calculate dose response by
linear regression curve fitting.
[b]Solvent control value (0% S9): 21+4
[c]Response < 2X solvent control values
[d]Solvent control value (4% S9): 38+5
[e]Solvent control value (4% S9): 29+4
[f]Solvent control value (4% S9): 31+4
[g]Solvent control value (4% S9): 38+2
[h]Solvent control value (4% S9): 46+6

azadibenzothiophenes are listed in Table 2. The 2- and 3-aminodibenzothio-
phenes are strongly mutagenic, and their average mutagenic response was ten to
one hundred times greater than the average response of benzo[a]pyrene (200-300
revertants/plate at 4 μg and 4% S9) (16). All isomers of the azadibenzo-
thiophenes were inactive. A comparison of the structures of aminodibenzo-
thiophenes to the aminophenanthrenes reveals a geometric similarity between
them. The 2-, 3-, and 9-aminophenanthrenes demonstrated the highest muta-
genicity of the aminophenanthrene isomers (17). The 3-aminophenanthrene
isomer had the strongest mutagenicity (30,300 rev/μg average response), and
this structure is analogous to 2-aminodibenzothiophene which is the most
active of the aminodibenzothiophene isomers.

REFERENCES

1. Wilson, B.W.; Pelroy, R.A.; Cresto, J.T. Mutat. Res. 1980, 79, 193-202.
2. Guerin, M.R.; Ho, C.-h.; Rao, T.K.; Clark, B.R.; Epler, 1980, 23, 42-53.
3. Haugen, D.A.; Peak, M.J.; Suhrbler, K.M.; Stamoudis, V.C. Anal. Chem. 1982, 54, 32-37.
4. Later, D.W.; Lee, M.L.; Pelroy, R.A.; Wilson, B.W. In "Polynuclear Aromatic Hydrocarbons: Physical and Biological Chemistry"; Cooke, M.; Dennis, A.J.; Fisher, G.L., Eds; Battelle Press: Columbus, OH, 1982, pp. 427-438.
5. Kudo, H.: Castle, R.N.; Lee, M.L. J. Heterocyclic Chem., submitted.
6. Castle, R.N., unpublished results.
7. Later, D.W.; Lee M.L.; Bartle, K.D.; Kong, R.C.; Vassilaros, D.L. Anal. Chem. 1981, 53, 1612-1620.
8. Later, D.W.; Andros, T.G.; Lee, M.L. Anal. Chem. 1983, 55, 2126-2132.
9. Kuei, J.C.; Shelton, J.I.; Castle, L.W.; Kong, R.C.; Richter, B.E.; Bradshaw, J.S.; Lee M.L. J. High Resoln. Chromatogr./Chromatogr. Commun. 1984, 7, 13-18.
10. McCann, J; Ames, B.N. Proc. Nat. Acad. Sci. 1976, 73, 950-954.
11. Later, D.W.; Lee, M.L.; Wilson, B.W. Anal. Chem. 1982, 54, 117-123.
12. Burchill, P.; Herod, A.A.; Pritchard, E. Fuel, 1983, 62, 20-29.
13. Burchill, P.; Herod, A.A.; Mahon, J.P.; Pritchard, E. J. Chromatogr. 1983, 265, 223-238.
14. Schmid, B.K.; Jackson, D.M. 85th National Meeting of AIchE, Philadelphia, PA, June 4-8 (1978)
15. Nishioka, M.; Lee, M.L.; Castle, R.N. in preparation.
16. McFall, T.; Booth, G.M.; Lee, M.L.; Tominaga, Y.; Pratap, R.; Tedjamulia, M.; Castle, R.N. Mutation Res. 1984, 135, 97-103.
17. Later, D.W.; Pelroy, R.A.; Stewart, D.L.; McFall, T.; Booth, G.M.; Lee, M.L.; Tedjamulia, M.; Castle, R.N. Environ. Mutagen. 1984, 6, 497-515.

NEW CHEMICAL STRUCTURAL FEATURES OF COAL. STRUCTURE OF COAL DERIVATIVES (1)

Ben M. Benjamin and E. C. Douglas

Oak Ridge National Laboratory, P. O. Box X, Oak Ridge, Tennessee 37831

INTRODUCTION

The transalkylation reaction has been used by several researchers to investigate the structure of coal and other fossil fuels. Heredy and Neuworth (2) first applied the method to depolymerize coal under conditions that were mild enough so that unaltered monomeric units could be recovered. Their procedure consisted of heating coal with boron trifluoride in phenol. The boron trifluoride catalyst served to cleave aromatic-aliphatic bonds and phenol served as solvent and acceptor to give alkylphenols. The product fraction containing the alkylphenols was recovered and analyzed (3,4). This fraction was found to contain iso-propylphenol, ethylphenol and dihydroxydiphenylmethanes, thus confirming the presence of iso-propyl, ethyl, and methylene groups in coal. Further work was done with the coal-BF$_3$-phenol system by Ouchi (5) and Larsen (6). Later Franz (7) showed that certain phenolic derivatives undergo condensation reactions to give heterocyclic compounds which are not directly derived from coal.

The transalkylation reaction was further developed by Farcasiu (8), who used trifluoromethanesulfonic acid, CF$_3$SO$_3$H, as catalyst and xylene as solvent and acceptor. The method was useful in obtaining qualitative and quantitative information on methylene connecting groups and alkyl substituents in petroleum resids. We have modified this method for use in probing the structure of coal. Our method employs CF$_3$SO$_3$H as catalyst and toluene as solvent and acceptor (9). Using our version of the translkylation reaction, we identified a large number of groups in coal (9) and compared the structures of nine different coals (10). Relevant model compound experiments were also reported. In this paper, we present preliminary information on the structure of the following products derived from coal: Pyridine extract and pyridine insoluble residue from Ky #9 coal, O-methylated Ill #6 coal, Birch reduced Ill #6 coal, Coke from Ill #6 coal, and SRC from Ky #9 coal.

EXPERIMENTAL

The procedure used here is the same as that used earlier (9,10). Briefly, 4 g of starting material are mixed with 20 ml of toluene after which 2 ml of CF$_3$SO$_3$H are added. The mixture is stirred under reflux for 48 hrs and then the reaction is quenched by adding NaHCO$_3$ and H$_2$O. An integration reference is added and the toluene solution is isolated and analyzed by capillary gc and capillary gc-ms. The original procedure calls for four consecutive reaction steps, or cycles, to recover most of the excisable groups. Here we report only selected data from the first reaction cycle. The data are recorded in Tables 1 and 2.

Coke was prepared by heating powdered Ill #6 coal in a quartz tube to 800°C for 1 hour in a stream of argon. O-Methylated coal was prepared by an adaptation of the Liotta procedure (11). Birch reduced coal was prepared by an adaptation of the Hombach procedure (12).

The material referred to as SRC is filtered SRC T102 bottoms, Run No. 72, K125, Date-4/19/76, SN No. 74690, supplied by W. H. Webber, EPRI.

RESULTS AND DISCUSSION

The mechanism (13) for transfer of ethyl groups, or other n-alkyl groups, from benzene to toluene is shown in Figure 1. Extension of the mechanism suggests that 1,1-ditolylethane also should appear in the product mixture. Assuming that the benzene ring is replaced by a coal aromatic cluster and ethyl is any n-alkyl group, it is anticipated that n-alkyltoluenes, 1,1-ditolylalkanes and a variety of free

aromatics will appear in the product mixture. Tertiary alkyl groups transfer through free cationic intermediates while secondary alkyl and benzylic groups probably transfer through mixed mechanisms.

Actually, a large number of derivatives of toluene as well as other compounds are found in the product mixture (9,10). For the present discussion we have selected a limited number of these compounds. The selection is made on the basis of two criteria: these groups are the most prevalent in most of the samples, and they represent groups which demonstrate similarities or differences between the samples. Other important aspects of the results will be presented in a future paper along with 2nd-4th cycle results.

Table 1 contains data obtained from the transalkylation of Ill #6 coal and its derivatives, while the data for Ky #9 coal and its derivatives are collected in Table 2.

From Table 1 it is seen that O-methylation of Ill #6 coal causes only small changes in the numbers of excisable groups. Only ethyl and propyl are significantly lower in value. From these results, we suggest that O-methylation of coal by the Liotta procedure (12) produces only minor structural changes.

Results from the transalkylation of Birch reduced coal are found in Table 1, column 4. These results also show reduced amounts of certain monosubstituted alkyl groups, while the amounts of 1,1-diarylalkanes are larger. The increased values of 1,2-ditolylethane can be a consequence of reaction of triglyme, used as solvent in the Birch reduction, which may not have been completely removed by washing and drying the coal. The methine cross linking group, represented by tritolylmethane, has been lowered in concentration relative to the parent coal, while the trisubstituted ethane has been increased. The observation relative to trisubstituted ethane will be resolved in future control experiments. Another observation not shown in the Tables is that changes in coal structure during Birch reduction resulted in the production of large numbers of substituted indane and tetralins during transalkylation.

The data on coke presents an interesting case. The coking process effectively drives off volatile matter and causes thermal cleavage of many bonds so that many substituent groups are removed. The remaining residue is thought to be a network of polynuclear aromatics with few excisable side chains. This expectation is borne out by the experimental data in Table 1. Only small amounts of ethyl and methylene substituents are found. The most abundant transalkylation product is an assembly of isomers of a compound which has a molecular weight of 214. This compound, not shown in the Tables, has not yet been identified.

The pyridine extract and pyridine insoluble residue from Ky #9 coal, Table 2 and Figure 2, show some large differences. The soluble part shows increased amounts of monosubstituted alkyl substituents, while the insoluble part is partially depleted in these groups. There is a decrease in the amount of 1,1-diarylethane in both fractions. The relationship between 1-substituted alkyls and 1,1-disubstituted alkyls can be explained by reference to the mechanistic scheme in Figure 1, and the proposed presence of larger numbers of hydride abstractors as set forth in the section on model systems.

The most dramatic change is seen in the differences in concentrations of ditolylmethane and tritolylmethane in the soluble and insoluble fractions. The soluble part contains the larger amount of ditolylmethane which represents methylene (-CH_2-) connecting groups between aromatic clusters. On the other hand, the insoluble part contains the larger amount of tritolylmethane which represents methine (>CH-) crosslinking groups. These data are in agreement with the accepted opinion that pyridine extracts the material with a lower cross-link density and leaves a residue with a higher cross-link density.

SRC contains smaller molecules and more soluble materials. It is about 90% soluble in toluene. It is observed to contain a larger number of alkyl substituents and, as expected, a lower number of methylene connecting groups relative to the starting coal.

We have performed numerous experiments with model compounds in order to better understand results with coal and coal products. The most significant aspects of

100

these experiments are summarized as follows: In an earlier paper (9), we showed
that n-alkylbenzenes transalkylate slowly under our experimental conditions. In
contrast, n-alkyl substituents on polynuclear aromatics, such as phenanthrene,
anthracene and pyrene, transalkylate 10-100 times faster. We also found that alkyl
substituted aromatics transalkylate 2-5 times faster when the reaction mixture
contains polynuclear aromatics. The latter observations are probably a result of
the much larger basicity of the polynuclear aromatics and the hydride abstracting
ability of their protonated intermediates. Because transalkylation takes place
through a chain mechanism, the presence of more hydride abstractors increases the
rate by increasing the number of chain initiation steps. With these concepts in
mind, it is reasonable that the polynuclear nature of coal accounts, at least in
part, for the rapid production of numerous toluene derivatives under our reaction
conditions.

CONCLUSIONS

The above discussion is based on preliminary data observed from coal deriva-
tives. The data show certain trends, such as:
1. O-methylation does not appear to change the structure of coal greatly.
2. The treatment of coal under alkali metal reducing conditions appears to
    lower the number of excisable short chain alkyl substituents while also
    changing the structure to give new compounds under transalkylation
    conditions.
3. Pyridine extraction produces two fractions which have widely different
    substituent features.

REFERENCES

1. Research sponsored by the Division of Chemical Sciences, Office of Basic Energy
    Sciences, U. S. Department of Energy, under contract DE-AC05-840R21400 with
    Martin Marietta Energy Systems, Inc.
2. L. A. Heredy and M. B. Neuworth, Fuel, 1962, 41, 221.
3. L. A. Heredy, D. E. Kostyo, and M. B. Neuworth, Fuel, 1963, 42, 182.
4. Ibid., Fuel, 1964, 43, 414.
5. K. Ouchi and J. D. Brooks, Fuel, 1967, 46, 367.
6. J. W. Larsen and E. W. Kuemmerle, Fuel, 1976, 55, 162.
7. J. A. Franz, J. R. Morrey, G. L. Tingey, W. E. Skiens, R. J. Pugmire, and D. M.
    Grant, Fuel, 1977, 56, 366.
8. M. Farcasiu, T. R. Forbus, and R. L. LaPierre, Preprints, Div. Pet. Chem., Am.
    Chem. Soc., 1983, 28, 279.
9. B. M. Benjamin, E. C. Douglas, and D. M. Canonico, Fuel, 1984, 63, 888.
10. A Comparison of Several Coals, submitted to Fuel.
11. R. Liotta and G. Brons, J. Am. Chem. Soc., 1981, 103, 1735.
12. K. Niemann and H. P. Hombach, Fuel, 1979, 58, 853.
13. A. Streitwieser and L. Reif, J. Am. Chem. Soc., 1960, 82, 5003.

TABLE 1.

Results from the transalkylation of products derived from Ill #6 coal compared with the parent coal.[a]

	Parent	-OCH₃	Birch Red.	Coke
Ethyltoluene	0.47	0.30	0.17	0.029
Propyltoluene	0.25	0.19	0.089	0.0066
Butyltoluene	0.053	0.040	0.045	---
Pentyltoluene	0.008	0.014	0.010	---
Phenyltolylmethane	0.018	0.022	0.016	---
Ditolylmethane	1.09	1.14	0.55	0.036
1,1-Ditolylethane	0.098	0.014	0.21	0.0010
1,2-Ditolylethane	0.037	0.039	0.088	0.0018
1,1-Ditolylpropane	0.021	0.040	0.041	---
Tritolylmethane	0.025	0.028	0.011	0.0012
1,1,2-Tritolylethane	0.019	0.023	0.070	---
Naphthalene	0.009	0.0079	0.0025	---
Methylnaphthalene	0.045	0.040	0.011	---
Dimethylnaphthalene	0.034	0.034	0.016	---
Trimethylnaphthalene	0.014	0.011	tr	---
Methyltolylnaphthalene	0.014	0.029	tr	---

[a] Results are in mmol per 4 g of starting coal.

TABLE 2.

Results from the transalkylation of products derived from Ky #9 coal compared with the parent coal.[a]

	Parent	PySol	Insol	SRC
Ethyltoluene	0.30	0.41	0.058	0.50
Propyltoluene	0.16	0.21	0.056	0.19
Butyltoluene	0.041	0.12	0.028	0.063
Pentyltoluene	0.016	0.020	0.0047	0.037
Phenyltolylmethane	0.029	0.018	0.035	0.012
Ditolylmethane	1.11	0.988	0.614	0.59
1,1-Ditolylethane	0.19	0.11	0.019	0.027
1,2-Ditolylethane	0.025	0.036	0.0069	0.012
1,1-Ditolylpropane	0.060	0.054	0.042	0.014
Tritolylmethane	0.057	0.019	0.12	0.006
1,1,2-Tritolylethane	0.049	0.024	0.019	---
Naphthalene	---	0.012	0.0027	0.027
Methylnaphthalene	0.067	0.057	0.040	0.037
Dimethylnaphthalene	0.027	0.056	0.019	0.022
Trimethylnaphthalene	0.0092	0.028	0.0055	tr
Methyltolylnaphthalene	0.013	0.12	0.015	---

[a] Results are in mmol per 4g of starting coal.
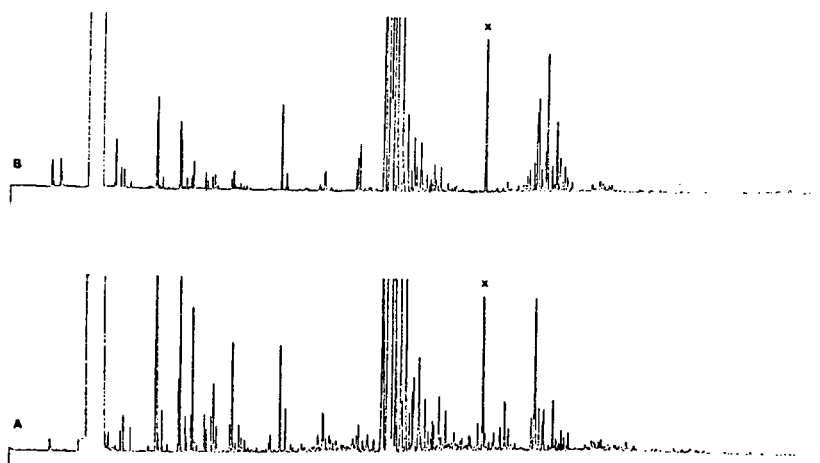
Figure 2. GC Traces of Transalkylation Products from A) Pyridine Soluble Fraction of Ky #9 Coal. B) Pyridine Insoluble Fraction. The Peak Marked X is Triphenylmethane Added as Internal Reference.

ORNL DWG 84-18170
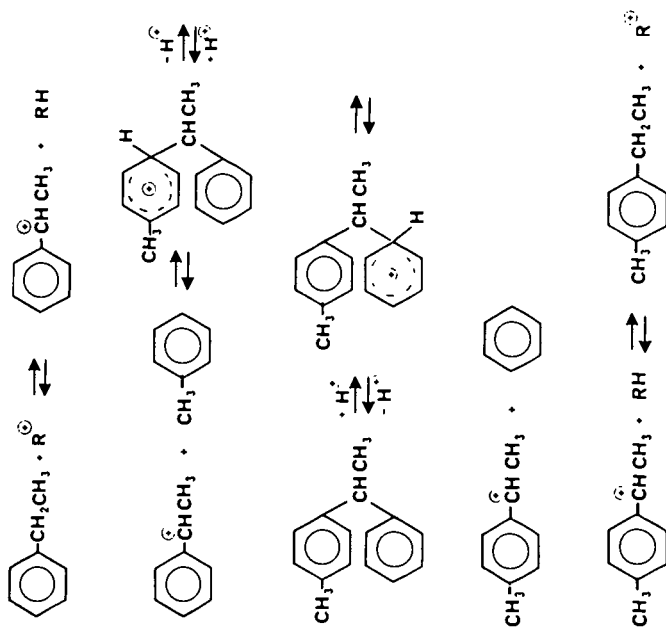
Figure 1. Mechanism of Transalkylation of Ethyl-Benzene in Toluene

NMR ANALYSIS OF HEAVY CRUDE OIL RESIDS

Judith C. Ware and Charles M. Schramm

Union Oil of California
Science and Technology Division
376 S. Valencia Avenue
Brea, CA 92621

SUMMARY

We have analyzed pentane-insoluble asphaltenes from a number of feeds and hydro-treated products. Processing reduced the asphaltenes levels by 29-77%. The hydro-gen-to-carbon atom ratio and fraction of aromatic carbon atoms were nearly the same for all of the feed and product asphaltenes, while other values varied widely. These results are taken to mean that aromaticity along with large molecular size is the factor determining whether a molecule is an asphaltene and that some degree of reduction of the asphaltene's aromatic system can convert it to a maltene. Crack-ing of the long aliphatic straight substituent chains does not seem to be necessary. An essential function of an asphaltene conversion catalyst appears to be reduction of aromatics.

INTRODUCTION

Asphaltenes are the light paraffinic hydrocarbon-insoluble but toluene- or benzene-soluble portions of crude oils. The are concentrated in the heavy ends when crude oils are distilled and are considered to be coke precursors in processing. The heavier oils, which constitute a growing proportion of the crudes available for processing, usually contain substantial quantities of asphaltenes.

Asphaltenes are a mixture of many different types of compounds and tend to be polar because they contain heteroatoms, in particular nitrogen, sulfur, oxygen and metals. Nickel and vanadium are the leading metallic elements. These materials associate so that their true molecular weights are hard to determine. It is estimated that the isolated molecules have an average molecular weight of the order of 1000-2000 amu (1).

When a crude oil or residuum is processed, the asphaltenes must be converted, preferably to more soluble products. In order to learn how asphaltenes are trans-formed in the upgrading process and how that process might be improved, we have examined feeds-and products- that were run sequentially over a typical hydrotreating catalyst. Asphaltenes and maltenes were separated from each and characterized by elemental analysis and by NMR techniques. Results of these studies suggest a common factor in asphaltene structure and an essential function of an upgrading catalyst.

EXPERIMENTAL

A series of residual feeds and blends was treated over the same charge of hydro-treating catalyst under typical conditions in order to compare their reactivity. The pressure was 2200 psig and temperatures ranged from 382-393°C. Properties of the resids are summarized in Table 1. Numbers 1 and 2 are blends; 3 and 10 are California offshore; 6 and 7 are California OCS; 11 and 12 are from the California central valley; 4, 5, 8, 9 and 14 are from Mexico, Iran, Alaska, Long Beach and Canada respectively.

Heavy Arabian resid was processed between each pair of resids in order to bring the catalyst to a "standard" condition and to check that its performance was consistent

throughout the run. The reactor temperature was increased as necessary to maintain approximately constant metals conversion of the Heavy Arabian blend. It was believed that all the resids tested would have been subjected to essentially the same catalyst.

Pentane asphaltenes were separated from each feed and product, using a modified Union Oil procedure. The resid was dissolved in a small amount of dichloromethane and then pentane was added at a solvent:sample ratio of about 100:1 to precipitate asphaltenes. The volume was reduced by 60% under nitrogen, and additional pentane was added to restore the solvent:sample ratio to 100:1. Precipitation was at room temperature. The mixtures were Millipore filtered after one hour, and the asphaltenes were washed with pentane and then dissolved through the filter with toluene. After evaporation of toluene the asphaltenes were vacuum dried in a pistol at 105°C and the maltenes were "dried" in a Rotavap at ca 0.3 mm at 60°C for one hour. Both fractions were analyzed for C, H_n S, N, Fe, Ni and V. Some IR spectra and thermal data were obtained, and ^{13}C- and ^{1}H-NMR spectra were obtained for all.

^{13}C-NMR spectra were obtained on spectrometers operating at 2.1, 4.7 and 6.3 Tesla, corresponding to ^{13}C resonance frequencies of 22.5, 50.3 and 67.9 MHz. In general, only sensitivity was improved by using higher field spectrometers to obtain the ^{13}C NMR spectra. A time factor improvement of almost 10 fold was achieved with the 6.3 Tesla spectrometer relative to the 2.1 Tesla spectrometer. However, the data obtained on all instruments were quite comparable. The improved resolution at higher fields did not result in better quality data, since resolution at 2.1 Tesla was sufficient for the measurements undertaken. All samples were run as $CDCl_3$ solutions in 10-mm or 12-mm sample tubes. Ninety degree pulses and 30-second recycle delays were used along with broadband, gated decoupling during acquisitions only. Line broadening equivalent to 1 Hz (whole resids and maltene fractions) or 2 Hz (asphaltenes) was applied prior to Fourier transformation. Sweep widths and data sizes were set, depending on applied field, to cover a 220 ppm range and to give approximately a 1-second acquisition time.

DEPT type spectra and quaternary carbon-only spectra were obtained on the 6.3 and the 2.1 Tesla instruments as described by Bendall and Pegg (2). A heteronuclear J-resolved two-dimensional experiment was performed on the 6.3 Tesla instrument using the software provided with the instrument.

Solid state ^{13}C-CPMAS experiments on the asphaltenes were performed with a Chemagnetics accessory attached to the 2.1 Tesla instrument. Experimental parameters used to obtain the spectra were a 1 ms contact time, 1 second recycle delay, and matched 40 kHz ^{1}H and ^{13}C R.F. field strengths. Samples were spun in Kel-F rotors at 3-3.5 kHz. Ten to twelve thousand scans were accumulated for each sample. Spectra of nonprotonated carbons were generated by inserting a 50 μsec delay between the end of the cross polarization period and the beginning of data acquisition during which the ^{1}H decoupler channel was gated off. Thirty Hz of line broadening was applied prior to Fourier transforming the data to enhance the signal-to-noise ratio.

RESULTS AND DISCUSSION

Figures 1-4 summarize the elemental analyses on the feed and product maltene and asphaltene fractions. From Figure 1 it can be seen that the H/C atom ratios for feed and product asphaltenes were all within the range 1.20±0.09, and the value could go up or down in a product. At the same time, asphaltenes were reduced by as much as 77 wt.%. The values of the ratios were also nearly the same for maltenes: 1.60±0.08 for feeds and 1.67±0.07 for products. In every instance the ratio increased in going from a given feed to its product. Some sort of increase would be expected for a hydrotreating process.

By contrast, nitrogen and sulfur levels varied widely in both fractions (Figures 2 and 3). Nitrogen levels were lower in maltenes but changed relatively little during processing. If any conversion did occur, it must have led to materials that remained in the liquid portions of the resids. Sulfur levels were usually lower in maltenes and decreased significantly on treatment. Sulfur also decreased in the product asphaltenes. Sulfur could have been removed as H_2S or insoluble sulfides, neither of which would have remained in the liquid phase.

Metals content, as represented by (Ni+V) values, was much higher in asphaltenes than in maltenes and decreased on treatment. Levels in product maltenes were very low, suggesting that soluble metals were readily removed. Metals reduction exceeded asphaltene reduction in most cases (Figure 5); evidently metals are removed more easily than asphaltenes are converted.

For all of the fractions ^{13}C-NMR spectra were measured; for each, the fraction of aromatic carbon atoms, f_a, and the average chain length parameter, $c_n/\bar{c}_1$ (3), were calculated. For several of the asphaltene fractions, the aromaticity was measured by ^{13}C CPMAS (cross polarization - magic angle spinning) NMR directly on the solid sample. Measured aromaticities were found to be identical whether measured on solution or solid samples. This suggests that we are examining the whole sample in solution, and that solubility of the asphaltenes is not a problem when chloroform is used as a solvent. The data are presented graphically in Figures 6 and 7. The calculation of $c_n/\bar{c}_1$ was modified by substituting for c_1 the average of the heights of the c_1-c_4 peaks that are characteristic of long straight chain hydrocarbons (chemical shifts 14.2, 20.4, 32.2 and 29.7 ppm respectively). Figure 6 shows that the values of $c_n/\bar{c}_1$ varied widely, corresponding to an average straight chain length range from 10 to 22 carbon atoms. The only obvious trend in the data is that $c_n/\bar{c}_1$ increases in product asphaltenes. It appears not to change much in maltenes. These results indicate that asphaltenes do contain long carbon chains, contrary to some earlier statements (4). The chain length assignment was calibrated with pentadecyl-phenol, and the results agreed with those of Netzel et al (3). When one LAR asphaltene sample was Soxhlet extracted with pentane for eight hours, the $c_n/\bar{c}_1$ value did not change appreciably. Thus, the long chains were not due to occluded paraffins; they are an integral part of the asphaltenes.

For several of the resid fractions, we have also calculated some additional parameters from the ^{13}C-NMR spectra. The fraction of paraffinic carbon was calculated as the fraction of alkyl carbon contained in resolved resonances (by integration) as described by Galya and Young (5). In addition, the fraction of straight chain paraffinic carbon was calculated from the ratio of the sum of the integrals of the 14.2, 20.4, 32.2, 29.7, and 29.9 ppm resonances to the total paraffinic carbon integral. Figure 7 shows the change in straight chain paraffinic contents after processing for the maltene and asphaltene fractions of six resids. Only the asphaltene paraffin content changes appreciably after processing, increasing for the resids examined. This suggests that hydrotreating reduces the naphthene carbon content relative to the paraffin content in the asphaltene fraction. Further work in this area is underway.

We have also used a variety of techniques to calculate the fraction of nonprotonated aromatic carbon for the maltenes and asphaltenes fractions. For the asphaltenes, ^{13}C CPMAS, DEPT, and heteronuclear J-resolved 2D NMR methods were evaluated. Of these methods, the latter two were found to be too time consuming. By obtaining the normal spectrum plus the interrupted decoupling spectrum, nonprotonated aromatic carbon was determined in just two hours, versus 12-48 hours for the DEPT and 2D methods. For the maltenes the DEPT technique allows determination of nonprotonated carbon in typically 2-3 hours versus overnight for 2D methods. Thus, DEPT is preferred when additional information available from the 2D NMR (such as coupling constants) is not deemed necessary. To date, we have not found any correlations

between nonprotonated carbon content and hydrotreating.

Figure 8 shows the values of f_a for all of the maltene and asphaltene fractions. The values for feed and product[a] asphaltenes very remarkably little; all are in the range 0.47 ± 0.06. At the same time, the asphaltene levels were reduced up to 77% by the processing (Figure 5). Maltene values also fall within a narrow range: 0.22 ± 0.05. In every case the value of f_a for maltenes either decreased or remained the same with hydrotreating.

Thus, only aromaticity and the H/C atom ratio, which is a rough indicator of aromaticity, maintained the same levels in feed and product asphaltenes. Sulfur, nitrogen and (Ni+V) levels varied greatly in the same asphaltenes. Such a wide variety of resids has been examined that these results cannot be coincidental. The data suggest that aromaticity along with high molecular weight is the primary criterion for asphaltene classification.

Once the asphaltene aromatics are hydrogenated to some degree, they evidently cease to be asphaltenes and pass into the maltene fraction. Metals or sulfur removal do not necessarily have the same effect. It appears that hydrogenation of the aromatic ring system is the one reaction necessary for asphaltene conversion to more soluble materials. The chain length data, which are harder to reproduce and therefore less reliable, show that in some instances the asphaltenes with shorter sidechains were more readily converted, but it does not appear that cracking of sidechains is generally required for asphaltenes reduction.

Aromatics reduction would cause a planar aromatic system to become nonplanar. If the stacking proposal of Yen (6) for asphaltene planar aromatic systems is correct, then the hydroaromatics thus formed might no longer fit into such an assembly, and the hydrogenated molecules might therefore no longer be asphaltenes.

These conclusions are at considerable variance with those of Plumail et al for the conversion of Boscan crude asphaltenes (7). Boscan resid was treated under the same conditions that we have reported here, and in our hands the results were in line with the present ones. Namely, asphaltene aromaticity and H/C ratio change little on processing, and sulfur and metals levels (including nickel) drop. Nitrogen values are virtually unchanged, while average straight alkyl chain length decreases somewhat in product asphaltenes but remains the same for product maltenes. We believe that hydrogenation of aromatic structures is the principal requisite for conversion of Boscan as well as other petroleum asphaltenes.

ACKNOWLEDGMENTS

BIBLIOGRAPHY

1. See the discussion by J. F. Speight and S. E. Moschopedis, Preprints, ACS Division of Petroleum Chemistry, 24(4), pp. 919-920 (1979).

2. M. R. Bendall and D. T. Pegg, J. Mag. Reson., 53, 272 (1983).

3. D. A. Netzel, D. R. McKay, R. A. Heppner, F. D. Guffey, S. D. Cooke, D. L. Varie and O. E. Linn, Fuel, 60, 307 (1981).

4. e.g., T. F. Yen, C. S. Wen, J. T. Kwan and E. Chow, "Oil Sand and Oil Shale", Verlag Chemie International, 1978, pp. 321-322.

5. I. G. Galya and D. C. Young, Preprints, ACS Division of Fuel Chemistry, 28(5), 1316 (1983).

6. T. F. Yen, J. G. Erdman and S. S. Pollack, Anal. Chem., 33, 1587 (1961).

7. J. C. Plumail, H. Toulhoat, Y. Jacquin and G. Martino, 8th Intern. Congr. Catal., Proc., 2, 317 (1984).

Table. Properties of Feed Resids

Ident. No.	Resid	Minimum B.Pt., C	API Gravity	%Asph	%N	%S	ppm (Ni+V)
1	HVY ARAB.	343	12.6	15.5	0.26	4.23	115
2	LAR	343	11.0	13.7	0.67	2.77	222
3	SA. MARIA	204	14.6	23.0	0.61	3.82	319
4	MAYA	343	9.4	23.4	0.52	4.42	496
5	GACH SARAN	343	15.6	8.7	0.41	2.60	144
6	HONDO	204	13.4	19.8	0.70	5.10	321
7	FRODO	232	9.3	30.0	0.80	5.95	658
8	N. SLOPE	343	15.3	5.1	0.31	1.60	57
9	LA BASIN	204	9.5	12.2	0.92	1.94	151
10	GILDA	232	14.6	13.9	0.73	3.60	318
11	BREMER	232	10.9	8.8	1.20	1.46	160
12	MIDWAY	260	11.6	8.1	0.83	1.41	150
13	ORCUTT	232	14.7	11.7	0.66	2.84	192
14	LLOYDMSTR	232	13.5	13.2	0.16	3.24	150

Fig. 1. Variation of H/C Atom Ratio
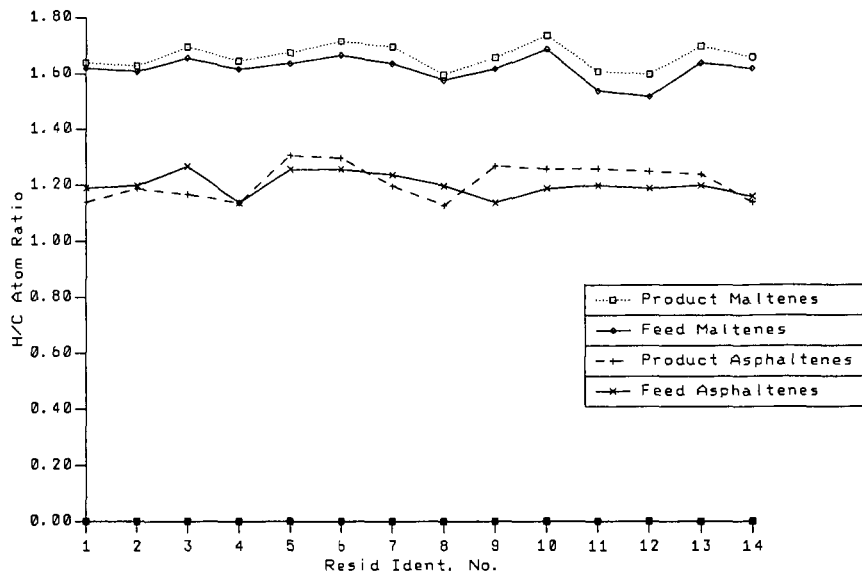
Fig. 2. Nitrogen Content of Resid Fractions
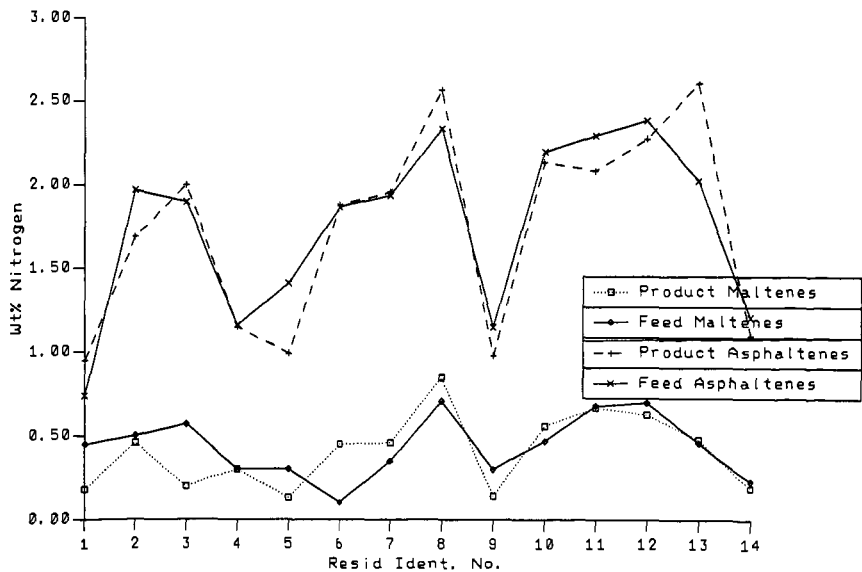
Fig. 3. Sulfur Content of Resid Fractions
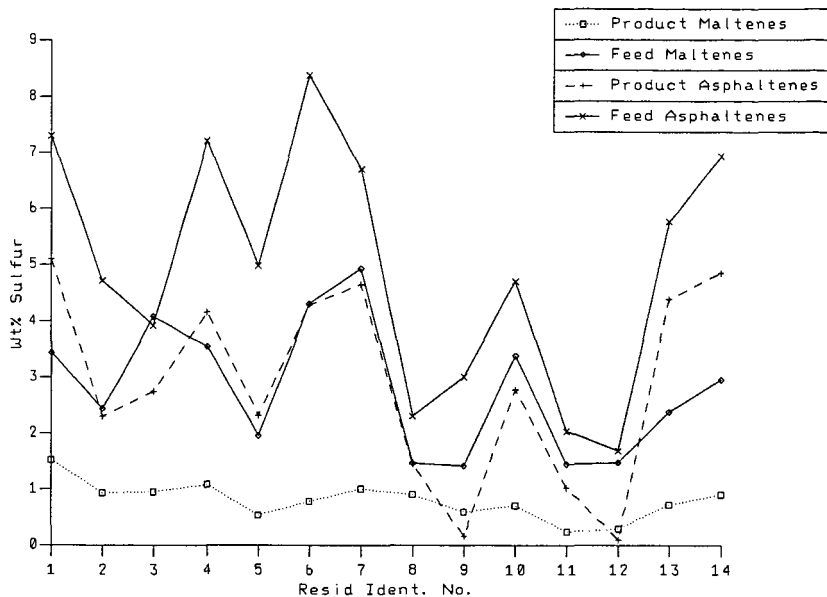
Fig. 4. (Ni+V) of Resid Fractions
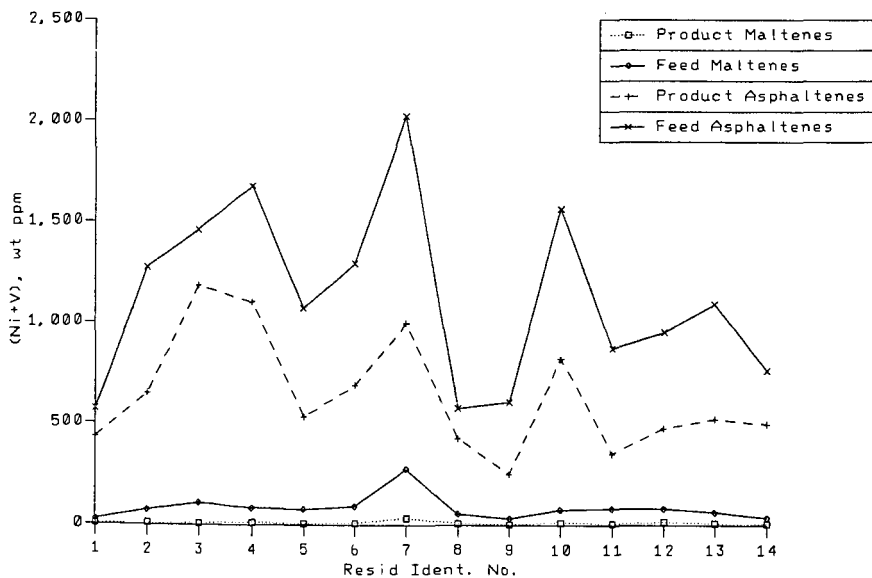
Fig. 5. Asphaltene Metals Reduction
vs Asphaltenes Conversion
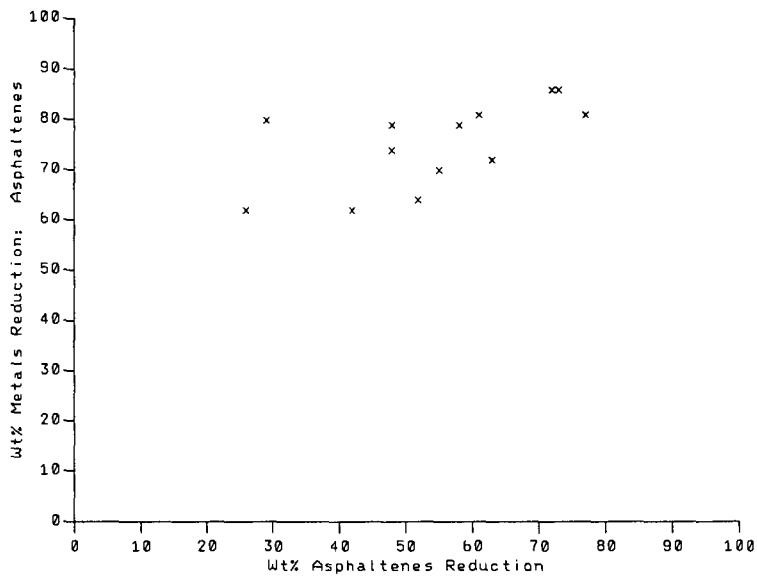
Fig. 6. cn/c1 for Resid Fractions

111
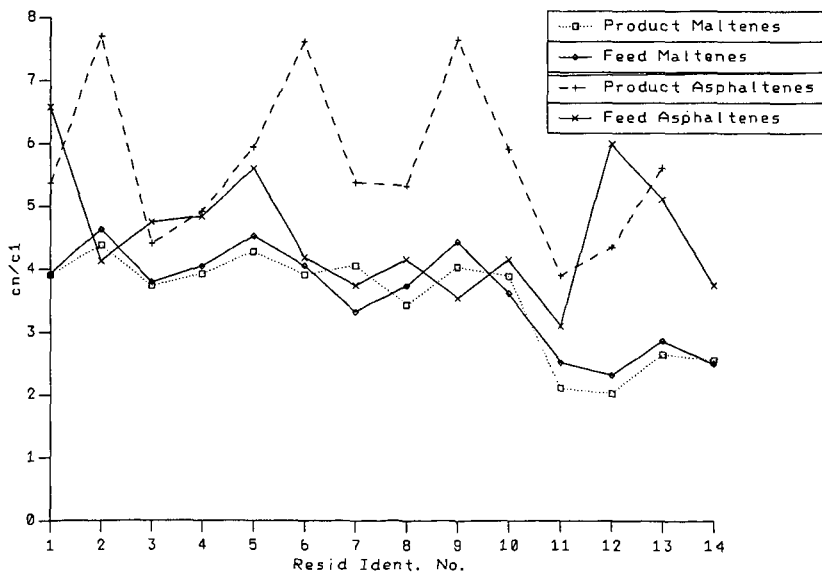
Fig. 7.   Percentage of Saturated Carbons
that Are Straight Chain
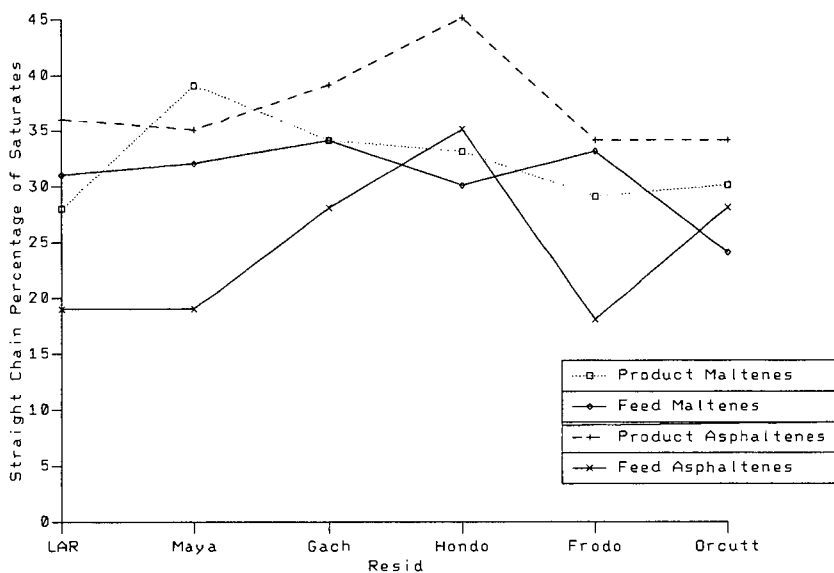
Fig. 8.   Fraction of Aromatic Carbon
in Resid Fractions
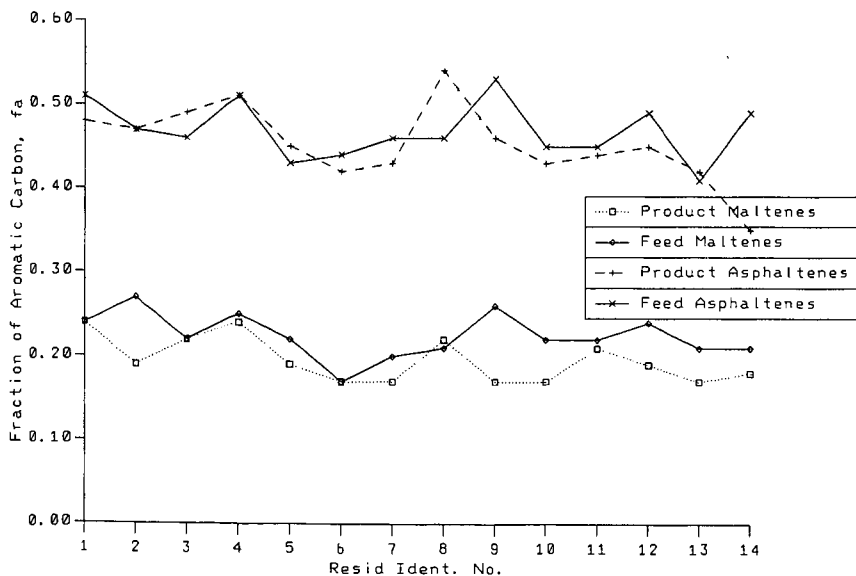
ADDUCTION IN DONOR SOLVENT CONVERSION OF EASTERN SHALE

L. G. Galya
D. C. Cronauer
J. Solash

Gulf Research & Development Company
P.O. Drawer 2038
Pittsburgh, PA 15230

INTRODUCTION

Rich deposits of Devonian oil shale are found east of the Mississippi. The carbon in oil shales from Kentucky have been shown to have a higher aromatic carbon content (~54% aromatic carbon) than oil shales from the Green River formation (~22% aromatic carbon).[1] This, along with the low H/C atomic ratio of 1.0-1.2 in eastern shales, suggests that these shales have a structure similar to that of coal. During coal liquefaction, as with eastern oil shale conversion, one objective is to decrease the extent of recombination of thermally produced free radicals through the use of a donor solvent. The donor solvent donates hydrogen to the substrate and, therefore, becomes more aromatic. In addition to donating hydrogen, the solvent can isomerize and/or be adducted. The objective of this work is to identify the types of adduction of donor solvents tetralin, octahydrophenanthrene, and mesitylene in eastern oil shale runs.

EXPERIMENTAL

The shale sample was provided by IMMR (Lexington, KY). It was taken from the Hilpat site (Fleming Co., KY) and it is classified as a Cleveland member, Ohio shale. It has a Fischer assay of 10.1 g/ton and a carbon content of 12.2 wt% (MF). The unlabeled solvents were obtained from Fisher Scientific and were used as received. The labeled solvents (see Figure 1) were prepared by E. J. Eisenbraun of Oklahoma State University.

Batch conversion experiments were made using equal charges of shale and solvent to a small microreactor which was lowered into a preheated sand-batch to bring its contents quickly to reaction temperature. The experiments were made at a temperature of 450°C and reaction times between 0 (allowing 2.5 min. for heating) and 30 min. Mixing was provided by up-and-down agitation at about 800 strokes/min. Further details are given in Reference 2.

The total reaction product was transferred to a small test tube and the solvent was stripped with a nitrogen flow to ensure a minimum of cosolvent effects during extraction. The product was then sequentially Soxhlet extracted to give pentane and toluene solubles. Percent solubles is defined as 100% minus Soxhlet residue. Selected samples of the toluene insolubles were also extracted with tetrahydrofuran (THF). The THF Soxhlet extract was stripped with a nitrogen flow at 80°C overnight to remove solvent and recover a sample of preasphaltenes for analysis.

^{13}C NMR spectra were obtained at 50.3 MHz on a Varian associates XL-200 spectrometer. Samples were made up in $CDCl_3$ with $Cr(acac)_3$ added at a level of 0.05 M. Spectra were obtained with 90° pulses, 0.4 second acquisition time, 2 second delay between pulses and gated decoupling. Spectra were referenced internally to TMS. In some cases, only 10-20 mg of each fraction were available so spectra were accumulated for 50-61 hours. In some cases, the spectral quality even then was poor, so only major types of adduction are discernable. A reference spectrum of the run made with unlabeled donor solvent was obtained for each labeled donor solvent run.

DISCUSSION

Tetralin Adduction

Tetralin can be adducted as tetralin, naphthalene, or isomerized tetralin, e.g., methylindane or butylbenzene. The possible fates of tetralin are given in Figure 2.

Pentane Solubles

The spectra from this fraction are shown in Figure 3.

Adduction of tetralin can occur in either the aromatic or aliphatic portion of the molecule. Adduction through the aromatic portion is difficult to identify because it does not perturb the chemical shift of the labeled carbon. Attachment at the aliphatic portion can occur in any of the four positions, but two of them are equivalent. Attachment at the labeled position, which is α to the aromatic ring, will move the chemical shift from its normal position of 29.9 ppm to 37.2 ppm or 42-46 ppm, depending on whether the attachment is by an aliphatic or aromatic structure. There are two signals at 45.4 ppm and 45.9 ppm, indicating attachment at the labeled carbon by an aromatic structure. In addition, there is a small amount of signal intensity at 41-42 ppm, also indicating attachment of the tetralin at the labeled position by an aromatic structure. The signal at 37.8 ppm can be due to attachment at the labeled position of tetralin by an alkyl group or attachment at the tetralin position β to the aromatic ring by an aromatic substituent. Because the α to aromatic position is the most active, it is assumed that this signal is due to attachment at that position by an alkyl substituent. The large signal at 29.9 ppm is due both to long chain material from shale and to tetralin adducted through a position which does not perturb the chemical shift of the labeled carbon, i.e., through the aromatic ring. This represents the largest amount of adducted tetralin.

The amount of each type of adducted tetralin is given in Table 1. They were estimated based on a comparison of signals in the spectra of the labeled and unlabeled runs.

Butyl Benzene Adduction

Tetralin can open to form n-butyl benzene with the label either in the position α to the aromatic ring or at the terminal methyl. The signals due to the label would then be at 36 ppm or 14 ppm, respectively, unless

adduction occurred through the alkyl chain. There is a signal at 36 ppm that is not present in the spectrum from the unlabeled run. This signal is due to butyl benzene with the label in the α position. The relative intensities of the signal at 22.4 and 14 ppm in both the labeled and unlabeled runs are the same. This indicates that there is little contribution to the signal at 14 ppm from n-butyl benzene. However, there is a signal at 36 ppm which indicates that n-butyl benzene is present and the label is in the α position. The amount of tetralin present as n-butyl benzene is given in Table 1.

Tetralin can also open to form 1-phenyl 1-methyl propane. In this case, the label would be present in the methyl group and would have its signal at 22.5-23 ppm. There is a signal present in both the labeled and unlabeled spectra at this position. However, it is present in the same amount relative to the signal at 22.4 in both spectra, indicating that it is due to the unlabeled β carbon of tetralin rather than the propane derivative.

Methyl Indane/Methyl Propyl Benzene Adduction

Tetralin can rearrange to form methyl indane or open to form ortho methyl propyl benzene. In either case, the label would be present on the methyl group and would have its signal at 20 ppm. One or both of these isomers is present as indicated by the signal at 20 ppm in the labeled run. Adduction of these isomers has probably occurred through the aromatic ring. The amount of these isomers is given in Table 1.

Naphthalene Adduction

Tetralin converted to naphthalene can be adducted at either of two equivalent positions. The labeled carbon has its signal at 127.9 ppm. The aromatic region of the spectrum has a large amount of signal intensity in this region, indicating that naphthalene has been adducted through the unlabeled ring. In addition, there are signals at 126 and 125.5 ppm, indicating adduction ortho to the label by either aromatic or short alkyl chain substituents. There is a signal at 131.2 ppm that only can be due to adduction para to the label and the labeled carbon must also contain a methyl group. The signal at 134.2 is indicative of naphthalene with an attached methyl group. In this case, adduction must be through the unlabeled ring. There are two signals at 137 and 138.4 ppm that are due to naphthalene adducted through the position para to the label and the labeled carbon must contain a short (C_{2-3}) alkyl group. There are also signals present at 140.1 and 140.4 ppm that are due to naphthalene adduction by an aromatic group.

Asphaltene Fraction

The aromaticity of the asphaltene fraction obtained from the unlabeled tetralin run of 5 min. was 70.7%. There are sharp signals in the spectrum at the classic positions for long alkyl chain material. The aromatic region is broad and featureless. The asphaltene fraction obtained from the ^{13}C labeled tetralin run of 5 min. has an aromaticity of 81.5%. The aliphatic region has the same classic signals for long chain material that were present in the unlabeled run.

There are two small signals at 32.5-33 ppm and at 36 ppm in the labeled asphaltene spectrum. These are due to small amounts of attachment of the hydroaromatic ring to the asphaltenes. The hydroaromatic ring is not attached at the labeled position. Otherwise, a signal would be present at either 37.2 ppm or 48 ppm for an alkyl or aryl aromatic attachment, respectively. The tetralin is probably attached at the position alpha to the label. Attachment at this position would move the chemical shift of the labeled carbon to 33.9 for attachment through an alkyl substituent or 36.9 ppm for attachment through an aromatic substituent. Both the positions α and β to the labeled carbon should be substituted to the same extent. However, some types of substitution at the β position would shift the signal under signals present from long alkyl chain material and hence would not be seen.

In addition to the aliphatic signals, there are several sharp signals present in the aromatic region at 126.0, 127.7, and 128.3 ppm. These indicate that some of the tetralin has been converted to naphthalene. The unperturbed chemical shift of the labeled carbon would be at 127.9 ppm. Attachment at the labeled carbon would move the chemical shift into the range of 134-148 ppm. Since there are no sharp signals in this region, the naphthalene must not be adducted at this position. Attachment ortho to the label would move the chemical shift of the labeled carbon upfield into the region of 124.8-128.8 ppm. The signal at 126.0 ppm can be due to alkyl attachment at this position. Attachment at the position meta to the label moves the signal only slightly for alkyl attachments but down to 128.3 ppm for an aryl substituent. There is a signal at 128.3 ppm which may be due to aromatic attachment of naphthalene to asphaltenes at the 3-position. Attachment para to the label would move the labeled carbon signal upfield into the region of 125.0-125.5 ppm or 126.9 for an alkyl or aryl attachment, respectively. Since no attachment was seen at the labeled position, it is unlikely that there will be any attachment at the position para to it.

Attachment in the ring without the labeled carbon will not significantly perturb the chemical shift of the labeled carbon. The signal at 127.7 ppm is due to unperturbed label indicating attachment to the unlabeled ring.

Adduction of Mesitylene

Asphaltene Fraction

The ^{13}C NMR spectrum of asphaltenes recovered from the run with unlabeled mesitylene shows an aromaticity of 88.5%. The sharpest signal in the spectrum is at 29.0 ppm. The spectrum of the asphaltene fraction obtained from the run with ^{13}C labeled mesitylene has an aromaticity of 75.9%. The decrease in aromaticity is due to an increase in aliphatic structure which comes from the ^{13}C label on one of the methyls of mesitylene.

The aliphatic region of the spectrum has two sharp signals at 29.4 ppm and 21.1 ppm. The signal at 21.1 ppm is due to the labeled methyl group on mesitylene. Adduction of mesitylene has not taken place through this

methyl group since its original chemical shift of 21.0 ppm is not significantly perturbed. Had adduction occurred through this methyl group, the chemical shift would move to 42 ppm if the attached group were aromatic, 29-36 ppm if the attached group were an alkyl chain, and 43-48 ppm if more than one alkyl group were attached. Adduction of the mesitylene on the aromatic carbon ortho be the labeled methyl group by an alkyl group would move the chemical shift of the labeled methyl group upfield by 2-3 ppm. Adduction at the aromatic carbon para to the labeled methyl group would have little effect on the chemical shift of the labeled methyl group. Similarly, adduction through one of the meta methyl groups would have little effect on the chemical shift of the labeled methyl group. It, therefore, appears that the mesitylene has been adducted through either the unlabeled methyl groups or the aromatic carbon para to the labeled methyl group.

Preasphaltene Fraction

The ^{13}C NMR spectrum of this fraction obtained from the run with unlabeled mesitylene shows an aromaticity of 84.7%. The most defined signal in the spectrum is at 29.6 ppm. The spectrum of the preasphaltene from the run with ^{13}C labeled mesitylene has an aromaticity of 81.0%. This decrease again is due to incorporation of the labeled methyl group from mesitylene. The most predominant signals in the spectrum are at 29.7 ppm and 21.5 ppm, the latter due to the labeled methyl group of mesitylene. It again appears that the mesitylene is not adducted through the labeled methyl group nor through the aromatic carbon ortho to the methyl group.

Adduction of Octahydrophenanthrene

Preasphaltene Run

The aromaticity of the preasphaltenes obtained from the run made without the labeled octahydrophenanthrene was 75.3%. The only sharp signal in the spectrum was at 29.6 ppm. The aromaticity of the preasphaltenes obtained from the run made with ^{13}C labeled octahydrophenanthrene was 77%. There are two sharp signals in the spectrum of the fraction. The signal at 128.4 ppm is the unperturbed chemical shift of carbon 1 in phenanthrene. This indicates that at least some of the adducted octahydrophenanthrene has been dehydrogenated to phenanthrene. The point of attachment of the phenanthrene to the preasphaltenes is not on the labeled carbon. Such attachment would move the chemical shift into the region of 137.6-150.7 ppm, depending on the nature of attached groups. It also is not attached at the carbon para to the label which moves the signal to 119.5-120 ppm for an alkyl attachment and 127.3 ppm for an aromatic attachment. Attachment of the phenanthrene at the ring position ortho to the label by some groups, some types of alkyl attachments, attachment at the position meta to the label, and attachment at one of the unlabeled rings will not be seen in the chemical shift position of the labeled carbon. Since the sharp signal is in a virtually unperturbed position, the phenanthrene must be adducted at one of the unlabeled rings or at the position ortho or meta to the labeled carbon.

Some phenanthrene is also attached as octahydrophenanthrene. There are sharp signals at 29.6 ppm in both the unlabeled and labeled runs.

117

However, in the labeled run, the ratio of aromatic carbon area, corrected for the sharp signal at 128.4 ppm to the area of the signal at 29.6 ppm is less by a factor of 7 than the same ratio in the unlabeled run. This indicates that there is substantially more area in this region in the labeled run. The chemical shift of the labeled carbon in octahydrophenanthrene is 30.3 ppm, which could overlap with the signal at 29.6 ppm under conditions where $Cr(acac)_3$ is added to the spectrum. In fact, there appears to be a downfield shoulder on the peak at 29.6 ppm in the labeled run. This indicates that there is some labeled octahydrophenanthrene adducted. The fact that the chemical shift of the labeled carbon is not moved substantially from its unadducted position indicates that it is adducted at either of the two aromatic rings or at the γ aliphatic carbon in the saturated ring. By analogy with tetralin, if it were attached at the labeled carbon, the chemical shift would be at 38.4 ppm. If it were attached at the aliphatic carbon α or β to the labeled carbon, the chemical shift of the labeled carbon would be 34.3 ppm or 26.8 ppm, respectively. Attachment in the γ position would not perturb the chemical shift of the labeled carbon. Since the chemical shift is virtually unperturbed, the point of attachment must be at the γ aliphatic carbon or on the two aromatic rings.

CONCLUSIONS

Adduction of donor solvents occurs during eastern shale conversion. Tetralin is adducted as tetralin, naphthalene, and isomerized tetralin. Mesitylene is adducted through the aromatic ring or unlabeled methyl groups rather than the labeled methyl group. Octahydrophenanthrene is adducted both as octahydrophenanthrene and phenanthrene.

REFERENCES

1. Miknis, F. D. and Maciel, G. E., Atomic and Nuclear Methods in Fossil Energy Research, Filby, R. H., ed., Plenum, NY, 1982, pg. 349.

2. Cronauer, D. C., McNeil, R. I., Young, D. C., and Ruberto, R. G., Fuel (1982), 61, 610.

Table 1

^{13}C NMR Analysis of Naphthalene/Tetralin
Adduction in Pentane Solubles

Shale Derived Material	81.6%
Adducted Tetralin	9.6%
at α position by aromatics	1.6%
at α position by alkyls	1.4%
not in aliphatic ring	6.6%
Adducted n-Butyl Benzene	1.0%
Adducted Methyl Indane/Methyl Propyl Benzene	1.0%
Adducted Naphthalene	6.8%
at α position by aromatics	0.7%
at para position with alkyl and methyl	0.3%
at α position by methyl	0.2%
at m position or in unlabeled ring	4.7%
at α by short alkyl with para alkyl	0.3%
0 to label by aromatics	0.5%
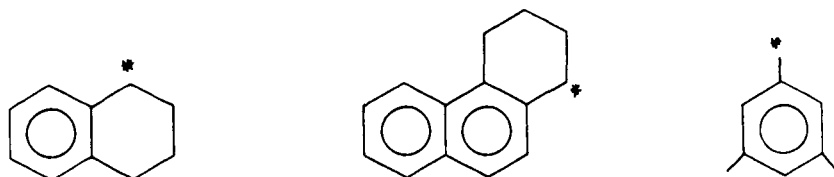
FIGURE 1. ^{13}C LABELED (*) COMPOUNDS USED IN ADDUCTION STUDY
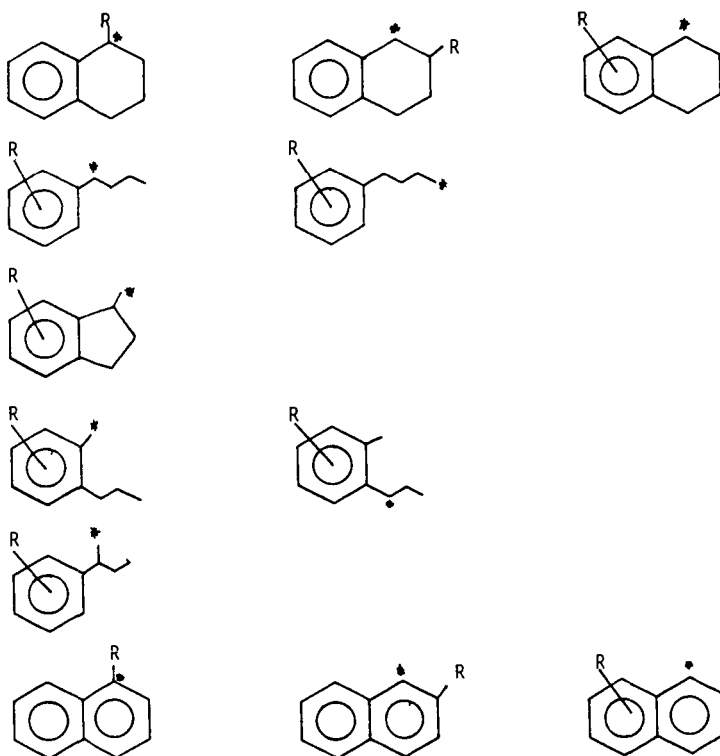
FIGURE 2. POSSIBLE FATES OF TETRALIN DURING ADDUCTION

LABELED RUN

UNLABELED RUN

180　　　　　　　　　90　　　　　　　　　0

CHEMICAL SHIFT (PPM)
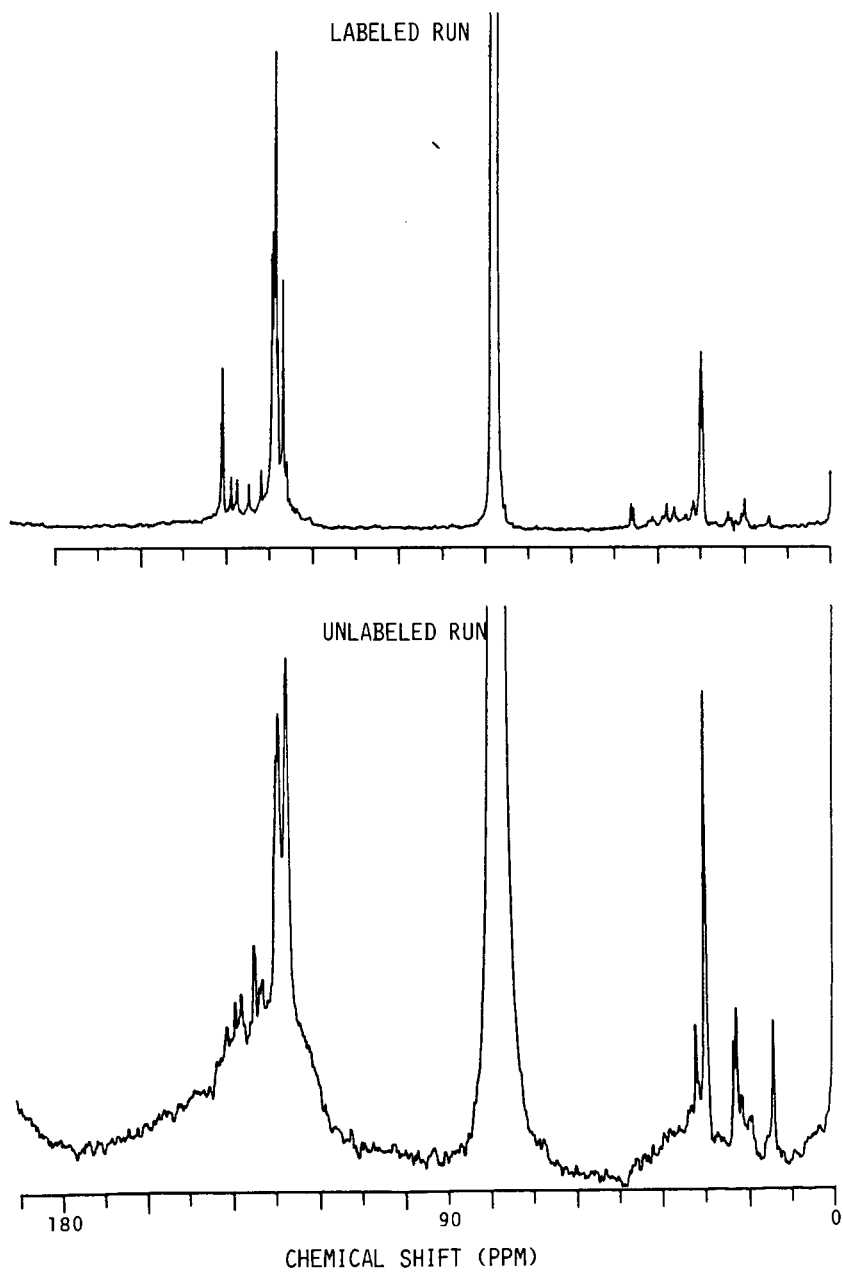
FIGURE 3. ^{13}C NMR SPECTRA OF PENTANE SOLUBLES FROM TETRALIN RUN

DETAILED CHARACTERIZATION OF SYNTHETIC FUEL STREAMS

by

Thomas Aczel, S. G. Colgrove, L. W. Dennis and S. D. Reynolds
Exxon Research and Engineering Company
Baytown Research and Development Division
P. O. Box 4255
Baytown, TX 77522-4255

INTRODUCTION

In depth characterization of synfuels requires the combination of several analytical tools and approaches. This requirement is due both to the complexity of the materials to be analyzed and to the information content that is desirable to obtain on semi-routine, research type samples.

Synfuels generally contain a large variety of hydrocarbons, including paraffins, cycloparaffins, aliphatic and aromatic olefins, one to eight-ring aromatics, and the corresponding aromatic furans, aromatic thiophenes, hydroxy-aromatics, dihydroxy-aromatics, aromatic pyrroles and aromatic pyridines. Minor amounts of polyfunctional components, such as thiophenofurans, hydroxy-nitrogen compounds, etc., are also present, as well as ketones, aldehydes, acids, amides, nitriles and dinitrogen compounds. Alkyl substitution of the above can range from zero to up to 50 carbon atoms. All considered, a typical synfuel sample contains as many as 1000 to 3000 carbon number homologs and many more positional isomers.

In our Laboratories, the information content required in general includes at least the identification and determination of most carbon number homologs, that is most discreet formulas, and as many individual isomers as can be separated by gas chromatography (GC) or gas chromatography/mass spectrometry (GC/MS). These are numerous, in particular in the lower boiling ranges up to about C_{12}, where the number of isomers is sufficiently small to be resolved by capillary column GC.

This presentation deals with the methodology developed at our laboratories for the detailed characterization of synfuels. This methodology will be illustrated with examples taken from the detailed analysis of a standard Colorado shale oil purchased from the National Bureau of Standards (SRM 1580). Issues discussed will include separation procedures and the analysis of the separated fractions by high and low resolution mass spectrometry (HRMS and LRMS), GC/MS, nuclear magnetic resonance (NMR) and other methods.

DISCUSSION

A. Overall Procedure

The analytical scheme devised for the characterization of complex synfuels that include significant amounts of non-hydrocarbons consists essentially of a separation step followed by extensive instrumental analysis of the separated fractions. A schematic of the procedure is given in Figure 1.

The extensive separation steps used yield important information on the chemical classes of components present, enrich trace components, facilitate subsequent instrumental analyses by greatly simplifying the samples to be analyzed, and eliminate many uncertainties related to composition as the presence of a given component in one or the other fraction is a clue to its identification. For example, high resolution MS can not determine in complex mixtures whether a component whose formula contains one oxygen atom is aromatic furan or a hydroxy-aromatic; but the component can be safely assigned a furanic or a hydroxy-aromatic structure according to whether it occurs in a neutral aromatic or in an acidic fraction. The number of fractions separated depends on the amount of information desired; and varies from three (saturates, aromatics, polars) to twelve, as discussed in this presentation. Unseparated materials can also be analyzed; the loss of information content is compensated by the faster response time and lower analytical expenditure. Furthermore, composition uncertainties can be resolved reasonably well in many such cases by using assumptions based on information obtained from separated samples.

Instrumental tools used for in depth analysis of the fractions include high resolution MS, GC/MS, ^{13}C and ^{1}H NMR, GC distillations and elemental analyses. Data from these analyses are integrated to provide the user with a multi-faceted insight into the overall composition.

B. Separations

The separation scheme used for the NBS shale oil is shown in Figure 2. It is based largely on procedures developed at the Laramie Energy Technology Center of the Department of Energy, now Western Research Institute. Generally, the procedure yields sharp fractions, although overlaps exist, in particular between some of the aromatic and the lower polarity "polar" fractions, such as the "neutral polars". As will be shown below, most of the overlaps can be corrected by the subsequent instrumental analyses of the fractions. In fact, if, as mentioned above, separations improve the overall characterization, one can also state that the characterization steps can improve the quality of the separations by correcting for separation overlaps. Both analytical steps are necessary for in depth understanding.

Another advantage of the above separation scheme is that it isolates some components that are not generally detected by high resolution, low voltage mass spectrometry and that would be very difficult to detect by GC/MS in very complex mixtures. These are mainly the aliphatic ketones and nitriles that are found in the neutral polars, weak acids, and weak bases.

Quantitative data on the fractions separated from the NBS shale oil are given in Table I. Major components are saturates and olefins (mostly linear), strong bases, neutral polars and the 1-ring aromatics. Loss was only about 9 percent, a small amount considering that the sample contained significant concentrations of relatively low-boiling materials in the C_8-C_{12} range.

The aliphatic fraction was separated further into saturates and olefins. Although the purity of the fractions was high, recovery was low. For this reason, quantitative data were obtained on total aliphatics.

123

C. Instrumental Analysis

The aliphatic fractions were analyzed by low resolution, high voltage MS, GC/MS, ^{1}H and ^{13}C NMR. All other fractions were analyzed by the same methods, except that the MS analyses were obtained in the much more powerful high resolution, low voltage mode, rather than under low resolution, high voltage conditions.

The type of information available from the above methods is summarized.

Low Resolution, High Voltage MS: Concentration of saturate and aromatic compound types (homologous series). In the present work, the approach was used only on the aliphatic fraction. A major disadvantage is the impossibility of distinguishing cycloparaffins from olefins, dicycloparaffins from cyclic olefins or diolefins, etc., due to the fact that they have the same general formulas.

High Resolution, Low Voltage MS: Concentration of aromatic and polar aromatic carbon number homologs. The method can determine several thousand components per sample, including hydrocarbons and heterocompounds and yields both very detailed and summarized data. Its main disadvantage is that it cannot be applied to aliphatic components.

GC/MS: Identifications and semi-quantitative analysis of individual components -- usually several isomers for each carbon number homolog. Applicable to both aromatic and aliphatic components, but limited by the resolution of the GC and the MS, boiling point and the unavailability of reference spectra for many of the components found in shale oils.

^{13}C and ^{1}H NMR: Overall saturate, olefinic or aromatic character; semi-quantitative insight into average structural features.

D. Typical Results

The major compound types determined in the various fractions are listed in Table II. The wide variety is an indication of the complexity of the shale oil studied. Most of the hydrocarbons, furans, thiophenes, hydroxy-aromatics and aromatic nitrogen types were detected both by high resolution MS and GC/MS. Some of the more condensed materials were determined only by high resolution MS; conversely aliphatic polar types such as ketones and nitriles were seen only by the GC/MS as these materials generally do not give significant molecular ions at low voltages.

A summary of the high resolution MS analyses of the fractions is given in Tables III-V. Most of the data is self-explanatory; several comments are, however, in order.

● Overall condensation is low; most of the components are either linear, or contain one or two aromatic or polar aromatic rings.

● Separation is rather sharp in most of the fractions; including the aromatic sub-fractions. Aromatic overlaps found mainly in the "less polar" polar fractions, such as the weak bases and the neutral polars, and these aromatics are the most condensed types, that indeed possess

some polar (basic) character. As most of the aliphatic polars not seen by high resolution MS are concentrated in these same fractions, they are probably more enriched in polar components than indicated by the high resolution MS data.

● Asphaltenes contain a very large amount of non-volatile components. We are now developing quantitative methods for determining at least the molecular weight distribution of this type of materials in the 500-3000+ molecular weight range using field desorption mass spectrometry.

Selected NMR parameters of the fractions are shown in Table VI. Aromatic character increases, as expected, with nominal condensation, in good agreement with the MS data. Fractions that contain aliphatic polars, such as the neutral polars and the bases have lower aromaticity, as expected. In general, the NMR analyses confirm the efficiency of the separations. The consistency of the NMR characterization is evident from the very good agreement between the experimental data obtained on the total sample before the separation and the composite values calculated from the eleven fractions analyzed separately (Table VII).

The GC/MS procedure is illustrated by partial chromatograms of the aliphatic (saturates plus olefins) and the neutral polar fraction that contains nitriles and ketones (Figures 3, 4). The composition pattern shown repeats itself in the higher carbon number range, up to about C_{25}-C_{30}.

The ideal analytical approach in this type of effort is the integration of all the analytical data. This is implicit in the data reported in the previous sections. A more explicit procedure is to identify as many individual isomers of a given carbon number homolog, say C_{10} benzenes or C_7 pyridines, as possible by GC/MS and then to normalize this data to the total concentration of the homolog as determined by high resolution MS, using these powerful techniques in a complementary way. The validity of the approach is confirmed by the data in Table VIII that shows good agreement between quantitative HRMS data on the total carbon number homologs and the sums of the corresponding isomers as determined by GC/MS. One can thus assume that if the high resolution MS data on a given carbon number homolog show much higher values than the corresponding sums of the isomers found by GC/MS, the deviation is due to isomers not detected by GC/MS.

CONCLUSION

The data reported in this work show that very complex mixtures, such as synfuels, can be characterized accurately and in great detail by a combination of analytical techniques. This multitechnique approach is essential for any in depth understanding of the composition of these materials. Much more work is needed to corroborate and to extend the information gathered in this work but we believe we have the means to do so.

Table I

NBS SRM 1580 SHALE OIL PREP LC DATA

Fraction	Weight Percent
Asphaltenes	1.60%
Weak Acids	5.00%
Strong Acids	0.^5%
Weak Bases	1.84%
Strong Bases	15.43%
Saturates + Nonaromatic Olefins	34.05%
1-Ring Aromatics	8.10%
1-2 Ring Aromatics	5.05%
2-3 Ring Aromatics	1.84%
3+ Ring Aromatics	0.89%
Neutral Polars	16.46%
Hold-Up & Losses	9.28%
Total	100.00%

Table II

MAJOR COMPOUND TYPES IN NBS SHALE OILS FRACTIONS

1. Saturate Fraction
   n-Paraffins
   Isoprenoid Paraffins
   Cycloparaffins

2. Olefin Fraction
   Alpha Olefins
   Internal Olefins

3. "1-Ring Aromatic" Fraction
   Benzenes
   Styrenes
   Indans/Tetralins
   Thiophenes

4. "2-Ring Aromatic" Fraction
   Indans, Tetralins
   Indenes
   Naphthalenes
   Biphenyls
   Acenaphthenes
   Benzothiophenes
   Benzofurans

5. "3-Ring Aromatic" Fraction
   Naphthalenes
   Biphenyls
   Fluorenes
   Phenanthrenes
   Pyrenes

6. "3+Ring Aromatic" Fraction
   Phenanthrenes
   Chrysenes
   Benzoanthracenes

7. Neutral Polar Fraction
   Linear Cyclic Ketones
   Aliphatic & Nitriles
   Benzonitriles/Indoles

8. Weak Acid Fraction
   Phenols
   Carbazoles
   Pyrroles
   Aliphatic Nitriles

9. Strong Acid Fraction
   Phenols
   Hydroxy-Indans/Tetralins
   Carbazoles

10. Weak Base Fraction
    Nitriles
    2-Ketones
    Acetophenones

11. Strong Base Fraction
    Pyridines
    Quinolines
    Tetrahydroquinolines
    Tetrahydrocarbazoles

12. Asphaltenes
    Non-Volatiles
    1-3 Ring Nitrogen Compounds

Table III

SUMMARY COMPOSITION OF NEUTRAL FRACTIONS AS DETERMINED BY HIGH AND LOW RESOLUTION MS

| | Weight Percent | | | | |
| | | Aromatics | | | |
Component Type	Aliphatics	1 Ring	2 Ring	3 Ring	4 Ring
Aliphatics	95.6	0.0	0.0	0.0	0.0
Aromatic Hydrocarbons	4.4	82.2	87.0	83.6	78.7
1 Ring	4.4	73.1	16.8	1.4	3.1
2 Ring	0.0	9.2	62.3	29.1	12.1
3 Ring	0.0	0.0	6.9	42.9	38.0
4 Ring	0.0	0.0	0.9	9.6	24.9
5+Ring	0.0	0.0	0.1	0.6	0.6
Aromatic Thiophenes	0.0	17.5	7.4	7.1	8.8
1 Ring	0.0	15.5	0.2	1.4	2.9
2 Ring	0.0	2.0	6.3	5.6	2.9
3+Ring	0.0	0.0	0.9	0.1	3.0
Aromatic Furans	0.0	0.3	4.0	5.7	3.1
1 Ring	0.0	0.3	2.3	1.0	0.0
2 Ring	0.0	0.0	1.6	3.4	0.5
3 Ring	0.0	0.0	0.1	0.7	1.1
4+Ring	0.0	0.0	0.0	0.6	1.5
Aromatic Difurans	0.0	0.0	0.0	0.3	1.5
Nitrogen Cpds.	0.0	0.0	1.6	3.3	6.3
Residue	0.0	0.0	0.0	0.0	1.6

Table IV

SUMMARY COMPOSITION OF POLAR FRACTIONS AS DETERMINED BY HIGH RESOLUTION MS

Component Type	Weight Percent					
	Neutral Polars	Weak Acids	Strong Acids	Weak Bases	Strong Bases	Asphaltenes
Mono-Oxygen Cpds. (mostly hydroxy-aromatics)	11.9	15.2	43.4	4.1	0.2	1.7
1 Ring	9.2	11.7	35.6	2.8	0.1	0.7
2 Ring	1.4	2.1	6.4	1.1	0.1	0.8
3 Ring	0.8	0.6	1.3	0.2	0.0	0.2
4+Ring	0.5	0.8	0.1	0.0	0.0	traces
Di-Oxygen Cpds. (mostly dihydroxy-aromatics)	0.0	2.5	6.0	0.0	0.0	0.6
1 Ring	0.0	1.7	4.5	0.0	0.0	0.5
2+Ring	0.0	0.8	1.5	0.0	0.0	0.1
Nitrogen Cpds.	57.1	54.0	8.5	63.1	88.0	10.5
1 Ring	2.2	5.2	0.3	4.3	45.3	1.9
2 Ring	37.4	25.0	3.0	30.5	25.6	5.0
3 Ring	15.5	18.2	4.6	22.6	13.5	3.0
4+Ring	2.0	5.6	0.6	5.7	3.6	0.6
Nitrogen-Oxygen Cpds.	0.7	3.5	10.4	4.9	0.4	1.4
1 Ring	0.1	1.4	6.9	1.0	0.1	0.4
2 Ring	0.3	1.4	2.9	2.3	0.1	0.8
3+Ring	0.3	0.7	0.6	1.6	0.2	0.2
Misc. N. Compounds	0.4	3.0	1.2	0.0	2.0	1.0
Aromatic Hydrocarbons	22.0	2.1	0.5	7.0	1.9	0.3
1-3 Ring	6.5	2.1	0.4	1.9	1.7	0.2
4-6 Ring	15.5	0.5	0.1	5.1	0.2	0.1
Thiophenes	0.3	0.3	0.2	0.2	0.0	Traces
Furans	0.0	0.0	0.0	0.0	0.0	0.0
Residue	7.6	19.4	29.8	20.6	7.5	84.5

129

Table V

SUMMARY COMPOSITION OF SHALE OIL AS CALCULATED FROM ANALYSES OF FRACTIONS

Component	Wt. Pct.	Component	Wt. Pct.
Aliphatics	32.53	Polar Aromatics	31.49
Neutral Aromatics	21.43	Mono-Oxygen Cpds.	3.04
		1 Ring	2.35
Hydrocarbons	18.98	2 Ring	0.41
1 Ring	8.86	3 Ring	0.17
2 Ring	4.94	4+Ring	0.11
3 Ring	2.01		
4 Ring	2.76	Di-Oxygen Cpds.	0.16
5+Ring	0.41	1 Ring	0.11
		2 Ring	0.04
Thiophenes	2.07	3+Ring	0.01
1 Ring	1.33		
2 Ring	0.63	Nitrogen Cpds.	27.23
3 Ring	0.10	1 Ring	7.74
4+Ring	0.01	2 Ring	12.08
		3 Ring	6.12
Furans	0.36	4+Ring	1.29
1 Ring	0.16		
2 Ring	0.14	Nitrogen-Oxygen Cpds.	0.51
3 Ring	0.02	1 Ring	0.14
4+Ring	0.04	2 Ring	0.21
		3+Ring	0.15
Difurans	0.02		
		Misc./Nitrogen Cpds.	0.55
		Residue	5.27
		Separation Loss	9.28

Table VI

SELECTED NMR DATA ON FRACTIONS

Carbon Type	Mole Percent							
	Alipha-tics	Aromatics			Neutral Polars	Acids	Bases	Asphaltenes
		1 Ring	2 Ring	3 Ring				
Aromatics	0.0	33.5	54.2	54.3	33.0	55.1	40.4	66.3
Olefinic	2.3	1.4	0.0	0.0	0.0	0.0	0.0	0.0
Aliphatic	97.6	65.2	45.8	45.7	67.0	44.9	59.6	33.7

Table VII

COMPARISON OF NMR DATA ON FRACTIONS AND TOTAL SAMPLE

Carbon Type	Mole Percent	
	Composite Calculated from Fractions	Experimental Value Found for Total Sample
Aromatic	25.8	27.2
Olefinic	1.0	1.6
Aliphatic	73.2	71.2

Table VIII

COMPARISON OF HIGH RESOLUTION MS (HRMS) AND GC/MS DATA
ON SELECTED COMPONENTS IN VARIOUS FRACTIONS

Components	Concentration HRMS	GC/MS	No. of Components
Alkylbenzenes, wt. pct.			
C_8	0.48	0.25	4
C_9	1.27	1.42	8
C_{10}	6.06	6.61	17
C_{11}	7.02	6.34	19
C_{12}	2.90	2.53	26
Phenols, ppm			
C_6	4.3	8.0	1
C_7	28.4	26.0	3
C_8	16.9	17.8	6
Pyridines, wt. pct.			
C_5	0.10	0.19	1
C_6	1.02	1.11	3
C_7	0.69	0.60	9
C_8	0.19	0.10	4

FIGURE 1

OVERALL ANALYTICAL APPROACH

```
                    ┌─────────────┐
                    │  SHALE OIL  │
                    └─────────────┘
                          │           ┌──────────────┐
                          ├──────────▶│  ASPHALTENES │
                          ▼           └──────────────┘
                    ┌─────────────┐
                    │     OILS    │
                    └─────────────┘
                          │
                        ╱ PREP ╲
                       ╱  HPLC  ╲
                      ╱──────────╲
                          │
              ┌───────────────────────┐
              │  3 TO 12 FRACTIONS    │
              └───────────────────────┘

   ╱ MS ╲     ╱ NMR ╲    ╱ GC/MS ╲    ╱ ELEM.     ╲
                                      ╱ ANALYSIS   ╲
```

133
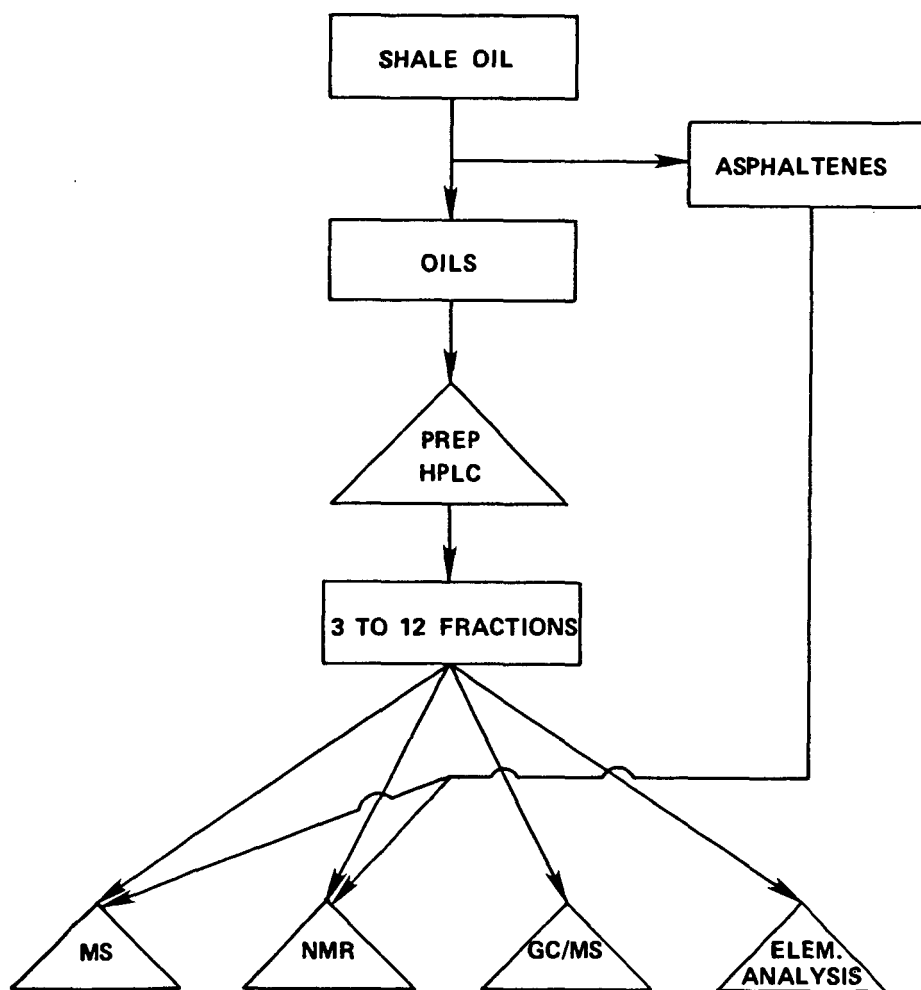
FIGURE 2

DETAILED SEPARATION SCHEME

```
                    ┌─────────────────┐
                    │  DEASPHALTENED  │
                    │   SHALE OIL *   │
                    └────────┬────────┘
                             ▼
                    ┌─────────┐  IRA-904
                    │/////////│  ANION EXCHANGE RESIN
                    └─────────┘
```

PENTANE   CH₂Cl₂   CH₃OH

BASE NEUTRALS   WEAK ACIDS *   STRONG ACIDS *

AMBERLIST 15 CATION EXCHANGE RESIN

PENTANE   1. CH₂Cl₂   1. 1:1 CH₃OH:IPA (1)
                 2. CH₃OH   2. IPA
                                    3. 1:9 IPA:CH₃OH (SOXHLET EXTRACT)

NEUTRALS   WEAK BASES *   STRONG BASES *

SILICA GEL + NH₂

PENTANE   PENTANE   PENTANE   PENTANE   PENTANE   CH₂Cl₂

ALIPHATICS*   1 RING * AROMATICS   2 RING * AROMATICS   3 RING * AROMATICS   3+ RING * AROMATICS   NEUTRAL * POLARS

AgNO₃ + SILICA

PENTANE

SATURATES *   ALIPHATIC * OLEFINS

* FRACTIONS SUBMITTED TO INSTRUMENTAL ANALYSES (MS, GC/MS, NMR, ETC.)

(1) ISOPROPYL-AMINE

FIGURE 3

PARTIAL GC/MS CHROMATOGRAM OF WBS SHALE OIL
SATURATES & OLEFINS
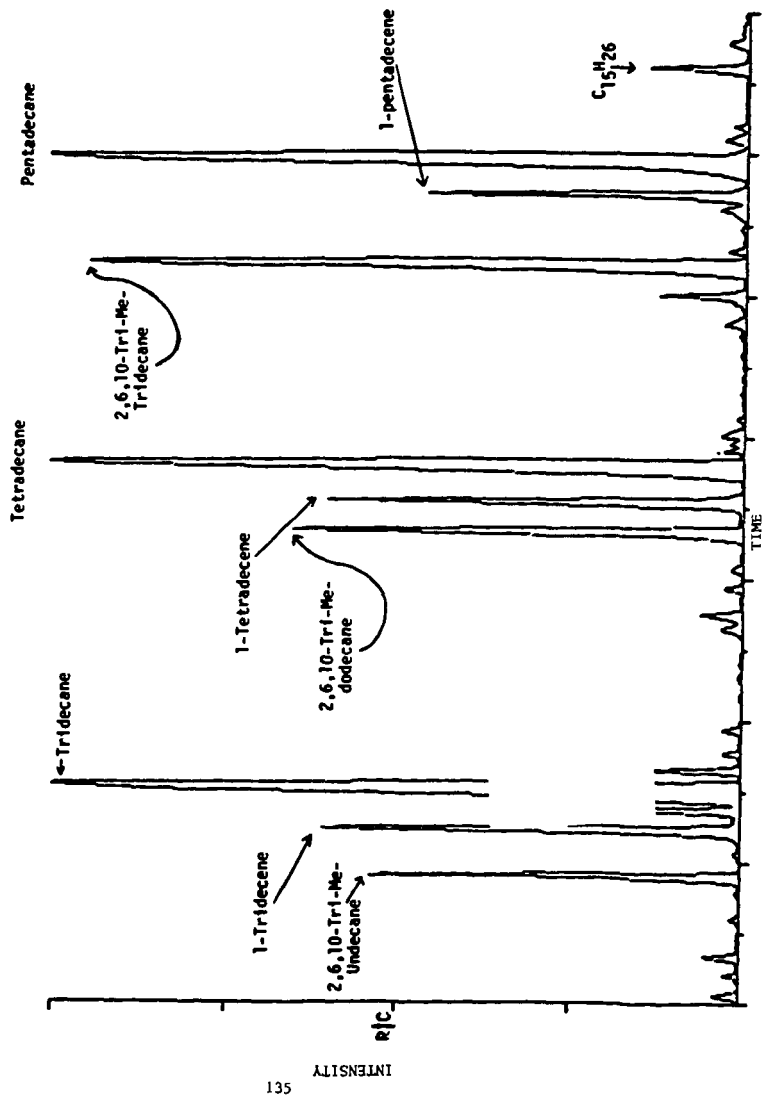
FIGURE 4

PARTIAL GC/MS CHROMATOGRAM OF NBS SHALE OIL
NEUTRAL POLARS
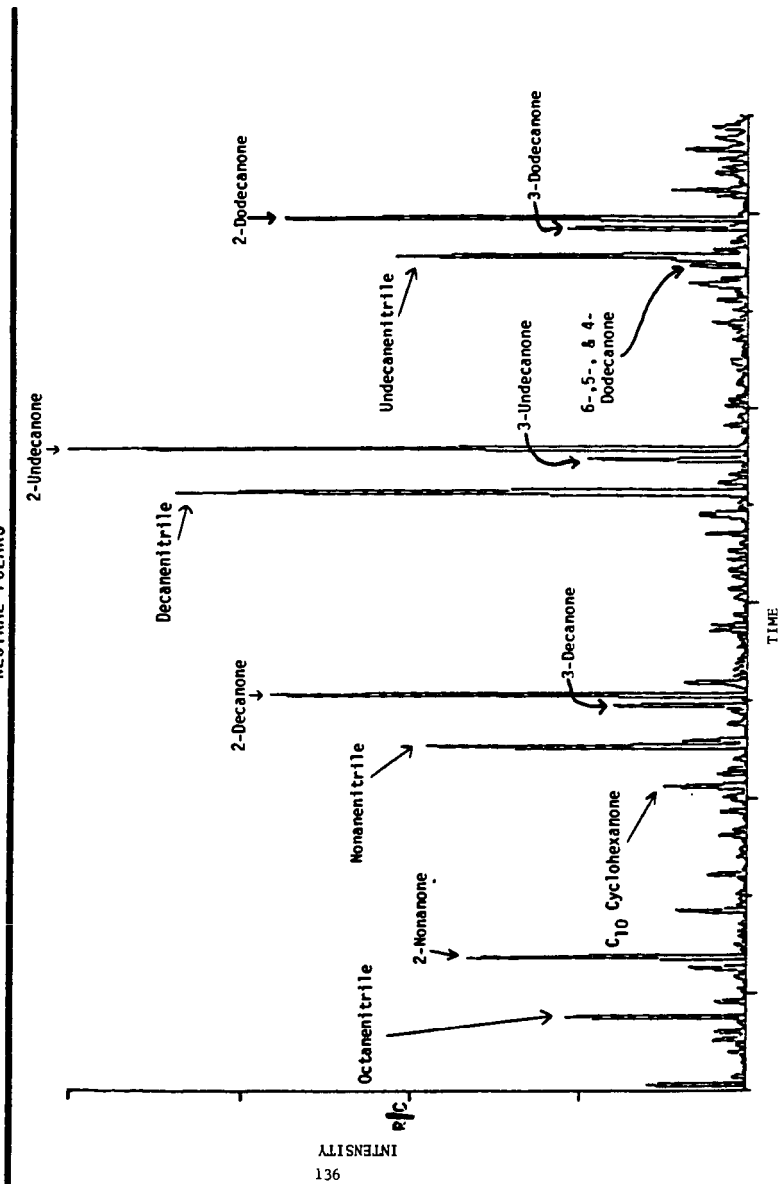
WEATHERING EFFECTS ON YIELD AND COMPOSITION OF PYROLYTIC COAL TARS

Emma Jakab, William H. McClennen, Barbara Hoesterey,
Henk L.C. Meuzelaar and George R. Hill

University of Utah, Biomaterials Profiling Center
391 S. Chipeta Way, Suite F, Research Park
Salt Lake City, Utah 84108

INTRODUCTION

Over the past few years the main thrust of our fossil fuels research program at the University of Utah Biomaterials Profiling Center has been to investigate the oxidation ("weathering") behavior of coals and coal liquids. Specific objectives of this program are: elucidation of relevant structure/reactivity relationships and of regressive reaction mechanisms; determination of the influence of weathering on technological properties (e.g., caking, calorific value, flotability and extractibility as well as liquefaction and gasification behavior); and development of novel, reliable methods for measuring the "weathering index" of coal samples from a given seam or field.

Our experimental approach has been primarily based on a combination of conventional coal pyrolysis and characterization methods and more advanced instrumental techniques, such as pyrolysis mass spectrometry (Py-MS), thermogravimetry (TG) and liquid chromatography (LC), with sophisticated numerical analysis methods, such as factor and discriminant analysis (1,2,3).

In previous reports we have discussed our findings with regard to weathering effects on structure/reactivity relationships (1), free swelling index (1,2), calorific value (1,2), extractability (1,4) and tubing bomb reactor (TBR) conversion yields (1). In many instances, interpretation of our findings appeared to benefit from - and thus lend additional support to - a "binary" coal structure model, recently proposed by Given (5). According to this model, most coals contain a sizeable fraction of "mobile phase" components, many of which are physically trapped in clathrate-like structures formed by the "network phase". From our weathering studies on HVB Hiawatha coal we concluded that the main weathering effect could be explained as a loss of mobile phase components through "grafting" onto the network phase (1).

In this paper, we present the results of a study on the effects of weathering on pyrolytic tars produced by a vacuum micropyrolysis technique (Curie-point Py-MS) which can be used as a model system for short contact time pyrolysis processes in bench scale, as well as pilot plant scale reactors.

EXPERIMENTAL

Coal samples were obtained from fresh channel cuts in the Hiawatha and Adaville #6 (Kemmerer field, Wyoming) seams as well as from a recent, carefully preserved, drill core of the Anderson seam (Powder River basin, Wyoming). All samples were milled to <60 mesh in nitrogen atmosphere. Sample storage took place under nitrogen in hermetically closed glass bottles at -20°C in the dark. A fresh Blind Canyon seam (Wasatch Plateau field, Utah) coal tar sample was obtained from a pilot plant scale Wellman-Galusha gasifier run (3) and stored in tough fluorocarbon plastic containers immersed in liquid nitrogen.

In the laboratory weathering experiments, 15-20 g aliquots of coals were exposed to air at different temperatures using a specially constructed bench scale weathering equipment described elsewhere (6). Weathering temperatures and times of the coals

studied are listed in Table I. Weathering of the coal tar took place in oxygen
heating 150-300 mg samples in sealed glass vials at 80°C for 64 hours. Control coal
and tar samples were exposed to nitrogen atmosphere under similar conditions as the
air and oxygen weathered samples.

Pyrolysis experiments were performed using an Extranuclear 5000-1 Curie-point Py-MS
system (7). Twenty five μg coal samples were coated on ferromagnetic wires from
methanol or toluene suspensions. Pyrolysis and mass spectrometry conditions were as
follows: heating rate approx. 100°C/s, end temperature 610°C, total heating time
10 s, electron energy 12 eV, mass range scanned m/z 20-260. Tar evaporation/-
pyrolysis spectra were obtained under the same conditions by coating 10 μg samples
on the wires from dichloromethane solutions. Time-resolved spectra of fresh and
weathered Hiawatha coals were obtained by scanning 3-8 mass peaks during each pyrol-
ysis experiment and recording the envelopes of the ion intensities.

Computerized data analyses were performed on the Py-MS data sets of fresh, N2
exposed and air/oxygen weathered coal and tar samples. Weathering-induced differ-
ences were analyzed using factor and discriminant analysis methods (8,9).

RESULTS AND DISCUSSION

A systematic investigation of the effects of coal weathering on the yield and com-
position of pyrolytic tars requires the availability of suitable model systems for
controlled weathering and pyrolysis of well defined coal samples. Bench scale
equipment for weathering coal samples in controlled atmospheric environments has
been described in previous reports (6,10). Moreover, tubing bomb reactor (TBR)
equipment has been used widely to study coal pyrolysis behavior and is reported to
provide a valid model for pilot plant scale coal conversion processes (11).

Unfortunately, even TBR runs require time-consuming equipment preparation and
product work-up steps. One of the largest TBR studies reported in the literature,
involving 104 U.S. coals, was carried out by Given and co-workers (12) over a one
year period. The size of the study was dictated by the need to perform a thorough
statistical analysis of the relationships between coal characteristics and coal
yield. In contrast, a vacuum micropyrolysis study of 102 U.S. coals by means of
Curie-point Py-MS, as reported by Meuzelaar *et al*. (13), was carried out in only two
weeks while including quadruplicate runs of each sample to further enhance statis-
tical analysis possibilities.

Moreover, several other studies have provided strong indications that Curie-point
Py-MS can be used as a valid model for short contact time pyrolysis processes in TBR
systems. For instance, the composition of pyrolytic tars obtained by means of a
rapid heating TBR system has been shown to be comparable to that of coal pyrolyzates
obtained by direct Py-MS (1). Moreover, pyrolysis tar from a pilot plant scale
Wellman Galusha fixed bed reactor (Figure 1a) can be seen to be quite similar to a
Curie-point pyrolyzate (Figure 1b) when allowing for the loss of gaseous products
during collection of the Wellman-Galusha tar. More recently, a systematic Py-MS
study of 47 U.S. coals, carried out by Voorhees and co-workers (14), has further
demonstrated the validity of Curie-point Py-MS as a coal pyrolysis model capable of
predicting tar yields in TBR experiments as well as in larger scale pyrolysis re-
torts.

Examples of the use of the Curie-point Py-MS technique to study the composition of
pyrolytic coal tars from three Western coals, a Hiawatha high volatile A bituminous
coal, an Adaville #6 subbituminous coal and an Anderson seam lignite, are shown in
Figure 2. As expected, rank related differences between the three coals, e.g.
reflected by an increase in dihydroxybenzenes and phenols and a relative decrease in
naphthalenes and short chain aliphatic hydrocarbons (13) are dominant in the spectra.

Nevertheless, weathering-induced changes (marked by arrows on the spectra of fresh coals in Figure 2), e.g., involving an increase in aliphatic carboxylic acids and ketones accompanied by decreased yields of phenols and dihydroxybenzenes in the lignite and subbituminous coal samples as well as a strong reduction in naphthalenic peak intensities in the hvb coal, are also easily recognizable. Earlier studies on weathered Hiawatha coal samples showed that conversion yields obtained by short contact time pyrolysis in a tubing bomb reactor (25 s at 420°C) decreased by 50% (1), whereas micropyrolysis (Curie-point Py-MS at 610°C for 5 s) yields decreased by an estimated 20% (4). Preliminary results from Py-MS experiments on all three Western coals discussed here indicate that vacuum micropyrolysis conversion yields decrease by an estimated 10-30% upon weathering.

Comparison of the ion intensities as a function of pyrolysis time (time profile curves) reveals that the evolution shape of several ion intensity curves is different between fresh and air weathered coals as shown for Hiawatha coal in Figure 3. Increased solvent (methanol; m/z 32) retention indicates increased polarity in the weathered coal. The fact that carbon dioxide (m/z 44) as well as benzene (m/z 78) curves both show an increasing, early component may indicate aromatic carboxylic acid formation during weathering. Moreover, aliphatic carboxylic acid ions show increased early components as well (e.g., CH_3COOH^+ in Figure 3f). On the other hand alkylnaphthalenes (e.g., the C_2-alkylnaphthalene in Figure 3c) show a strong decrease at lower temperatures in the weathered coal.

The discriminant analysis results shown in Table I and Figure 4 reveal characteristic changes in the composition of the pyrolytic tars obtained from coals weathered in air, whereas little or no change is observed in the control samples exposed to N_2 atmospheres. Although a quantitative comparison of weathering-induced changes in the different coals is not possible because of variations in the total duration of the three experiments as well as in the weathering temperatures, qualitative analysis of the three discriminant spectra in Figure 4 reveals marked differences. For example, the pyrolytic tar obtained from weathered Anderson lignite shows a decreased contribution of dihydroxybenzenes, whereas the spectrum of the subbituminous Adaville #6 tar exhibits a more pronounced decrease in phenolic compounds as well. Moreover, slight increases in the relative contributions of aromatic hydrocarbons (benzenes + naphthalenes) can be noted in the latter. Furthermore, the pyrolyzate of weathered hvb Hiawatha coal tar shows a pronounced loss of naphthalenic compounds.

Although the detailed mechanism behind these changes are not yet understood the differences between three discriminant spectra in Figure 4 are more or less consistent with the differences observed between the composition of the pyridine extractable fractions of each of the three coals (not shown here). Consequently, our earlier interpretation of the loss of naphthalenic components in the pyrolyzate of Hiawatha coal as due to "grafting" of extractable mobile phase components onto the network phase (1), may well hold true for the two lower rank coals as well. Obviously, further work is required to confirm these findings and interpretations.

Finally, it should be noted that whereas changes in the relative abundance of aromatic compound series appear to be quite specific for each coal, all three coals show increased mass peak intensities at m/z 28 (e.g., $CO^{+\cdot}$), 44 (e.g. $CO_2^{+\cdot}$) and 60 (e.g. $CH_3COOH^{+\cdot}$). Apparently, the formation of polar functional groups, e.g. in short chain aliphatic moieties, is a general characteristic of oxidative changes in Western coals independent of differences in rank.

Whereas our experiments demonstrate that coal weathering influences the composition of pyrolytic tars it is also known that such tars are often quite reactive and prone to regressive reactions which may cause marked changes in the physical and chemical properties of the tar (15). In order to compare the effect of "regressive" reactions on the composition of pyrolytic tars with that of coal weathering processes,

carefully preserved samples of "fresh" tar from the Wellman Galusha gasifier and tar samples exposed to oxygen as well as control samples exposed to N_2 were analyzed by low voltage MS. Minor, but highly characteristic changes in chemical composition were found in the oxygen exposed samples by means of discriminant analysis techniques. The discriminant spectrum in Figure 5 reveals a decrease in the relative abundance of dihydroxybenzene peaks along with several other peak series thought to represent naphthols and phenols (and/or quinones). These observations are in agreement with earlier studies by McMillan *et al.* (15).

The Blind Canyon coal used to produce the Wellman Galusha tar is closely related to the Hiawatha coal and shows similar weathering behavior (10). Therefore it is interesting to note that whereas naphthalene moieties play a prominent role in coal weathering related changes they do not appear to be directly involved in oxidative tar processes. This would seem to indicate that both types of oxidative processes involve quite different reaction mechanisms. Whereas weathering induced loss of aromatic and hydroxyaromatic tar components is thought to be due primarily to "grafting" reactions between the mobile and the network phase, loss of hydroxyaromatic components during tar oxidation is more likely to be caused by simple condensation reactions. Additional evidence for such reactions is found in Figure 5 showing an increased abundance of small mass peaks in the high mass range (possibly representing condensed tar components) upon weathering.

CONCLUSIONS

Weathering-induced decreases in relative yields of pyrolytic tars from Western coals of different rank (lignite to hvb) may range from 20 to 50%, depending on pyrolysis conditions.

Pyrolytic coal tars of remarkably similar composition are obtained from a Wellman Galusha reactor and from a vacuum micropyrolysis experiment in spite of 8-9 orders of magnitude differences in sample size.

Vacuum micropyrolysis experiments on three Western coals of different rank (lignite, subbituminous and hvb-A) which were oxidized ("weathered") under controlled laboratory conditions show marked differences in the behavior of aromatic tar components but an overall similarity in the increase of polar, aliphatic compounds.

In each coal the observed changes in the relative abundance of aromatic compounds appear to be explainable by a loss of mobile phase components through "grafting" reactions with the network phase during coal weathering.

Small but characteristic changes which occur in the composition of a Wellman Galusha reactor coal tar during exposure to oxygen at 80°C point to the occurrence of condensation reactions involving dihydroxybenzenes and other hydroxyaromatic compounds.

REFERENCES

1. Meuzelaar, H.L.C., McClennen, W.H., Cady, C.C., Metcalf, G.S., Windig, W., Thurgood, J.R., Hill, G.R., "Pyrolysis Mechanisms and Weathering Phenomena in Rocky Mountain Coals" ACS Preprints (Div. of Fuel Chem.) Vol. 29, No. 5 (1984) pp. 166-177.

2. Hill, G.R., Meuzelaar, H.L.C., Cady, C.C., Metcalf, G.S., "Weathering Losses in Coal Piles", Report to UP&L, R&D-1011-84.

3. Meuzelaar, H.L.C., Hoesterey, B.M., McClennen W.H., Hill, G.R., "Composition and Stability of Pyrolytic Tars from HVB Wasatch Plateau Coals" Proceedings 10th Annual EPRI's Contractors' Conference on Coal Liquefaction, 1985.

4. Hill, G.R., Meuzelaar, H.L.C., Futrell, J.H., Harper, A.M., McClennen, W.H., "Role of Preasphaltenes in Coal Conversion Reactions", Final report to DOE, Contract No. DE-FG22-82PC50970, 1984.

5. Given, P.H., "An Essay on the Organic Geochemistry of Coal" in Coal Science, Vol. 3, M.L. Gorbaty, J.W. Larsen and I. Wender (eds.), Academic Press, 1984, pp. 63-341.

6. Meuzelaar, H.L.C., Hill, G.R., Hoesterey, B., "Weathering Losses in Coal Storage Piles", Report to UP&L, in press.

7. Meuzelaar, H.L.C., Haverkamp, J., Hileman, F.D., "Curie-point Pyrolysis Mass Spectrometry of Recent and Fossil Biomaterials: Compendium and Atlas", publ. Elsevier, Amsterdam (1982).

8. Windig, W., Meuzelaar, H.L.C., Anal. Chem. 56, (1984) 2297-2303.

9. Meuzelaar, H.L.C., Windig, W., Harper, A.M., Huff, S.M., McClennen, W.H., Richards, J.M., Science, Vol. 226, No. 4672, Oct. 19, 1984, 268-274.

10. Hill, G.R., Meuzelaar, H.L.C., Kithany, S., Tai, W. Cady, C.C., "Free Swelling Index of Utah High Volatile Bituminous Coals" Report to Utah Power & Light (R&D-1003-83).

11. Maa, P.S., Neavel, R.C., Vernon, L.W., "Tubing Bomb Coal Liquefaction Techniques" Industrial Engineering Chemistry (Process Design and Development Section) 23, (1984) 242.

12. Yarzab, R.F., Given, P.H., Spackman, W., Davis, A., Fuel 59, (1980) 81.

13. Meuzelaar, H.L.C., Harper, A.M., Hill, G.R., Given, P.H., Fuel 63, (1984) 640.

14. Durfee, S.L., Voorhees, K.J., "Pyrolysis Mass Spectrometric Prediction of Liquefaction Reactivity and Structural Analysis of Coals" submitted to Anal. Chem., (1985).

15. McMillen, D.F., Chang, S.J., Malhotra, R., Ogier, W.C., Ross, D.S., "The Effects of Oxygen Functionalities on Bond Scission and Retrograde Reactions in Coal Liquefaction", Proceedings Ninth Annual EPRI Contractors' Conference on Coal Liquefaction, EPRI AP-3825-SR.

ACKNOWLEDGEMENTS

TABLE I

WEATHERING CONDITIONS OF THE COALS STUDIED

Sample Treatment	Hiawatha	Adaville # 6	Anderson
Air weathered	100°C, 96 hr.	100°C, 96 hr.	80°C, 232 hr.
N_2 exposed	80°C, 120 hr.	100°C, 96 hr.	80°C, 232 hr.

TABLE II

SCORES OF THE FIRST DISCRIMINANT FUNCTIONS OBTAINED FOR PYROLYSIS MS DATA ON

FRESH, N_2 EXPOSED AND AIR WEATHERED SAMPLES

Sample* Treatment	Discriminant Scores (DI)		
	Hiawatha	Adaville #6**	Anderson
Fresh	1.61 ± 0.34	0.88 ± 0.07	1.68 ± 0.34
N_2 exposed	1.20 ± 0.27	0.88 ± 0.44	1.09 ± 0.10
Air weathered	-1.13 ± 0.31	-0.98 ± 0.33	-0.85 ± 0.43

 * Weathering conditions are shown in Table I.

** Discriminant function rotated for maximum discrimination.
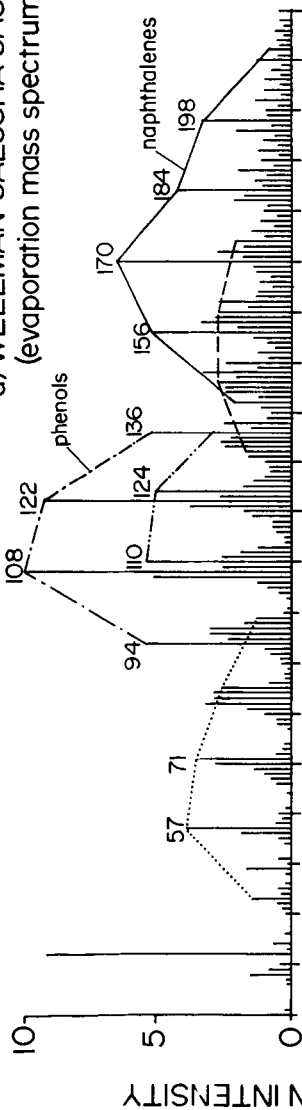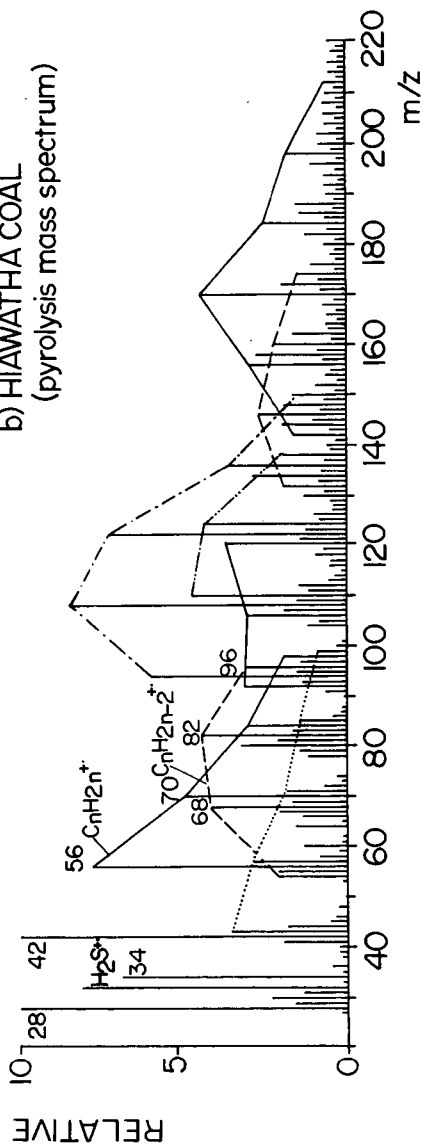
Figure 1. Comparison of low voltage mass spectra of (a) Wellman-Galusha gasifier tar (Blind Canyon seam) and (b) Curie-point pyrolyzate of a coal from a related Wasatch Plateau seam (Hiawatha seam). Note marked correspondence in high mass range.

143
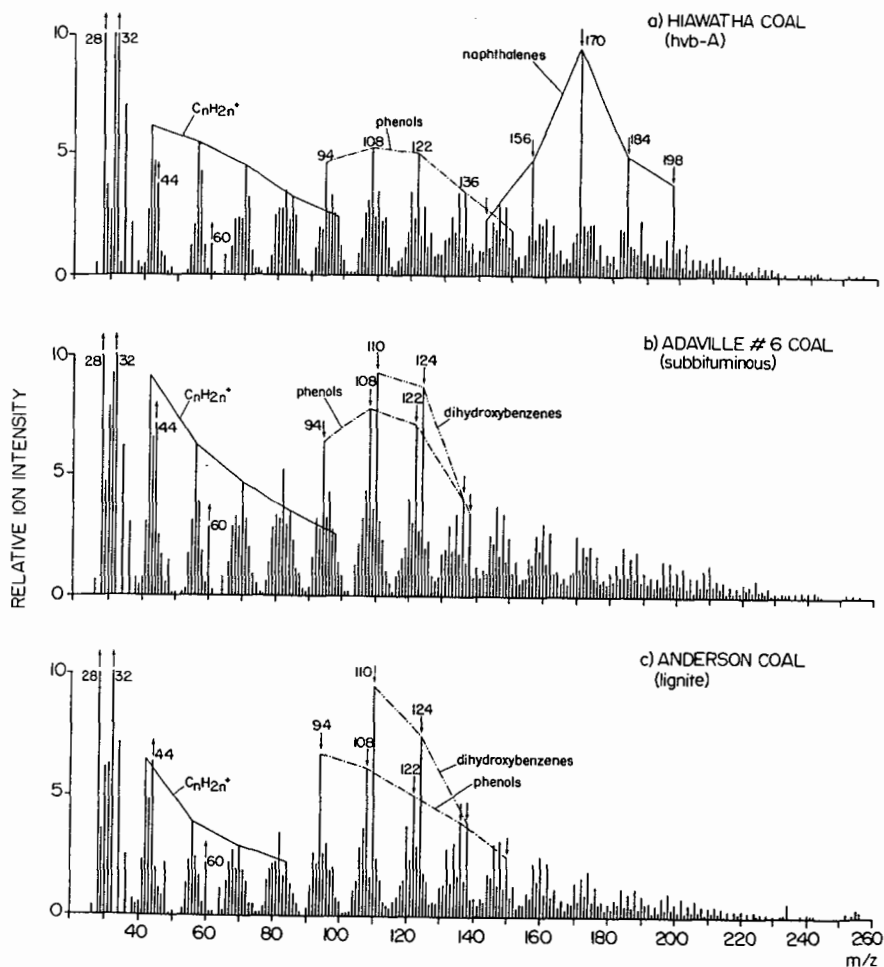
Figure 2. Low voltage pyrolysis mass spectra of fresh coal samples from (a) Hiawatha seam (b) Adaville #6 seam and (c) Anderson seam. Arrows indicate changes in mass peak intensities in the air weathered coals. Note that mass spectrometry conditions were different from that in Figure 1 resulting in increased sensitivity in high mass range.

144
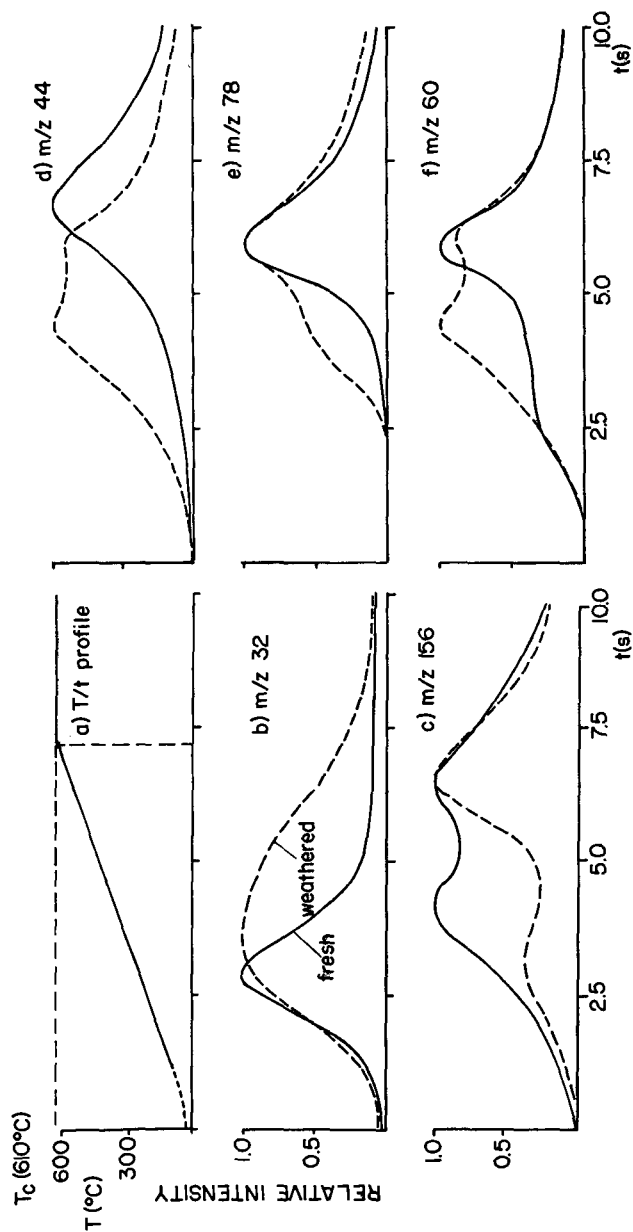
Figure 3. Time-resolved recording of ion signals at: (b) m/z 32 (methanol); (c) 156 (e.g., C₂-alkylnaphthalenes); (d) m/z 44 (mainly carbon dioxide); (e) m/z 78 (e.g., benzene); and (f) m/z 60 (e.g., acetic acid) during Curie-point pyrolysis of fresh (——) and air weathered (---) Hiawatha coal. Estimated temperature/time profile is shown in (a).

145
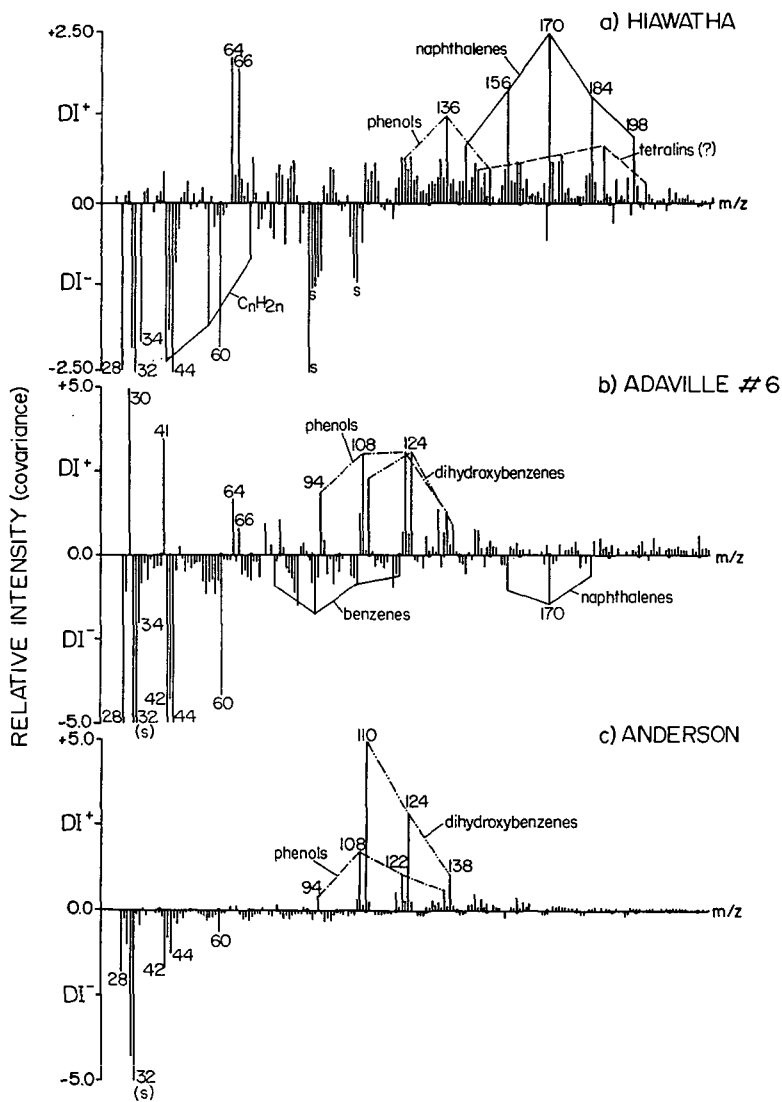
Figure 4. Discriminant spectra obtained on Py-MS data sets of fresh and air weathered coals from: (a) Hiawatha seam; (b) Adaville #6 seam; and (c) Anderson seam. Positive components (DI$^+$) represent mass peaks decreased in weathered samples. Negative components (DI-) represent compounds increased in weathered samples. (s) denotes peaks originating from solvent(s).
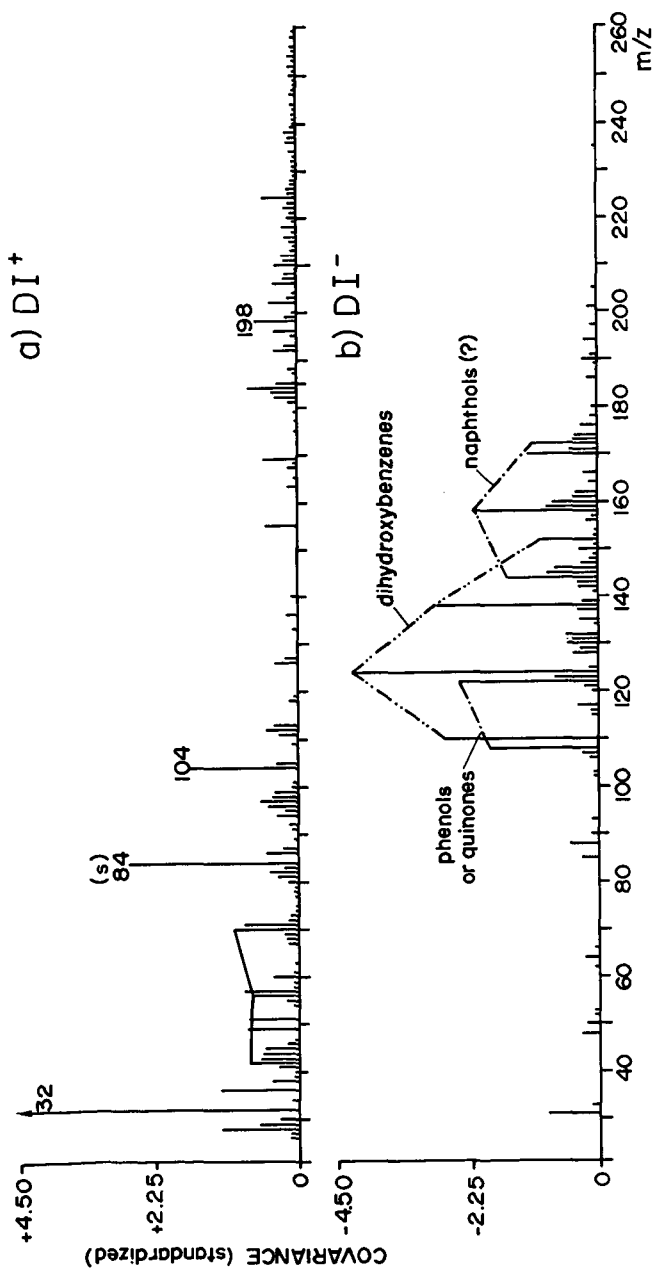
Figure 5. Discriminant spectrum showing the effect of oxygen exposure on the Wellman-Galusha gasifier tar. The negative component (DI⁻) represents compounds decreased in oxidized tar. The positive component (DI⁺) represents ion signals increased in oxidized tar. (s) indicates dichloromethane solvent peaks.

DEACTIVATION OF DIRECT COAL LIQUEFACTION CATALYSTS BY CARBONACEOUS DEPOSITS*

Frances V. Stohl and Howard P. Stephens
Sandia National Laboratories
Albuquerque, NM 87185

INTRODUCTION

The accumulation of carbonaceous deposits on direct coal liquefaction catalysts has long been known to cause significant, rapid deactivation. We have previously shown that greater than 75% of the catalyst hydrogenation activity and 50% of the hydrodesulfurization activity is lost due to carbonaceous deposits within the first few days of coal processing.[1] The objective of the work reported here, which is part of a larger study aimed at extending catalyst life by mitigating the effects of carbonaceous deposits, was to determine the impact of several hydrotreater feed components and distillate cuts on catalyst activity. This work differs from previous studies[2,3] in that we have not only characterized the catalyst but have also quantitatively measured catalyst activity losses resulting from the contaminants. As a result of this study, we have found that losses of catalyst extrudate hydrogenation activity ranged from 23% for experiments with the lowest boiling fraction to 82% for a high boiling point feed component. Although HDS activity was not affected by the low boiling fraction, a 70% loss resulted from hydrotreating the highest boiling point component.

EXPERIMENTAL PROCEDURES

Two process streams and various distillate cuts of a coal liquefaction hydrotreater feed were catalyticlly hydrogenated in microreactors. The starting feeds, products and catalysts of these experiments were characterized and the catalysts were tested for hydrodesulfurization and hydrogenation activities.

Materials

The catalyst used in these studies was Shell 324M with 12.4 wt % Mo, 2.8 wt % Ni and 2.7 wt % P on an alumina support. The catalyst is in the form of extrudates measuring about 0.8 mm in diameter and 4 mm in length. Prior to use, the catalyst was presulfided with a 10 mol % H_2S/H_2 mixture at 400°C and atmospheric pressure for 2 hours. The hydrotreater feed was obtained from the Wilsonville Advanced Coal Liquefaction R&D Facility's run 247 which processed Illinois No. 6 bituminous coal. This hydrotreater feed was made up of two process streams derived from the first stage thermal liquefaction unit. The two streams are identified by the number of the storage tank (V-178) and separator (T-102) from which they were obtained just before entering the hydrotreater. The V-178 process stream is lighter than the second process stream which consisted of the bottoms from T-102. Samples of each of these streams were used in this study. The feed to the hydrotreater at Wilsonville consisted of 35 wt % V-178 and 65 wt % T-102 bottoms.

Apparatus and Procedures

A Perkin-Elmer 36" adiabatic spinning band distillation column was used to separate V-178 into five boiling point fractions and to obtain boiling point information on the T-102 bottoms. Distillations were performed at 0.1 torr pressure. Boiling temperatures are reported as atmospheric pressure values.

Both process streams, the five distillate cuts, and a mixture of V-178 and T-102 bottoms comparable to the hydrotreater feed at Wilsonville, were each hydrotreated with presulfided catalyst in 40 cc microreactors at 350°C for 2 hours. The microreactors were charged with 6 g of feed, 2 g of catalyst and 1200 psig of H_2. All of the feeds, products and catalysts from these experiments were analyzed for carbon, hydrogen, nitrogen and sulfur contents. The catalysts were Soxhlet extracted with tetrahydrofuran prior to analysis or activity testing.

Both hydrodesulfurization (HDS) and hydrogenation activities were determined for the catalysts. HDS testing was performed at atmospheric pressure and 350°C using a fixed bed flow reactor with thiophene as the model compound. HDS activity was measured by conversion to n-butenes and n-butane as analyzed by gas chromatography.

Hydrogenation activity was determined using the hydrogenation of pyrene to dihydropyrene as has been previously reported.[4] This testing was carried out in 26 cc microreactors at 300°C with 500 psig H_2 cold charge. Experiments performed on both catalyst ground to -200 mesh and whole extrudates enabled determination of the losses of both intrinsic and extrudate activities.

RESULTS AND DISCUSSION

Feed, Product and Catalyst Compositions

Results of distilling the two process streams showed that 96.1 wt % of the V-178 boiled below 850°F whereas only 16.4 wt % of the T-102 bottoms boiled below 825°F. The initial boiling points of the V-178 and T-102 bottoms were 400°F and 720°F respectively. The boiling point ranges and weight fractions of the five distillate cuts from the V-178 stream are given in Table 1, along with analyses on all the feed components. The most significant differences in elemental compositions between the V-178 and T-102 bottoms are the higher H/C ratio of the V-178 and the higher nitrogen content of the T-102 bottoms. The V-178 distillate fractions show decreasing H/C ratios with increasing boiling point.

Results of analyses of the products from the hydrotreating experiments are also given in Table 1. All of the microreactor products showed higher hydrogen contents and decreased nitrogen contents compared to the starting feeds. The greatest increase in H/C ratio was 28% for the run with T-102 bottoms. Products from all other experiments also showed increased H/C ratios between 9 and 14%. Hydrotreating a 35 wt % V-178 + 65 wt % T-102 bottoms mixture yielded an increase in hydrogen content that approximated that obtained by hydrotreating similar amounts of each stream separately. This indicates that the presence of the lower boiling process solvent did not improve T-102 bottoms hydrogen uptake.

Analyses of the catalysts retrieved from these runs are given in Table 2. These catalysts show an increasing carbon content with increasing boiling point of the feed processed. The nitrogen

content is highest on the catalyst used to process T-102 bottoms although all of the catalysts have at least 0.40 wt % nitrogen. All of the nitrogen removed from the V-178 feed was deposited on the catalyst whereas only 40% of the nitrogen removed from the T-102 bottoms was found on the catalyst. Processing of the V-178 + T-102 bottoms mixture yields a similar catalyst carbon content to processing the T-102 bottoms alone.

Hydrodesulfurization Activity

HDS activity testing results obtained for whole catalyst extrudates from the microreactor runs are given in Figure 1. The standard deviation for this testing procedure is $\pm$ 2% absolute. Catalyst from the hydrotreating of the V-178 stream shows a small but statistically significant decrease in HDS activity compared to fresh catalyst. Catalyst used to hydrotreat T-102 bottoms, however, shows a 46% decrease in thiophene conversion which is equivalent to losing ∿70% of fresh catalyst HDS activity. Catalysts used in microreactor runs with the -550°F and 550-650°F distillate cuts have the same HDS activity as fresh catalysts. HDS activities of catalysts from experiments with higher boiling point cuts decrease with increasing boiling point. Comparison of these results with the carbon deposition on the catalyst shows that catalyst carbon contents $\leq$ 1.58 wt % do not affect HDS activity. However, above this carbon content, HDS activity loss is proportional to carbon content. It is observed that the +850°F portion of the V-178 causes significantly less carbon buildup and HDS activity loss than obtained with the T-102 bottoms which contain 83.6 wt % +825°F material.

Hydrogenation Activity

A quantitative, mathematical expression, reported previously,[4] relates catalyst extrudate activity remaining (F) to the intrinsic activity loss (α). Use of the relationship between F and α enables determination of the effective diffusivities of these catalysts. For catalyst from the run with V-178 feed, no significant decrease in effective diffusivity, as compared to fresh catalyst (5 x 10^6 $cm^2/sec/cm^3$), was observed. However, catalysts from the run with the V-178 + T-102 bottoms mixture and from the run with only T-102 bottoms showed ∿70% decreases in effective diffusivity which are due to the higher carbon content of these catalysts. The relationship between F and α enables differentiation of two limiting modes of deactivation-- homogeneous and shell-progressive poisoning.[4] A plot of F vs α for the effects of carbonaceous deposits alone is shown in Figure 2. Since the α values increase more rapidly than the F values, the dominant mode of deactivation is due to homogeneous poisoning. A smaller F value indicates higher deactivation so that deactivation increases with higher boiling point of the microreactor feed. The catalysts used to hydrotreat T-102 bottoms and the V-178 + T-102 bottoms mixture have lost ∿80% of their hydrogenation activity after only 2 hours in the batch microreactor runs. The +850°F component of the V-178 yields a 50% decrease in hydrogenation activity. The difference between the activities of the catalysts used to hydrotreat the +850°F portion of the V-178 and the T-102 bottoms must be due to compositional differences between these high boiling point materials.

Comparison of the catalyst carbon contents in Table 2 with the F and α values in Figure 2 shows that the greatest changes in F and α as a function of carbon content occurred for the first sample with a carbon content of $\sim$1.25 wt %. Additional accumulation of carbon produces smaller changes of F and α. There appears to be no correlation between losses of hydrogenation activity (or HDS activity) and nitrogen content of the catalyst.

CONCLUSIONS

Hydrotreating the high boiling materials for only 2 hours yielded up to $\sim$80% loss of hydrogenation activity and 70% loss of catalyst HDS activity. Combining a lighter solvent with the T-102 bottoms did not have any impact on the extent of deactivation. These results show that, in order to extend catalyst life, it is necessary to either eliminate the high boiling material from the hydrotreater feed or change the feed to eliminate the harmful components of these high boiling materials. Current studies are aimed at identifying and separating different chemical classes of compounds in the high boiling fractions to determine their individual effects on catalyst activity.

REFERENCES

1. Stohl, F. V. and Stephens, H. P. Proceedings Tenth Ann. EPRI Contractors' Conf. on Coal Liquefaction, Palo Alto, CA, April 1985.

2. Ternan, M., Furimsky, E. and Parsons, B. I. Fuel Proc. Tech. 2, 45-55 (1979).

3. Furimsky, E. Fuel Proc. Tech. 6, 1-8, 1982.

4. Stephens, H. P. and Stohl, F. V. ACS Proc. Div. of Fuel Chemistry 29 (6), 79-89, 1984.

Table 1. Analyses of feeds and products from microreactor runs reported in weight percent.

Analyses of Hydrotreater Feed

	35% V-178 + 65% T-102	V-178	T-102 Bottoms	V-178 Distillate Cuts				
				-550F	550-650F	650-750F	750-850F	850F+
Distillate Wt %				21.84	28.89	32.46	12.86	3.95
Carbon	87.16*	87.69	86.88	86.28	87.65	88.40	88.13	(93.19)
Hydrogen	7.44*	10.05	6.03	10.62	10.14	9.75	9.38	8.86
Nitrogen	0.91*	0.23	1.27	0.22	0.31	0.25	0.32	0.48
Sulfur	-	0.13	N.A.	0.22	0.10	0.08	0.12	N.A.
H/C	1.02*	1.38	0.83	1.48	1.39	1.32	1.28	1.14

Analyses of Microreactor Products

	35% V-178 + 65% T-102	V-178	T-102 Bottoms	-550F	550-650F	650-750F	750-850F	850F+
Carbon	(93.46)	86.39	90.36	87.09	88.09	87.99	88.23	88.62
Hydrogen	9.02	10.86	7.99	11.79	11.20	10.69	10.35	9.54
Nitrogen	0.49	0.10	0.69	0.03	0.07	0.08	0.13	0.26
Sulfur	N.A.	<0.01	N.A.	<0.01	<0.01	<0.01	0.05	0.04
H/C	1.16	1.51	1.06	1.62	1.53	1.46	1.41	1.29

* Calculated from V-178 and T-102 data.

( ) Poor reproducibility in analysis.

N.A. = Not analyzed.

Table 2. Analyses of used catalysts from microreactor
runs reported as weight percent.

Feed	Carbon	Hydrogen	Nitrogen
35% V-178 + 65% T-102 bottoms	11.42	1.46	0.57
V-178	1.96	0.82	0.50
T-102 bottoms	11.71	1.44	0.61
V-178 Distillate Cuts			
-550°F	1.25	0.82	0.55
550-650°F	1.58	0.84	0.47
650-750°F	1.92	0.90	0.46
750-850°F	2.64	0.82	0.40
+850°F	4.20	0.93	0.49

Figure 1. HDS activity of fresh catalyst and catalysts from micro-
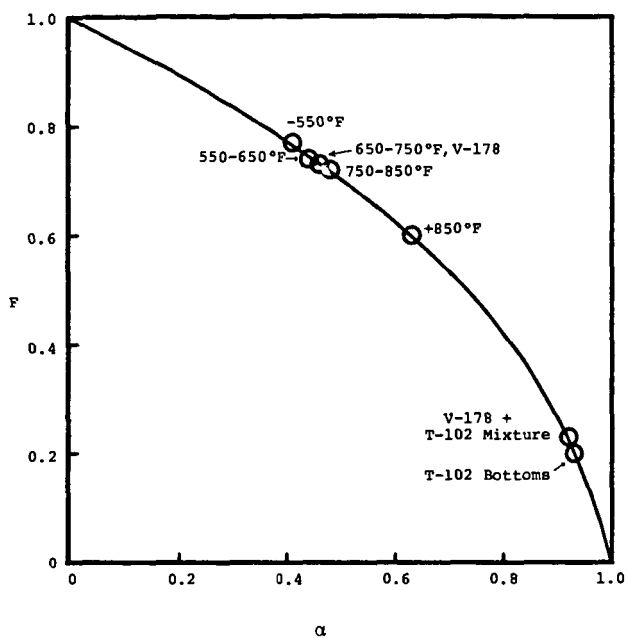reactor runs with different feed components.

Figure 2. F vs α for catalysts from microreactor experiments. Results shown for carbonaceous deposits only.

PHENOLIC -OH AS A PROCESS-PERFORMANCE INDICATOR
IN TWO-STAGE LIQUEFACTION

G. A. Robbins, R. A. Winschel and F. P. Burke

CONOCO INC.
Coal Research Division
4000 Brownsville Road
Library, PA   15129

ABSTRACT

Phenolic -OH concentrations were measured for process oil samples taken throughout the year-long Run 3LCF9 of the Lummus Integrated Two-Stage Liquefaction PDU, and a 25-day run of HRI's bench scale Catalytic Two-Stage Liquefaction process unit. The phenolic -OH concentration of the Lummus product resid responded to changes in catalyst age and space velocity. The phenolic -OH concentration of the HRI second-stage products also increased in response to catalyst age, the only process variable during that run. These results demonstrate that phenolic concentration is a sensitive indicator of coal liquefaction process performance. These data were obtained using a quantitative infrared spectroscopic method, applicable to tetrahydrofuran-soluble coal liquids, which permits analysis of the entire range of converted coal products. This analytical method is rapid, reproducible and accurate, and also provides qualitative information about the molecular structure of the phenolic components.

INTRODUCTION

The successful operation of a coal liquefaction process requires some means to monitor process performance as a function of time and changes in operating conditions. Operating history and material balance data are essential, but require substantial time for analysis, calculations and compilation. Alternatively, selective chemical characterization techniques can provide a great deal of process performance information within minutes after samples are obtained. A principal objective of our coal liquefaction research has been to develop rapid reproducible analytical methods for coal liquids characterization and process monitoring.

Extensive application of these techniques has shown that the phenolic OH concentrations of coal liquids are very useful in monitoring process performance. These data give evidence of approach to or achievement of steady-state operation. They provide information on the extent of deoxygenation, which can be used to assess catalyst deactivation in a process such as two-stage liquefaction. Changes in phenol concentration can also result from changes in operating conditions. Phenolic OH concentrations supplement other data to provide a broad picture of process performance and product characteristics.

This paper presents two applications of an infrared spectroscopic method for phenolic OH.

RESULTS AND DISCUSSION

Summary of Infrared Method

In this method, the phenol concentration is determined from the height of the peak in the infrared spectrum produced by the stretching vibration of the phenolic O-H bond in dilute tetrahydrofuran (THF) solution (Figure 1). The infrared spectra were obtained using a Nicolet Model 7199C Fourier transform infrared (FTIR)

instrument operated at a nominal resolution of 4 cm^{-1} (data were collected every 2 cm^{-1}).

A software peak-picking routine was used to locate the maximum in the phenolic OH stretch band found around 3300 cm^{-1}. The baseline value used was the average absorbance over 3750-3650 cm^{-1}. The net absorbance used for quantitation was the OH stretch peak absorbance minus the baseline absorbance. Measurements were limited to the 0.3 - 1.0 net absorbance range. A linear least-squares fit of absorbance vs (concentration x path length) for standard solutions provided the calibration (extinction coefficient) for phenols determination in actual samples. A detailed description of this method and its verification by an independent ^{19}F-NMR technique have been reported (1).

Other methods for the determination of phenols in coal liquds (using nuclear magnetic resonance (NMR) spectrometry or infrared (IR) spectroscopy) have typically employed chloroform or methylene chloride as solvents for analysis. However, because THF is a much better solvent than these for dissolving coal liquids, almost the entire sample from any liquid process stream becomes available to the analysis method, particularly if "THF solubles" is used to define converted coal products. A significant advantage of the IR technique is that minimal sample preparation is required. In addition, because the instrument produces digitized data, the peak location and background and peak absorbances are determined auto-matically, greatly facilitating the analysis. Using this method, we can routinely complete 3-4 phenolic -OH determinations per hour, including sample preparation and clean-up.

Possible common interferences to determination of phenolic OH content by this method are water and amine groups (particularly pyrroles). Water in moderate amounts poses no particular problem, and the question of interferences by amines remains to be resolved and is an active area of our investigation.

Based on the model compound data, phenol concentrations are accurate to ±0.1 meq OH/g sample (95% confidence) over the range of concentrations typical for coal liquids. Reproducibility for resid samples was ±0.09 meq OH/g sample for concentration and ±1 cm^{-1} for frequency.

Consistent calibration data for quantitative analysis were obtained from a wide range of model compound phenols (Figure 2). This is necessary for accurate quantitation. The frequencies of the peaks varied somewhat from one model phenol to another, demonstrating a trend with ring condensation and with phenol aqueous acidity (Figure 3). The frequency observed for a particular phenol depends on the O-H bond strength, which is related to the chemical structure and is reflected in the acidity (as the aqueous dissociation constant). A low frequency results from a weaker O-H bond (more acidic) as in the multiple-ring phenols. Ring condensation withdraws electrons, thus weakening the O-H bond. Conversely, alkyl substituents donate electrons, producing a stronger O-H bond, lower acidity, and higher infrared frequency. Thus, the infrared frequency of the OH peak is roughly related to ring condensation and alkyl substitution. The model compound data indicate a single- vs multiple-ring frequency cutoff in the 3275-3300 cm^{-1} region. Because of these observations, we explored the potential utility of the frequency data to provide qualitative information on process samples. These results are discussed below.

Lummus ITSL Run 3LCF9 Process Description and Run Summary

Run 3LCF9 was a year-long run of the Integrated Two-Stage Liquefaction (ITSL) process at Lummus' 30 lb/h PDU. The three major process units are: 1) plug flow, short contact time, first stage (SCT unit) operated at 830-865°F, 2 to 10 min, and 2000-2400 psig, 2) an interstage antisolvent deashing unit (ASDA), and

3) an expanded-bed catalytic hydrotreater second-stage (LC-Finer), operated at 720-750°F, 2700 psig, and 0.6 - 1.8 lbs feed/lb cat h. These three sub-units serve distinct functions. The SCT unit dissolves the coal (~92% MAF), the ASDA removes solids, and the LC-Finer converts resid to lighter products, prepares a suitable donor solvent and removes heteroatoms from the net product.

Run 3LCF9 was made with clean Burning Star (Illinois 6) coal and a single charge of fresh Shell 324M (Ni/Mo) catalyst. Major variables during the run were catalyst age, space velocity, temperature, and feed source.

During the first third of Run 3LCF9, the PDU was operated as described above. During the middle of the run the order of the ASDA and LC-Finer was inverted, i.e., the LC-Finer processed ash-containing feed and the LC-Finer product was deashed. Later in the run, the ASDA and LC-Finer were returned to their original order and a partially back-mixed soaker reactor was added to the SCT unit. The soaker was operated at a lower temperature (830°F) and pressure (1000-2000 psig) but longer residence time (10-15 min) than the SCT coil-only reactor.

The discussion below describes characterization of the second-stage (LC-Finer) operations in terms of the -OH concentrations of the THF-soluble 850°F$^+$ feeds and products. A detailed description of Run 3LCF9 (4, 5, 6) and thorough analytical characterization results (1, 7) have been reported.

Phenol Concentration Response

Figure 4 plots the change in phenolic concentration (feed minus product) for the soluble resid samples of ITSL Run 3LCF9 as a function of catalyst age: the greater the value, the greater the reduction in phenolic functionality in the LC-Finer system. Phenolic concentrations ranged from 1.1 to 1.6 meq/g for the feed resids and from 0.4 to 1.6 meq/g for the product resids.

The general decrease in phenolic removal with catalyst age at constant space velocity is apparent. It is also evident during the parts of the run operated with all variables held constant, such as those at 750°F (early in the run) and at 780°F. This represents deactivation of the catalyst's deoxygenation activity.

The data around 600 and 1800 lb 850°F$^+$/lb cat show the clear effect of space velocity. Operation of the process at lower space velocity increased phenol removal by decreasing the phenolic OH concentration in the products. Conversely, operation at higher space velocity decreased phenol removal by increasing the phenol content in the products. Although temperature and feed source were also variables during Run 3LCF9, the phenol concentrations in the products showed no obvious response to these changes. Thus, the phenol concentrations of Run 3LCF9 products were sensitive to catalyst age and space velocity, but not to the other variables.

In addition to showing response to certain planned process variables, phenolic OH concentration is also sensitive to unplanned changes in conditions, as the following example shows. Three points between catalyst age 400-500 lb 850°F$^+$/lb cat show anomalously low phenol removals (Figure 4). For these three run periods, the product samples had unusually high phenolic concentrations. These three were the earliest samples we received following a departure from planned operating conditions which was reported by Lummus (4, 5). If frequent sampling and analysis were performed on a continuing basis during plant operations, such deviations from desired conditions might be recognized and corrected earlier.

Phenol Frequency Response

The phenol peak frequency was sensitive to catalyst age, but not to the other variables (Figure 5). These data show much less variation than the concentration data. The product resid peaks consistently occur at higher frequency than the feed resid peaks (product 3289-3306 cm^{-1} vs feed 3282-3288 cm^{-1}), in agreement with the structural interpretation of the model compound frequency data. The upgraded product resids have a lower degree of ring condensation than the feed resids, hence the higher frequency of the product resid peaks. For the same reason, the distillate phenol peaks occur at higher frequencies than the peaks from the corresponding resids. In the present application, the decrease of the product resid peak frequency with increasing catalyst age is an indication of catalyst deactivation. Both the concentration and frequency data indicate that two stages of catalyst deactivation may be present. A very rapid deactivation for the initial part of the run is followed by a more gradual one for the remainder of the run.

CTSL Run 227-20 Process Description and Run Summary

HRI's catalytic two-stage liquefaction (CTSL) process consists of two catalytic ebullated-bed reactor stages for coal hydrogenation and liquefaction. In the first stage, a coal slurry prepared from process-derived heavy recycle oil is treated with hydrogen at temperatures below 800°F. These conditions are designed to hydrogenate the coal matrix while maintaining the solvent donor quality. The low temperature minimizes dehydrogenation, cracking, polymerization, and condensation reactions. The first-stage products pass directly to the second stage, where higher temperature hydrotreatment, liquefaction, and heteroatom removal take place. Atmospheric still bottoms, vacuum still overheads, and pressure filter liquid (PFL) from the atmospheric still bottoms are combined to make the recycle oil. A summary of CTSL development has been reported (8).

Run 227-20 was conducted as a bench-scale demonstration of CTSL technology. Burning Star (Illinois 6) coal was processed at constant conditions for 22 days after a three-day startup period. Operating conditions reported by HRI (8) are given below:

<div align="center">

OPERATING CONDITIONS
HRI CTSL Run 227-20

</div>

Feed: Illinois No. 6 Coal, Burning Star Mine, ~70 US mesh,
             2.5/1 Solvent/Coal
Catalyst: First Stage - Amocat 1C (Ni/Mo)
             Second Stage - Amocat 1A (Co/Mo)

First Stage Temperature - 750°F
Second Stage Temperature - 825°F
Unit Back Pressure - 2500 psig
Dry Coal Space Velocity (each Stage), lb Dry Coal/h/ft^3 cat - 68

Conoco received daily PFL samples from the run and performed analyses on selected samples. The PFL represents the solids-free portion of the major second-stage product, which is recycled to the first stage. The complete characterization data have been reported (1).

Phenol Concentration Response

Phenolic OH concentrations of 850°F$^-$ distillate and THF-soluble 850°F$^+$ resid samples from Run 227-20 are plotted in Figure 6 as a function of run day. There

<div align="center">158</div>

is an initial reduction in distillate and resid phenolic OH content during the three day startup period, as the startup solvent was replaced by coal liquids low in phenols, produced over the fresh catalyst. From day 4 to day 25, as the catalyst aged, the phenol concentrations of the PFL distillates and resids increased as shown in Figure 6.

The observation that these samples became more phenolic with time is consistent with HRI's process performance data which also show a decrease in catalyst activity with time (see below).

CTSL RUN 227-20 PROCESS PERFORMANCE DATA (Reference 8)

Period	5	10	15	19	24
Avg Cat Age,					
lb Dry Coal/lb Cat	216.3	441.3	664.3	844.2	1069.1
$975°F^+$ Conversion, wt % MAF	86.9	83.6	82.2	80.6	77.2
C_4 - 975°F, wt % MAF	72.3	68.0	67.2	65.4	62.6
Organic Sulfur Removal, wt %	98.0		96.6		94.6
Nitrogen Removal, wt %	79.2		66.5		56.4

The increase in phenolic concentration represents deactivation of the catalyst's deoxygenation activity. The deactivation exhibited by the distillate phenol data is highly linear with catalyst age and showed no evidence of subsidence at the end of the run.

The increase in phenolic content of the $850°F^+$ resid samples was not linear (Figure 6). There was a rapid increase in phenolic content up to about day 12 followed by a more gradual increase. This may indicate that the catalysts' initial activity for removal of phenols from the resid was substantially lost by day 12. One would expect the resid molecules to be excluded from the active catalyst sites by pore mouth blockage before the distillate molecules would be excluded. The observed difference between the distillate and resid phenolic OH concentration response with time suggests that the distillate and resid fractions have different rates and/or mechanisms of deactivation toward deoxygenation.

Phenol Frequency Response

The phenol infrared peak frequency data from the distillate and resid samples are plotted in Figure 7 as a function of run day. The distillate peaks were consistently observed at higher frequency than the resid peaks. This fits the structural model for these data, with the distillates containing phenols of smaller ring size than the resids. These frequencies decrease throughout the run, consistent with a continual catalyst deactivation. In contrast to the concentration data, the frequency data do not show a trend reversal after startup. The reason for this is not clear, but the result implies that the concentration and frequency data are independent measurements, even through a high peak frequency and low phenol concentration tend to correlate. It is probable that the two concentration and frequency trends during startup reflect differences in the molecular composition of the startup and process oils, and that inventory replacement was complete by day 4, as the concentration data indicate.

The distillate and resid frequency appear to follow curves of nearly identical shapes, in contrast to the concentration data. The interpretation of the frequency data is not completely straightforward, but future application of the data may suggest a more meaningful interpretation of the results.

CONCLUSIONS

Phenolic OH concentration can be a useful indicator of coal liquefaction process performance. Such data are sensitive to process variables such as catalyst age and space velocity, and to changes during startup and process upsets. The infrared spectroscopic method employed permits useful data to be obtained from residual oils, for which few analytical methods are available. Data from CTSL Run 227-20 suggest that distillate and residual oils may have different rates and/or mechanisms for deactivation of the catalyst toward deoxygenation reactions.

Use of the infrared frequency data provided by the method may give qualitative information about the molecular structure of phenols present in each sample. Interpretation of these data may not be straightforward, but might be improved after broader application.

Continued application of this method to liquefaction process monitoring should lead to a clearer picture of changes during specific process runs, and should aid in a general understanding of liquefaction chemistry, particularly in the heavier materials.

ACKNOWLEDGEMENT

REFERENCES

1. Burke, F. P. and Winschel, R. A., "Recycle Slurry Oil Characterization – Technical Report: 10/1/83 – 3/31/84", DOE Contract No. DE-AC22-80PC30027, March, 1985.

2. CRC Handbook of Chemistry and Physics, 50th Edition (1969), The Chemical Rubber Co., Cleveland, Ohio, Robert C. Weast, Editor.

3. "pKa Prediction for Organic Acids and Bases", Perrin, D. D., Dempsey, B., and Serjeant, E. P., Chapman and Hall, Publisher, New York (1981).

4. Schindler, H. D., Chen, J. M. and Potts, J. D., "Integrated Two-Stage Liquefaction, Topical Technical Progress Report, Steady State Illinois No. 6 Program, Period April 1, 1982 – July 6, 1982", DOE Contract DE-AC22-79ET14804, April, 1983.

5. Schindler, H. D., Chen, J. and Potts, J., "Integrated Two Stage Liquefaction Final Technical Report, Volume I, Period July 1, 1979 – July 6, 1982", DOE Contract DE-AC22-79ET14804, June, 1983.

6. Schindler, H. D., Chen, J. M., and Potts, J. D., "Integrated Two-Stage Liquefaction, Topical Technical Progress Report, Process Flow Modification, Period: July, 1982 – February, 1983", DOE Contract DE-AC22-82PC50021, January, 1985.

7. Winschel, R. A. and Burke, F. P., "Recycle Slurry Oil Characterization – Technical Report: 10/1/82 – 3/31/83", DOE Contract No. DE-AC22-80PC30027, February, 1984.

8. Comolli, A. G., Mac Arthur, J. B., McLean, J. B., "HRI's Two-Stage Catalytic Coal Liquefaction Program – A Status Report", Proceedings of the 1984 DOE Direct Liquefaction Contractors' Review Meeting, Albuquerque, NM, October, 1984.
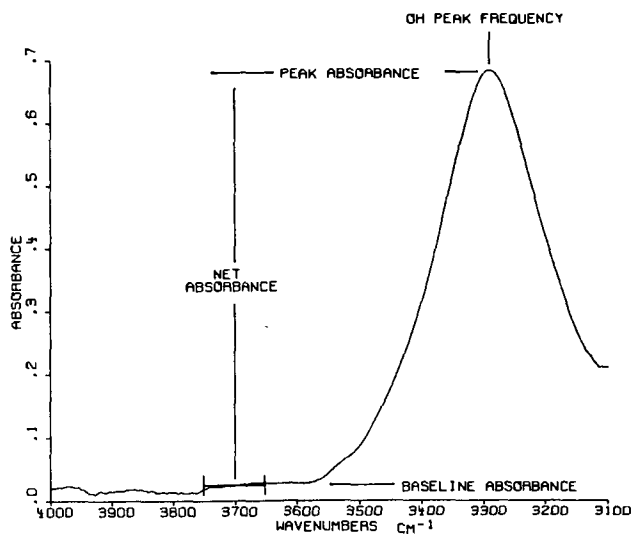
Figure 1. Infrared Spectrum of a Distillate Sample in THF.

Figure 2. Model Compound Phenol Calibration Data and Least-Squares Line.

161

Figure 3. Relationship of Phenolic OH Peak Frequency to Phenol Structure.

Figure 4. Change in Phenol Concentration - Run 3LCF9.
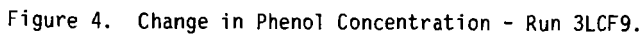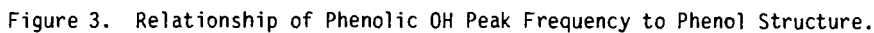
Figure 5. Frequency of Phenol Peak Maximum – Run 3LCF9.

Figure 6. Phenolic OH Content vs
Run Day – Run 227-20.
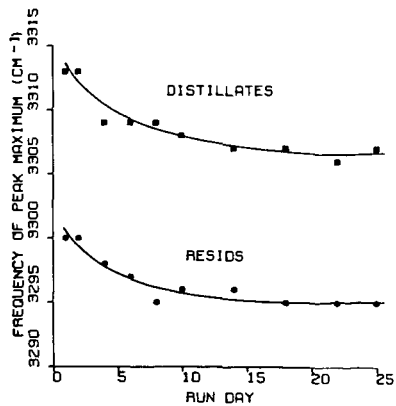
Figure 7. Phenol Peak Frequency vs
Run Day – Run 227-20.

163

THE EFFECT ON PRODUCT YIELD STRUCTURE AND PRODUCT QUALITY
IN THE HYDROTREATMENT OF COAL DERIVED EXTRACT PRIOR TO
DEASHING IN A TWO-STAGE LIQUEFACTION PILOT PLANT OPERATION

M. J. Moniz, R. V. Nalitham

Catalytic, Inc., Wilsonville, AL 35186

and T. W. Johnson

Southern Company Services, Inc., Wilsonville, AL 35186

INTRODUCTION

A two-stage liquefaction (TSL) operation typically consists of the sequential processing of coal in three distinct steps. These are: a thermal liquefaction first stage, an intermediate deashing step, followed by a second-stage hydro-treating unit. The TSL operation provides flexibility in that a number of process options are possible, depending on the sequencing of process units, and recycle of process streams (1, 2). This paper provides a comparison of the effects of resequencing process units in a TSL operation on product yields and product quality for processing bituminous coal (Illinois No. 6, Burning Star Mine).
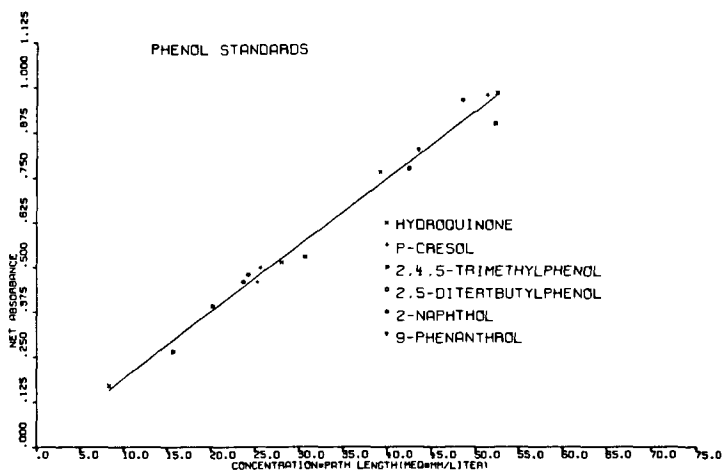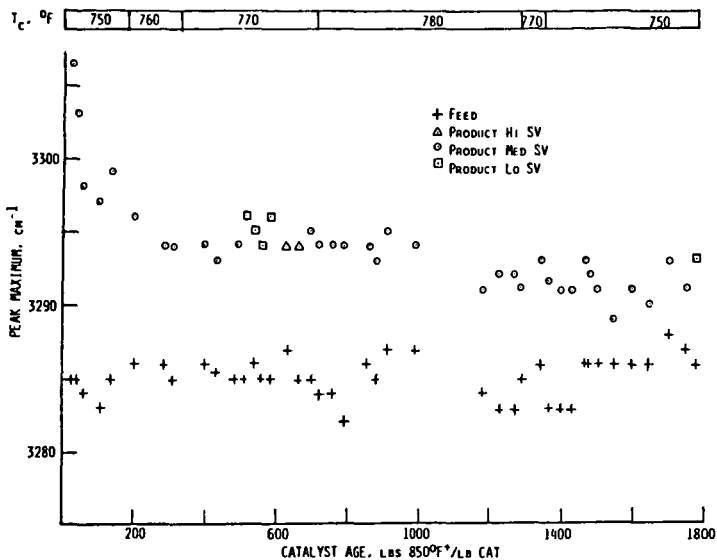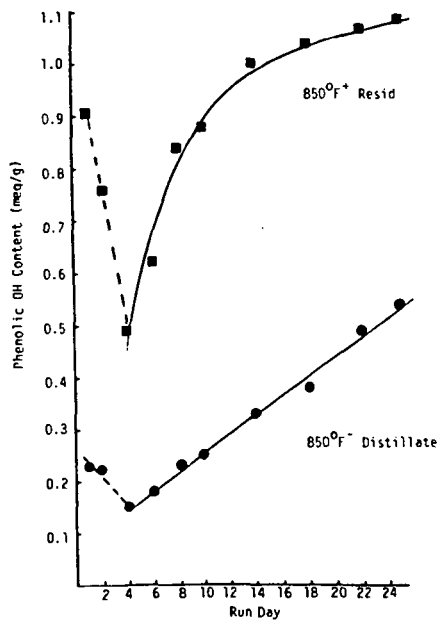
The configuration modes compared were the integrated TSL (ITSL) mode (Figure 1) and the reconfigured integrated TSL (RITSL) mode (Figure 2). In both modes, the reaction stages are coupled by recycling full-range hydrotreated resid and distillate solvent from the hydrotreater to the thermal liquefaction step. The RITSL mode differs from the ITSL mode in that for the RITSL mode, the vacuum-flashed product from the thermal stage is hydrotreated prior to being deashed.

PRODUCT YIELD COMPARISON

A wide range of thermal and hydrotreater reaction conditions were investigated in the ITSL mode to determine their effects on product yield structure (3). For comparison purposes, Table 1 lists a typical set of RITSL conditions relative to three sets of ITSL conditions. Thermal stage reaction conditions are comparable for the runs listed in Table 1. Catalytic stage reactor conditions for ITSL-1 are fairly comparable to RITSL, with a 10°F higher reactor temperature for ITSL-1. A higher temperature of 740°F was used at an extended catalyst age for ITSL-2. In ITSL-3, catalyst age was maintained in the 1300-1400 lb resid/lb catalyst range with catalyst addition and withdrawal, and space velocity was decreased to 0.75 lb feed/(hr·lb catalyst).

For a similar reaction severity, RITSL indicates a higher distillate yield, accompanied by a significantly higher hydrogen consumption. Hydrogen efficiency is hence lower for RITSL as compared with ITSL.

A typical set of process unit yields is given in Table 2 for the RITSL and ITSL modes. Gaseous hydrogen consumption was comparable for both modes in the thermal stage, but was significantly higher for the RITSL mode in the hydrotreater stage, despite a slightly lower hydrotreater temperature employed for RITSL mode. The thermal unit resid yield for the RITSL mode was higher than that typically observed for the ITSL mode, which may be attributed to differences in the process solvent. Resid conversion in the hydrotreater was significantly higher for the RITSL mode, resulting in a higher distillate yield. The amount of organics rejected with the ash concentrate in the CSD unit was comparable for

164

both modes. The H/C atomic ratio of the organics was higher for the RITSL mode, which implies a slightly higher rejection, on an energy basis for the RITSL mode.

The conversion of coal to cresol solubles in the individual process units and for the TSL system are shown in Table 3, for the ITSL and RITSL configuration modes. For similar thermal unit reaction conditions, observed coal conversions for the ITSL mode (92.5±1.1) were similar to the RITSL mode (91.7±1.4). In the ITSL mode, a statistically significant increase is observed in unconverted coal yield, in the fractionation and deashing steps (-4.8±1.4), downstream of the thermal reactor. In the RITSL mode, conversion of coal in the hydrotreating unit (0.7±1.5), and downstream of the reaction stages (-1.4±0.9) is statistically insignificant. Hence, for similar thermal unit coal conversions, the two-stage coal conversion is higher for RITSL mode as compared with ITSL mode. In both configuration modes, there was pressure letdown, and absence of hydrogen atmosphere between reaction stages. In the RITSL mode, the cool-down and heat-up temperature cycles of the liquefaction extract and the hold-up time between stages is reduced in comparison to the ITSL mode. The adverse effect of interstage cooling on regressive reaction occurrence, leading to reduced coal conversion and distillate yield has been reported (4). This interstage processing difference between configuration modes may have reduced the potential for regressive reaction occurrence for the RITSL mode, explaining the observed differences in overall coal conversion.

PRODUCT QUALITY COMPARISON

"Synthetic crude blends" were prepared for the RITSL and ITSL product slates, by combining all product streams in proportion to their respective flow rates. A comparison of the elemental contents for various boiling-point ranges of the crudes is shown in Table 4.

A slightly lower naphtha yield but a higher distillate yield was obtained for the RITSL crude in comparison to the ITSL crude. The hydrogen contents for comparable fractions were much higher for the RITSL crude. This result is to be expected because of the comparatively higher hydrogen consumption observed for RITSL mode, for similar hydrocarbon gas yield. The heteroatomic content in the product fractions was also lower for the RITSL crude, indicating an overall, better quality product compared with the ITSL crude.

CATALYST REQUIREMENT COMPARISON

Batch deactivation trends for resid conversion in the hydrotreater were developed for the RITSL and ITSL modes (1), using a first-order resid conversion model (5). The trends showed an initial period of rapid deactivation, followed by slower deactivation rates, for the deashed (ITSL) extract as well as for the nondeashed (RITSL) extract. The deactivation rates were comparatively higher for the nondeashed extract. However, the nondeashed resid was observed to be more reactive (higher resid conversion rate constants) as compared to the deashed resid, over the range of catalyst age investigated.

The batch deactivation data developed for the deashed and nondeashed bituminous runs may be used to estimate catalyst requirements in a steady-state, catalyst addition/withdrawal operation. The equilibrium activity is computed by combining the equilibrium catalyst residence time distribution (RTD) function and the activity function as shown below:

$$K_{eq} = \int_0^\infty RTD(t)K(t)dt \qquad\qquad 1)$$

The RTD function for a continuous, stirred-tank, recycle reactor (6), is given as:

$$RTD(t) = \frac{1}{\bar{t}} e^{-t/\bar{t}} \qquad\qquad 2)$$

where $\bar{t}$ = catalyst hold-up/catalyst addition rate.

Integration of Equation 1 for a batch catalyst activity function has been reported (7).

The projected catalyst requirement for deashed and nondeashed bituminous extracts for steady-state operation is shown in Figure 3. The catalyst requirement is projected for a fixed level of resid conversion and for similar reactor space rates. Owing to a higher resid reactivity, the catalyst requirement for the nondeashed extract, in the temperature range of 680-730°F, is projected to be lower than the catalyst requirement for the deashed extract.

CONCLUSIONS

Significant changes were observed in product yields and product quality by hydrotreating coal derived extract prior to the deashing step. At approximately comparable reaction conditions, overall coal conversion and hydrotreater resid conversion were higher for the RITSL mode. A higer distillate yield accompanied by a significantly higher hydrogen consumption was reported for the R1TSL mode, yielding product fractions of higher hydrogen and lower heteroatomic content, as compared to the ITSL mode. For a fixed level of resid conversion and for similar reactor space rates, catalyst requirement is projected from batch deactivation trends to be lower for the nondeashed extract (RITSL) mode.

ACKNOWLEDGEMENT

REFERENCES

1. Moniz, J. J., Nalitham, R. V., Davies, O. L., Lamb, C. W., "Effect of Feedstock Characteristics and Reaction Conditions on Hydrotreatment of Coal Derived Extracts in a Two-Stage Coal Liquefaction Process", Presented at the Spring National AIChE Meeting, Houston, TX, March 1985.

2. Janka, R. C., Paranjape, A. S., "Investigation of Various Process Options in Two-Stage Liquefaction -- Bench Scale Results", Proceedings of the Eighth Annual EPRI Contractors' Conference on Coal Liquefaction, May 1983.

3. Rao, A. K., Moniz, M. J., Lee, J. M., Pillai, R. S., "Advances in Integrated Two-Stage Coal Liquefaction", Chem. Eng. Prog. p.33, November 1984.

4. Derbyshire, F.J., Odoerfer, G. A., Varghese, P., "Fundamental Studies in the Conversion of Coals to Fuels of Increased Hydrogen Content", Research Project 1655-1, Mobil R & D Corpn., EPRI Report AP-2912, March 1983.

5. Rao, A.K., Gadiyar, H. J., Pate, F. L., "Catalytic Hydrogenation of SRC-1 Product at Wilsonville Pilot Plant", Proceedings of the Seventh Annual EPRI Contractors' Conference on Coal Liquefaction, May 1982.

6. Levenspiel, O., "The Chemical Reactor Omni Book" Oregon State University Press, Corvalis, OR, 1979.

7. Nalitham, R. V., Moniz, M. J., Davies, O. L., "Studies on ITSL System Response to Hydrotreating Catalyst Addition and Withdrawal Operations at Wilsonville", Proceedings of the Ninth Annual EPRI Contractors' Conference on Coal Liquefaction, May 1984.

Table 1

Two-Stage Reaction Conditions and Yields for RITSL and ITSL Modes

Mode Catalyst Operating Mode	RITSL Batch	ITSL-1 Batch	ITSL-2 Batch	ITSL-3 Addition/ Withdrawal
Thermal Stage				
Reactor temperature (°F)	810	810	810	810
Inlet hydrogen partial pressure (psi)	2160	2040	2040	2040
Coal space velocity [(lb/hr-ft^3(>700°F)]	27	28	28	26
Catalytic Stage				
Reactor temperature (°F)	710	720	740	720
Space velocity (lb feed/hr-lb cat)	0.9	1.0	1.0	0.75
Catalyst Age (lb resid/lb cat)	445-670*	350-400	1200-1350	1300-1400**
Two-Stage Yield*(% MAF Coal)**				
C_1-C_3 Gas	6	7	6	6
C_4+ Distillate	62	59	57	61
Resid	3	4	7	3
Hydrogen Consumption	-6.1	-5.3	-5.4	-5.6
Hydrogen Efficiency (lb C_4+Dist/lb H_2 Cons.)	10.2	11.1	10.6	10.8

  * Resid contains unconverted coal and coal ash components.
 ** Average catalyst age: catalyst addition/withdrawal rate of 1.0 lb/ton (MF) coal
    employed.
*** Elementally balanced yield structure.

Table 2

Process Unit Yields for RITSL and ITSL Modes

Mode	RITSL	ITSL
Thermal Unit Yield (% MAF Coal)		
C_4+ Distillate	27.0	34.1
Resid	50.0	46.5
Hydrogen Consumption	-1.7	-1.5
Hydrotreater Unit Yield (% MAF Coal)		
C_4+ Distillate	35.0	24.9
Hydrogen Consumption	-4.4	-3.8
CSD Unit (% MAF Coal)		
Organic Rejection with Mineral Ash	19.6	21.0
[Atomic (H/C) of Rejected Organics]	0.68	0.75

Table 3

Effect of Configuration Mode on Coal Conversion*

Mode	Thermal Stage Conversion	Catalytic Stage Conversion	CSD Unit "Conversion"	Two-Stage Conversion**
ITSL	92.5±1.1		-4.8±1.4	87.7±1.3
RITSL	91.7±1.4	0.7±1.5	-1.4±0.9	91.0±0.8

 * Conversion of Coal to Cresol Solubles.
** Two-Stage Conversion = Sum of Process Unit Conversions.

Table 4

Product Quality Comparison for RITSL and ITSL "Synthetic Crudes"

Distillation Cut	Wt % of Crude	Elemental (Wt %)				
		C	H	N	S	O (diff)
ITSL*						
Naphtha (IBP-360°F)	18.4	85.21	12.86	845 ppm	0.36	1.50
Distillate (360°F-650°F)	45.7	86.34	10.73	0.23	0.22	2.48
Gas Oil (650°F-1000°F)	35.0	89.07	9.69	0.31	0.16	0.76
Resid (1000°F)	0.9	86.71	6.94	1.13	0.60	3.15
RITSL**						
Naphtha (IBP-360°F)	14.9	85.50	14.07	500 ppm	0.35	0.03
Distillate (360°F-650°F)	49.8	86.74	11.54	0.23	0.16	1.33
Gas Oil (650°F-1000°F)	35.3	89.48	10.44	0.06	0.02	-

*Samples obtained with hydrotreater temperature of 730°F; catalyst age of approximately 1,400 lb resid/lb catalyst.

**Samples obtained with hydrotreater temperature of 700°F; catalyst age of approximately 350 lb resid/lb catalyst.
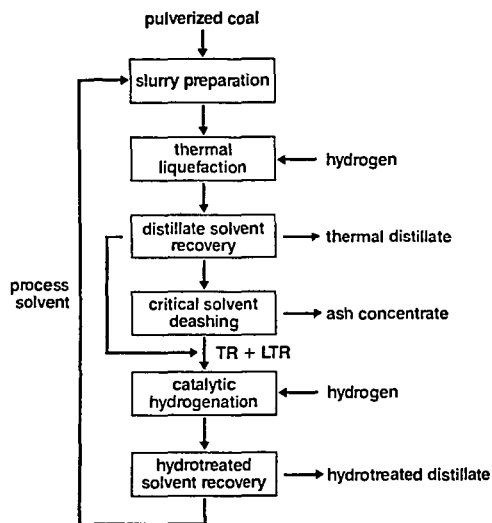
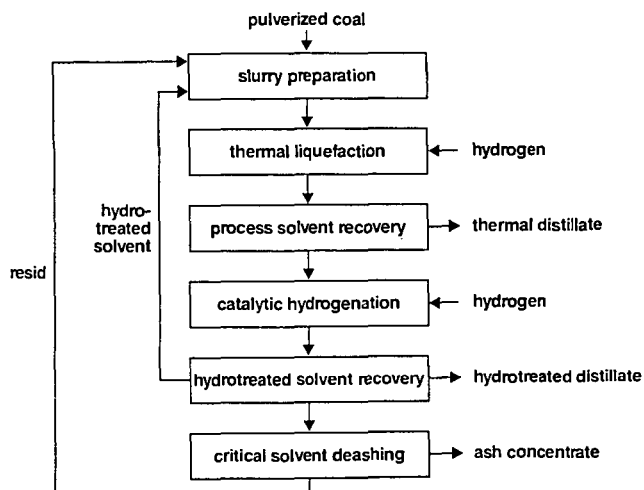Figure 1. Block Diagram of the ITSL Configuration Mode

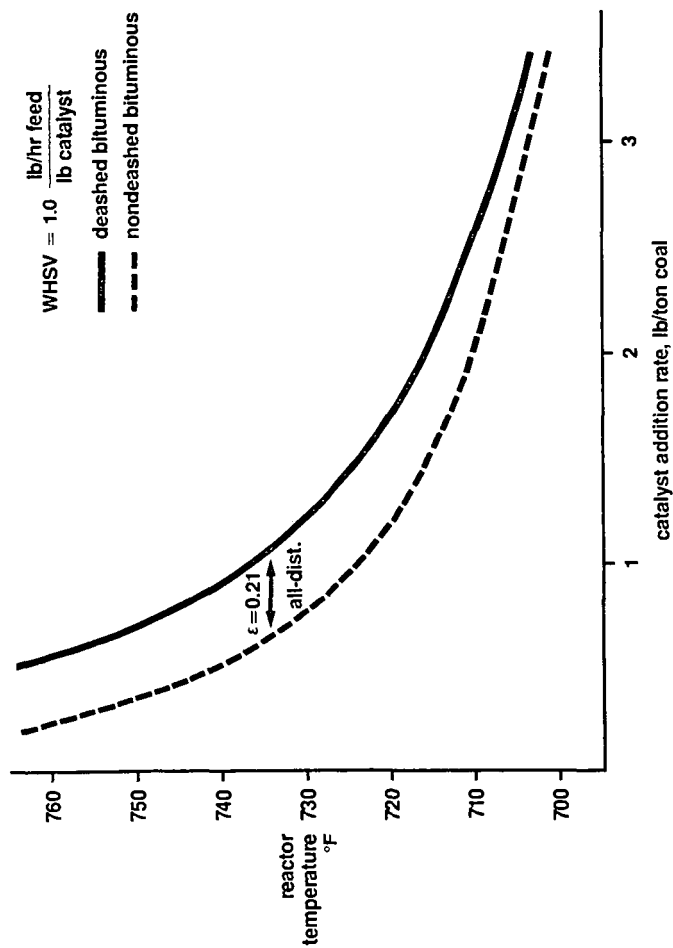Figure 2. Block Diagram of the RITSL Configuration Mode

Figure 3. Projected Catalyst Requirement for RITSL and ITSL Modes

PROCESS-OIL CHARACTERISTICS
IN INTEGRATED TWO-STAGE LIQUEFACTION (ITSL):
COMPARISON OF PDU AND PILOT-PLANT OPERATIONS WITH BITUMINOUS COAL

R. A. Winschel and F. P. Burke

CONOCO INC.
Coal Research Division
4000 Brownsville Road
Library, PA 15129

ABSTRACT

Recycle and other process oils taken during Integrated Two-Stage Liquefaction (ITSL) operations of Lummus' 30 lb/h process development unit (PDU) and the Wilsonville, AL, pilot plant (200 lb/h) were analyzed to compare the two ITSL operations. Samples were obtained from Lummus PDU Runs 3LCF7 (Indiana 5 coal), 3LCF8 and 3LCF9 (Illinois 6 coal), and Wilsonville pilot plant Run 242 (Illinois 6 coal). The process oils from pilot plant Run 242 are significantly different from the corresponding process oils from the Lummus PDU, although both were ITSL operations. Much of the difference may be ascribed to differences between the first-stage (thermal) severities and the selectivities of the deashing operations. Characteristics of the start-up solvents may also have influenced this comparison. Laboratory experiments showed that the second-stage residual feed to pilot plant run 242 was significantly less reactive toward conversion to distillate than the corresponding material from PDU Run 3LCF9 at thermal/donor, i.e., non-catalytic conditions, consistent with the process oil analysis.

INTRODUCTION

Wilsonville Run 242 is generally considered to have successfully demonstrated a scale-up of the Integrated Two-Stage Liquefaction (ITSL) process from the 0.35 ton/day process development unit (PDU) scale as operated by the Lummus Co. to the 2.5 ton/day pilot plant scale. The PDU and pilot plant have similar, though not identical, configurations. Two major differences are the interstage deasher and the second-stage hydrotreater. Lummus uses antisolvent deashing (ASDA) and a three-reactor train LC-Finer unit. Wilsonville uses critical solvent deashing (CSD) and a single-reactor H-Oil unit.

Many direct comparisons of the performances of the pilot plant and PDU cannot be made because of the lack of a uniform analytical scheme. Most notably, the distillation used to determine "resid" differs between the two operations; Wilsonville uses a 975°F (1) end point and Lummus uses an 850°F end point (2). Such parameters as resid space velocity and resid conversion, therefore, are not uniformly determined at the two plants. One of our objectives in this work was to analyze a large suite of comparable samples from the two plants, using an identical analytical scheme, to permit direct comparisons of process-oil characteristics and other derived parameters.

We analyzed several hundred samples of recycle oils and other process streams from Lummus Runs 3LCF7, 3LCF8 and 3LCF9 and daily process-oil samples from Wilsonville Run 242. In each case, the catalyst was Shell 324M (Ni/Mo on alumina) and the feed coal was Burning Star mine Illinois 6 (Run 3LCF7 used Indiana 5). The large number of samples studied has enabled us to describe "typical" compositions, to discern effects of process variables and to describe long-term trends. This paper presents a comparison of the Wilsonville and Lummus ITSL results based on our analysis of process-oil samples.

The set of Wilsonville Run 242 samples we obtained included 121 samples of V-1064 (second-stage feed), V-1067 (second-stage flashed bottoms product, recycle to first stage), T-102 bottoms (first-stage product vacuum bottoms, feed to CSD), and V-178 (first-stage heavy distillate product, second-stage distillate feed).
Run 242 was two months long. Runs 3LCF7 and 3LCF9 were each nearly one year long. Run 3LCF8 was five months long. Analyses included distillation, solvent fractionation, H-NMR, phenolic determinations and microautoclave extractions.

This paper will demonstrate first that the characteristics of the process oils from Wilsonville Run 242 were relatively constant, then that the oils differed significantly from those produced in the PDU. Causes of these differences will be suggested. Finally, the results of a set of batch experiments will be presented that demonstrate an inherent difference in "thermal" reactivities of the $850°F^+$ resids from the two operations.

Complete descriptions of the subject liquefaction runs have been published: Wilsonville Run 242 [1], and Lummus Runs 3LCF9 [2,3], 3LCF8 [2] and 3LCF7 [2]. Our complete analytical data have also been reported in References 4, 5, 6 and 7, respectively.

DISCUSSION

RUN 242 - PROCESS OIL CHARACTERISTICS RELATIVELY CONSTANT

Resid Content in Process Oils Increased Slightly with Time

The $850°F^+$ resid content of both the feed and product of the hydrotreater generally increased as Run 242 progressed. There were three periods of relatively constant resid content as shown below:

	Wt % $850°F^+$ in Sample, Average	
Date, 1982-83	V-1064	V-1067
12/03 - 12/16	57.4	51.8
12/18 - 12/29	63.6	58.5
01/07 - 01/21	66.6	60.1

The step increase in resid content on 12/17 was an intentional change made by the plant operators to reduce resid inventory [1].

Distillate Composition Nearly Constant - Run 242

Though the absolute amount of distillate in lbs/hr and the proportion of distillate in any stream did change with time in Run 242, the compositions of the $850°F^-$ process oil distillates were remarkably steady after 11/28/82. The proton distributions of the V-1064 and V-1067 distillates and the V-178 samples showed little change over the course of the run; in fact, the calculated standard deviations approach our experimental reproducibility [8]. This indicates 1) that the hydrogen content of these distillates is nearly constant, and 2) that the donor-solvent quality of the distillates is also nearly constant. This was confirmed by the donor solvent quality as measured by microautoclave tests, which was nearly constant for each type of process oil tested.

Resid Composition Fairly Constant

As noted above, the resid content in the various process streams increased in a step-wise fashion with time in Run 242. However, the compositions of the first-

stage product resid (T-102 bottoms) and the second-stage feed resid (V-1064) were fairly constant as measured by solvent fractionation. The scatter in the solvent fractionation data for these samples was certainly greater than experimental uncertainty, but there is no obvious trend to the data.(4) The proton distributions of the samples from these two streams may show some increase in aromaticities as the run progressed.(4) This may be a result of the recycle of hydrotreater product which showed a relatively large increase in aromaticity with time, as discussed below.

As with the hydrotreater feed resids, the HTR product resid (V-1067) compositions showed no trend as measured by solvent fractionation data. However, the aromaticity of the HTR product resid increased from about 18 to 25% over the course of the run. This indicates decreasing hydrogenation of the resids which may result partially from the increasing hydrotreater temperature. Higher temperature is thermodynamically unfavorable to hydrogenation. It appears likely that there was an additional cause, perhaps catalyst deactivation, because the decrease was fairly continuous whereas temperatures were increased in steps.

EFFECT OF CSD ON RESID COMPOSITION

In Run 242 the CSD unit removed solids from the first-stage product resid to prepare the second-stage feed resid. The T-102 bottoms (pilot plant distilled first-stage product resid) are about 89% THF soluble and contain nearly equal levels of IOM and ash. After CSD processing, the IOM and ash levels are generally reduced to well below 0.5% of the non-distillate second-stage feed. Other than removing solids, the CSD unit also tends to selectively reject the pre-asphaltenes fraction of the soluble resid. This is clearly seen by comparing the compositions of the second-stage feed soluble resid and the first-stage product soluble resid which are summarized below:

	Average wt % of THF-Soluble Resid		
Resid Sample	Oils	Asphaltenes	Preasphaltenes
First-stage product (T-102 Bottoms)	51	22	27
Second-stage feed (V-1067)	56	25	19

This selective fractionation of the resid may well be important to the performance of the second stage.

LUMMUS AND RUN 242 PROCESS OILS VERY DIFFERENT

It was demonstrated above that many Run 242 process-oil characteristics were relatively invariant over the course of the run. This is not usually the case in the Lummus PDU runs. That plant has been used to investigate a large number of variables. Commonly, seven or more first-stage "runs" and perhaps ten deasher "runs" are made for every second-stage "run". Also, modes of recycle are sometimes changed. Consequently, the compositions of the process oils undergo discontinuous changes.

Some of the text that follows presents comparisons of data from Run 242 and various Lummus PDU runs. Complete data are available in our reports on Wilsonville Run 242 (4) and Lummus Runs 3LCF7 (7), 3LCF8 (6) and 3LCF9 (5). For the sake of brevity, many comparisons will be made based on average values. Because averages are not always meaningful without knowledge of the distribution of the individual data, we have included standard deviations and sometimes a range of data for many of the averages.

Resid Quality in Run 242 Superior to Lummus Runs/Deashing Differences

One major difference between the practice of ITSL at the PDU (Lummus) and the pilot plant (Wilsonville) is the interstage deashing process. The critical solvent deashing (CSD) process employed at Wilsonville selectively rejects a portion of the preasphaltene fraction of the soluble resid as demonstrated above. On the other hand, our analyses of twenty-six Lummus antisolvent deasher (ASDA) runs with bituminous coal products demonstrated no consistent fractionation of the THF-soluble resid (5, 6, 7). This is certainly one reason (out of perhaps several) that the second stage feed resid contained fewer preasphaltenes in Run 242 than in typical Lummus operations. Since resid is recycled around the entire integrated process, each resid stream from Run 242 had relatively fewer preasphaltenes than the correspondong resid sample from Lummus runs. As a general rule, preasphaltenes are less hydrogenated than benzene solubles. As expected, therefore, Run 242 resids were lower in aromaticity than typical Lummus resids.

Soluble Resid Sample	Run #	Average Value ± Std Dev	
		wt % Preasphaltenes	H-Aromaticity, %
Second-stage feed	242	19 ± 2	34 ± 2
	3LCF7	43 ± 4	-
	3LCF8	36 ± 5	44 ± 3
	3LCF9	35 ± 5	47 ± 3
Second-stage product	242	13 ± 3	22 ± 3
	3LCF7	28 ± 6	-
	3LCF8	23 ± 6	30 ± 5
	3LCF9	22 ± 4	37 ± 6

For both units, the resids are upgraded, i.e., preasphaltenes and aromaticity are reduced, in the second stage. However, these data also demonstrate the significant difference in resid compositions for Run 242 and the Lummus runs. Both aromaticities and preasphaltene contents differ from one unit to the other by at least two standard deviations. This may have a significant bearing on process performance, e.g., second-stage conversion. It is expected that preasphaltenes may react kinetically differently than asphaltenes and residual oils and may require more hydrogen and produce more hetero-gases upon upgrading to equivalent products. Additionally, resids of different solubility characteristics and hydrogen contents may deactivate the catalyst at different rates.

In Run 242, the CSD unit consistently reduced the solids (IOM and ash) concentration in the second-stage feed to less than 0.5% (4). The Lummus runs all operated on feeds containing significant levels of solids (IOM plus ash) as shown below.

ITSL Run No.	Solids Concentration in Second-Stage Feed wt %, Average (Range)
242	0.1 (<0.1 - 0.6)
3LCF7	8 (1 - 17)
3LCF8	8 (1 - 11)
3LCF9; deashed	5 (1 - 12)
3LCF9; non-deashed	12 (5 - 17)

These solids are typically composed of two parts IOM and one part ash. The high solids contents in the Lummus feeds result from periods during which the deasher was not operating at full efficiency or was bypassed. Once the solids entered the feed tank, they purged out slowly.

Solids concentration may also have significant bearing on process performance, both mechanically (e.g., deposits, erosion or viscosity problems) and chemically (e.g., second-stage conversion). Metals may deposit on catalyst surfaces and cause deactivation.

Process Streams Contain More Resid in Run 242 than in Lummus Runs

The hydrotreater feed in Run 242 contained a somewhat greater resid (lower distillate) concentration than for typical Lummus second-stage feeds as shown below.

Run No.	$850°F^+$ Content of Second-Stage Feed, wt %, range
242	57 - 67
3LCF7	52 - 75
3LCF8	50 - 61
3LCF9	45 - 63

As discussed earlier, the Run 242 $850°F^+$ resids were essentially ash-free whereas the Lummus resids contained significant amounts of ash. Therefore, the difference in ash-free resid content is even greater than shown in the above table.

Distillate Process Oil Comparison

The following table compares the compositions of the second-stage $850°F^-$ distillates from Run 242 and from several Lummus ITSL runs in terms of proton distributions and microautoclave extractions. The microautoclave tests were all performed at our modified equilibrium conditions which are designed such that donor concentration is the limiting factor in coal conversion (7).

		Average Value		
				Microautoclave Conversion wt %
$850°F^-$ Sample	Run	H Aromaticity % (Range)	$\frac{Cyclic}{Alkyl} H$	MAF Coal ± Std Dev
Second-stage feed	242	17.4 (17-20)	0.64	70 ± 1
	3LCF7	40.2 (31-50)	0.98	–
	3LCF8	40.8 (35-48)	1.07	78 ± 7
	3LCF9	38.3 (34-47)	1.04	83 ± 6
Second-stage product	242	11.3 (10-12)	0.68	83 ± 1
	3LCF7	17.3 (11-28)	0.98	–
	3LCF8	18.0 (17-20)	1.07	90 ± 2
	3LCF9	22.9 (18-33)	1.01	89 ± 2

Aromaticity relates inversely to hydrogen content. The ratio of cyclic to alkyl aliphatic protons at constant aromaticity correlates with donor solvent quality (9)

and relates inversely to paraffin content. The increase in hydrogen content (decreased aromaticity) and donor solvent quality between the second-stage feed and product distillates is evident for all these runs. However, the Run 242 distillates are significantly different from those produced in the Lummus PDU. Although the compositions of the Lummus distillates spanned a fairly broad range, the Wilsonville distillate compositions were considerably outside that range.

A GC/MS investigation of these oils revealed that the Run 242 distillates are much more complex because of extensive alkyl substitution on aromatic rings and contain considerably greater concentrations of paraffins relative to most Lummus samples from equivalent process streams. This is consistent with the ^{1}H-NMR and micro-autoclave data. The Run 242 distillates are more highly hydrogenated but a lower proportion of the hydrogen is found in the desirable hydroaromatic form.

Elemental analyses obtained at Lummus and supplied by Mr. M. Peluso confirm the difference in hydrogen content for various ASTM D-1160 boiling cuts:

	H/C Atomic Ratio	
		Run 242
	3LCF9	V-1067
Boiling Fraction	Product	12/10/82
500 x 650°F	1.40	1.50
650 x 850°F	1.16	1.38
850°F$^+$	0.86	1.04

One potential cause of the observed differences in distillate oils is the effect of the different start-up oils used in the Wilsonville and Lummus programs. Lummus uses creosote oil/hydrogenated creosote oil as a start-up solvent. Run 242 used solvent produced from prior runs (1). Hydrogenated creosote oil is relatively aromatic, non-alkylated and non-paraffinic compared to most coal liquids and is an excellent donor solvent. An exhaustively recycled oil might be expected to be relatively paraffinic and alkylated (9). The solvents from each plant appear to retain certain characteristics of their respective start-up oils long after start-up. This could indicate inefficient solvent turn-over or perhaps it could be an example of multiple steady states (10).

RUN 242 - GREATER SCT SEVERITY AND COAL CONVERSION THAN LUMMUS RUNS

First-stage conversions of coal to THF solubles, calculated based on analyses of T-102 bottoms samples, average 91 ±1% for the samples from Run 242. This is in excellent agreement with the conversions to cresol solubles during "special product work-up periods" reported by Catalytic, Inc., which also averaged 91% (1). Each of the periods discussed above was operated at 860°F and 2400 psig (nominal). The SCT unit of the Lummus plant has been operated at conditions as mild as 830°F and 2000 psig, but has also been operated at the more severe conditions for a large part of the PDU program. THF conversions for those periods (850-860°F and 2400 psig), determined by Conoco, averaged 87% (7) for Runs SCT14 through SCT21 and 88% (7) for Runs 2SCT3 through 2SCT6. Lower severity conditions resulted in even lower coal conversions (5). Quinoline conversions, determined by Lummus, were typically 92% for the same periods (2). The greater first-stage conversion of coal to THF solubles, comparing Conoco's data for Run 242 and the PDU, is consistent with the greater SCT distillate yield reported by Rao, et al. (11) for Run 242 relative to the Lummus PDU and may reflect a greater SCT reaction severity during Run 242. The Lummus system has operated at coal space rates as low as 82 lbs/hr·ft^3 (2SCT15-1014) but is more typically operated at coal

space rates of between 110 and 190 lbs/hr·ft³. Run 242 was consistently operated at about 92 lbs/hr·ft³ based on reactor volume and at about 44 lbs/hr·ft³ when the volume of the heated transfer line is included. The more severe first-stage conditions present during Run 242 as compared to typical PDU runs would be expected to affect SCT yields, thus changing the composition of the second-stage feed.

SECOND-STAGE CONVERSIONS AND CONVERSIONS ACTIVITIES

$850°F^+$ conversions during Run 242 were calculated based on Conoco's analyses as detailed in Reference 4. Average $850°F^+$ conversions changed over the course of Run 242 in the following manner:

Date, 1982-83	Catalyst Age lbs SRC/lb Cat	T, °F	$850°F^+$ Conversion, % Average
12/01 - 12/14	72 - 204	679 - 685	13
12/15 - 12/17	216 - 242	699 - 704	16
12/18 - 01/04	253 - 467	718 - 721	16
01/08 - 01/21	520 - 685	745 - 750	21

It should be noted that these values average 5-7 absolute percentage points lower than the SRC conversions reported by Catalytic, Inc., (1) because of the different distillation procedures used (4).

At the end of Run 242, catalyst age was 500-700 lbs SRC/lb cat, H_2 partial pressure was 2500 psig, temperature was 750°F, the overall space velocity was 1 lb feed/lb cat·hr and the $850°F^+$ space velocity was 0.6 lbs $850°F^+$/lb cat·hr. At similar second-stage conditions the Lummus PDU typically obtains 30-35% $850°F^+$ conversion. The comparison shown below is based on Conoco data.

Run	Period	Cat Age	T, °F	$850°F^+$ Conversion % Average ± Std Dev
242	1/8 - 1/21	520 - 685	745 - 750	21 ± 3
3LCF7	58 - 85	527 - 930	749 - 759	34 ± 3
3LCF8	27 - 49	299 - 526	732 - 751	33 + 2
3LCF9	0826 - 0122	697 - 1474	723 - 756	28 ± 6

The catalyst age units above are lb SRC/lb cat for Run 242 and lb $850°F^+$/lb cat for the Lummus runs. The Run 242 catalyst age values should be increased by about 13% for an equal catalyst age comparison because of the difference in resid determinations (4). The closest comparison shown above in terms of catalyst age and temperature is for Runs 242 and 3LCF7. In that comparison, the average $850°F^+$ conversion for Run 3LCF7 is four standard deviations greater than that for Run 242. Run 3LCF7 was made with a different Illinois basin coal (Indiana 5, Old Ben No. 1). Runs 242, 3LCF8 and 3LCF9 were all made with Illinois 6, Burning Star coal. Even though the data for Runs 3LCF8 and 9 shown above were obtained at generally lower temperatures than the data for Run 242, average $850°F^+$ conversions are greater for the Lummus runs. Clearly the second-stage $850°F^+$ conversion in Run 242 was lower than in typical Lummus runs at operating conditions (T, S.V., catalyst age, pressure, catalyst type, coal) that were ostensibly similar.

First order kinetic rate constants (k) and pre-exponential factors (A) were calculated for second-stage $850°F^+$ conversion for Runs 242 (4) and 3LCF9 (5)

based on Conoco's analyses. Lummus uses an activation energy of 23,500 cal/mol for 850°F$^+$ conversion in the second stage ($\underline{2}$). If it is assumed, for the sake of argument, that the activation energy is the same in the Wilsonville system, pre-exponential factors can be calculated to compare the resid conversion activities of the two systems. The data for Run 242 are compared to the data from Run 3LCF9 in Figure 1. It should be noted that the catalyst age units in Figure 1 are consistent. The catalyst ages of the Run 242 data, which were obtained from the report by Catalytic, Inc., ($\underline{1}$) were increased by 13% to put them on a basis equivalent to the Run 3LCF9 data, i.e., on a lbs 850°F$^+$/lb cat basis. As shown in Figure 1, 850°F$^+$ conversion activity decreased with time for both runs as measured by the first-order pre-exponential factor. The data for Run 242 are consistently lower than the Run 3LCF9 data indicating that within the limits of the assumptions used in this model, 850°F$^+$ conversion activity was significantly lower in Run 242 than in Run 3LCF9.

There are several possible reasons for the difference in the calculated conversion activities in the two systems: 1) Simple first-order kinetics may not be a good description of the conversion reactions. Additionally, it may be more appropriate to use space velocity based on reactor volume rather than on catalyst weight for the resid conversion reaction since there may be a large thermal contribution to conversion. 2) The inherent reactivities of the feedstocks are almost certainly different. The clearly demonstrated differences in feed composition are expected to result in different reactivities. This could be caused in part by the different selectivities of the deashing processes as well as the different first-stage reaction severities. Batch experiments demonstrating different "thermal" reactivities of the feedstocks are described below in this paper. Different reactivities would require the use of different activation energies in the kinetic calculations. In fact, Catalytic, Inc., uses an activation energy value of 50,000 Btu/lb mol (27.8 kcal/mol) for Run 242 data($\underline{12}$) as opposed to the 23.5 kcal/mol used in our calculations. 3) One or both runs may have been operated with non-equilibrated solvent. 4) The use of the "effective" (average) temperature in the kinetic calculations for the Lummus system may give incorrect results because the LC-Finer operation is not strictly isothermal. Temperature differentials over the LC-Finer are often 50°F or greater ($\underline{13}$).

YIELD DIFFERENCES CONSISTENT WITH CONVERSION DIFFERENCES

The greater first-stage severity and lower second-stage conversions of Run 242 in relation to Lummus Run 3LCF9 were discussed above. It would be expected that these differences would be reflected in the product yields of the two runs. A comparison of the yield structures of the two runs was reported by Rao, et al ($\underline{11}$). The table below, based on those data, compares the net C$_5^+$ distillate yields by stage.

	Net C$_5^+$ Distillate Yield			
	Run 242		Run 3LCF9	
	As wt % MAF Coal	As % of Total Distillate Yield	As wt % MAF Coal	As % of Total Distillate Yield
First Stage	35.6	57	8.5	15
Second Stage	27.3	43	49.0	85
Total	62.9	100	57.5	100

Although total distillate yields are similar for the two runs, a much greater proportion of the distillate was produced in the first stage during Run 242. These results are consistent with conclusions drawn from our analyses of the runs.

179

THERMAL REACTIVITIES OF RUNS 3LCF9 AND 242 RESIDS

The comparison of Wilsonville Run 242 with typical Lummus operations described above showed that when second-stage samples were analyzed on an equivalent basis, the resid ($850^\circ F^+$) conversion activity, as measured by the first-order kinetic pre-exponential factor, was lower in the Wilsonville system than the Lummus system. To examine the reactivities of the different feed resids, we performed a set of experiments to compare the "thermal" reactivities of the residual feeds to Lummus Run 3LCF9 and Wilsonville Run 242. One reason the compositions of the second-stage feed resids are different is the different deashing technologies in use at the two plants. Wilsonville uses CSD which selectively rejects preasphaltenes. In order to determine if the difference in reactivities (if any) of the second-stage feed resids were caused solely by deashing differences, we also tested a T-102 bottoms (first-stage product resid, non-deashed) sample from Run 242.

The conversion of resid in the second stage of ITSL is promoted by the distillate hydrogen donors in the solvent. Since the second stage of each plant is back-mixed, the product distillate better models the reactor inventory than the feed distillate. Therefore, the distillates used in this work were second-stage products whereas the resids were second-stage feeds.

The samples used for these experiments are described below:

3LCF9 Resid: A composite sample of the $850^\circ F^+$ resid fraction of LC-Finer feed samples from Run 3LCF9.

3LCF9 Distillate: Same, but composited from the $850^\circ F^-$ distillate products.

V-1064 Resid: The residual ($850^\circ F^+$) portion of the V-1064 (second-stage feed) sample from 1/13/83 of Run 242. A typical sample.

242 Distillate: A composite sample of the $850^\circ F^-$ distillate fraction of the V-1067 (second-stage product) samples from Run 242.

T-102 Bottoms: The first-stage product resid from 12/19/82 of Run 242. A typical sample.

The method used for these experiments follows. The 30 ml microautoclave was charged with 9 g of the resid sample and 6 g of the distillate sample to be investigated. This approximates a "typical" resid/distillate ratio in the continuous units. The microautoclave vessel has heat-up and cool-down times of less than 2 min and is agitated vigorously to overcome mass transfer limitations. The vessel was charged with 1000 psig cold H$_2$ (<2300 psig at 750°F). Reactions were carried out for two hours at 750°F. 750°F was used because both continuous units were operated for some time at that temperature. Two hours is thought to approximate the average liquid residence times in the second-stages of the two continuous units. It is recognized that a batch microautoclave can only approximate the performance of the continuous unit; however, this work was done to obtain a comparison, not absolute reactivities. After each microautoclave run, the microautoclave contents were extracted with THF to separate the IOM and ash. The solubles were distilled to 320°C pot/270°C column/5 torr (850°F) using a microstill. Conversions and yields were determined from known feed and product compositions. Ash was assumed to carry through unchanged. $850^\circ F^-$ was determined by difference and includes both distillate and total gas make. Each experiment was performed at least twice to obtain a measure (pooled standard deviation) of reproducibility. Each distillate sample was reacted with each resid sample at least in duplicate to determine the relative "thermal" reactivities of the resids and the effect of the distillates. The data are summarized in Table 1. As

shown in Table 1, the pooled standard deviation of our measurement of $850°F^+$ conversion is 0.6% absolute.

No difference was observed that was dependent on the distillate solvent used in these tests even though there is a significant difference in their abilities to convert coal in a donor-only system (4, 5).

Unlike the distillate, the resids made a large, experimentally significant difference. About 15% of the resid from Run 3LCF9 converted to lighter materials, regardless of distillate. This compares to about 5 to 6% for the two Run 242 resids which did not react to significantly different extents from one another.

These results support the conclusion that the resid conversion activities calculated for Runs 3LCF9 and 242 were different, at least in part, because of a difference in the reactivities of the feedstocks. The results indicate that the lower resid conversions obtained in Run 242 as compared to Run 3LCF9 during periods of generally comparable operating conditions resulted at least partly from a less reactive second-stage feedstock. This is consistent with the first-stage distillate yields in Run 242 being higher than in Run 3LCF9 (12), thus leaving only the more refractory materials for second-stage conversion.

SUMMARY

● The compositions and relative proportions of both the $850°F^-$ distillate and $850°F^+$ resid fractions in the process streams were fairly constant in Wilsonville Run 242.

● The Critical Solvent Deashing (CSD) unit selectively rejected preasphaltenes during Run 242. The reduced level of preasphaltenes thus fed to the hydrotreater could affect hydrotreater performance.

● The characteristics of the process oils from Run 242 are significantly different from the characteristics of the corresponding process oils from Lummus PDU operations, although both operations were conducted in the ITSL mode. For many measured parameters, the data from Run 242 and the Lummus operations do not share a common range. Much of the difference may be ascribed to differences in the first-stage (thermal) severities and to selectivities of the deashing operation between the Lummus and Wilsonville operations. Characteristics of the start-up solvents may also have influenced this comparison.

● First-stage coal conversions to THF solubles averaged 91% for Run 242. This is 3 to 4% absolute greater than the THF conversions calculated for Lummus PDU runs operated at similar temperature and pressure conditions and is consistent with the generally lower first-stage space velocity used in Run 242. The more severe first stage conditions used in Run 242 may be one reason for the different first-stage yields and different second-stage feed compositions in that run as compared to PDU operations.

● Second-stage $850°F^+$ conversions in Run 242 were clearly lower than in typical PDU runs at operating conditions that were ostensibly similar. A possible reason for this is the dissimilar second-stage feed composition, again partially a result of the deashing process and first-stage severity differences.

● A statistically-designed set of experiments showed that the second-stage residual feed from Wilsonville Run 242 was significantly less reactive than the corresponding material from Lummus Run 3LCF9 at thermal/donor, i.e., non-catalytic conditions. This is consistent with the analytical results.

ACKNOWLEDGEMENT

REFERENCES

1. Catalytic, Inc., "Run 242 with Illinois 6 Coal", Technical Progress Report, DOE Contract No. DE-AC22-80PC50041, July, 1983.

2. Schindler, H. D., Chen, J. M. and Potts, J. D., "Integrated Two-Stage Liquefaction – Final Technical Report – Volume I", DOE Contract No. DE-AC22-79ET14804, June, 1983.

3. Schindler, H. D., Chen, J. M. and Potts, J. D., "Integrated Two-Stage Liquefaction - Topical Technical Progress Report - Process Flow Modification – Period: July, 1982 – February, 1983", DOE Contract No. DE-AC22-82PC50021, January, 1985.

4. Burke, F. P., Winschel, R. A. and Robbins, G. A., "Recycle Slurry Oil Characterization - Third Annual Report", DOE Contract DE-AC22-80PC30027, October, 1984.

5. Burke, F. P. and Winschel, R. A., "Recycle Slurry Oil Characterization – Technical Report: 10/1/82 – 3/31/83", DOE Contract No. DE-AC22-80PC30027, February, 1984.

6. Burke, F. P. and Winschel, R. A., "Recycle Slurry Oil Characterization – Second Annual Report", DOE Contract No. DE-AC22-80PC30027, August, 1983.

7. Burke, F. P. and Winschel, R. A., "Recycle Slurry Oil Characterization – First Annual Report", DOE Contract DE-AC22-80PC30027, July, 1982.

8. Burke, F. P. and Winschel, R. A., "Recycle Slurry Oil Characterization – Final Report", DOE Contract DE-AC22-80PC30027, March, 1985.

9. Burke, F. P., Winschel, R. A., and Pochapsky, T. C., Fuel, 60, 562 (1980).

10. Klunder, E., Krastman, D., Mima, J., "Iron Pyrite Catalysis and Gas Velocity Effects in Coal Liquefaction", Proceedings of the 1983 International Conference on Coal Science, p. 118-121, August, 1983.

11. Rao, A. K., Pillai, R. S., Lee, J. M. and Johnson, T. W., "Recent Advances in Two-Stage Liquefaction at Wilsonville", Proceedings of the Eighth Annual EPRI Contractors' Conference on Coal Liquefaction, EPRI Report AP-3366-SR, February, 1984.

12. Rao, A. K., Lee, J. M., Moniz, M. J. and Pillai, R. S., "Recent Developments in Two-Stage Coal Liquefaction at Wilsonville", Proceedings of the 1983 DOE Direct Liquefaction Contractors' Review Meeting, Pittsburgh, PA, November, 1983.

13. Schindler, H. D., Chen, J. M. and Potts, J. D., "Integrated Two Stage Liquefaction, Topical Technical Progress Report, Steady State Illinois No. 6 Program, Period April 1, 1982 – July 6, 1982", DOE Contract No. DE-AC22-79ET14804, April, 1983.

TABLE 1

THERMAL REACTIVITIES OF RUNS 3LCF9 AND 242 RESIDS
SUMMARY OF RESULTS

Samples		850°F$^+$ Conversions, wt %			
Distillate	Resid	Trial 1	Trial 2	Trial 3	Average
3LCF9	3LCF9	15.8	14.4	–	15.1
	V-1064	5.6	6.4	–	6.0
	T-102 Bottoms	5.1	5.8	–	5.4
242	3LCF9	15.6	15.4	–	15.5
	V-1064	4.8	4.0	4.9	4.6
	T-102 Bottoms	6.8	5.8	–	6.3

Pooled standard deviation = 0.6% absolute

Average conversion using 3LCF9 distillate = 8.8% $\Big\}$ No significant
Average conversion using 242 distillate = 8.8% difference

Average conversion using 3LCF9 resid = 15.3% $\Big\}$ 3LCF9 resid more
Average conversion using V-1064 resid = 5.3% reactive than either
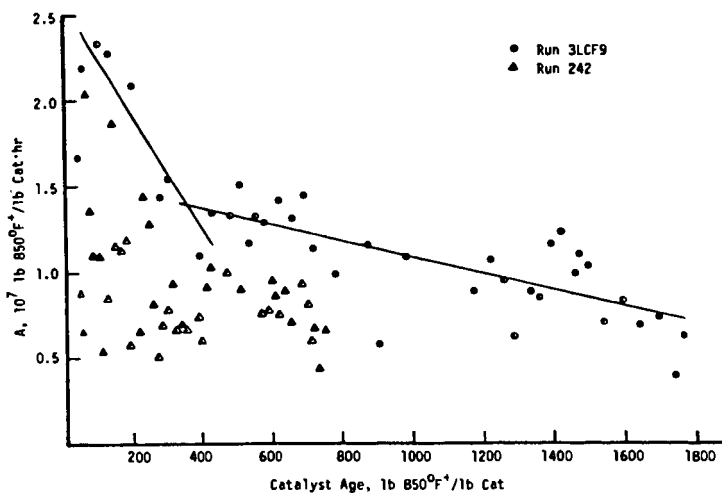Average conversion using T-102 bottoms resid = 5.9% 242 resid

Figure 1. Comparison of First-Order Pre-Exponential Factors vs Catalyst Age.
Runs 242 and 3LCF9.

183